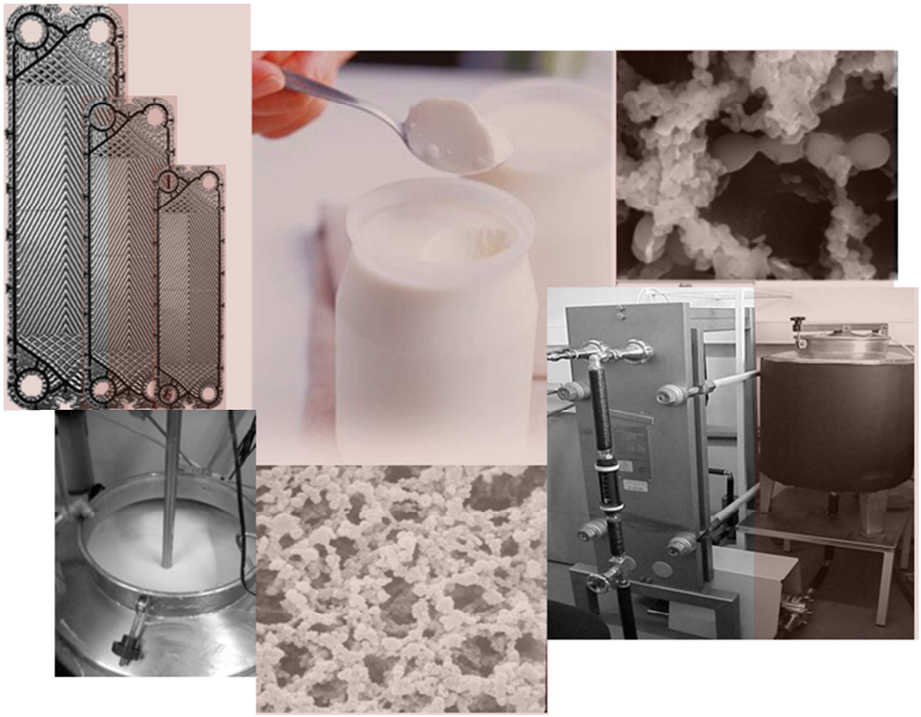
Universidade do Porto
Faculdade de Engenharia
FEUP
Chemical Engineering Department

Lepae
Laboratory for Process, Environmental and Energy Engineering

Heat Transfer in Non-Newtonian Food Fluids in a Plate Heat Exchanger



Isabel Maria Barreira Afonso Paula

Doctoral Programme in Chemical and Biological Engineering

Dissertation submitted in partial fulfilment of the requirements for the degree of Doctor of Philosophy in Chemical and Biological Engineering

Porto, 2012

This thesis was supervised by:

Supervisor: Professor Dr. Luís Manuel Ferreira de Melo

LEPAE – Laboratory for Process, Environment and Energy Engineering

Department of Chemical Engineering

Faculty of Engineering, University of Porto

Co-Supervisor: Associate Professor João Manuel Luis Lopes Maia

I3N - Department of Polymer Engineering, Institute for Nanostructures, Nanomodelling and Nanofabrication, Universidade do Minho, Guimarães

Department of Macromolecular Science and Engineering

Case Western Reserve University, Cleveland, Ohio

HEAT TRANSFER IN NON-NEWTONIAN FOOD FLUIDS IN A PLATE HEAT EXCHANGER

ISABEL MARIA BARREIRA AFONSO PAULA

Doctoral Programme in Chemical and Biological Engineering

Philosophiae Doctor (Ph.D.) in Chemical and Biological Engineering

Chemical Engineering Department

LEPAE - Laboratory for Process, Environmental and Energy Engineering

Faculty of Engineering of the University of Porto

JUNE 2012

“It does not matter how slowly you go so long as you do not stop”

Confucius (551-479 BC)

ACKNOWLEDGEMENTS

During the last fourteen years I have the privilege of working with Professor Luis Melo to whom no words can express my sincere gratitude and appreciation for his guidance, encouragement and support throughout this long scientific journey. I am eternally grateful for being an always available advisor, always providing a soothing presence in bad moments. I would also like to acknowledge Professor João Maia for his guidance and support since the beginning of my scientific journey in the "Rheology world" and for friendly welcoming me in the Rheology Laboratory.

I acknowledge Dr Ulf Bolmstedt from Tetra Pak Processing Components AB (Lund, Sweden) for making possible the fulfilment of this thesis by having made available the industrial plate heat exchanger used in the experimental set-up of this study. I am very grateful for this opportunity.

I acknowledge the late Dr Jean-Claude Leuliet from INRA-LGPTA (Institut National de la Recherche Agronomique - Laboratoire de Génie des Procédés et Technologie Alimentaires, Lille) for the useful help and discussion of the instrumentation and control of the plate heat exchanger and Dr Thierry Bénézech for making possible my technical visit to LGPTA and organizing the technical meetings that have been of great value for the present thesis.

I acknowledge Professor João Campos for the useful help and discussion on heat transfer subjects.

My gratitude also goes to Carla Ferreira (Carlinha) for being my other "pair of hands" when work seemed to never end. For me is a privilege to have you as a friend, you were/ are a source of energy and encouragement in good and bad moments. No words can express my gratitude for your support and care. Stirred yoghurt experiments were performed with your enormous help.

My thanks also go to Ana Pereira for being a precious help in the meticulous welding of temperature probes and for all help and technical support concerning the data acquisition system. Thank you Ana for all the care and friendship above all.

Looking back in time I cannot forget the feelings of joy, fun and drama that my dearest friend Roxane Rosmaninho filled out hers and my days on Lab 303. Now I can say that I have missed your singing/ shouting moments.

I acknowledge Paulo Cruz for the important contribution for the simulation analysis performed in this thesis and Afonso Leite for the useful help concerning MATLAB programming.

I thank Pablo Garrido, my Spanish friend, for his exceptional work in the beginning of my PhD, together we solved a lot of technical problems related with the plate heat exchanger ("LUPITA" as you named it).

I thank all my co-workers in Lab 303, Joana Teodósio and the newest members.

A PhD is not only a scientific project but also an individual strength probation, a life passage that comprises thrilling and encouraging moments but very often tough moments. In all these moments Artur was by my side trying to make my life easier, cheering and helping me when I needed. Thank you for all the love, patience and friendship.

I also thank Francisco, my treasured son, for brightening my days (even the darkest ones) with his outstanding happiness and energy. I hope you forgive me for my absence and (sometimes) impatience during the last months.

I would like to express my gratitude to my lovely family. I thank my Parents, Olinda and Telémaco and my brother Zé for their support, patience and love during all these years. I also want to thank my parents in law for their care and friendship, a special thanks to my mother in law, D. Alice, for taking good care of my diet. Thank you all for being there when I needed most and for being exceptional grandparents. Special thanks also go to my best friend Tini for her cheerfulness, help and for just being there.

A special thank goes to Nuno Ratola, Olga, Tiago and to the other new members of the FEUP lunch group for the nice and funny moments at lunch. For several years, lunch time was a therapy for depression.

I would also like to acknowledge all my co-workers in Food Quality and Safety Group at ESA-IPVC, special thanks to Ana Paula Vale, Ana Ferraz and Ana Cristina

Rodrigues for their friendship, support and help concerning projects and classes. I thank Álvaro Queiróz for the useful help concerning Statistics methodologies.

I thank Sr Manuel Santos for his help on the assembling of my stirred yoghurt production setup, for teaching me the techniques that enabled me to perform changes and to solve problems by myself. This was not a “man´s job”.

I would like to thank to Paulino Amorim, Elisa Duarte and D. Fátima Faustino for their help regarding administrative issues.

ABSTRACT

Thermal processing in the food industry involves heating and cooling of highly viscous fluids. Frequently, plate heat exchangers (PHE) are used for liquid–liquid heat transfer duties that require uniform and rapid heating or cooling, as is often the case when treating thermally sensitive fluids such as food fluids. During such operations, physical modifications affecting the structure and stability of the final product occur. To reach an appropriate balance between thermal efficiency and properties of the food products, a combined study of heat transfer and product rheology is needed.

The aim of this thesis was to increase the current knowledge about several distinct, but complementary, subjects related with thermal processing of complex food fluids in plate heat exchanger in order to obtain semi- empirical correlations for the determination of mean and local convective heat transfer coefficients of stirred yoghurt cooling in a plate heat exchanger. This thesis comprised the development of empirical models of the rheological and thermo-physical properties of the selected food fluids (water, stirred yoghurt and aqueous solutions of carboxymethyl cellulose (CMC) used as a thickening agent in stirred yoghurt production). The studies were mainly focused on the characterization of rheological properties of the stirred yoghurt produced from different non-fat milk based formulations and their correlation with the operating features of the plate heat exchanger. The optimization of the operating conditions in order to achieve reduced processing costs and quality improvement of the final product was attempted.

Steady shear and dynamic oscillatory rheological experiments were carried out in order to evaluate the non-Newtonian behaviour of stirred yoghurt, particularly pseudoplasticity and viscoelasticity characteristics. The relationship between rheological properties, microstructure, and susceptibility to syneresis in yoghurt made from milk base mixture as affected by total solids content added was assessed. The experiments allowed to verify that yoghurts produced with starter culture YF-L812 exhibited, in general, better rheological and texture characters, apparently with less susceptibility to syneresis.

Heat transfer experiments were performed in a plate heat exchanger CLIP 6 – RM (Tetra Pak Processing Components AB, Sweden) operating in countercurrent flow on a 2×2 arrangement with two channel per pass instrumented with thermocouples type J and platinum resistance probes Pt100 for temperature control along the PHE channels. Heat transfer experiments were carried out with water on both sides of the PHE in order to obtain mean and local heat transfer coefficients of cooling water. Four correlations for determination of local heat transfer coefficients of cooling water for each section were obtained, and one correlation for determination of mean heat transfer coefficients of cooling water. From heat transfer experiments performed during cooling of stirred yoghurt, the local correlations obtained showed a great dispersion mainly on the channel entrance zone due to instabilities on the thermocouples caused by stirred yoghurt highly viscous flow. The correlations obtained for the determination of mean heat transfer coefficient of stirred yoghurt, in different product formulation tested, evidenced a laminar flow in plate heat exchanger considering the Reynolds number values ($Re<3$) and its exponents in the correlation. The correlations obtained for the local heat transfer coefficient of stirred yoghurt confirmed the significant effect of temperature on the rheological properties of stirred yoghurt (significant variation of Reynolds number along PHE channels was observed).

This study enabled to verify the complexity of heat transfer of non-Newtonian food fluids in a plate heat exchanger, enhancing the hydrodynamic aspects related to fluid thermo-rheological behaviour. The correlations obtained for the determination of local heat transfer coefficients of stirred yoghurt during cooling in a plate heat exchanger revealed distinguished thermal profiles in both sections analysed in a plate heat exchanger with a 2×2 arrangement.

KEYWORDS

Yoghurt; food rheology; food processing; Convective heat transfer coefficient; heat exchanger

RESUMO

O processamento térmico na indústria alimentar envolve o aquecimento e arrefecimento de fluidos altamente viscosos. Frequentemente, os permutadores de calor de placas são utilizados em operações de transferência de calor líquido-líquido que requerem aquecimento ou arrefecimento uniforme e rápido, como é frequente o caso quando se trata fluidos termicamente sensíveis como os fluidos alimentares. Durante estas operações podem ocorrer modificações físicas que afectam a estrutura e a estabilidade do produto final. Para obter um equilíbrio adequado entre a eficiência térmica e as propriedades dos produtos alimentares, é necessário um estudo combinado da transferência de calor e reologia do produto.

Esta tese teve como objectivo aumentar o conhecimento actual sobre vários assuntos distintos, mas complementares, relacionados com o processamento de fluidos alimentares complexos em permutadores de calor de placas de modo a obter correlações semi-empíricas para a determinação dos coeficientes convectivos de transferência de calor médio e local do iogurte batido arrefecido num permutador de calor de placas. Esta tese contempla o desenvolvimento de modelos empíricos das propriedades reológicas dos fluidos alimentares seleccionados (água, iogurte batido e soluções aquosas de carboximetilcelulose (CMC) usado como espessante na produção de iogurte batido). A abordagem seguida está relacionada com a caracterização das propriedades reológicas do iogurte batido produzido a partir de diferentes formulações da mistura base do leite magro e a sua correlação com as características operacionais do permutador de calor de placas. A optimização das condições operacionais tendo em vista a diminuição do custo do processo e a melhoria de qualidade do produto final foi outro dos objectivos traçados.

Foram realizados ensaios reológicos em escoamento estacionário e ensaios dinâmicos oscilatórios com os iogurtes produzidos a partir de diferentes formulações da mistura base do leite magro, que permitiu verificar o comportamento não-Newtoniano dos diferentes iogurtes, particularmente, o comportamento pseudoplástico com características viscoelásticas. A relação entre propriedades reológicas, a microestrutura

e susceptibilidade à sinérese dos iogurtes produzidos a partir das diferentes formulações da mistura do leite base foi avaliada tendo em consideração os efeitos do teor em sólidos totais e cultura láctica (YC-380 e YF-L812) adicionados. Os ensaios realizados permitiram verificar que os iogurtes produzidos com a cultura láctica YF-L812 apresentaram, de um modo geral, melhores características reológicas e textura, aparentemente menor susceptibilidade à sinérese.

Os estudos de transferência de calor foram realizados no permutador de calor de placas CLIP 6- RM (Tetra Pak Processing Components AB, Sweden), a operar em contracorrente num arranjo 2×2, com dois canais por secção instrumentados com termopares tipo J, para ler as temperaturas dos fluidos, e termoressistências Pt100. Nos ensaios realizados com água de modo a obter as correlações para a determinação dos coeficientes convectivos de transferência de calor médios e locais da água de arrefecimento foram obtidas quatro correlações locais, para cada secção, uma correlação global. Nos ensaios de transferência de calor com iogurte batido as correlações locais obtidas apresentam uma grande dispersão principalmente nas zonas de entrada devido ao escoamento viscoso do iogurte que provoca perturbações nos termopares de leitura de temperatura no seio do fluido. As correlações obtidas para a determinação dos coeficientes convectivos de transferência de calor médio do iogurte batido, nas diferentes formulações testadas, evidenciam um escoamento laminar no permutador de calor pelos valores do número de Reynolds ($Re < 3$). As correlações locais obtidas comprovam o efeito significativo da temperatura nas propriedades reológicas dos fluidos (Re variável ao longo do canal).

Este trabalho permitiu avaliar a complexidade da transferência de calor de fluidos alimentares não-Newtonianos num permutador de calor de placas, realçando os aspectos hidrodinâmicos relacionados com o comportamento termo-reológico do fluido. As correlações semi-empíricas para a determinação dos coeficientes convectivos de transferência de calor local do iogurte batido arrefecido num permutador de calor de placas obtidas revelaram o perfil térmico diferenciado nas duas secções analisadas no permutador de calor de placas com arranjo 2×2.

PALAVRAS-CHAVE

Iogurte; reologia de alimentos; processamento de alimentos; coeficiente convectivo de transferência de calor; permutadores de calor.

RÉSUMÉ

Le traitement thermique dans l'industrie alimentaire implique le chauffage et le rafraîchissement de liquides fortement visqueux. Fréquemment, les échangeurs de chaleur à plaques (PHE) sont utilisés pour les performances de transfert de chaleur liquides-liquides qui exigent le chauffage ou le rafraîchissement uniforme et rapide, comme est souvent le cas en traitant des liquides thermiquement sensibles comme des fluides alimentaires. Pendant ces opérations, des modifications physiques affectant la structure et la stabilité du produit final arrivent. Pour atteindre un équilibre approprié entre l'efficience thermique et les propriétés des produits alimentaires, une étude combinée de transfert thermique et la rhéologie de produit est nécessaire.

La présente thèse vise l'accroître des connaissances actuelles sur plusieurs sujets différents, mais complémentaires, liés à traitement des fluides alimentaires complexes dans l´échanger de chaleur à plaques pour obtenir corrélations semi-empiriques pour la détermination des coefficient de transfert de chaleur moyen et local de yaourt brassé rafraîchissant dans un échangeur de chaleur à plaques. Cette thèse a compris le développement des modèles empiriques des propriétés rhéologiques des fluides alimentaires choisis (l´eau, le yaourt brassé et les solutions aqueuses de carboxyméthylcellulose utilisée comme un agent d'épaississement dans la production de yaourt brassé). Les études sont principalement centrées sur la caractérisation des propriétés rhéologiques du yaourt brassé produit avec différentes formulations de la mixture basée du lait sans matières grasses et sa corrélation avec les caractéristiques opérationnelles de l'échangeur de chaleur à plaques. L'optimisation des conditions d'opération pour réaliser la diminution de coût de traitement et pour l'amélioration de qualité du produit final a été essayée.

Expériences avec fixe vitesse de cisaillement et des expériences rhéologiques oscillantes dynamiques ont été effectuées pour évaluer le comportement non-newtonien de yaourt brassé, particulièrement la pseudoplasticité et des caractéristiques viscoélastiques. La relation entre des propriétés rhéologiques, la microstructure et la sensibilité à synérèse dans les yaourts produits avec différentes formulations de la

mixture basée du lait comme affecté par le contenu de solides totaux, et la culture lactique (YC-380 et YF-L812) supplémenté a été évaluée. Les expériences ont effectué permise la vérification de cela des yaourts produits avec la culture lactique YF-L812 présenté, en général, mieux caractéristiques rhéologiques et de texture, apparemment avec moins de sensibilité à synérèse.

Les expériences de transfert thermique ont été exécutées dans un échangeur de chaleur à plaques et joints CLIP 6-RM (Tetra Pak Processing Components AB, Sweden) opérant en contrecourant sur le configuration 2×2, avec deux canaux par passe, instrumenté avec des thermocouples type J et des sondes à résistance de platine Pt100 pour le contrôle de température le long des canaux de l´échangeur à plaques. Les expériences de transfert thermique ont été effectuées avec l'eau dans le deux côtés de l´échangeur à plaque pour obtenir les coefficients de transfert de chaleur moyens et local de l'eau de rafraîchissant. Quatre corrélations pour la détermination des coefficients de transfert de chaleur locaux de rafraîchir l'eau pour chaque section ont été obtenues et une corrélation pour la détermination des coefficients de transfert thermique moyens de l'eau. D'expériences de transfert thermique exécutées pendant le rafraîchissement de yaourt brassé, les corrélations locales obtenues ont montré qu'une grande dispersion principalement sur les zones d'entrée de canal en raison des instabilités sur les thermocouples causés par l´écoulement fortement visqueux de yaourt brassé. Les corrélations obtenues pour la détermination de coefficient de transfert de chaleur moyen de yaourt brassé, dans les différentes formulations de produit évaluées, ont fait la preuve d'un régime d´écoulement laminaire dans l'échangeur à plaques considérant les valeurs du nombre de Reynolds ($Re < 3$) et son indice dans la corrélation. Les corrélations obtenues pour la détermination de coefficient de transfert de chaleur local de yaourt remué brassé ont confirmé l'effet significatif de la température sur les propriétés rhéologiques de yaourt brassé (la variation significative du nombre de Reynolds le long des canaux a été observée).

Cette étude a permis vérifier la complexité de transfert de chaleur de fluides alimentaires non-Newtoniens dans un échangeur de chaleur à plaques améliorant les aspects hydrodynamiques liés au comportement thermo-rhéologique du fluide. Les corrélations obtenues pour la détermination des coefficients de transfert de chaleur

locaux de yaourt brassé pendant le rafraîchissement dans un échangeur à plaques ont révélé des profils thermiques distincts dans les deux sections analysées dans l´échangeur à plaques avec la configuration 2 × 2.

MOTS-CLÉS

Yaourt; rhéologie des aliments; traitement alimentaire; coefficient de transfert de chaleur; échangeur de chaleur

CONTENTS

ACRONYMS XIX

NOMENCLATURE XXI

Greek Symbols xxiii

Subscripts xxiv

1. STATE OF THE ART 1

1.1 The Problematic of Food Fluids in Plate Heat Exchangers 1

1.2 Plate Heat Exchangers 2

1.2.1 Plate Heat Exchanger – Basic Construction **3**

1.2.2 Flow arrangements **7**

1.2.3 Advantages and Limitations **8**

1.2.4 Experimental and numerical studies on plate heat exchanger **10**

1.3 Transport Phenomena in Food Processing 11

1.3.1 Momentum transport 11

1.3.2 Heat Transfer 12

1.3.3 Rheological properties and their relation to food processing 12

1.3.4 Thermophysical properties and their relation to food processing 13

1.4 Dairy Products 13

1.4.1 Dairy products based on proteins 14

1.4.2 Yoghurt 14

2. ROADMAP FOR THE THESIS 17

3. MATERIALS AND METHODS 23

3.1 Introduction 23

3.2. Experimental set-up 23

3.2.1 Main features 23

3.2.2 Temperature measurement in the plate heat exchanger channels..... 25

3.3 Yoghurt production..... 31

3.3.1 Set-style yoghurt production..... 31

3.3.2 Stirred yoghurt..... 36

3.3.3 Microbiological control 38

3.4 Physicochemical analysis of yoghurt 39

3.4.1 pH measurements..... 39

3.4.2 Dry matter..... 39

3.4.3 Fat content 40

3.4.4 Protein content..... 41

3.4.5 Total ash..... 44

3.4.6 Syneresis quantification..... 44

3.4.7 Titratable acidity..... 45

3.4.8 Density determination..... 45

3.5 Rheological methods..... 46

3.5.1 Oscillatory rheology tests 46

3.5.2 Viscometric tests..... 46

3.6 Microscopy methods..... 46

3.6.1 Gram staining..... 46

3.6.2 Scanning Electron Microscopy (CryoSEM)..... 47

3.7 Heat transfer experiments 48

3.7.1 Water/ water heat transfer experiments 48

3.7.2 CMC / Water heat transfer experiments 49

3.7.3 Stirred yoghurt/ water heat transfer experiments..... 50

3.8 Heat transfer analysis 50

3.8.1 Mean convective heat transfer coefficients 50

3.8.2 Determination of Local Heat Transfer Coefficients 57

3.8.3 Pressure drop 60

3.9 Statistical Analysis..... 61

4. DETERMINATION OF MEAN AND LOCAL HEAT TRANSFER COEFFICIENTS OF COOLING WATER IN A PLATE HEAT EXCHANGER..... 63

4.1 Introduction 63

4.2 Experimental methodology..... 64

4.3 Results and Discussion 65

4.3.1. Determination of mean convective heat transfer coefficients of cooling water 65

4.3.2. Determination of local convective heat transfer coefficients of cooling water714.3.3. Determination of Fanning friction factor correlations 95

4.4 Conclusions 97

5. DETERMINATION OF MEAN AND LOCAL CONVECTIVE HEAT TRANSFER COEFFICIENTS OF NEWTONIAN AND NON-NEWTONIAN FLUIDS IN A PLATE HEAT EXCHANGER 99

5.1 Introduction 99

5.2 Experimental methodology..... 100

5.2.1 Thermophysical properties 100

5.2.2 Heat transfer experiments..... 101

5.3 Results and Discussion 103

5.3.1. Rheological behaviour..... 103

5.3.2. Determination of the mean convective heat transfer coefficients of CMC solutions..... 114

5.3.3. Determination of the local convective heat transfer coefficients of CMC solutions 126

5.3.4. Determination of Fanning friction factor correlations 156

5.4 Conclusions 159

6. DETERMINATION OF MEAN AND LOCAL CONVECTIVE HEAT TRANSFER COEFFICIENTS OF STIRRED YOGHURT COOLING IN A PLATE HEAT EXCHANGER 163

6.1 Introduction 163

6.2 Experimental methodology 164

6.2.1 Thermophysical properties 165

6.2.2 Structure analysis by CryoSEM 166

6.2.3 Heat transfer experiments 166

6.3 Results and Discussion 168

6.3.1 Rheological characterisation 168

6.3.2 Temperature dependence 177

6.3.3. Determination of the mean convective heat transfer coefficients of stirred yoghurt 179

6.3.4. Determination of the local convective heat transfer coefficients of stirred yoghurt 187

6.3.5. Determination of Fanning friction factor correlations 207

6.3.6. Effect of cooling stage in the structure of the stirred yoghurt 210

6.4 Conclusions 217

7. MAIN CONCLUSIONS AND SUGGESTIONS FOR FORTHCOMING WORK 221

7.1 Main conclusions 221

7.2 Forthcoming work 222

BIBLIOGRAPHY 223

ANNEXES..... 239

Annex A1 - Complementary data and results..... 241

Annex A2 - Simplified numerical simulation to obtain heat transfer correlations for stirred yoghurt in a plate heat exchanger..... 253

LIST OF FIGURES

In the main text

Figure 1.1- Examples of plate heat exchangers. 3

Figure 1.2- Structure of a typical gasketed plate heat exchanger with chevron plates (Gut *et al.*, 2004). 4

Figure 1.3- Flow pattern in a plate heat exchanger..... 5

Figure 1.4- Alignment of chevron plates and contact points formation. 6

Figure 1.5- Plate patterns: (a) washboard; (b) zigzag; (c) chevron or herringbone; (d) protrusions and depressions; (e) washboard with secondary corrugations; (f) oblique washboard (Shah *et al.*, 2003). 6

Figure 1.6- Single- and multipass plate heat exchanger arrangements. Looped or single-pass arrangements: (a) U-arrangement; (b) Z-arrangement. Multipass arrangements: (c) 2 pass – 1 pass, (d) 3 pass – 1 pass, (e) 4 pass – 2 pass, and (f) series flow (Shah *et al.*, 2003). 8

Figure 2.1- Experimental set-up in initial stage of assembling. 18

Figure 2.2- Schematic representation of temperature probes location along the PHE channels. 19

Figure 2.3- Detailed view of temperature probes location along PHE plates..... 20

Figure 3.1- Flow diagram of the experimental set-up (1: Fermentation tank; 2: flow regulation valve; 3: lobules pump; 4: plate heat exchanger; 5: water refrigerating unit; 6: centrifuge pump (cooling water); 7: stirred yoghurt storage tank (after cooling); 8: flowmeter; 9: hot oil tank; 10: oil centrifuge pump; T1, T3: inlet/ outlet tested fluid temperature probes; T2, T4: inlet/ outlet cooling water temperature probes. 24

Figure 3.2- Main dimensions of the plate heat exchanger (Tetra Pak Processing Components AB, 2000). 26

Figure 3.3- Detail of thermocouple positioning in tube connector to PHE. 27

Figure 3.4- Detailed positioning of Pt 100 in a PHE plate: (a) attached probe, (b) final aspect of plate assembling with Pt100 probes and thermocouples. 28

Figure 3.5- Schematic representation of temperature probes location along the PHE channels. 29

Figure 3.6- Experimental set-up. View of a PHE channel..... 30

Figure 3.7- Reconstituted milk for set-style yoghurt production, for several milk formulations..... 31

Figure 3.8- Set-style yoghurt obtained with milk formulation F38. 36

Figure 3.9- Yoghurt coagulum in the incubation tank of test facility..... 37

Figure 3.10- Stirred yoghurt cooling in the PHE of test facility..... 38

Figure 3.11- Fluid flow pattern of the plate heat exchanger with a multipass configuration 2×2/2×2 in countercurrent..... 51

Figure 3.12- Representation of flow pattern and thermal analysis for section 1 (a) and section 2 (b) of plate heat exchanger. 58

Figure 5.1- Viscosity data obtained of 0.25% CMC solution, at a constant spindle speed rotation (12 rpm), for different fluid temperatures. 104

Figure 5.2- Displacement factor dependency on temperature of the 0.25% CMC solution. 105

Figure 5.3- Viscosity data obtained of 1.0% CMC solution, at a constant spindle speed rotation (12 rpm), for different fluid temperatures. 106

Figure 5.4- Displacement factor dependency on temperature of the 1.0% CMC solution. 107

Figure 5.5- Mechanical spectrum for 1.0% CMC solution in the linear domain (τ=1.0 Pa), at 20ºC. 107

Figure 5.6- Dynamic viscosity as a function of angular frequency, at 20ºC, for 1.0% CMC solution. 108

Figure 5.7- Flow curves of the 2.0% CMC solution, as a function of temperature. 110

Figure 5.8- Displacement factor dependency on temperature of the 2.0% CMC solution. 111

Figure 5.9- Mechanical spectrum for 2.0% CMC solution in the linear domain (τ=1.0 Pa), at 20ºC. 111

Figure 5.10- Dynamic viscosity as a function of angular frequency, at 20ºC, for 2.0% CMC solution. 112

Figure 5.11- The Cox-Merz superposition of shear viscosity versus shear rate and complex viscosity versus oscillation frequency for 2.0% CMC solution, at 20ºC (closed symbol: η_{app}, open symbol: η^*)..... 113

Figure 5.12- PHE ports temperatures (entrance/exit) along experiment time of each fluid, in 0.25%CMC solution / water experiment (Re_{CMC}=2.56). 114

Figure 5.13- Thermal correlation for the mean convective heat transfer coefficient of the 0.25% CMC solution, as a function of the Reynolds number. 116

Figure 5.14- Comparison among obtained and published thermal correlations, for viscous Newtonian fluids. 117

Figure 5.15- Experimental and predicted overall heat transfer coefficients as a function of Reynolds number of 0.25% CMC solution. 118

Figure 5.16- PHE ports temperatures (entrance/exit) along experiment time of each fluid, in 1.0% CMC solution / water experiment (Re_{CMC}=23.5). 119

Figure 5.17- PHE ports temperatures (entrance/exit) along experiment time of each fluid, in 2.0% CMC solution / water experiment (Re_{CMC}= 4.0). 120

Figure 5.18- Thermal correlation for the mean convective heat transfer coefficient of the 1.0% CMC solution, as a function of the Reynolds number. 121

Figure 5.19- Thermal correlation for the mean convective heat transfer coefficient of the 2.0% CMC solution, as a function of the Reynolds number. 123

Figure 5.20- Comparison among obtained and published thermal correlations, for non-Newtonian fluids. 124

Figure 5.21- Experimental and predicted overall heat transfer coefficients as a function of Reynolds number of 1.0% CMC and 2.0% CMC solutions. 126

Figure 5.22- Temperature profiles of working fluids ((a) cooling water channel, (b) warm CMC channel) along the PHE section 1 channels, as a function of time, for 0.25% CMC solution (Re=2.56). 127

Figure 5.23- Wall temperature profiles along plate 2 ((a) cooling water side, (b) warm CMC side), as a function of time, for 0.25% CMC solution (Re=2.56). 128

Figure 5.24- Wall temperatures (Plate 2) and working fluids temperatures at channels inlet and outlet ((a) cooling water side, (b) warm CMC side), as a function of time, for 0.25% CMC solution. 129

Figure 5.25- Temperature profiles of working fluids ((a) cooling water channel, (b) warm CMC channel) along the PHE section 2 channels, as a function of time, for 0.25% CMC solution. 130

Figure 5.26- Wall temperature profiles along plate 8 ((a) cooling water side, (b) warm CMC side), as a function of time, for 0.25% CMC solution. 131

Figure 5.27- Wall temperatures (Plate 8) and working fluids temperatures at channels inlets ((a) cooling water side, (b) CMC side), as a function of time, for 0.25% CMC solution. 132

Figure 5.28- Working fluids temperatures along channels 1 and 2 corrugated zone, for different times ((a) cooling water channel, (b) warm CMC channel), for 0.25% CMC solution. 133

Figure 5.29- Working fluids temperatures along channels 7 and 8 corrugated zone, for different times ((a) cooling water channel, (b) warm CMC channel), for 0.25% CMC solution. 134

Figure 5.30- CMC solution (0.25%) local Nusselt number variation along channel length (channel 2, section 1), for several Reynolds numbers. 137

Figure 5.31- CMC solution (0.25%) local Nusselt number versus Graetz number (channel 2, section 1). 138

Figure 5.32- Comparison of local heat transfer correlations in the thermal entry region obtained in the present work (0.25% CMC solution) and those published in the open literature. 139

Figure 5.33- Temperature profiles of working fluids ((a) cooling water channel, (b) warm CMC channel) along the PHE section 1 channels, as a function of time, for 2.0% CMC solution (Re=4.02). 141

Figure 5.34- Wall temperature profiles along plate 2 ((a) cooling water side, (b) warm CMC side), as a function of time, for 2.0% CMC solution (Re= 4.02). 142

Figure 5.35- Wall temperatures (Plate 2) and working fluids temperatures at channels inlet and outlet ((a) cooling water side, (b) warm CMC side), as a function of time, for 2.0% CMC solution (Re=4.02). 143

Figure 5.36- Temperature profiles of working fluids ((a) cooling water channel, (b) warm CMC channel) along the PHE section 2 channels, as a function of time, for 2.0% CMC solution. 145

Figure 5.37- Wall temperature profiles along plate 8 ((a) cooling water side, (b) warm CMC side), as a function of time, for 2.0% CMC solution. 146

Figure 5.38- Wall temperatures (Plate 8) and working fluids temperatures at channels inlet and outlet ((a) cooling water side, (b) warm CMC side), as a function of time, for 2.0% CMC solution (Re=4.02). 147

Figure 5.39- CMC solution (1.0%) local Nusselt number variation along channel length (channel 2, section 1), for several Reynolds numbers. 152

Figure 5.40- CMC solution (2.0%) local Nusselt number variation along channel length (channel 2, section 1), for several Reynolds numbers. 152

Figure 5.41- CMC solutions (1.0% and 2.0%) local Nusselt number versus Graetz number (channel 2, section 1)..... 154

Figure 5.42- Comparison of local heat transfer correlations in the thermal entrance region obtained in the present work (1.0% and 2.0% CMC solutions) and those published in the open literature. 155

Figure 5.43- Overall pressure drop versus Reynolds number of different CMC solutions. 157

Figure 5.44- Fanning friction factor versus Reynolds number, comparison of correlations obtained in the present work and those published in the open literature.. 157

Figure 6.1- Time-course of pH reduction during fermentation for both starter culture used in this study. 169

Figure 6.2- Storage and loss moduli as a function of oscillation stress of stirred yoghurt in fermentation tank (13%ST-YF). 171

Figure 6.3- Comparison of the mechanical spectra of the stirred yoghurt in the fermentation tank for all the formulations. 172

Figure 6.4- Complex viscosity (η^*) and tan δ, at 20ºC, for the different stirred yoghurt formulations. 173

Figure 6.5- Effect of the starter culture in the mechanical spectra of the stirred yoghurt produced. 174

Figure 6.6- Storage and loss moduli of stirred yoghurt as function of time (BT- sample collected in the fermentation tank; PHE- sample collected after cooling in the PHE). 176

Figure 6.7- Temperature dependence, stirred yoghurt in the fermentation tank (13%ST-YF). 177

Figure 6.8- Temperature dependence, stirred yoghurt after cooling stage (13%ST-YF). 178

Figure 6.9- PHE ports temperatures (entrance/exit) along experiment time of each fluid, in 12%TS stirred yoghurt / water experiment (Re_{YOG}=1.10). 180

Figure 6.10- Thermal correlation for the mean convective heat transfer coefficient of the stirred yoghurt, as a function of the Reynolds number, for all the formulations tested. 183

Figure 6.11- Comparison among obtained and published thermal correlations, for non-Newtonian fluids. 185

Figure 6.12- Temperature profiles of working fluids ((a) cooling water channel, (b) warm stirred yoghurt) along the PHE section 1 channels, as a function of time, for 12% TS-YF stirred yoghurt (Re=1.10). 188

Figure 6.13- Wall temperature profiles along plate 2 ((a) cooling water side, (b) warm stirred yoghurt), as a function of time, for 12%TS-YF stirred yoghurt (Re=1.10). 189

Figure 6.14- Wall temperatures (Plate 2) and working fluids temperatures at channels inlet and outlet ((a) cooling water side, (b) warm stirred yoghurt), as a function of time, for 12%TS-YF stirred yoghurt (Re=1.10). 190

Figure 6.15- Temperature profiles of working fluids ((a) cooling water channel, (b) warm stirred yoghurt channel) along the PHE section 2 channels, as a function of time, for 12%TS-YF stirred yoghurt (Re=1.10). 192

Figure 6.16- Wall temperature profiles along plate 8 ((a) cooling water side, (b) warm stirred yoghurt side), as a function of time, for 12%TS-YF stirred yoghurt (Re=1.10). 193

Figure 6.17- Wall temperatures (Plate 8) and working fluids temperatures at channels inlets ((a) cooling water side, (b) warm stirred yoghurt side), as a function of time, for 12%TS-YF stirred yoghurt (Re=1.10). 194

Figure 6.18- Working fluids temperatures along channels 1 and 2 corrugated zone, for different times ((a) cooling water channel, (b) warm stirred yoghurt channel), for 12%TS-YF stirred yoghurt (Re=1.10). 195

Figure 6.19- Working fluids temperatures along channels 7 and 8 corrugated zone, for different times ((a) cooling water channel, (b) warm stirred yoghurt channel), for 12%TS-YF stirred yoghurt (Re=1.10). 196

Figure 6.20- Stirred yoghurt (12%TS-YF) local Nusselt number variation along channel length (channel 8, section 2), for several Reynolds numbers. 202

Figure 6.21- Stirred yoghurt (13%TS-YC) local Nusselt number variation along channel length (channel 8, section 2), for several Reynolds numbers. 202

Figure 6.22- Stirred yoghurt (12%TS-YF and 13%TS-YC) local Nusselt number versus Graetz number (channel 8, section 2). 204

Figure 6.23- Comparison of local heat transfer correlations in the thermal entrance region obtained in the present work (12%TS-YF and 13%TS-YC stirred yoghurt) and published in the open literature. 205

Figure 6.24- Computed average Nusselt number as a function of Graetz number and activation energy (E), for constant wall temperature boundary condition, for parallel flat plates. Comparison with empirical correlations obtained: a) 12%TS-YF and b) 13%TS-YC stirred yoghurt. 207

Figure 6.25- Overall pressure drop versus generalised Reynolds number of different stirred yoghurt formulations. 208

Figure 6.26- Fanning friction factor versus generalised Reynolds number, comparison of correlations obtained in the present work and those published in the open literature. 209

Figure 6.27- Mechanical spectrum of yoghurt coagulum in fermentation tank (13%ST-YF). 211

Figure 6.28- Comparison of mechanical spectra stirred yoghurt in fermentation tank and after cooling in the PHE at a shear rate (13%ST-YF). 212

Figure 6.29- Comparison of mechanical spectra of the stirred yoghurt after cooling stage at different shear rates (13%ST-YF). 213

Figure 6.30- Microstructure and storage and loss moduli of stirred yoghurt (with 12% total solids) in the fermentation tank (ST), after cooling stage in a PHE at different shear rates: PHE1 (γ=94 s^{-1}) and PHE 2 (γ=158 s^{-1}). 214

Figure 6.31- Microstructure and storage and loss moduli of stirred yoghurt (13% total solids with 1% HP50) in the fermentation tank (ST), after cooling stage in a PHE at different shear rates: PHE1 (γ=113 s^{-1}) and PHE 2 (γ=221 s^{-1}). 215

Figure 6.32- Comparison of mechanical spectra of the cooled stirred yoghurt and after an incubation stage post-cooling (13%ST-YF). 216

In the annexes

Figure A.1- Temperature profiles during a heat transfer experiment (in-line reading). 241

LIST OF TABLES

In the main text

Table 2.1- Main geometrical characteristics of the chevron plates 18

Table 3.1- Dimensions and technical data of the plate heat exchanger (Tetra Pak Processing Components AB, 2000)..... 26

Table 3.2- Design of Experiments for yoghurt formulation screening..... 32

Table 5.1- Reynolds number and Prandtl number ranges of CMC solutions and cooling water, for each concentration used. 102

Table 5.2- Average values of heat transfer rate transferred to cooling water (Q_{cw}), heat transfer rate transferred from CMC solution (Q_{CMC}) and Reynolds numbers of 0.25% CMC solution (Re_{CMC}), for each experiment. 115

Table 5.3- Statistical parameters obtained by nonlinear regression analysis. 116

Table 5.4- Average values of heat transfer rate transferred to cooling water (Q_{cw}), heat transfer rate transferred from CMC solution (Q_{CMC}) and Reynolds numbers of CMC solution (Re_{CMC}), for each experiment at different % CMC solution..... 121

Table 5.5- Statistical parameters obtained by nonlinear regression analysis of 1.0% CMC experimental data..... 122

Table 5.6- Statistical parameters obtained by nonlinear regression analysis of 2.0% CMC experimental data..... 123

Table 5.7- Average values of and local overall heat transfer coefficients (U_{ij}) and local Reynolds number (Re_{ij}) of 0.25% CMC solution for the four sub-sections analysed in section 1, for each experiment..... 135

Table 5.8- Statistical parameter obtained by nonlinear regression analysis, for the four sub-sections analysed in section 1, for 0.25% CMC solution. 135

Table 5.9- Local thermal correlation as a function of channel length, for several local Reynolds numbers of 0.25% CMC solution, in channel 2. 137

Table 5.10- Statistical parameters obtained by nonlinear regression analysis for channel 2 (section 1). 138

Table 5.11- Average values of and local overall heat transfer coefficients (U_{ij}) and local Reynolds number (Re_{ij}) of 1.0% and 2.0% CMC solutions for the four sub-sections analysed in section 1, for each experiment. 148

Table 5.12- Statistical parameter obtained by nonlinear regression analysis, for the four sub-sections analysed in section 1, for 1.0% CMC solution. 149

Table 5.13- Statistical parameter obtained by nonlinear regression analysis, for the four sub-sections analysed in section 1, for 2.0% CMC solution. 150

Table 5.14- Local thermal correlation as a function of channel length, for several local Reynolds numbers of both 1.0% and 2.0% CMC solution, in channel 2. 153

Table 5.15- Statistical parameters obtained by nonlinear regression analysis for channel 2 (section 1). 154

Table 6.1- Stirred yoghurt formulations used in heat transfer experiments 164

Table 6.2- Flow rates ranges of stirred yoghurt and cooling water, for each yoghurt formulation tested. 167

Table 6.3- Reynolds number and Prandtl number ranges of stirred yoghurt and cooling water, for each yoghurt formulation tested. 167

Table 6.4- Yoghurt production conditions, pH of milk before innoculation, fermentation temperature and pH variation (mean values). 168

Table 6.5- Composition parameters of stirred yoghurt for each formulation tested (mean values). 170

Table 6.6- Physical and rheological parameter of stirred yoghurt, for each formulation (mean values). 175

Table 6.7- Energy activation values, at constant oscillation stress, stirred yoghurt with 12% and 13% total solids content (TS%). 179

Table 6.8- Average values of heat transfer rate transferred to cooling water (Q_{cw}), heat transfer rate transferred from stirred yoghurt (Q_{yog}) and generalised Reynolds numbers of stirred yoghurt (Re_{yog}), for each yoghurt formulation tested. 182

Table 6.9- Statistical parameters obtained by nonlinear regression analysis of stirred yoghurt experimental data, for all formulations tested. 184

Table 6.10- Average values of and local overall heat transfer coefficients (U_{ij}) and local Reynolds number (Re_{ij}) of 12% TS-YF stirred yoghurt for the four sub-sections analysed in section 2, for each experiment. 197

Table 6.11- Statistical parameter obtained by nonlinear regression analysis, for the four sub-sections analysed in section 2, for 12%TS-YF stirred yoghurt..... 198

Table 6.12- Average values of and local overall heat transfer coefficients (U_{ij}) and local Reynolds number (Re_{ij}) of 13% TS-YC stirred yoghurt for the four sub-sections analysed in section 2, for each experiment. 199

Table 6.13- Statistical parameter obtained by nonlinear regression analysis, for the four sub-sections analysed in section 2, for 13%TS-YC stirred yoghurt. 200

Table 6.14- Local thermal correlation as a function of channel length, for several local Reynolds numbers of both stirred yoghurts 12%TS-YF and 13%TS-YC, in channel 8. 203

Table 6.15- Statistical parameters obtained by nonlinear regression analysis for channel 8 (section 2). 204

In the annexes

Table A.1- Average values of the mass flow rate, Reynolds (Re) and Prandtl (Pr) numbers of the cold and hot water and of the overall heat transfer coefficients (U), for each water/ water heat transfer experiment. 242

Table A.2- Average values of the overall heat transfer coefficients (U), mean convective heat coefficients of cooling water (hcw) and mean convective heat coefficients of hot water (hhw) for each water/ water heat transfer experiment. 243

Table A.3- Average values of the local Nusselt number (Nu_L) of cooling water along the channel length (x_L) as a function of local Reynolds number, for section 1. 244

Table A.4- Average values of the local Nusselt number (Nu_L) of cooling water along the channel length (x_L) as a function of local Reynolds number, for section 2. 245

Table A.5- Average values of the mass flow rate, Reynolds (*Re*) and Prandtl (*Pr)* numbers of the CMC solutions and cooling water and of the overall heat transfer coefficients (*U*), for each CMC/ water heat transfer experiment. 246

Table A.6- Average values of the local Nusselt number (Nu_L) of 0.25% CMC solution along the channel length (x_L) as a function of local Reynolds number, for section 1. 247

Table A.7- Average values of the local Nusselt number (Nu_L) of 1.0% CMC solution along the channel length (*xL*) as a function of local Reynolds number, for section 1. 247

Table A.8- Average values of the local Nusselt number (Nu_L) of 2.0% CMC solution along the channel length (x_L) as a function of local Reynolds number, for section 1. . 248

Table A.9- Average values of the mass flow rate, Reynolds (*Re*) and Prandtl (*Pr*) numbers of the stirred yoghurt and cooling water and of the overall heat transfer coefficients (*U*), for each stirred yoghurt/ water heat transfer experiment. 249

Table A.10- Average values of the local Nusselt number (Nu_L) of 12%TS-YF stirred yoghurt along the channel length (x_L) as a function of local generalised Reynolds number, for section 2. 250

Table A.11- Average values of the local Nusselt number (Nu_L) of 13%TS-YC stirred yoghurt along the channel length (x_L) as a function of local Reynolds number, for section 2. 251

ACRONYMS

AISI	American Iron and Steel Institute
CMC	Carboxymethyl cellulose
NTU	Number of Transfer Units
PHE	Plate heat exchanger
TS	Total solids
YC	YC380 starter culture
YF	YF-L812 starter culture

NOMENCLATURE

a, b, c, c', d	constant (-)
A_c	channel cross-sectional area (m^2)
A_p	projected area (m^2)
A_t	heat transfer area of the heat exchanger (m^2)
b	distance between plates (m)
C	molar concentration (mol m^{-3})
C_1, C_2	constant (-)
C_p	specific heat of fluids ($Jkg^{-1}K^{-1}$)
D	mass diffusivity (m^2s^{-1})
D_e	equivalent diameter (m)
D_h	hydraulic diameter (m)
E	activation energy ($Jmol^{-1}$)
f	Fanning friction factor (-)
F	correction factor (-)
G´	storage modulus (Pa)
G´´	loss modulus (Pa)
Gz	Graetz number (-)
h	heat transfer coefficient ($Wm^{-2}K^{-1}$)
J	mass flux (kg $m^{-2}s^{-1}$)

K	constant (-)
k_1, k_2	consistency index ($Pa.s^n$)
L	effective length (m)
L_T	length (m)
M	mass flow rate per channel (kgs^{-1})
m_v	volumetric flow rate per channel (m^3s^{-1})
M_v	total volumetric flow rate (m^3s^{-1})
n	flow behaviour index (-)
N_c	number of channels per pass (-)
N_p	total number of plates (-)
Nu	Nusselt number (-)
p_c	wavelength of corrugation (m)
Pr	*Prandtl number (-)*
P_w	wetted perimeter (m)
Q	heat transfer rate (W)
q	heat flux (Wm^{-2})
r	cylindrical coordinate (m)
R	ideal gas constant ($Jmol^{-1}K^{-1}$)
Re	Reynolds number (-)
T	absolute temperature (K)

u	mean velocity (ms^{-1})
U	overall heat transfer coefficient ($Wm^{-2}K^{-1}$)
v	local velocity (ms^{-1})
w	effective width (m)
w_T	width (m)
x_p	plate thickness (m)
x, y, z	spatial coordinates (m)

Greek Symbols

α	thermal diffusivity (m^2s^{-1})
β	corrugation angle (º)
ΔP	pressure drop (Pa)
ΔT_{ml}	mean logarithmic temperature difference (K)
ϕ	surface enlargement factor (-)
$\dot{\gamma}$	shear rate (s^{-1})
η'	dynamic viscosity (Pa.s)
η^*	complex viscosity (Pa.s)
η_{app}	apparent viscosity (Pa.s)
η_f	average fluid viscosity (Pa.s)
η_w	fluid viscosity at the wall temperature (Pa.s)

λ_p	thermal conductivity of the plates ($WK^{-1}m^{-1}$)
ω	angular frequency (rad s^{-1})
ρ	fluid density (kgm^{-3})
τ	shear stress (Pa)
ν	kinematic viscosity (m^2s^{-1})
τ_0	yield stress (Pa)

Subscripts

cw	cold water
g	generalised
i	heat exchanger section identification
in	inlet
hw	hot water
j	heat exchanger sub-section identification
L	local
out	outlet
PHE	plate heat exchanger
wat	cooling water
yog	yoghurt

1. STATE OF THE ART

1.1 The Problematic of Food Fluids in Plate Heat Exchangers

In the chemical and food processing industries, many similarities exist in the way by which the raw materials are modified or processed into the final product, since many of these processes have in common certain fundamental principles or mechanisms and equipment.

In food industry, transport phenomena of food materials are crucial issues in the relationship between the processing of these materials and the quality and safety of the products. Although important, it did not yet draw the attention it deserves in industrial practice (Edwards, 1988; Welti-Chanes, Vergara-Balderas *et al.*, 2005). Material and energy balances have major importance in food industry in the design, control and improvement of control food processing and in the reducing of energy consumption.

Thermal processing of food products is a common operation in the food industry aimed at preserving its quality and preventing spoilage (Corrieu, Noël *et al.*, 1985). During such operations, physical modifications affecting the structure and stability of the final product occur. To reach an appropriate balance between thermal efficiency and properties of the food products, a combined study of heat transfer, product rheology and product texture is needed.

In the case of heat treatment operations, the knowledge of engineering properties, such as density, specific heat and thermal conductivity, as well as of the flow characteristics of food processing fluids is a pre-requisite for the proper design of industrial plants, the reduction of energy consumption, the definition of levels of product quality and control of manufacturing processes.

Heat exchangers are found widely scattered throughout the food process industry, comprising a wide range of equipment that goes under many names, such as boilers, pasteurizers, jacketed pans, freezers, air heaters, etc.

Very frequently, plate heat exchangers (PHE) are used for liquid–liquid heat transfer duties that require uniform and rapid heating or cooling, as is often the case when treating thermally sensitive fluids such as food fluids (Afonso, Hes *et al.*, 2003).

Although the industrial development of plate heat exchangers was considerable in recent decades, particularly in the food industry for viscous food fluids, the published information available for the design of PHE's using real food fluids, such as stirred yoghurt, is somewhat scanty. The design methods are mostly owned by the equipment manufacturers and are suited only for the marketed exchangers (Gut and Pinto, 2003a).

Fermented milk products, such as yoghurt, are subjected to various shear rates during their manufacturing process. Thus, there is a need to optimize the appropriate fluid flow pattern during the different unit operations, whilst taking into account the previous shear history of the fluids (Maingonnat, Muller *et al.*, 2005). Variations in the rheological properties of stirred yoghurt may be due to several factors. These can be related with milk composition and type of starter culture or with processing conditions, such as post-incubation stages (including: stirring, pumping, cooling and packaging).

The present work intends to bring an additional contribution to the existing general knowledge on the field of thermal processing in plate heat exchangers, more precisely by trying to obtain thermal correlations for the determination of the local heat transfer coefficients for stirred yoghurt during cooling in a plate heat exchanger, optimizing the cooling conditions in order to attain the processing conditions that minimize the negative impact on yoghurt texture properties and keep the thermal efficiency at the desired levels (controlling energy consumption).

1.2 Plate Heat Exchangers

Plate heat exchangers have been the focus of interest since the 1930s when they first appeared in the present form. A great deal of technical information has been published in the literature since the 1930s regarding almost all aspects of plate heat exchangers. Nevertheless, much of design data for plate heat exchangers remain proprietary (Mehrabian, 2009).

The first PHE, dated in 1923, used plates of bronze molten bearing a pressure of 2 bar. There are also letters of the patent in a similar equipment in Germany for the year 1878 (Gut, 2003).

Nowadays, plate heat exchangers (PHEs) are extensively used for heating, cooling and heat-regeneration applications in the chemical, food and pharmaceutical industries. This type of exchanger was originally developed for use in hygienic applications such as the pasteurization of liquid food products (Gut, Fernandes *et al.*, 2004). In recent times, the range of applications of this type of exchanger (see Figure 1.1) largely expanded due to the continual design and construction improvements.

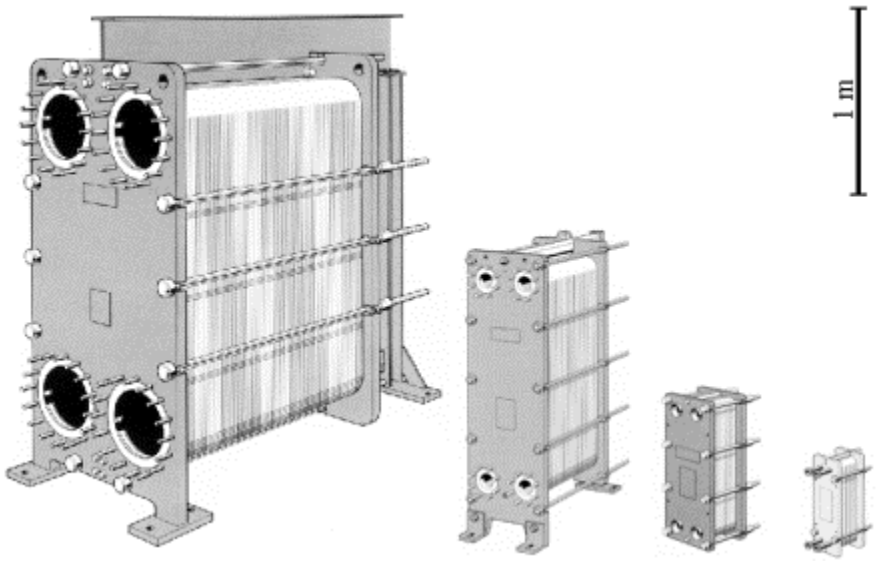


Figure 1.1- Examples of plate heat exchangers.

In the last 20 years they have also been used for two-phase heat transfer, particularly as evaporators and condensers in chillers and heat pumps (Longo, Gasparella *et al.*, 2004).

1.2.1 Plate Heat Exchanger – Basic Construction

The plate-and-frame or gasketed plate heat exchanger (PHE) consists of a number of thin rectangular metal plates sealed around the edges by gaskets and held together in a frame (Shah, Sekuli *et al.*, 2003) as shown in Figure 1.2. The frame usually has a fixed end cover (headpiece) fitted with connecting ports and a movable end cover (pressure plate, follower, or tailpiece). In the frame, the plates are suspended from an upper carrying bar and guided by a bottom carrying bar to ensure proper alignment. The plate

pack with fixed and movable end covers is clamped together by long bolts, thus compressing the gaskets and forming a seal (Kakaç and Liu, 2002; Shah *et al.*, 2003).

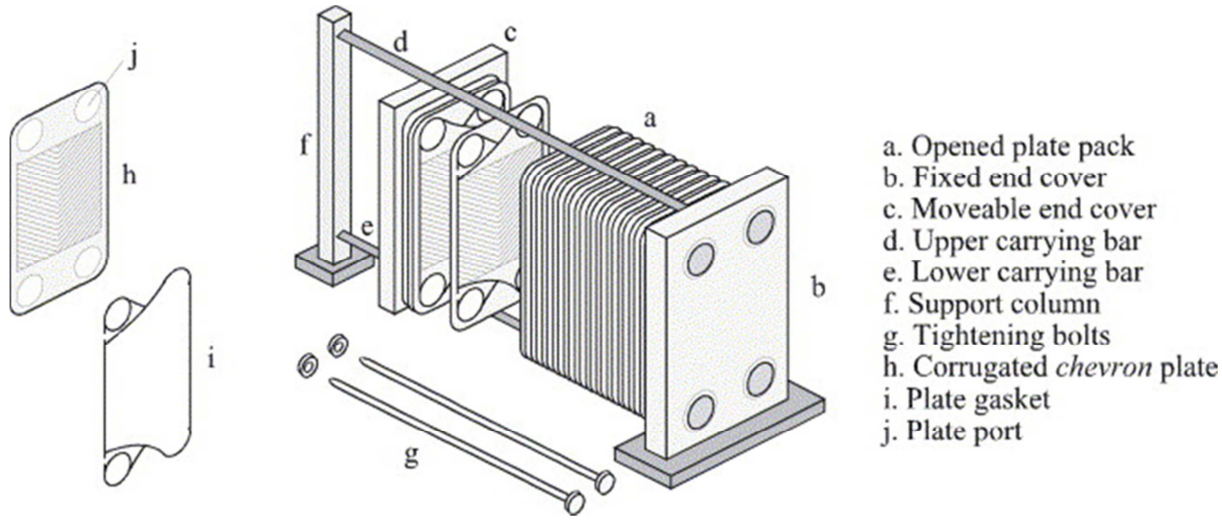


Figure 1.2- Structure of a typical gasketed plate heat exchanger with chevron plates (Gut *et al.*, 2004).

The gaskets on the corners of the plates form a series of parallel flow channels, where the fluids flow alternately and exchange heat through the thin metal plates (see Figure 1.3). Alternate plate are assembled such that the corrugations on successive plates contact or cross each other to provide mechanical support to the plate pack through a large number of contact points. The resulting flow passages are thin, highly interrupted, and tortuous, and enhance the heat transfer rate and decrease fouling resistance by increasing the shear stress, producing secondary flow, and increasing the level of turbulence (Shah *et al.*, 2003).

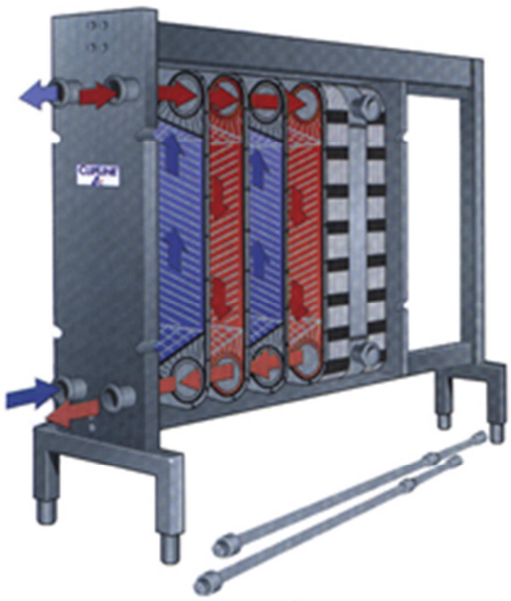


Figure 1.3- Flow pattern in a plate heat exchanger.

The number of plates, their perforation, the type and position of the gaskets and the location of the inlet and outlet connections at the covers characterize the PHE configuration, which affects the flow distribution inside the plate pack. The flow arrangement can be parallel, series or any of their various possible combinations (Kakaç and Liu, 2002; Gut and Pinto, 2003a).

Continuing improvements were introduced as the development of the chevron plates trned PHEs turned into more compact and efficient heat exchangers, so that they became an alternative to the traditional of Shell- and-tubes heat exchanger.

The most common plate materials are stainless steel (AISI 304 or 316) but other ductile materials such as titanium, Incoloy 825, Inconel 625, and Hastelloy C-276 are also available (Shah and Sekulic, 2003).

The corrugations also improve the rigidity of the plates and form the desired plate spacing, avoiding plate curvature (see Figure 1.4.).

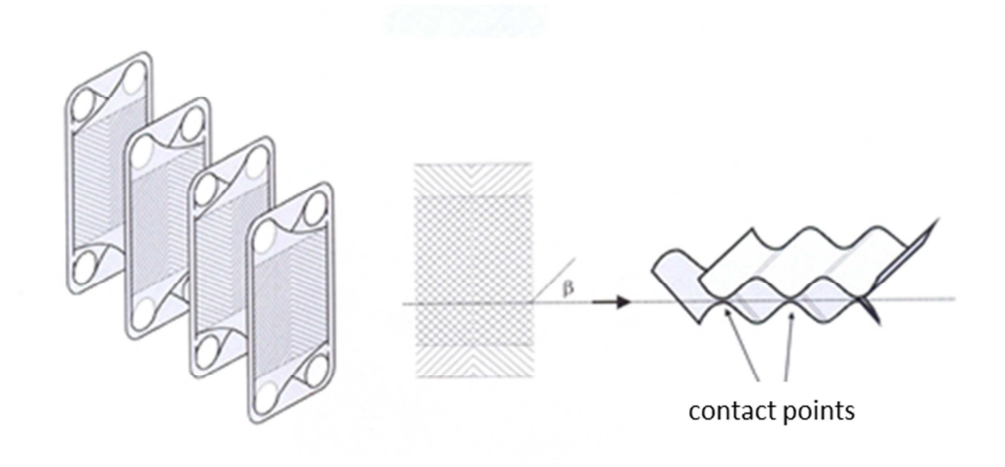


Figure 1.4- Alignment of chevron plates and contact points formation.

Typical plate geometries (corrugated patterns) are shown in Figure 1.5 and over 60 different patterns have been developed worldwide (Shah *et al.*, 2003).

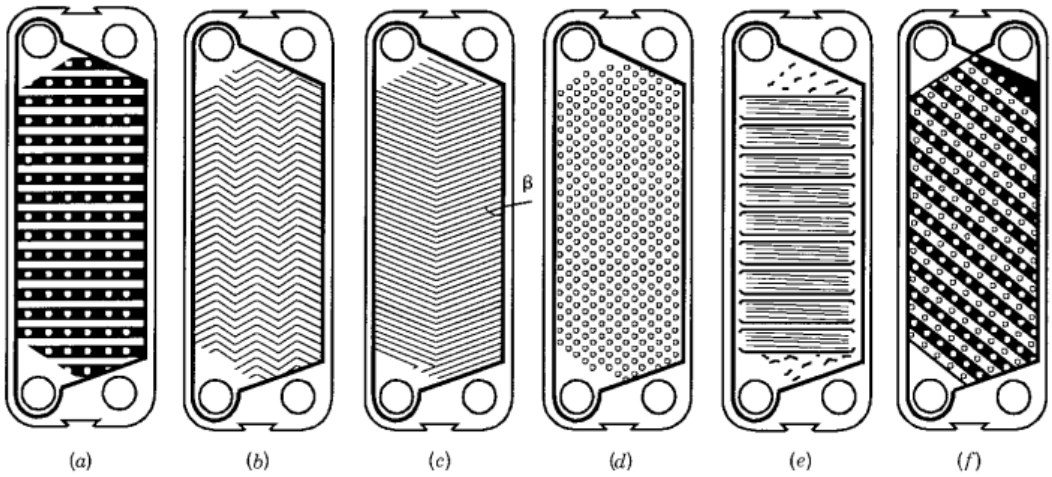


Figure 1.5- Plate patterns: (a) washboard; (b) zigzag; (c) chevron or herringbone; (d) protrusions and depressions; (e) washboard with secondary corrugations; (f) oblique washboard (Shah *et al.*, 2003).

The type of corrugation and the corrugation angle have a great influence in the hydraulic performance of the equipment. The corrugations increase the turbulence in the fluid flow and reduced the value of critical Reynolds number (transition for the

turbulent regime for values between 10 and 400, whereas for a smooth pipe of circular section the transition happens in nearby Reynolds to 2100 (Gut, 2003).

High corrugation angles (β) are related to higher turbulence in fluid flow resulting in the increase of the heat transfer and the pressure drop. Different assemblies can be done by alternating plates with corrugation angles of 30º and 60º resulting in an intermediate solution in order to obtain a better thermal duties with less heat transfer area as possible (Kakaç and Liu, 2002).

1.2.2 Flow arrangements

A large number of flow arrangements are possible in a plate heat exchanger (see Figure 1.6), depending on the heat transfer duty requirements, available pressure drops, minimum and maximum velocities allowed, and the flow rate ratio of the two fluid streams (Gut, 2003; Shah *et al.*, 2003). One of the most common flow arrangements in a PHE is a 1-pass–1-pass U configuration (Figure 1.6a), since this design allows all fluid ports to be located on the fixed end cover, permitting easy disassembly and cleaning of a PHE without disconnecting any piping . In multipass arrangement, the ports and fluid connections are located on both fixed and movable end covers.

A multipass arrangement is generally used when the flow rates are considerably different or when one would like to use up the available pressure drop by multipassing and hence getting a higher heat transfer coefficient (Gut, 2003; Shah *et al.*, 2003).

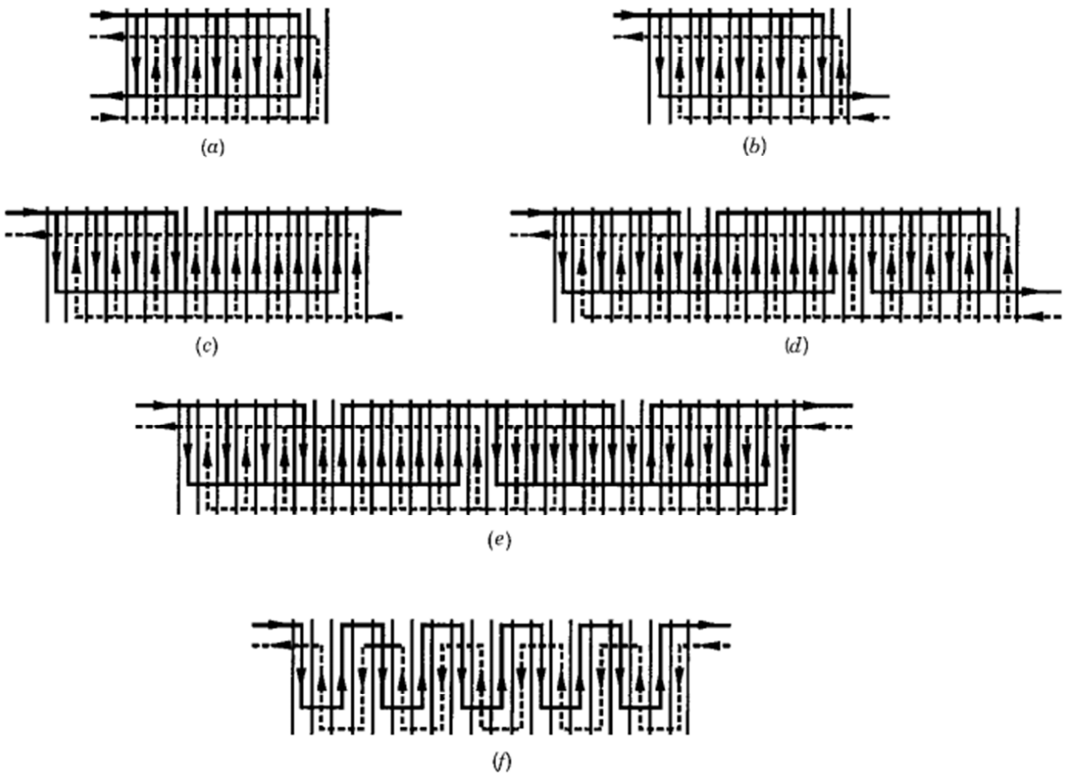


Figure 1.6- Single- and multipass plate heat exchanger arrangements. Looped or single-pass arrangements: (a) U-arrangement; (b) Z-arrangement. Multipass arrangements: (c) 2 pass – 1 pass, (d) 3 pass – 1 pass, (e) 4 pass – 2 pass, and (f) series flow (Shah *et al.*, 2003).

1.2.3 Advantages and Limitations

The main advantages of plate heat exchangers are as follows (Raju and Bansal, 1986; Hewitt, Shires *et al.*, 1994a; Kakaç and Liu, 2002; Gut, 2003):

- *High efficiencies and NTU:* PHEs display high heat transfer coefficients and can work in pure countercurrent arrangement, allowing to reach very small temperature differences concerning heat recovery processes. Very high heat transfer coefficients are achieved due to the breakup/ separation and reattachment of boundary layers, swirl or vortex flow generation, and small hydraulic diameter flow passages (Shah *et al.*, 2003).
- *Good temperature control*: temperature distribution is more uniform in PHEs, without stagnant or overheated zones which is an advantage for heat-sensitive products.

- *Flexibility*: the heat transfer surface area can readily be changed or rearranged for a different task or for anticipated changing loads, through the flexibility of plate size, corrugation patterns, and pass arrangements. PHEs with joints enable to add more plates to the heat exchanger, increasing the heat transfer area.
- *Cleaning and Maintenance*: PHEs can easily be taken apart into their individual components for cleaning, inspection and maintenance.
- *Compactness*: Because of high heat transfer coefficients, reduced fouling, the absence of bypass and leakage streams, and pure counterflow arrangements, the surface area required for a plate exchanger is one-half to one-third that of a shell-and-tube exchanger for a given heat duty.
- *Reduced cost*: compactness, high thermal efficiencies and operating conditions are features that result in reduced processing costs, overall volume and space requirement for the exchanger.
- *Reduced fouling*: High shear rates and shear stresses, secondary flow, high turbulence, and mixing due to plate corrugation patterns reduce fouling to about 10 to 25% of that of a shell-and-tube exchanger, enhancing heat transfer.

Some inherent limitations of the plate heat exchangers are caused by plates and gaskets as follows (Raju and Bansal, 1986; Hewitt *et al.*, 1994a; Kakaç and Liu, 2002; Gut, 2003):

- *Pressure limitation*: the plate exchanger is capable of handling up to a maximum pressure of 16 bar. In case of the welded PHEs this pressure can reach values of 21 bar. In addition, the application is also limited for services with reduced pressure drop (<5 kPa).
- *High pressure drop*: pressure drop in a plate exchanger is very high compared to that of a shell-and-tube exchanger. However, the flow velocities are usually low and plate lengths are ‘‘short,’’ so the resulting pressure drops are generally acceptable. High pressure drop increases the pumping costs.
- *Gaskets*: considering the diversity of gaskets types, their use is limited by the temperature of operation value up to a maximum of 260 ºC. In addition, the utilization of the gaskets also is incompatible with some fluids, namely corrosive and very inflammable fluids (due to leakage risk). Because of the long gasket periphery, PHEs are not suited for high-vacuum or high pressure applications.

- *PHEs are not suitable for*: for erosive duties or for fluids containing fibrous materials; suspensions can be handled but to avoid clogging, the largest suspended particle should be at most one-third the size of the average channel gap; extremely viscous fluids lead to flow maldistribution problems, especially on cooling; lower-density gas-to-gas applications.

1.2.4 Experimental and numerical studies on plate heat exchanger

Several studies have been published focusing on heat transfer in plate heat exchanger using non-food fluids viscous Newtonian and non-Newtonian, mainly pseudoplastic fluids (Bassiouny and Martin, 1984a; Bassiouny and Martin, 1984b; Leuliet, Maingonnat *et al.*, 1987; Leuliet, Maingonnat *et al.*, 1990a; Rene, Leuliet *et al.*, 1991b; Delplace, 1995; Kho and Müller-Steinhagen, 1999; Muley, Manglik *et al.*, 1999; Afonso *et al.*, 2003). For such fluids, the performances of plate heat exchangers both from a thermal and hydraulic viewpoint have been studied by several authors taking into account several aspects such as hydraulic diameter (Leuliet *et al.*, 1990a); pressure drop ((Leuliet *et al.*, 1987); flow distribution and arrangement type (Bassiouny and Martin, 1984a; Bassiouny and Martin, 1984b; Heggs, Sandham *et al.*, 1997; Kho and Müller-Steinhagen, 1999; Thonon, Grandgeorge *et al.*, 1999) and plate type (Rene *et al.*, 1991b).

The thermal–hydraulic model of the PHE relies on correlations for the evaluation of the convective heat transfer coefficient and the friction factor for the flow inside the channels for any given plate surface type and geometry, several studies having been conducted in order to gather reliable information for the thermal model. These studies comprised numerical simulation (Croce and D'Agaro, 2002; Gut and Pinto, 2003a; Fernandes, Dias *et al.*, 2005b; Fernandes, Dias *et al.*, 2007), experimental investigation (Bobbili, Sunden *et al.*, 2006; Li, Meng *et al.*, 2010) and both (Gut and Pinto, 2003b; Gut *et al.*, 2004; Carezzato, Alcantara *et al.*, 2007) .

1.3 Transport Phenomena in Food Processing

The three fundamental transport phennomena involved in some way in each process are: momentum, heat and mass transfer. The basic mechanisms are the same whether the phases are gas or liquid (Coulson, Richardson *et al.*, 1999) and some are also common to solids..

The basic laws governing the flux of momentum, heat and mass transport due to molecular motion or vibration are, respectively, Newton´s Law (equation 1.1), Fourier´s Law (equation 1.2) and Fick´s Law (equation 1.3) which have the form:

$$\tau = \frac{\eta}{\rho}\frac{d}{dz}(\rho u) = \upsilon\frac{d}{dz}(\rho u) \tag{1.1}$$

$$q = -\frac{\lambda}{\rho C_p}\frac{d}{dz}\left(\rho C_p T\right) = -\alpha\frac{d}{dz}\left(\rho C_p T\right) \tag{1.2}$$

$$J_i = -D\frac{dC}{dz} \tag{1.3}$$

All three processes are quite different at a molecular level, though, there are certain analogies between them. In effect, kinematic viscosity (μ), thermal diffusivity (α) and diffusion (D) have the same dimensions (L^2/t) (Welti-Chanes *et al.*, 2005) and they can be related by theoretical and/or semi-empirical expressions.

1.3.1 *Momentum* transport

Momentum transfer is present in several processes of the food processing involving fluid flow and comprises motion of molecules (or groups of molecules). On the other hand, foods are complex systems, frequently with non-Newtonian behaviour and subjected to several conditions.

Among the situations in which momentum transfer phenomena are important, we can emphasize: fluid transport/motion, including several unit operations such as mixing, fluidization, pneumatic transport (Welti-Chanes *et al.*, 2005).

A better understanding of the phenomenon is intended in areas comprising the evaluation of the behaviour of food systems in different processes and the quantification of power requirements in the design of pipelines, mixing or different separation processes.

1.3.2 Heat Transfer

Knowledge of heat transfer and the parameters that govern it is essential for understanding food processing. In most heat transfer operations in food processing, particularly continuous thermal processing of fluid foods, the governing heat transfer mode is convection.

Operations involving heating and cooling of foods are performed in order to accomplish the reduction of the microbial population, enzymes inactivation and the modification of the functionality of certain food components.

The temperature gradient is the driving force in heat transfer processes, and several models have been developed to describe heat transfer behaviour in different systems under different conditions, taking into account the transfer mechanism involved (conduction, convection and/or radiation) (Cronin, Caro-Corrales *et al.*, 2010).

Besides the physical state, other thermo-physical properties such as form, size, structure, thermal conductivity, specific heat, density and viscosity, are of major importance in the thermal behaviour of a system

The study of heat transfer in food engineering involves more than one mode of heat transfer simultaneously, and frequently some of the physical characteristics of food, such as density, structure or viscosity, change as heat modifies the chemical structure, affecting its thermal behaviour.

1.3.3 Rheological properties and their relation to food processing

The importance of rheological properties in several unit operations has been treated in studies in which pipeline transport, mixing, pumping, mechanical separations, heating, cooling, evaporation, drying, fermentation, etc. depend on the knowledge of rheological properties of the foods handled in these processes (Sesták, Zitný *et al.*, 1983; Khalaf and Sastry, 1996; Anema and Klostermeyer, 1997; Buffo, Reineccius *et al.*, 2002; Chakrabandhu and Singh, 2005; Lee and Lucey, 2006; Baixauli, Sanz *et al.*, 2007; Anema, 2008; Chen, Kang *et al.*, 2008; Wang, Wang *et al.*, 2009; Wang and Hirai, 2011).

Several works combine the concepts of rheology and the improvement of design of equipment and processes (Afonso *et al.*, 2003; Fernandes, Dias *et al.*, 2006; Wang and

Hirai, 2011) and the design of new food products and processes (Chen and Dickinson, 1998; Buffo and Reineccius, 2002; Abu-Jdayil, 2003; Chen *et al.*, 2008)

1.3.4 Thermophysical properties and their relation to food processing

The importance of thermophysical properties in unit operations has been treated in several studies (Schwartzberg, 1976; Reddy and Datta, 1994; Tavman, Tavman *et al.*, 1997; Tavman and Tavman, 1999; Fricke and Becker, 2002; Otero, Guignon *et al.*, 2010), since values of the these food properties are required to perform the heat transfer calculations which are involved in the design of food processing equipment and optimization of operating conditions (Hamdami, Monteau *et al.*, 2004; Kowalczyk, Hartmann *et al.*, 2005; Kresic, Lelas *et al.*, 2008).

1.4 Dairy Products

Dairy products include a diverse group of foods made from milk, including concentrated milk, cream, butter, ice cream, yogurt and fermented milks, cheese, and powdered milk, which are the most commercially known, and other by-products that are less marketable.

Although milk has the appearance of a simple liquid, its structure is very complex and not even fully known. An understanding of the physico-chemical characteristics of this biological fluid is necessary to better understand the changes that occur during processing and the properties of intermediate and finished dairy products

From a physicochemical point of view, milk is a complex solution of salts, lactose, and other hydrophilic minor organic components where whey proteins, casein corpuscular micelles, and fat globules are dispersed (Vélez-Ruiz, Cánovas *et al.*, 1997).

The physical state of the dispersed phase represents two separate colloidal forms: a suspension and an emulsion. Milk constituents that interact in various ways lead to different microstructures and, consequently, develop particular properties and structures, depending on the manufacture process applied to elaborate each dairy product.

1.4.1 Dairy products based on proteins

Milk proteins have the capacity to form a gel consisting of a protein matrix with casein as the main structural element. This matrix may contain additional components such as whey proteins, fat globules, lactic acid bacteria, and other ingredients. The ability to immobilize milk serum or whey in a liquid phase is one of the most important characteristics of the gel matrix (Lucey, Teo *et al.*, 1998).

Casein micelles are one of the most important components of milk that make it possible to formulate a variety of products with very different characteristics, ranging from liquids such as evaporated milk, and "semiliquids" such as yogurt, to "semisolids" such as cheese (Vélez-Ruiz *et al.*, 1997) .

The ability of casein micelles to interact with whey proteins and to aggregate and hydrolyse under the effects of low pH, heat, and the presence of proteolytic enzymes, is the most important property of milk for making dairy products (Vélez-Ruiz *et al.*, 1997; Lucey, Tamehana *et al.*, 1998).

1.4.2 Yoghurt

Stirred yoghurt is a typical non-Newtonian fluid, which is the result of milk acidification by fermentation with lactic acid bacteria, e.g., *Lactobacillus delbrueckii subsp. bulgaricus* and *Streptococcus salivarius* subsp. *thermophilus* (Tamime and Robinson, 1999).

In stirred yoghurt production, milk is inoculated and incubated in a fermentation tank at a suitable temperature, normally 40-43ºC, for approximately 2 ½ - 4 h, and the formed yoghurt gel is subsequently broken during the stirring, cooling and packaging stages.

The influence of factors such as total solids content, type of starter culture, heat treatment and cooling conditions on the rheological properties of stirred yoghurt has been studied by several authors using different rheological methods ((Kalab, Allan-Wojtas *et al.*, 1983; Benezech and Maingonnat, 1993; Benezech and Maingonnat, 1994; Afonso and Maia, 1999; Domagala, Sady *et al.*, 2005; Amatayakul, Halmos *et al.*, 2006; Domagata, Sady *et al.*, 2006; Abbasi, Mousavi *et al.*, 2009; Aguirre-Mandujano,

Lobato-Calleros *et al.*, 2009). In various reports, its pseudoplastic flow behaviour, partial thixotropic and viscoelastic characteristics were identified (Rohm and Kovac, 1994; Rohm and Kovac, 1995; Smyth, Kudryashov *et al.*, 2001; Torre, Tamime *et al.*, 2003; Sodini, Mattas *et al.*, 2006; Sanz, Salvador *et al.*, 2008; Raudsepp, Feindel *et al.*, 2010) .

2. ROADMAP FOR THE THESIS

The work presented in this thesis started as part of a National project called DOPHE – Design and operating conditions optimisation of plate heat exchangers for foodstuff funded by Fundação para a Ciência e Tecnologia (FCT). This project was based on heat gathering reliable information to predict heat transfer rates of stirred yoghurt during the cooling process in plate heat exchangers. In order to do so, an experimental investigation (that takes into account the non-Newtonian behaviour of the stirred yoghurt) was conducted in order to obtain a correlation for the determination of convective heat transfer coefficients of stirred yoghurt in a plate heat exchanger.

The first experimental set-up revealed some technical deficiencies, namely, insufficient thermal isolation, impossibility of being scored and instrumented, with significant difficult to carry out experimental work in order to obtain local heat transfer coefficients of viscous food fluids. This was mainly due to the small dimension of the first plate heat exchanger used, a Pacetti RS22, with a plate length of 265 mm and a heat transfer area of 0.015 m^2. Therefore, a completely experimental set-up was assembled comprising a new plate heat exchanger, a CLIP 6-RM with chevron plate provided by Tetra Pak Processing Components AB (Sweden). The main geometrical characteristics of the chevron plates of the new plate heat exchanger are shown in table 2.1.

In the new installation besides the replacement of the previous plate heat exchanger, the cooling circuit was also modified by introducing a water cooler model Gerês (Friaque, Braga, Portugal). The above mentioned replacements originated deep changes in the initial installation. Further equipment was introduced in yoghurt production set-up, such as a lobe pump model B100 3280 (OMAC, Rubiera, Italy) and a yoghurt stirrer. In Figure 2.1 shows the initial stage of the experimental set-up assembling.

Table 2.1- Main geometrical characteristics of the chevron plates

Material	Stainless steel AISI 316
Plate model	CLIP 6-RM
Area, A (m^2)	0.18
Length, L (m)	0.859
Width, w (m)	0.200
Area enlargement factor, ϕ (-)	1.49
Distance between plates, $b \times 10^{-3}$ (m)	4.06
Thickness, $x_p \times 10^{-3}$ (m)	0.5
Thermal conductivity, k_p ($W\ m^{-1}K^{-1}$)	16.3



Figure 2.1- Experimental set-up in initial stage of assembling.

As the results obtained in the heat transfer experiments for determination of the heat transfer coefficient of transfer of stirred yogurt during the cooling in the experimental installation with the PHE with plates RS22 suggested the existence of a thermal layer

limit problem in the PHE channels, it was decided to install temperature probes in the channel of the new PHE in order to obtain local heat transfer coefficients.

Therefore, temperature probes were placed on the plate for wall temperature readings along the plate and in the channel for fluid temperature readings, located in the middle of the water and yoghurt channels as shown in Figure 2.2.

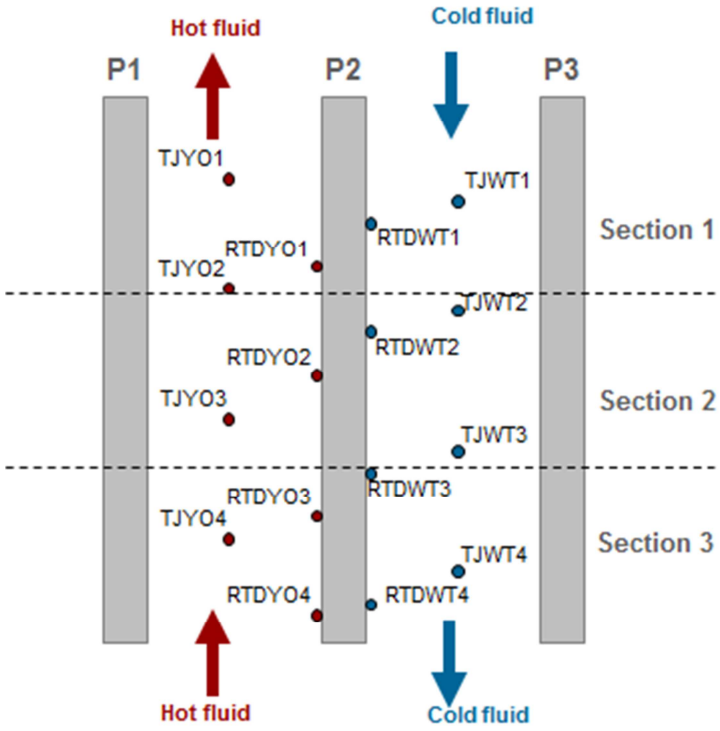


Figure 2.2- Schematic representation of temperature probes location along the PHE channels.

Platinum resistance probes Pt100 (M-FC 420, PT-100 B, Heraeus) were bonded to the stainless steel plate with Loctite and thermocouples type J were fastened underneath the nitrile gasket (see Figure 2.3 for details).

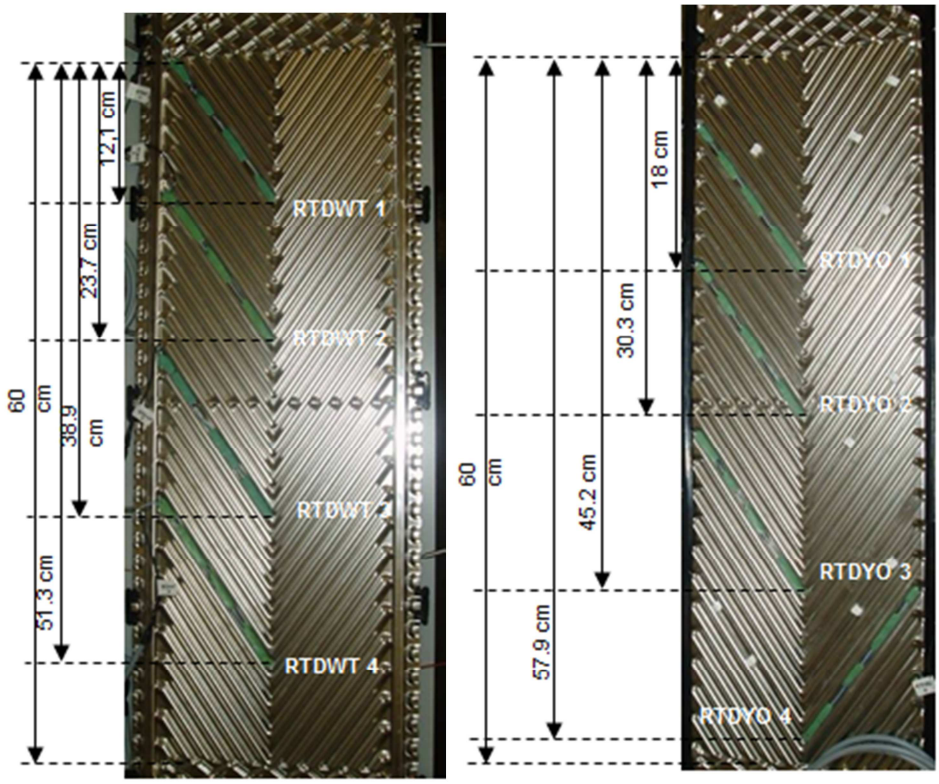


Figure 2.3- Detailed view of temperature probes location along PHE plates.

The interface used in the acquisition of the temperature data contained two modules of 8 channels each one of National Instruments, one of them used for the control of the Pt100 (model FP-RTD-122 16 bit) and other two for the thermocouples (model FP-TC-120 16 bit).

Heat transfer experiments procedures are detailed in Chapter 3 – Materials and Methods sub-section 3.7, and the heat transfer analysis procedures are presented in sub-section 3.8.

In Chapter 4, the empirical correlations obtained for the determination of mean and local heat transfer coefficients of water in a plate heat exchanger are presented. These experiments were carried out using water as working fluid in both cold and hot sides of the plate heat exchanger. The results enhanced the importance of the knowledge of design and operating conditions used in the production of empirical correlations in order to allow a more accurate selection of proper correlations in the analysis of the thermal and hydrodynamic performance of PHEs

In order to accurately analyse the rate and amount of heat transfer involved and its impact on the final product quality, thermal and physical properties of the products being processed must be known. From experimental rheological studies the rheological properties of the selected food fluids (stirred yoghurt and CMC) at different temperatures. This includes not only the final products but also monitoring the rheological changes along the manufacturing process.

The rheological properties of the selected food products, submitted to not only to different processing conditions but also different product formulation, were assessed by instrumental methods. This resulted in the definition of a rheological model for each yoghurt product and yielded information about the effect of the processing conditions on the final quality of the products.

From heat transfer experiments with yoghurt and CMC (Chapters 5 and 6), empirical correlations for average and local convective heat transfer coefficients for the selected food products in PHE were obtained. This allowed defining the thermal efficiency of PHE at different distances from the inlet. The characterisation of the rheological properties of the selected products and their correlation with the operating features of the plate heat exchangers was also obtained from these experiments.

Finally, in Chapter 7 conclusions and suggestions for future work are presented.

3. MATERIALS AND METHODS

3.1 Introduction

This chapter aims to overview all materials and procedures used in this study. The plate heat exchanger and the experimental facility used in the heat transfer experiments are presented,

An industrial plate heat exchanger CLIP Tetra Plex 6-RM (Tetra Pak, Sweden) was incorporated in the experimental facility in order to simulate operating conditions similar to the industrial cooling of stirred yoghurt.

An experimental facility was built for the production of stirred yoghurt, comprising a fermentation section, the cooling and heating sections of working fluids and the PHE with entrance/exit controlled temperatures and two channels with controlled temperatures along the plates and the flowing fluids.

Heat transfer experiments were performed using as working fluids, water, sodium carboxymethylcellulose solutions (with different viscous properties) and stirred yoghurt with different compositions (similar to commercial products).

The study of the influence of several dairy and non-dairy ingredients added to milk for yoghurt production comprised the preparation of several set-style yoghurt batches, using operating conditions similar to the industrial ones.

The methods applied in the characterisation of yoghurt (set and stirred) are divided in three major sections: physicochemical, rheological and microscopic methods.

Calculation procedures and statistical analysis applied in the result treatments are also described.

3.2. Experimental set-up

3.2.1 Main features

The experimental set-up used for determining mean and local heat transfer coefficients of stirred yoghurt during cooling in a plate heat exchanger was designed

and built up on purpose. Heat transfer experiments using other fluids, namely CMC and water, were performed in this facility, only changing the pumping system.

The experimental set-up flow diagram is illustrated in Figure 3.1. It consists, basically, of a 100 L stainless steel AISI 316 fermentation jacketed tank, a water refrigerating unit model Gerês (Friaque, Portugal), a plate heat exchanger CLIP 6-RM with chevron plate (Tetra Pak Processing Components AB, Sweden) and an oil heating unit. The facility comprises two GRUNDFOS UP-20-45 N150 centrifuge pumps in the cooling water circuit and a lobe pump model B100 3280 (OMAC, Italy) in the stirred yoghurt circuit. The total pressure drop was determined experimentally using Fischer & Porter differential pressure transmitters Type F 50 DPF 110-3-C (Sistimetra, Portugal) located at both hot and cold fluid sides of the PHE inlet and outlet, and connected to the AI-FP-110 module of the acquisition data system from National Instruments (NI, Portugal).

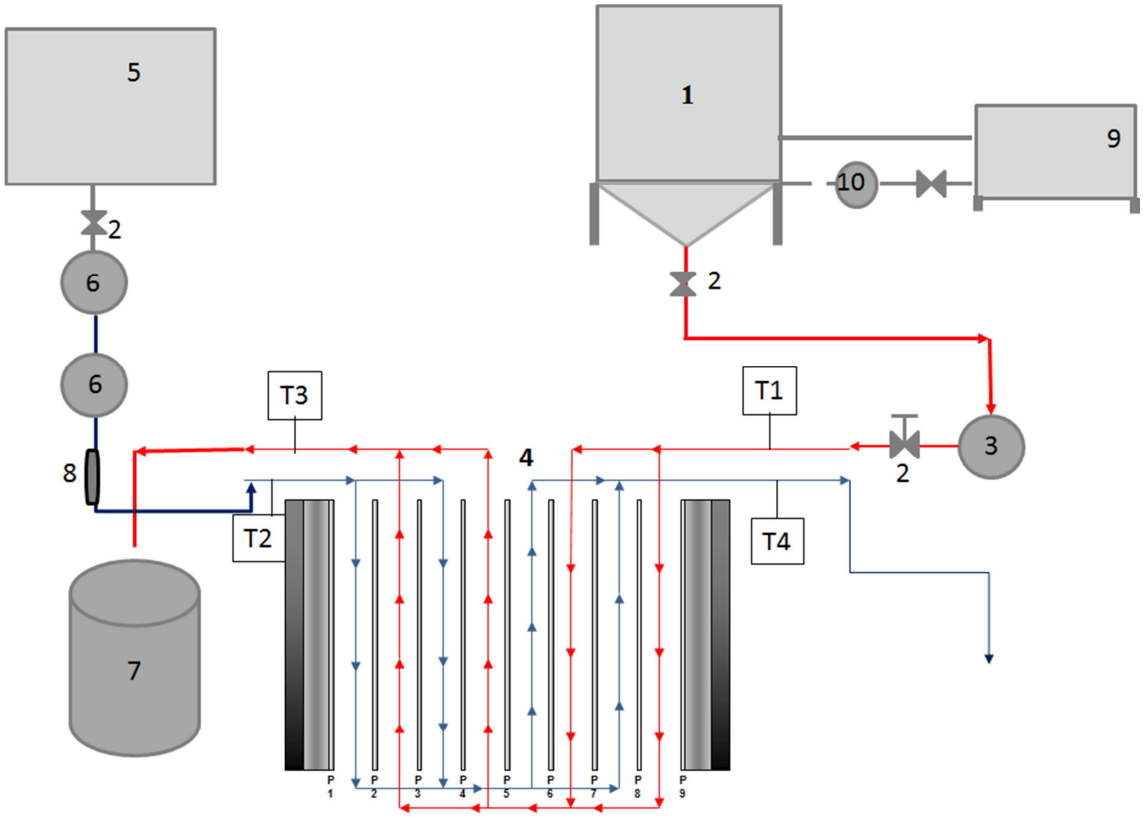


Figure 3.1- Flow diagram of the experimental set-up (1: Fermentation tank; 2: flow regulation valve; 3: lobules pump; 4: plate heat exchanger; 5: water refrigerating unit; 6: centrifuge pump (cooling water); 7: stirred yoghurt storage tank (after cooling); 8: flowmeter; 9:

hot oil tank; 10: oil centrifuge pump; T1, T3: inlet/ outlet tested fluid temperature probes; T2, T4: inlet/ outlet cooling water temperature probes.

Cold and hot fluids flow rates were settled and controlled by mean of a flowmeter and a pump rotation frequency controller, respectively.

The fermentation temperature, oil temperature used in the heating of jacketed tank and temperatures of both hot and cold fluid sides of the PHE inlet and outlet and along the channels were controlled and registered by means of type J thermocouples (Omega Engineering Inc., UK) and platinum resistance probes Pt100 (M-FC 420, PT-100 B, Heraeus, Spain) connected to the multichannel acquisition data modules of National Instrument with a Windows XP compatible FIELPOINT – Measurement operational software. Further details concerning temperature probes position will be presented in next section.

3.2.2 Temperature measurement in the plate heat exchanger channels

Temperature measurement is of major importance for the determination of heat transfer rates, and consequently, in the determination of convective heat transfer coefficients.

The main geometrical characteristics of the plate heat exchanger plates are given in Figure 3.2 and in Table 3.1.

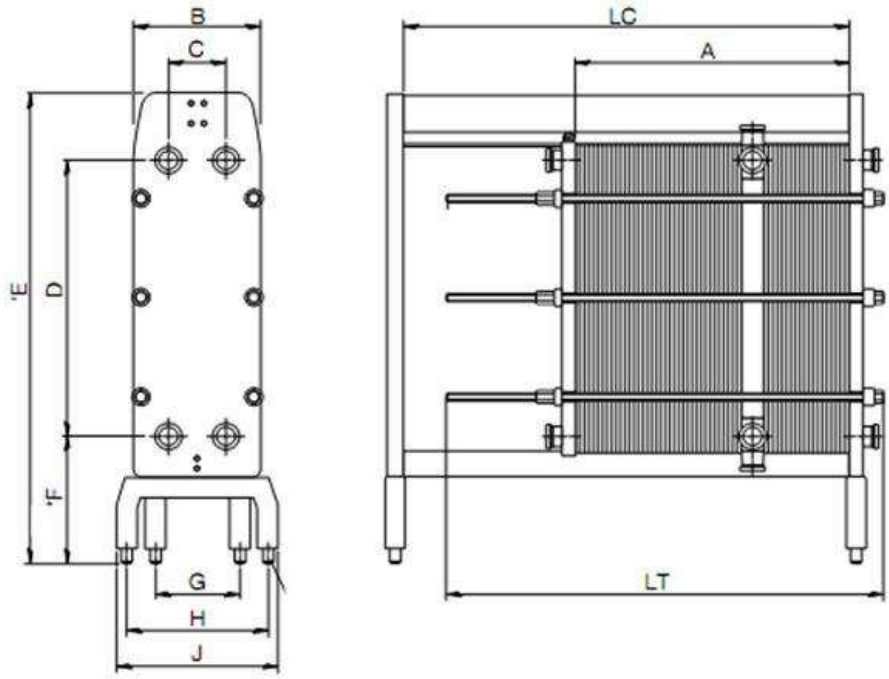


Figure 3.2- Main dimensions of the plate heat exchanger (Tetra Pak Processing Components AB, 2000).

Table 3.1- Dimensions and technical data of the plate heat exchanger (Tetra Pak Processing Components AB, 2000).

Frame		**Plates**	
Measurements (mm)		Plate pattern	Chevron
B	370	Surface, m^2	0.18
C	129	Overall dimensions, mm	1000×250
D	859	Port dimensions, mm	55
E	1420	Thickness, mm	0.5
F	400		
G	240		
H	460		
J	520		
Capacity			
Heating/Cooling, L/h	15000		
Water, L/h	30000		

In order to obtain temperature data for the determination of mean heat transfer coefficients of stirred yoghurt and other working fluids, temperatures of both hot and cold fluid sides of the PHE inlet and outlet were controlled and registered by means of type J thermocouples (Omega Engineering Inc.) positioned 10.0 cm away from the inlet and outlet of the PHE (details in Figure 3.3).

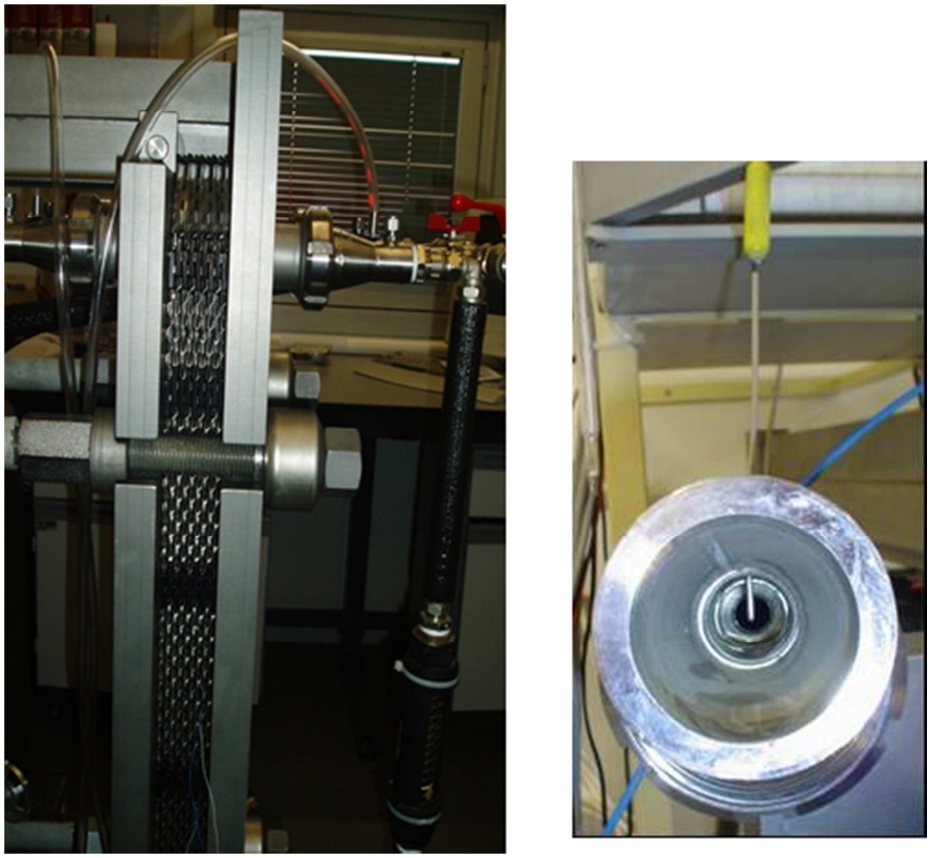


Figure 3.3- Detail of thermocouple positioning in tube connector to PHE.

To attain reliable information to predict local heat transfer rates in PHE channels, two channels of each fluid were adapted with Pt100 probes, bonded to stainless steel plate wall with Loctite epoxide glue (see Figure 3.4a). Due to high fragility of Pt100 resistance probes and high shear stress values in regular operating conditions, it was necessary to protect the temperature probes. Therefore, a loaded epoxy resin for stainless steel (Loctite) was used to cover the Pt100 in order to guarantee probes attachment (Figure 3.4b) and optimal control of wall temperature.

Hot and cold fluids temperatures along the PHE channel were monitored by means of thermocouples type J, with a diameter 1.0 mm and 150 mm length, which were fastened underneath the nitrile gasket and fixed with small fragments of self-adhesive Gore-

Tex®, in order to avoid that the thermocouples drop from the plate wall. This was a time-consumption work that was repeated each time a probe exhibited reading perturbations or the working fluid was changed.

The distribution of Pt100 along the plate wall and the thermocouples in both fluids channels was according to the scheme shown in Figure 3.5. Some fine-tunings were performed during the experimental work in order to improve the system response.



Figure 3.4- Detailed positioning of Pt 100 in a PHE plate: (a) attached probe, (b) final aspect of plate assembling with Pt100 probes and thermocouples.

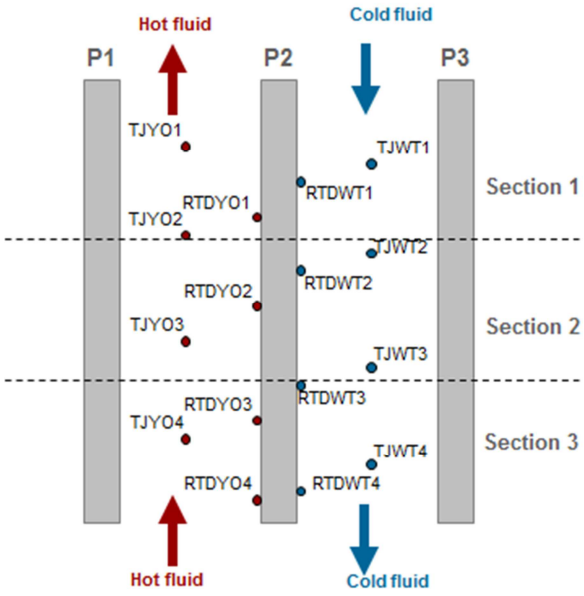


Figure 3.5- Schematic representation of temperature probes location along the PHE channels.

In Figure 3.6, an internal view of the plate heat exchanger is presented, before closing the PHE.



Figure 3.6- Experimental set-up. View of a PHE channel.

3.3 Yoghurt production

3.3.1 Set-style yoghurt production

Low-heat skim milk powder (max. 1.25 % butter fat, min. 34.0 % protein, appro. 50 %) was purchased from VETAGRI Humana S.A. (Cantanhede, Portugal) and used to prepare the several batches of set-style yogurts following the blending presented in table 3.2, in order to obtain different fortified milk compositions. The yoghurt formulations consisted of blending of skim milk powder with one or more of the following ingredients: high protein skim milk powder – HP50 (min. 50 % protein, max. 0.5 % of butter fat, max. 35 % lactose, max. 8.5 % ash) (FORMULAB – Aditivos Alimentares, Lda., Portugal), sodium carboxymethylcellulose WALOCEL CRT 1000 GA (Wolff Cellulosics GmbH & Co, Germany) and sweet whey powder (max. 15 % protein, max. 1.5 % butter fat, min. 60 % lactose, max. 8.8% ash) (FORMULAB – Aditivos Alimentares, Lda., Portugal).

The skim milk powder blends were reconstituted with tap water, preparing 1000 mL of each formulation, as shown in Figure 3.7.



Figure 3.7- Reconstituted milk for set-style yoghurt production, for several milk formulations.

Table 3.2- Design of Experiments for yoghurt formulation screening.

Formulation ID	Starter Culture	MSNF (%)	SMP	SMP HP50 (%)	CMC (%)	Sweet Whey (%)	Total Solids in Yoghurt (%)
F1	YF – L812	12	0	0	0	0	12
F2		12	0	1	0	0	13
F3		12	0	0	0	1	13
F4		12	0	0	1	0	13
F5		12	0	0.5	0.5	0	13
F6		12	0	0.5	0	0.5	13
F7		12	0	0	0.5	0.5	13
F8		12	1	0	0	0	13
F9		12	2	0	0	0	14
F10	YC-380	12	0	0	0	0	12
F11		12	0	1	0	0	13
F12		12	0	0	0	1	13
F13		12	0	0	1	0	13
F14		12	0	0.5	0.5	0	13
F15		12	0	0.5	0	0.5	13
F16		12	0	0	0.5	0.5	13
F17		12	1	0	0	0	13
F18		12	2	0	0	0	14

Table 3.2- Design of Experiments for yoghurt formulation screening. (cont.)

Formulation ID	Starter Culture	MSNF (%)	SMP	SMP HP50 (%)	CMC (%)	Sweet Whey (%)	Total Solids in Yoghurt (%)
F19	YF – L812	12	0	0	0	0	12
F20		12	0.5	0.5	0	0	13
F21		12	0.5	0	0.5	0	13
F22		12	0.5	0	0	0.5	13
F23		12	0	0.33	0.33	0.33	13
F24		12	0.33	0.33	0	0.33	13
F25		12	0.33	0.33	0.33	0	13
F26		12	0.33	0	0.33	0.33	13
F27		12	0.25	0.25	0.25	0.25	13
F28	YC-380	12	0	0	0	0	12
F29		12	0.5	0.5	0	0	13
F30		12	0.5	0	0.5	0	13
F31		12	0.5	0	0	0.5	13
F32		12	0	0.33	0.33	0.33	13
F33		12	0.33	0.33	0	0.33	13
F34		12	0.33	0.33	0.33	0	13
F35		12	0.33	0	0.33	0.33	13
F36		12	0.25	0.25	0.25	0.25	13

Table 3.2- Design of Experiments for yoghurt formulation screening. (cont.)

Formulation ID	Starter Culture	MSNF (%)	SMP	SMP HP50 (%)	CMC (%)	Sweet Whey (%)	Total Solids in Yoghurt (%)
F37	YF – L812	12	0	0	0	0	12
F38		12	0.625	0.125	0.125	0.125	13
F39		12	0.125	0.625	0.125	0.125	13
F40		12	0.125	0.125	0.125	0.625	13
F41		12	0.125	0.125	0.625	0.125	13
F42	YC-380	12	0	0	0	0	12
F43		12	0.625	0.125	0.125	0.125	13
F44		12	0.125	0.625	0.125	0.125	13
F45		12	0.125	0.125	0.125	0.625	13
F46		12	0.125	0.125	0.625	0.125	13

The reconstituted milks were subjected to a heat treatment at 80ºC for 30 minutes, cooled down and allowed to stabilise overnight, at 4ºC. Then, reconstituted milks flasks were placed into water bath at 43ºC for 30 minutes, and inoculated using 30 mL of a starter culture solution containing 25 U/ L. Two starter culture consortiums were used in this study, the freeze-dried DVS YC– 380® and the YF-L812® (CHR Hansen, Promolac, Lda., Portugal). The starter culture solutions were prepared by solubilisation of a pack of freeze-dried DVS starter culture containing 50 U in 2000 mL of sterile distilled water. Inoculated milk was aseptically poured into 100 mL sterile plastic containers (as shown in Figure 3.8) and into 20 mL conical centrifuge tubes and incubated for 4 to 5 hours at 43ºC in incubation chamber, until pH around 4.8 (taking into account the starter cultures growth specifications given by the producer). The fermentation process was monitored in a control cup by measuring pH value each 30 minutes along the fermentation time, and titratable acidity was determined in the beginning and at the end of process.

After incubation, the yoghurt samples were transferred to and kept in a refrigerator at 4ºC for 2 weeks, the latter being the maximum storage time to have all the analyses concluded. Most of analyses were performed in the day after production, except for three analyses: density determination, microstructure and rheological studies.

In microstructure analysis by Cryo-Scanning Electron Microscopy (section 3.6.2.), the yoghurt samples used in the studies had 1-2 days storage time.

Rheological studies (section 3.5.) were conducted one day after production, but due to the huge number of samples it was not possible to perform the analysis in the same day. Afonso and Maia (1999), when studying the influence of storage time on yoghurt samples, observed only small differences on the structure of undisturbed yoghurt coagulum (similar to set yoghurt), due to the increase of consistency.



Figure 3.8- Set-style yoghurt obtained with milk formulation F38.

3.3.2 Stirred yoghurt

Stirred yoghurt, produced in the experimental facility described previously in section 3.2, was used as case-study of non-Newtonian food fluids in heat transfer experiments. The main operating conditions concerning milk fortification, heat treatment and fermentation conditions were maintained in this production scale. The skim milk powder, food ingredients and starter culture were the same as those mentioned in section 3.3.1.

Low-heat skim milk powder was used to prepare the several batches of stirred yoghurt following some blends presented in table 3.2., in order to obtain different fortified milk compositions.

The skim milk powder blends were reconstituted with tap water in four containers of 25 L, preparing 100 L of reconstituted milk subjected to a heat treatment at 80ºC for 30 minutes in autoclave. After heat treatment, milk was transferred to the incubation tank and cooled in the plate heat exchanger until 43ºC. Then, the milk was inoculated using 3000 mL of starter culture and incubated for 4 to 5 hours at 43ºC, until pH around 4.8.

The starter culture was propagated, previously, in skim milk powder (12% w/v) sterilised at 115ºC for 10 minutes. Sterilised milk was cooled until 43ºC, inoculated with 90 mL of a starter culture solution containing 25 U/ L (section 3.3.1.) and

incubated at 42ºC for approximately 4 hours (see Figure 3.9). Starter culture was kept overnight at 4ºC. Prior to inoculation, the starter culture container was placed into a water bath at 43ºC for 30 minutes. The fermentation process was monitored in continuous mode by measuring pH value in the incubation tank.



Figure 3.9- Yoghurt coagulum in the incubation tank of test facility.

When pH reached an approximate value of 4.8, the yoghurt coagulum was disrupted by means of a mechanical stirrer during 5 minutes. In order to ensure that the yoghurt coagulum was completely broken and that whey incorporation was promoted, yoghurt was stirred manually ten times in slow helicoidal movements of a perforated stirrer. After this operation, the stirred yoghurt was circulated through the plate heat exchanger where it was cooled down by the cold water stream, until a temperature of approximately 20ºC was reached (see Figure 3.10).



Figure 3.10- Stirred yoghurt cooling in the PHE of test facility.

Yoghurt samples were collected in different stages of production for microbiological control and physicochemical analyses: yoghurt coagulum, stirred yoghurt in the incubation tank and yoghurt samples after cooling stage in the PHE, for each flow rate tested.

3.3.3 Microbiological control

Two 10 g samples of yoghurt were diluted with 90 mL of sterile 0.1% w/v Ringer solution. After uniform mixing, subsequent serial decimal dilutions were prepared in 9 mL of sterile 0.1% (w/v) Ringer solution. Duplicate plates of each set of dilutions were prepared. These procedures were performed in duplicate when the microbiological control was performed randomly either in set-style yoghurt batches or in stirred yoghurt production.

Enumeration of characteristic microorganisms of yoghurt was carried out using the reference process according to the Portuguese standard NP 1864:1987. In this method 90 mL of sterile Plate Count Agar PCA (OXOID) (121ºC/ 15 minutes) is mixed with 9.9 mL of sterile skim milk 10% total solids (sterilised at 115ºC/ 10 minutes) and 0.1

mL of a solution of 2,3,5-triphenyltetrazolium chloride (wt 2%). For each sample, 1 mL of each dilution was pour-plated in PCA modified medium, in duplicates. Plates were incubated at 43ºC ±1ºC for 48 hours, the number of CFU/ml was determined considering only the plates with a number of colonies between 30 and 300, according to the NP 1864:1987. All colonies were counted, considering their colour and/or size.

According to the NP 1864:1987, ***Streptococcus thermophilus*** colonies exhibit the following characteristics: colonies with 0.1 to 0.2 mm diameter, round or oval shape, regular edges, white with red center, involved by a clear zone. ***Lactobacillus bulgaricus*** colonies are large, 1.0 mm diameter, rhizoid, irregular red edges, involved by whitish blurry zone.

Alternatively, the microbiological control of yoghurt starter culture consortium was performed by pour-plating 1.0 mL of each dilution in Plate Count Skim Milk Agar medium (Merck), sterilised at 121ºC for 15 minutes. Plates were incubated at 35ºC for 24 hours. All colonies were counted, regardless their colour and/or size. Duplicates of each sample were analysed.

3.4 Physicochemical analysis of yoghurt

3.4.1 pH measurements

The pH values of the yogurts were measured at 20°C using a pH meter (HI 8424, HANNA Instruments, USA) after calibrating with fresh pH 4.0 and 7.0 standard buffers.

3.4.2 Dry matter

Dry matter percentage of yoghurt samples was determined according to the Portuguese standard NP 703:1982. The principle of this method is based on moisture evaporation from sample by oven drying and subsequent total dry matter determination by weighing the residue remaining after drying and cooling in desiccator.

For the determination of dry matter content of yoghurt samples, approximately 5.0 g of sample were weighed into an aluminium dish, previously dried at 105ºC for at least

1hour, cooled in a desiccator and tared. The aluminium dishes were placed into oven, preheated to 105ºC, left uncovered samples in oven overnight. Then, the samples were moved to desiccator and allowed to cool for at least 1 hour, and finally weighed. Duplicates of each sample were analysed.

The dry matter (DM) percentage is determined by the following equation:

$$\%\, DM = \frac{weight\ of\ residue weight\ of (\ sample+container)_{dry} - weight\ of\ container}{weight\ of (\ sample+container)_{wet} - weight\ of\ container} \times 100 \quad (3.1)$$

3.4.3 Fat content

The fat content of yoghurt samples was determined by the Gerber method according to the Portuguese standard NP 469:1983. This method is based on the solubilisation of casein and water-insoluble phosphates present in milk by concentrated sulfuric acid. Then, the fat is separated by the addition of amyl alcohol and centrifugation at 65ºC.

Yoghurt samples were previously homogenized with a glass stirrer and maintained at 20ºC. Then, 10.0 mL of Gerber sulphuric acid (density =1.82) were added to the Gerber butyrometer (0-4% Butterfat scale) followed by 11.0 mL of homogenized sample (avoiding the wetting of the neck of the butyrometer) and 1.1 mL of amyl alcohol (density=0.81; furfurol-free). The butyrometer was sealed with a rubber stopper and shaken carefully until the curd dissolves and no white particles could be observed. The butyrometer were placed in the centrifuge specific for Gerber butyrometer with temperature control system and centrifuged at 1100 rpm for 5 minutes at 65ºC. The butyrometer were placed in the centrifuge with the stem (scale) pointing towards the centre of the centrifuge.

The fat content (butterfat percentage) is determined form direct reading of fat column from the lowest point of the meniscus of the interface of the acid-fat to the 0-mark of the scale. Duplicates of each sample were analysed.

3.4.4 Protein content

The total protein content of dairy products is usually determined by Kjeldahl method, dye-binding methods and infrared (IR) and ultraviolet (UV) spectrophotometry.

The main methodologies can be divided into methods that require protein chemical degradation, such as Kjeldhal method, methods for fixation of dyes, colorimetric methods, such as Bradford method, by atomic absorption spectrophotometry in infrared (IR) and ultraviolet (UV) and by fluorescence (Veloso, Teixeira *et al.*, 2001).

In this study two methods were used in order to determine yoghurt samples total protein content: Kjeldhal method and Bradford method.

Kjeldhal method was first published in 1883 by Kjeldahl and is still considered a reference method for determination of nitrogen and protein in food or in routine analysis and calibration of different analytical equipment (Veloso *et al.*, 2001).

Kamizake *et al.* (2003) carried out a comparative study between the Kjeldahl method and several spectrophotometric methods for the determination of total proteins in a range of milk powder samples. These authors concluded that Bradford method showed the best results for the determination of total proteins in all the samples whose results were not statistically different from those obtained for total nitrogen by the Kjeldahl method.

The Bradford method was performed, after comparison of the protein content of several yoghurt samples determined by Kjeldhal method.

Kjeldhal method

Protein content of yoghurt samples was determined by Kjeldhal method according to the Portuguese Standard NP-1986:1991.

Method Principles: total nitrogen content is determined sample digestion by heating in the presence of concentrated sulphuric acid and a catalyst such as copper, selenium, titanium, or mercury (containing potassium sulphate) to speed up the reaction by raising the boiling point. Digestion promotes the conversion of organic nitrogen and other nitrogenous substances (such as nitrates or nitrites) into ammonia and other organic

matter to carbon dioxide and water. In the neutralisation stage, sodium hydroxide is added to digested solution, converting ammonium sulphate into ammonia gas which is distilled and collected in an excess of boric acid solution. Titration is the final stage, consisting in the determination of ammonium ions by titration with standard sulphuric acid.

Procedure: For the determination of total protein content of yoghurt samples, approximately 5.0 g of yoghurt were weighed into a digestion flask, added 3 catalyst tablets (Potassium sulphate / anhydrous Copper sulphate) and 25 mL of sulphuric acid (concentrated, 95-98%). The digestion flasks were placed on preheated burner in Block digestion system KJELDATHERM (Gerhardt GmbH & Co, UK) and heated until white fumes clear bulb of flask. The digestion time varied with sample composition and quantity, though average digestion time was around 4 hours. The digested flaks were cooled and placed in the distillation system VAPODEST 20s (Gerhardt GmbH & Co, UK). Titration flasks were prepared by adding 50 mL of standard solution of boric acid (4%wt) added with 3 to 4 drops methyl blue indicator solution (green-violet). The condenser tip was immersed in of boric acid solution. Titration of ammonia borate was performed with standard sulphuric acid solution (0.1N) to violet endpoint (colour change from green to uncoloured to violet). Duplicates of each sample were analysed.

The total nitrogen content is determined by the following equation:

$$\%\, Nitrogen = \frac{(V_{H_2SO_4} - V_0) \times \frac{N}{2} \times 1.407}{weight\ of\ sample} \times 100 \qquad (3.2)$$

where

V_{H2SO4} - mL standard sulphuric acid (H_2SO_4) needed to titrate sample

V_0 - mL standard sulphuric acid (H_2SO_4) needed to titrate a ammonia free sample (blank sample)

N – Normality of sulphuric acid

1.407 - milliequivalent weight of nitrogen

To determine % protein instead of % nitrogen, the calculated % N is multiplied by a factor. The magnitude of the factor depends on the sample matrix. For milk and dairy products and according to the analytical standard followed, this factor is 6.38.

The total protein content is determined as follows:

$$\%\, Protein = \%Nitrogen \times 6.38 \quad (3.3)$$

Bradford method

The Bradford method of protein determination is based on the binding of a dye, Coomasie Blue G, to the protein. This binding shifts the absorption maximum of the dye from red to blue. The absorbance of the solution is measured at 595 nm and is proportional to protein concentration when compared to a standard curve (Kruger, 2002).

Procedure: The reagent was prepared by dissolving 100 mg of Coomassie Blue G250 (BIO-RAD, Portugal) in 50 mL of 95% ethanol. The solution was then mixed with 100 mL of 85% phosphoric acid and made up to 1 L with distilled water. The reagent was filtered through Whatman no. 1 filter paper and then stored in an amber bottle at room temperature. Prior to the analysis of yoghurt samples, a protein calibration curve was prepared. Thus, a bovine serum albumin (BSA) standard at concentration of 10mg/mL prepared in distilled water was used as a stock solution. For the calibration curve, protein standards solutions were prepared at concentrations of 0.5; 1.0 and 5.0 mg/mL.

For the determination of protein content of samples, 50 µL of sample were pipetted into a test tube and added 2.50 mL of protein reagent to each tube and mixed well by gentle vortex. After 5 minutes of rest, absorbance of the samples and standards against the reagent blank was measured at 595nm in a UV/VIS spectrophotometer (model Pye UNICAM 8600, PHILIPS).

Yoghurt samples were previously diluted in arrange of dilutions (1, 1:5, 1:10; 1:20, 1:50, 1:100). Duplicates of each sample were analysed.

3.4.5 Total ash

Total ash (total mineral) content in yoghurt samples after incineration was determined according to AOAC Method 930.30 .

For the determination of total ash content of yoghurt samples, approximately 2.0 g of yoghurt were weighed into a previously ignited, cooled, and weighed porcelain crucible. After weighing, the samples were ignited in a muffle furnace equipped with automatic pyrometer (capable of operating at temperatures up to 600 ± 15°C) at about 550ºC until carbon-free. Finally, the crucibles with sample ashes were removed to a desiccator, cooled and weighed. Duplicates of each sample were analysed.

The total ash content is determined by the following equation:

$$\% \, Ash = \frac{weight \, of \, residue}{weight \, of \, sample} \times 100 \qquad (3.3)$$

3.4.6 Syneresis quantification

Syneresis or spontaneous whey separation on the surface of set yogurt is regarded as a defect. Several methods can be used to evaluate whey separation such as drainage and centrifugation methods. The centrifugation method is generally used to study the water-holding capacity of a product. A certain quantity of set yogurt (disturbed or undisturbed gel) is centrifuged at a specified speed over a certain period at a fixed temperature. The whey separation is calculated as the percentage weight of the separated whey over the initial weight of the gel. Although these methods give high-precision results, they do not represent the actual value of spontaneous whey separation in set-style yogurt (Amatayakul, Sherkat *et al.*, 2006).

Syneresis in set-style yoghurt samples was determined using the yoghurt samples fermented in the test tube (conical centrifuge tubes), containing approximately 20.0 g of yoghurt. The tubes containing approximately 20 g of sample were placed into centrifuge Eppendorf 5810R (VWR, Portugal) and centrifuged at 5000rpm for 25 minutes, at a controlled temperature of 20ºC. Both the separated whey and the coagulum were weighed. Duplicates of each sample were analysed.

The following equation is used for determination of syneresis:

$$\%\ syneresis = \frac{weight\ of\ separated\ whey}{total\ weight\ of\ gel} \times 100 \quad (3.4)$$

3.4.7 Titratable acidity

Titratable acidity (TA) was measured according to the Portuguese standard NP 701:1982, that defined this parameter as the amount of 0.1N NaOH (mL) required to neutralise the present acid in 100 mL of yoghurt sample. Here, 5.0 mL of yoghurt sample, previously homogenised, were measured into an Erlenmeyer flask, added 5.0 mL of distilled water and 3 drops 1% phenolphthalein indicator. The resulting mixture was then titrated with 0.1M NaOH until the yoghurt sample turned pink, which persisted for 30 seconds. Duplicates of each sample were analysed.

Titratable acidity (TA) is determined by the following equation:

$$\text{Titratable acidity } (TA) = V_{NaOH} \times 20 \quad (3.5)$$

where :

V - mL 0.1 N NaOH required.

3.4.8 Density determination

The density is a fundamental physical characteristic of any substance, which may be readily and reproducibly determined in the laboratory if the mass and volume of a sample can be determined, by means of a pycnometer. Therefore, a dry pycnometer (bottle and stopper) was weighed, recorded the mass and volume and filled with yoghurt with a 20.0 mL syringe. The bottles were filled until they were completely full. The stopper was inserted until yoghurt completely filled the capillary tube in the stopper, then the whole system was weighed. Duplicates of each sample were analysed.

The density (d) is determined by the following equation:

$$density, d = \frac{total\ weight\ of\ (pycnometer + sample) - total\ weight\ of\ pycnometer}{volume\ of\ pycnometer} \quad (3.6)$$

3.5 Rheological methods

3.5.1 Oscillatory rheology tests

Dynamic oscillatory time, frequency and stress sweeps were carried out at 20ºC, using a TA Instruments AR-G2 StressTech controlled-stress rheometer with 40 mm diameter parallel plate geometry (P 40 ETC) at 1.0 mm measuring gap distance.

Oscillation stress sweeps were performed at a constant frequency of 1.0 Hz, over the oscillation stress range of 0.01-100 Pa, in order to assure that the working conditions in frequency sweeps lied in the linear viscoelastic region.

Dynamic oscillatory time sweeps were carried out at a constant frequency of 1.0 Hz and oscillation stress of 1.0 Pa, for a short time period in order to avoid syneresis.

Frequency sweeps were performed in the 0.01-10 Hz range and the oscillation stress was fixed at 1.0 Pa.

The temperature effect in the rheological properties of yoghurt was studied by means of temperature ramp oscillatory procedure in the 20-45ºC range and a constant frequency of 1.0 Hz.

3.5.2 Viscometric tests

The temperature effect in the rheological properties of CMC solutions was studied by means of steady-shear viscosity measurements at constant spindle speed rotation (12 rpm) at temperatures of 20°C, 30°C, 40°C and 45°C, the experiments being performed using a FUNGILAB S.A. VISCO STAR Plus L viscometer using spindle PA.

3.6 Microscopy methods

3.6.1 Gram staining

Bacteria can be differentiated in two groups according to their cell walls using the Gram staining in which the ones with the thickest walls stain in purple (Gram-positive bacteria) and the others in pink (Gram-negative bacteria) (Madigan, Mortinka *et al.*, 2009).

The bacteria preparation was performed on a slide from a fresh and pure culture or from fresh yoghurt samples collected during and after fermentation process. The fresh samples were fixed by the flame. Then the stains were added sequentially as follows: firstly, the crystal violet stain (10 % wt. in ethanol at 95 %) was added to the preparation and washed 30 seconds after. Then, Gram's iodine (3.3 g iodine/L + 6.7 g KI/L) was added and after 30 seconds, the slide is washed. After this, the decolourizing solution (80 % ethanol + 20 % acetone) was applied while colour was being washed away. Finally, the safranin (0.25 % wt. in ethanol at 95 %) was added and the stain in excess was washed 30 seconds after. After air drying and oil mounting, the preparation was observed in a LEICA DMLB2 microscope, incorporating a CCD camera to acquire images using IM50 software (Leica).

3.6.2 Scanning Electron Microscopy (CryoSEM)

Scanning electron microscopy (SEM) is one of the most popular methods to obtain microstructural images, in which subjective parameters such as constituents distributions, arrangements, interactions, and compositions within the microstructure, structural uniformity of the texture, as well as particle size characteristics are evaluated (Mortazavian, Rezaei *et al.*, 2009).

The Cryo-Scanning Electron Microscopy observations (CryoSEM) were performed in the Materials Center of University of Porto (CEMUP) with a JEOL JSM-6301F microscopy coupled with the micro-analysis system OXFORD INCA/ENERGY 350.

The yoghurt samples were frozen in slush nitrogen (T<−210°C), fractured, etched (−90°C) and coated with gold (0.2 kPa and 40 mA) for imaging.

SEM observations were performed with different magnifications (1 000 - 15 000), at a working distance of 15 mm, with an energy beam of 10 - 15 keV.

3.7 Heat transfer experiments

The heat transfer experiments were performed in the PHE set-up previously described. Details about procedure and operating conditions for each working fluid will be given in the next sub-section.

3.7.1 Water/ water heat transfer experiments

Prior to the experiments for the determination of the mean and local heat transfer coefficient of stirred yoghurt and CMC aqueous solutions, the experimental set-up was operated with cold water and hot water in order to determine cooling water heat transfer coefficients (both mean and local coefficients) at different volumetric flowrates. Any variation in this operating parameter will be reflected in the fluid velocity and shear rate, influencing the flow pattern. Details about the Reynolds number range used will be given forward in chapter 5.

Cold water coming from the refrigerator was pumped by two centrifuge pumps (see Figure 3.1), the flowrates being adjusted by means of a flow regulation valve. The temperature of the hot water in the fermentation jacketed tank was stabilized by means of hot oil circulating in the jacket at temperature of 45–50ºC.

The flowrates were monitored by means of calibrated flowmeter and by weighing and measuring the volume of fluid exiting the heat exchanger during a given time interval. The mass and volumetric flowrates were found to be constant during the experiment, confirmed by random flowrates measurements in time.

While hot water was being heated and stabilised in the fermentation tank, five minutes before starting the heat transfer experiments cold water flowing was started in order to stabilise this fluid circuit. During this period, it was carried out the control and determination of cold water flowrate was carried out.

Simultaneously to the start of hot water flowing, data acquisitions were initiated, so one could follow the temperature profiles in-line in FIELPOINT interface with Windows XP (see Figure A.1 in Annex A.1). Hot water flowrate was adjusted to the desired value. The experiments were carried out until stabilisation of temperature profiles and switch off when all the hot water was used or when the PHE inlet

temperature of cold water temperature varied significantly after the initial temperature profile stabilisation.

Total pressure drop along the PHE was measured and data acquired by the same system.

This procedure was also performed several times with the same operating conditions, in order to obtain reproducible data.

3.7.2 CMC / Water heat transfer experiments

The experiments for the determination of heat transfer coefficients of the several aqueous solutions of CMC included two main stages: the aqueous solutions of CMC preparation and the heat transfer experiments.

Three completely dissolved concentrations (0.25, 1.0 and 2.0% w/w) of CMC WALOCEL CRT 1000 GA (Wolff Cellulosics GmbH & Co, Germany) were prepared in tap water, in four containers of 25 L. CMC solutions were dissolved by vigorous mixing (mechanical stirring and manual stirring with a perforated stirrer) and then were transferred to the fermentation tank and stayed overnight to release air bubbles. Test samples were then gently and carefully mixed before measurements to avoid air entrapment.

The tests in the plate heat exchanger with CMC solutions were carried out according to the procedure described in previous section 3.7.1.

In these experiments the flow measurement device in the circuit of CMC solutions was removed in order to minimize the head losses along the flow circuit that would require more powerful pumping systems with probable undesirable fluid heating.

Thus, CMC flowrate was determined and controlled by weighing the volume of fluid exited in the heat exchanger during a given time interval. The CMC flowrate was found to be constant during the experiment.

This procedure was carried out at different mass flowrates, by varying the frequency of the rotation of the lobules pump, using a frequency controller.

3.7.3 Stirred yoghurt/ water heat transfer experiments

The experiments for the determination of mean and local heat transfer coefficients of the stirred yoghurt included two successive main stages: the stirred yoghurt production and the heat transfer experiments.

The stirred yoghurt production was accomplished following the procedure described in section 3.3.2. The tests in the plate heat exchanger with stirred yoghurt were carried out according to the procedure described above for the evaluation of the heat transfer coefficients of the water and CMC.

3.8 Heat transfer analysis

3.8.1 Mean convective heat transfer coefficients

The determination of the convective heat transfer coefficients of the working fluids studied (water, stirred yoghurt and CMC aqueous solutions) in the plate heat exchanger was based on the following assumptions: average constant thermal properties (thermal conductivity and specific heat) and convective heat transfer coefficients along the heat exchanger, negligible internal heat generation, negligible axial convection or conduction and negligible free convection.

In the present study, the plate heat exchanger used has 9 plates (7 thermal plates) with a multipass arrangement with a configuration 2×2/2×2 (2 pass-2 pass, 2 pass of 2 channels per fluid) and is operated in countercurrent as shown in Figure 3.11.

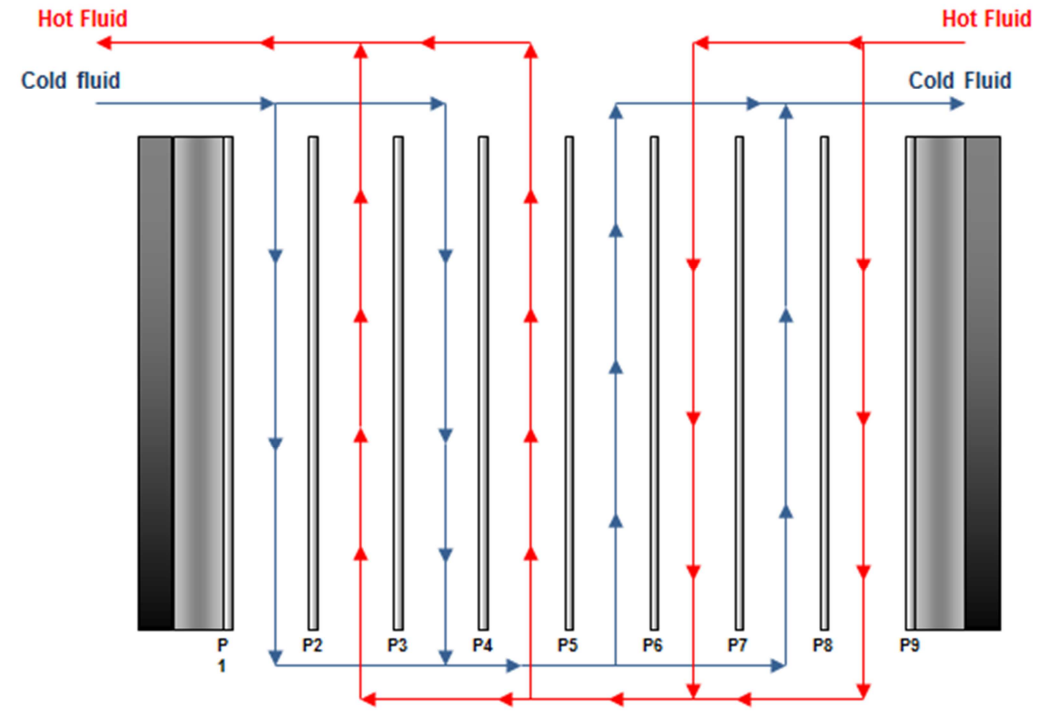


Figure 3.11- Fluid flow pattern of the plate heat exchanger with a multipass configuration 2×2/2×2 in countercurrent.

In order to determine the mean heat transfer coefficient of cooling water (h_{cw}), heat transfer experiments were performed with cold and hot water circulating through the heat exchanger at approximately equal flowrates. The heat transfer rate between the two fluids was calculated from the measured flowrates and temperatures of both hot and cold fluid sides at the PHE inlet and outlet.

The heat flow transferred to the cooling water is determined as follows:

$$Q=\dot{M}_{cw} \cdot c_{p_{cw}} \cdot \rho_{cw} \cdot \left(T_{cw,out} - T_{cw,in}\right) \quad (3.7)$$

The heat flow transferred from hot water is determined as follows:

$$Q=\dot{M}_{hw} \cdot c_{p_{hw}} \cdot \rho_{hw} \cdot \left(T_{hw,in} - T_{hw,out}\right) \quad (3.8)$$

The heat transfer design equation is:

$$Q = A_t \cdot F \cdot U \cdot \Delta T_{ln} \quad (3.9)$$

where A_t is the heat transfer area of the heat exchanger, U is the overall heat transfer coefficient, F is a correction factor and ΔT_{ln} is the mean logarithm temperature difference.

If it is assumed that no significant heat exchange takes place between the equipment and the surrounding air, then:

$$\dot{M}_{cw} \cdot c_{p_{cw}} \cdot \rho_{cw} \cdot \left(T_{cw,out} - T_{cw,in}\right) = \dot{M}_{hw} \cdot c_{p_{hw}} \cdot \rho_{hw} \cdot \left(T_{hw,in} - T_{hw,out}\right) \quad (3.10)$$

Considering the flow arrangement of this PHE, the volumetric flowrates of each fluid can be determined by can be expressed in terms of the number of channels per pass, as follows:

$$\dot{m}_v = \frac{\dot{M}_v}{N_c} \quad (3.11)$$

where N_c is the number of channels per pass, for each fluid, defined as:

$$N_c = \frac{N_p - 1}{2} \quad (3.12)$$

where N_p is total number of plates of the heat exchanger. The number of channels per pass is equal for the two fluids.

Taking into account the countercurrent flow in this PHE, the mean logarithm temperature difference equation is:

$$\Delta T_{ln} = \frac{\left(T_{hw,in} - T_{cw,out}\right) - \left(T_{hw,out} - T_{cw,in}\right)}{ln\left(\frac{T_{hw,in} - T_{cw,out}}{T_{hw,out} - T_{cw,in}}\right)} \quad (3.13)$$

The deviation from an ideal heat exchanger operating only in counter-current flow, as it happens in crossflow and multipass flow heat exchangers, is expressed by a correction factor F (Rene, Leuliet *et al.*, 1991a; Kakaç and Liu, 2002) . The factor *F*, used to correct the mean logarithm temperature difference, was determined graphically (Buonopane, Troupe *et al.*, 1963; Raju and Bansal, 1986):

$$F = 0.967$$

Considering valid the assumption that heat losses are negligible and the equality of volumetric flowrates of the fluids is kept, then the convective heat transfer rate of the cold and hot water will be equal:

$$Q_{cw} = Q_{hw} = F \cdot U \cdot A \cdot \Delta T_{ln} \quad (3.14)$$

The overall heat transfer coefficient (U) is defined as:

$$\frac{1}{U} = \frac{1}{h_{cw}} + \frac{1}{h_{hw}} + \frac{x_p}{\lambda_p} \tag{3.15}$$

where x_p is the plate thickness and λ_p is the plate thermal conductivity. .

If the overall heat transfer coefficient (U) is expressed in terms of the convective and conductive parameters, then equation (3.9) can be re-written as:

$$Q = A_t F \left(\frac{1}{\frac{1}{h_{cw}} + \frac{1}{h_{hw}} + \frac{x_p}{\lambda_p}} \right) \Delta T_{\ln} \tag{3.16}$$

The total heat transfer area, A_t, is calculated by the following equation:

$$A_t = A_p \left(N_p - 2 \right) \tag{3.17}$$

where A_p is the heat transfer area of one plate is 0.18 m^2 (value supplied by the producer), and $\left(N_p - 2 \right)$ is the number of plates really involved in the heat transfer process.

From the experimental data (inlet and outlet temperatures of cold and hot fluids, volumetric flowrates of the two fluids, total number of plates used, thermophysical properties: specific heat, thermal conductivity and density) of each fluid, it is possible to determine the heat transfer rate in the plate heat exchanger (Q). The convective heat transfer coefficients are then calculated from equation (3.16).

Due to the difficulty to obtain equal volumetric flowrates of the fluids in both sides of the PHE, it was necessary to introduce a correction in equation (3.14) that also included the effect of temperature on fluids viscosities.

According to McKillop and Dunkley (1960), Buonopane et al. (1963), Kakaç and Liu (2002), heat transfer coefficients in plate heat exchangers can be determined by means of correlations, obtained by dimensional analysis, defined as:

$$Nu = aRe^b Pr^c \left(\frac{\eta_f}{\eta_w} \right)^d \tag{3.18}$$

or

$$\frac{h \cdot D_e}{\lambda} = a \left(\frac{D_e \cdot \rho \cdot u}{\eta}\right)^b \left(\frac{c_p \cdot \eta}{\lambda}\right)^c \left(\frac{\eta_f}{\eta_w}\right)^d \quad (3.19)$$

where *a, b, c, d* are constants dependent on fluid and flow characteristics, D_e is the equivalent diameter , *Re* is the Reynolds number and *Pr* is the Prandtl number defined as:

$$Re = \frac{D_e \cdot \rho \cdot u}{\eta} \quad (3.20)$$

and

$$Pr = \frac{c_p \cdot \mu}{\lambda} \quad (3.21)$$

The viscosity terms includes the average fluid viscosity (η_f) and the fluid viscosity at the wall temperature (η_w). When fluids exhibit small viscosity variations along the cross section, $\eta_f \approx \eta_w$, and equations (3.18) and (3.19) can be simplified as following:

$$Nu = aRe^b Pr^c \quad (3.22)$$

or

$$\frac{h \cdot D_e}{\lambda} = a \left(\frac{D_e \cdot \rho \cdot u}{\eta}\right)^b \left(\frac{c_p \cdot \eta}{\lambda}\right)^c \quad (3.23)$$

In most presentations of heat transfer data for plate heat exchangers, the equivalent diameter is used (Hewitt *et al.*, 1994a):

$$D_e = 2b \quad (3.24)$$

where *b* is the mean plate spacing.

Based on heat exchanger plate geometry, the hydraulic diameter of the PHE channels (D_h) is defined as (Kakaç and Liu, 2002):

$$D_h = \frac{4A_c}{P_w} \quad (3.25)$$

where, A_c is the channel cross-sectional area and P_w is the wetted surface (wetted perimeter). Equation (3.25) can be re-written as:

$$D_h = \frac{4(b \cdot w)}{2(b + w \cdot \phi)} \quad (3.26)$$

where *w* is the plate width and ϕ is the surface enlargement factor, defined as the ratio of the developed length to the flat or projected area (Kakaç and Liu, 2002). The value of ϕ is a function of the plate corrugation pith and corrugation depth, and varies between 1.15 and 1.25 (Kakaç and Liu, 2002) (Fernandes, 2009). The value of ϕ of the plate heat exchanger used in this study is 1.49.

Equation 3.26 can be simplified since $b << L_w$:

$$D_h = \frac{2b}{\phi} \tag{3.27}$$

In the determination of the convective heat transfer coefficient of the cold water, using hot water as the heat source, from the ratio between heat transfer coefficients of the fluids, it is possible to obtain an expression that relates h_{hw} with h_{cw} in order to substitute h_{hw} in equation (3.16). Hence,

$$\frac{h_{hw}}{h_{cw}} = \left(\frac{Re_{hw}}{Re_{cw}}\right)^b \cdot \frac{Pr_{hw}^c}{Pr_{cw}^{c'}} \tag{3.28}$$

re-writing the equation as follow:

$$h_{hw} = h_{cw}\left(\frac{Re_{hw}}{Re_{cw}}\right)^b \cdot \frac{Pr_{hw}^c}{Pr_{cw}^{c'}} \tag{3.29}$$

where c and *c'* are the Prandtl number exponents that equal 0.4 or 0.3, for hot and cold water, respectively (Raju and Basal, 1986).

From equation (3.29) it is possible to obtain a correction factor, $\left(\frac{Re_{hw}}{Re_{cw}}\right)^b \cdot \frac{Pr_{hw}^c}{Pr_{cw}^{c'}}$, necessary to introduce the effects of the viscosity and flowrate differences on heat transfer, particularly on the convective heat transfer coefficients.

Applying equation (3.22) to each fluid and re-writing as follows:

$$h_{cw} = C_1 \cdot \mathrm{Re}_{cw}^b \tag{3.30}$$

and

$$h_{hw} = C_2 \cdot \mathrm{Re}_{hw}^b \tag{3.31}$$

where

$$C_1 = \frac{a \cdot \lambda_{cw}}{D_h} \cdot \mathrm{Pr}_{cw}^{c} \tag{3.32}$$

and

$$C_2 = \frac{a \cdot \lambda_{hw}}{D_h} \cdot \mathrm{Pr}_{hw}^{c'} \tag{3.33}$$

Correlating the constants C_1 and C_2:

$$\frac{C_2}{C_1} = \frac{\lambda_{hw}}{\lambda_{cw}} \cdot \frac{\mathrm{Pr}_{hw}^{c}}{\mathrm{Pr}_{cw}^{c'}} \tag{3.34}$$

Rearranging the equation,

$$C_2 = C_1 \cdot K \cdot \frac{\mathrm{Pr}_{hw}^{c}}{\mathrm{Pr}_{cw}^{c'}} \tag{3.35}$$

where $K = \frac{\lambda_{hw}}{\lambda_{cw}}$

Replacing in equation (3.29):

$$h_{hw} = C_1 \cdot K \cdot \frac{\mathrm{Pr}_{hw}^{c}}{\mathrm{Pr}_{cw}^{c'}} \cdot \mathrm{Re}_{hw}^{b} \tag{3.36}$$

The convective heat transfer coefficient of cold water is determined from equations (3.30) and (3.36) and (3.29), as described below:

$$\frac{1}{U} = \frac{1}{C_1 \cdot \mathrm{Re}_{cw}^{b}} + \frac{1}{C_1 \cdot K \cdot \frac{\mathrm{Pr}_{hw}^{c}}{\mathrm{Pr}_{cw}^{c'}} \cdot \mathrm{Re}_{hw}^{b}} + \frac{x_p}{\lambda_p} \tag{3.37}$$

The values of constants C_1 and b can be obtained by nonlinear regression analysis, considering fluid and flow characteristics. Therefore, a correlation for the determination of mean heat transfer coefficients of cooling water is obtained, after optimization.

In the case of the convective heat transfer coefficient of stirred yoghurt and CMC solutions (1% and 2%), “generalised” dimensionless numbers should be used so that the non-Newtonian behaviour of the fluids is taken into account:

$$Nu = a\,\mathrm{Re}_g^{b}\,\mathrm{Pr}_g^{c} \tag{3.38}$$

where the "generalised" Reynolds and Prandtl numbers are given by:

$$\mathrm{Re}_g = \frac{u\rho D_h}{\eta_{app}} \tag{3.39}$$

$$\mathrm{Pr}_g = \frac{c_p \eta_{app}}{\lambda} \tag{3.40}$$

The generalisation of these dimensionless numbers is obtained by introducing the viscosity dependency on the shear rate and temperature, correlated by the following general equation (Barnes, Hutton *et al.*, 1989):

$$\eta_{app} = \left[\eta_{app}(\dot{\gamma})\right] e^{\left(\frac{E}{RT}\right)} \tag{3.41}$$

where η_{app} is the apparent viscosity of food fluids, $\eta_{app}(\dot{\gamma})$ is the term that takes into account the dependency of viscosity on shear rate, E (J mol^{-1}) is the activation energy, R is the constant of ideal gas (R=8.31451 J K^{-1} mol^{-1}) and T the absolute temperature (K).

The determination of the heat transfer coefficients of stirred yoghurt and CMC solutions exhibiting non-Newtonian behaviour is a process less complex than cold water process, since the heat transfer coefficients of cold water has been determined previously. Consequently, the heat transfer coefficients of the working fluids (CMC solutions and stirred yoghurt) can be determined directly from equation (3.16).

3.8.2 Determination of Local Heat Transfer Coefficients

The approach embraced for the determination of local heat transfer coefficients of stirred yoghurt and CMC aqueous solutions is similar to the one described in section 3.8.1. Therefore, it is applied to the experimentally monitored channels in each pass of the plate heat exchanger.

Figure 3.12 shows the heat transfer sections considered in this heat transfer analysis for the determination of local heat transfer coefficients.

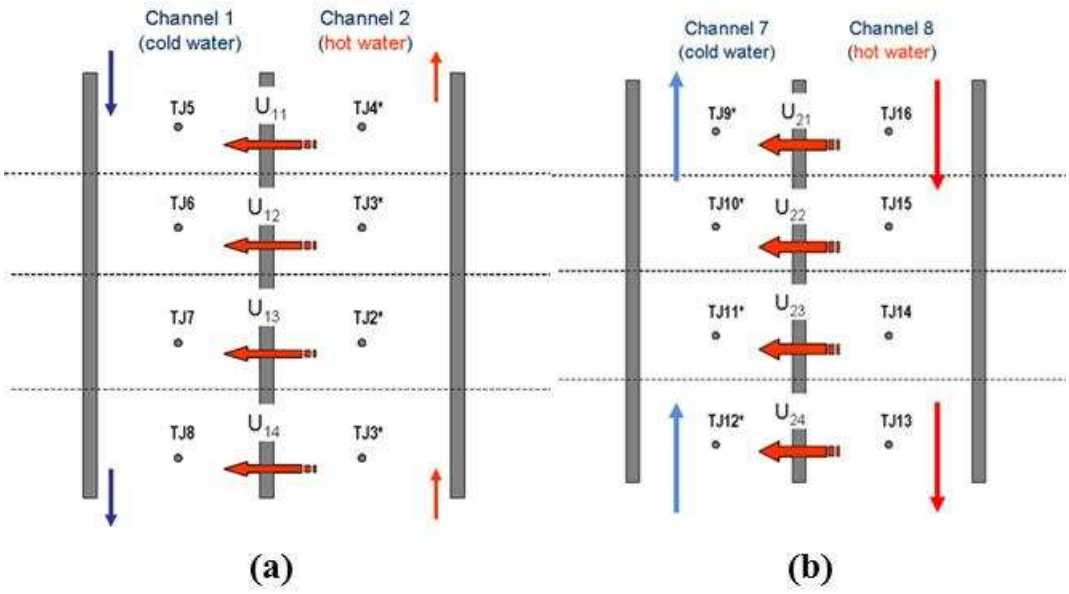


Figure 3.12- Representation of flow pattern and thermal analysis for section 1 (a) and section 2 (b) of plate heat exchanger.

Figure 3.12 represents the four sub-sections considered in thermal analysis. Each controlled section was divided in four sub-sections, with the same heat transfer area, in order to determine four local overall heat transfer coefficients (U_{ij}) along the PHE controlled plates.

The first monitored section, named section 1, was defined by channels 1 and 2 and plate 2 (P2), the assembled plate with Pt100 resistance probes.

For each section, four equations were written for the determination of heat transfer flow through the plate wall, represented by:

$$\frac{\dot{Q}_{ij}}{A_{p,ij}} = U_{ij} \cdot \left(T_{h,ij} - T_{c,ij}\right) \tag{3.42}$$

where $\dot{Q}_{ij}$ is the heat transfer rate for given sub-section ij, i=1 to 2 (section identification) and j= 1 to 4 (sub-section identification), $A_{p,ij}$ is the heat transfer area of a given sub-section, U_{ij} is the overall heat transfer coefficient for given sub-section, $\left(T_{h,ij} - T_{c,ij}\right)$ is the temperature difference between the hot and cold fluids in a given sub-section.

For each sub-section considered, the temperature difference was calculated by experimental data, and local heat transfer rates $\dot{Q}_{ij}$ were determined by means of the

heat capacity rates for each channel, considering average specific heat of each fluid, determined at the mean fluid temperature sub-section. The influence of temperature on the thermophysical properties of each fluid was taken into account in order to attain a more realistic thermal analysis approach.

Then, local heat transfer rate $\dot{Q}_{ij}$ is given by:

for cold fluid

$$\dot{Q}_{ij} = \dot{m}_c \cdot cp_{c,ij} \cdot \left(T_{c,out} - T_{c,in}\right)_{ij} \tag{3.43}$$

and for hot fluid

$$\dot{Q}_{ij} = \dot{m}_h \cdot cp_{h,ij} \cdot \left(T_{h,in} - T_{h,out}\right)_{ij} \tag{3.44}$$

where $\dot{m}_c$, $\dot{m}_h$ are the mass flowrates of cold and hot fluids, respectively and$cp_{c,ij}$, $cp_{h,ij}$ are the specific heat of cold and hot fluids, respectively.

The local overall heat transfer coefficients U_{ij} for given sub-section is determined by:

$$\frac{1}{U_{ij}} = \frac{1}{h_{c,ij}} + \frac{1}{h_{h,ij}} + \frac{x_p}{\lambda_p} \tag{3.45}$$

As it was mentioned before, this approach is similar to the approach used in the determination of the mean heat transfer coefficients of the studied fluids.

Therefore, the local convective heat transfer coefficient of cold water, in each sub-section was determined by applying equation (3.37), as follows:

$$\frac{1}{U_{ij}} = \frac{1}{C_{1,ij} \cdot \mathrm{Re}_{cw,ij}^{b,ij}} + \frac{1}{C_{1,ij} \cdot K_{ij} \cdot \frac{\mathrm{Pr}_{hw,ij}^{c,ij}}{\mathrm{Pr}_{cw,ij}^{c,ij'}} \cdot \mathrm{Re}_{hw,ij}^{b,ij}} + \frac{x_p}{\lambda_p} \tag{3.46}$$

Again, the values of constants $C_{1,ij}$ and b_{ij} can be obtained by nonlinear regression analysis, considering fluid properties and flow characteristics. Therefore, four correlations for the determination of local heat transfer coefficients of cooling water were obtained, for each section, after optimization.

The determination of local heat transfer coefficients of stirred yoghurt and CMC aqueous solutions in each sub-section is similar to the one described for the determination of the mean heat transfer coefficients.

3.8.3 Pressure drop

During the heat transfer experiments, total pressure drop was determined experimentally using differential pressure transmitters located at both hot and cold fluid sides of the PHE inlet and outlet, in order to evaluate the head losses in the heat exchanger, by means of a correlation including the friction factor.

For a Newtonian fluid of viscosity, μ, and density, ρ, flowing through non-circular duct of equivalent diameter D_e and the length L, in laminar flow regime, the basic relationship for relating the Fanning friction factor with the pressure drop is (Rene *et al.*, 1991a):

$$\frac{f}{2} = \frac{\Delta P \cdot D_e}{4L \cdot \rho \cdot u^2} \tag{3.47}$$

where, f is the Fanning friction factor, ΔP is the pressure drop and u is the average or bulk velocity.

Equation (3.47) may be written as:

$$\Delta P = \frac{2f \cdot L \cdot u^2 \cdot \rho}{D_e} \tag{3.48}$$

The friction factor is proportional to Reynolds number and can be expressed as:

$$f = aRe^b \tag{3.49}$$

Combining equations (3.48) and (3.49) one can obtain:

$$\Delta P = \frac{(aRe^b) \cdot 2 \cdot L \cdot u^2 \cdot \rho}{D_e} \tag{3.50}$$

Equation (3.50) may be written as:

$$\Delta P = C \cdot (aRe^b) \tag{3.51}$$

where $C = \frac{\cdot 2 \cdot L \cdot u^2 \cdot \rho}{D_e}$

The values of constants *a* and *b* can be obtained by nonlinear regression analysis, considering fluid and flow characteristics. Therefore, a correlation relating the friction factor to Reynolds number was obtained.

3.9 Statistical Analysis

The characterisation of physicochemical and rheological properties of set-style yoghurt comprised the study of the effect of addition of a few ingredients such as skim milk powder, high protein skim milk powder (HP50), sweet whey and carboxymethylcellulose (cellulose gum). Set-style yoghurt formulations were prepared based on a design of experiments (DOE) method, the ABCD mixture design. A mixture design for factor screening, specifying four ingredients, was performed using JMP 5.01 – The Statistical Discovery software (SAS Institute, Inc.).

The correlations for the determination of mean and local heat transfer coefficients were obtained, firstly by data analysis in Microsoft Excel and by nonlinear regression analysis performed using SPSS Statistics version 17.0 for Windows (SPSS, Inc.). Nonlinear regression analysis was performed using the Levenberg–Marquardt method for minimizing the sum of squared residuals function.

4. DETERMINATION OF MEAN AND LOCAL HEAT TRANSFER COEFFICIENTS OF COOLING WATER IN A PLATE HEAT EXCHANGER

4.1 Introduction

The plate heat exchangers are extensively used in warming, heating and cooling applications in chemical, pharmaceutical and food industries.

In the last decades, several studies have been conducted to evaluate the performance of PHEs by studying the efficiency of heat transfer, flow resistance, and the pressure capacity, considering different plate geometries, flow arrangements and flow regimes (e.g. (McKillop and Dunkley, 1960; Buonopane *et al.*, 1963; Rene *et al.*, 1991b; Leuliet and Maingonnat, 1992; Muley and Manglik, 1999; Wang and Sundén, 2003; Galeazzo, Miura *et al.*, 2006; Durmuş, Benli *et al.*, 2009).

Notwithstanding the number of works presented in the open literature, plate heat exchanger design continues to be proprietary, since PHEs manufacturers have developed their own empirical correlations for the prediction of thermal performance applicable to PHEs produced and marketed by them (Kuppan, 2000). Therefore, specific and accurate heat transfer correlations of specific PHE considering plate patterns and flow arrangements are not available in the open literature, though, in recent years, several studies were conducted on numerical simulation and modelling thermal–hydraulic performances of PHEs (e.g. (Bassiouny and Martin, 1984a; Bassiouny and Martin, 1984b; Rene and Lalande, 1987; Zettler and Müller-Steinhagen, 2001; Gut and Pinto, 2003a; Gut *et al.*, 2004; Palm and Claesson, 2005; Galeazzo *et al.*, 2006; Fernandes, Dias *et al.*, 2008; Luan, Zhang *et al.*, 2008; Han, Cui *et al.*, 2010).

The present chapter presents preliminary heat transfer experiments using water as working fluid in both cold and hot sides of the plate heat exchanger, in order to obtain empirical thermal correlations for cooling water heat transfer coefficients.

4.2 Experimental methodology

This chapter presents and discusses all the results obtained in the water/ water heat transfer experiments conducted in order to obtain accurate thermal correlations for the determination of cooling water heat transfer coefficients (both mean and local coefficients) in a PHE CLIP 6-RM with chevron plate (β=35º/35º) with a multipass configuration 2×2/2×2 in countercurrent, as shown in Figure 4.1.

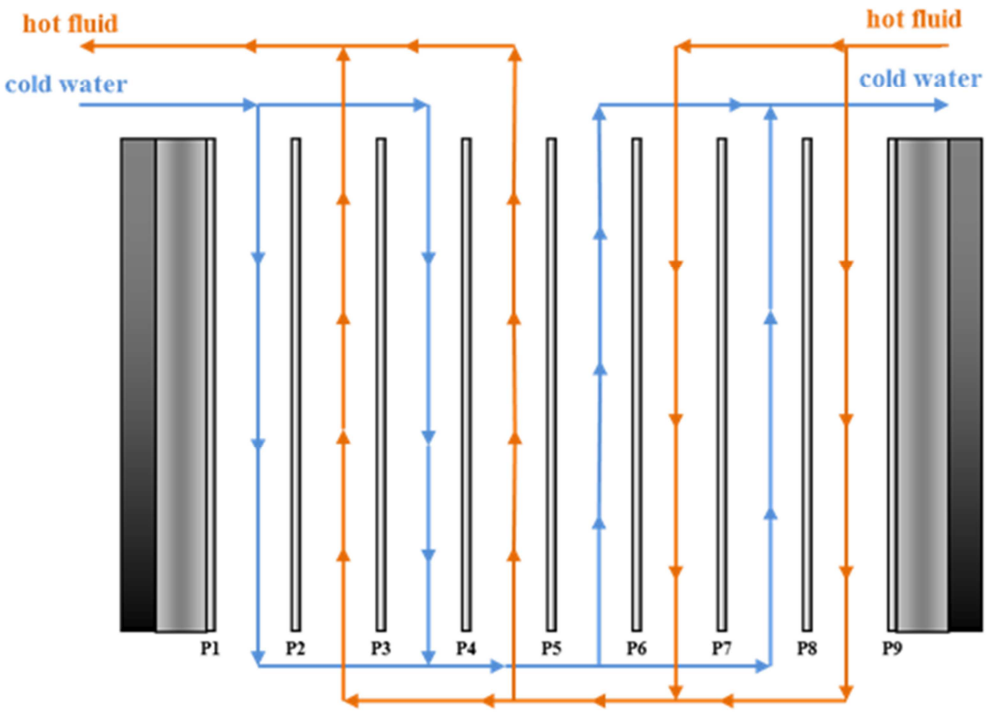


Figure 4.1- PHE flow arrangement used in water-water experiments.

The heat transfer experiments were carried out according to procedures described in section 3.7.1., with different the mass flow rates. The later were measured by calibrated flowmeter and controlled by weighing and measuring the volume of fluid exiting the heat exchanger during a given time interval. The mass flow rates were kept constant during the experiments. In the different experiments, the cold and hot water flows varied between 0.06 kg/s and 0.25 kg/s. The inlet temperature of cold water varied from 6 to 35ºC and the inlet hot water varied from 48 to 17ºC (average ranges).

In the experiments, Reynolds number varied in the range of 289 to 1296, and Prandtl number varied in the range of 6 to 8.

The mean heat transfer coefficients of cooling water were calculated according to procedures described in section 3.8.1, taking in consideration the following assumptions: average constant thermal properties (thermal conductivity and specific heat) and convective heat transfer coefficients along the heat exchanger, negligible internal heat generation, negligible free convection and negligible heat losses. Nonlinear regression analysis was performed using the Levenberg–Marquardt method for minimizing the sum of squared residuals function (section 3.9) in order to obtain a thermal correlation.

The local heat transfer coefficients of cooling water were calculated according to procedures described in section 3.8.2., considering the two experimentally monitored sections, with two controlled adjacent channels in each pass of the PHE. Each monitored section was divided in four sub-sections, with the same heat transfer area, in order to determine four local overall heat transfer coefficients along the PHE monitored plates. Therefore, the variation of the local overall heat transfer coefficients as well as the local convective heat transfer coefficients of cooling water along the PHE was determined, considering the temperature-dependent thermophysical properties of water (thermal conductivity, specific heat, density and viscosity) (ThermExcel, 2003). The local convective heat transfer coefficients were calculated from the four correlations obtained by nonlinear regression analysis as referred in section 3.9.

4.3 Results and Discussion

4.3.1. Determination of mean convective heat transfer coefficients of cooling water

For each heat experiment, temperatures of both hot and cold fluid sides of the PHE inlet and outlet were monitored and registered as mentioned in section 3.2.2. Figure 4.2 shows an example of PHE inlet and outlet temperatures during an experiment, in which it is possible to observe that temperatures became steady about two minutes after the beginning of the heat transfer experiment. Temperature profiles were analysed for each experiment in order to define the time period to be studied. In all experiments, the transient period observed in the temperature profiles was neglected for calculation purposes.

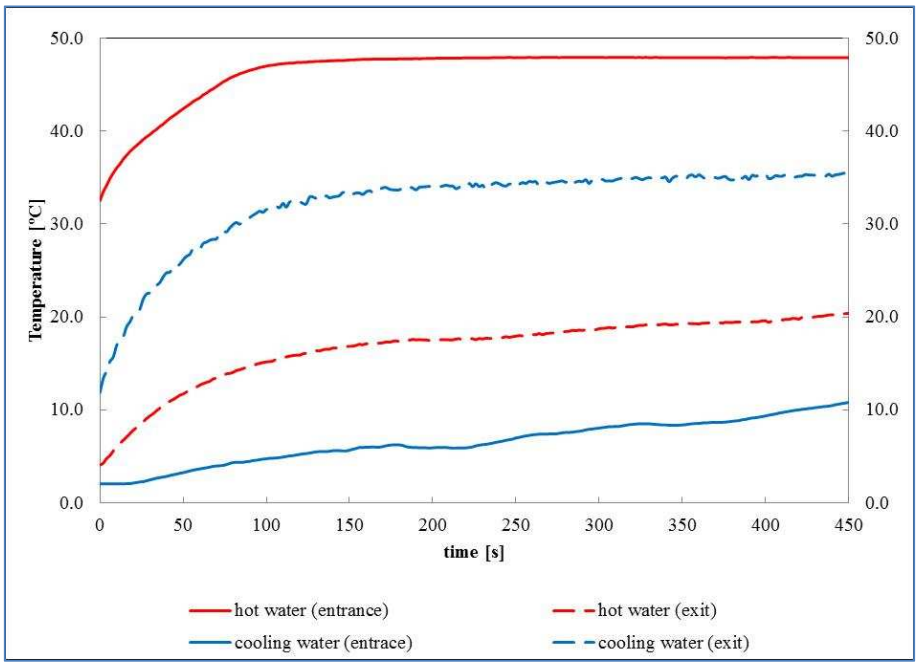


Figure 4.2- PHE ports temperatures (entrance/exit) along experiment time of each fluid (Re=289).

Figure 4.3 shows the fluids temperatures variation in the counterflow configuration of the PHE used in this work. This analysis was performed in all experiments in order to determine the mean logarithm temperature difference (ΔT_{ml}) considering the temperature difference between fluids at the PHE inlets.

From the experimental data (temperatures of both hot and cold water sides of the PHE inlet and outlet, mass flow rates of both fluids) it were determined the heat flow transferred to cooling water and the heat flow transferred from hot water was determined. Different process conditions were obtained by varying temperature and flow rate of the inlet fluids. Data were accepted only if the deviation between heat transfer rates from hot and cold sides were less than 20%.

Table 4.1 shows the values of the heat transfer rates in each experiment for different Reynolds numbers. Differences between the rates of heat transfer to the cold water and from the hot water can be observed in Table 4.1, evidencing the existence of some heat exchange with the surrounding air. The mean value of heat losses percentage was 9%. No relationship was observed between the occurrence of higher heat losses percentages and operating conditions (fluids temperature inlet and flow rates), as reported by Afonso

et al. (2003) in their work, where they found an increase of heat losses when increasing the total number of plates, due to the increasing surface area in contact with the exterior (the length and width of the plates in this PHE was much smaller than those used in the present study, but their thickness and plate gap was similar).

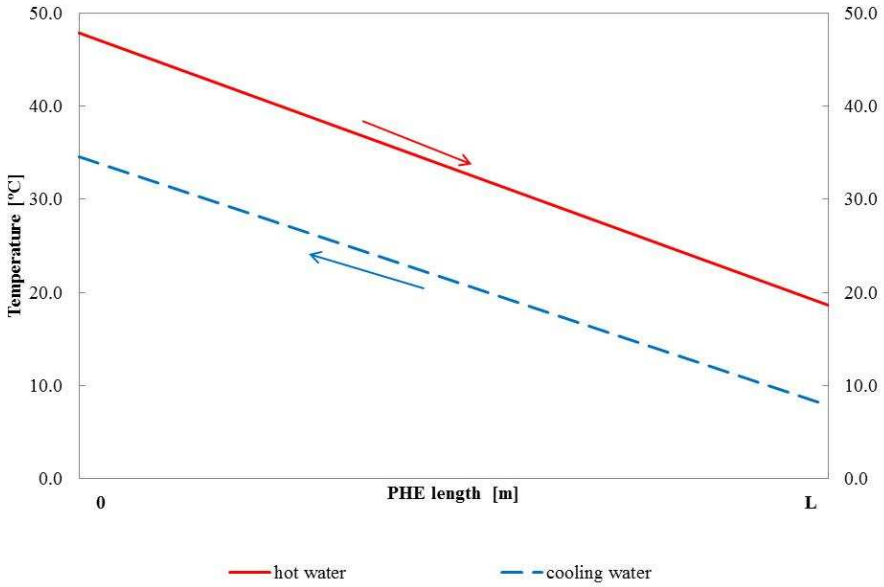


Figure 4.3- Fluids temperatures variation in the counterflow configuration of the PHE used (Re=289).

Due to the differences observed in the heat rates exchanged between the two fluids, a decision was taken on whether to calculate the overall heat transfer coefficients based on heat flow transferred to cooling water or the heat flow transferred from hot water. Assuming the heat losses to be higher in the hot fluid side, a criterion was established so that the overall heat transfer coefficients were determined from the data measured on the cooling water side. The overall heat transfer coefficients were obtained by Equation 3.9 (section 3.8.1.).

Table 4.1- Average values of heat transfer rate transferred to cooling water (Q_{cw}), heat transfer rate transferred from hot water (Q_{hw}) and Reynolds numbers of cooling water (Re_{cw}), for each experiment.

Experiment ID	**Reynolds number, Re_{cw} [-]**	**Heat transfer rate, Q_{cw} [W]**	**Heat transfer rate, Q_{hw} [W]**
1	977	19743	21923
2	393	8406	9122
3	414	9113	9915
4	524	8129	8756
5	1137	21777	24753
6	1168	20718	22434
7	291	7755	8344
8	289	6319	6714
9	1152	20186	22862
10	1151	21281	23668
11	1031	13263	14732
12	679	12401	13551
13	342	6965	7548
14	409	7954	9677
15	409	7054	5738
16	1078	15370	16993
17	1097	18886	20577
18	1296	22237	24632
19	666	11003	10771
20	536	9310	8980
21	959	14987	14909
22	582	4996	4784
23	574	5762	4870

From the results presented in Table 4.1, Table A.1 and Table A.2 (Annex A), by following the calculation procedures described in section 3.8.1 it was possible to obtain the relation between the mean Nusselt number and Reynolds number for cooling water, as shown in Figure 4.4.

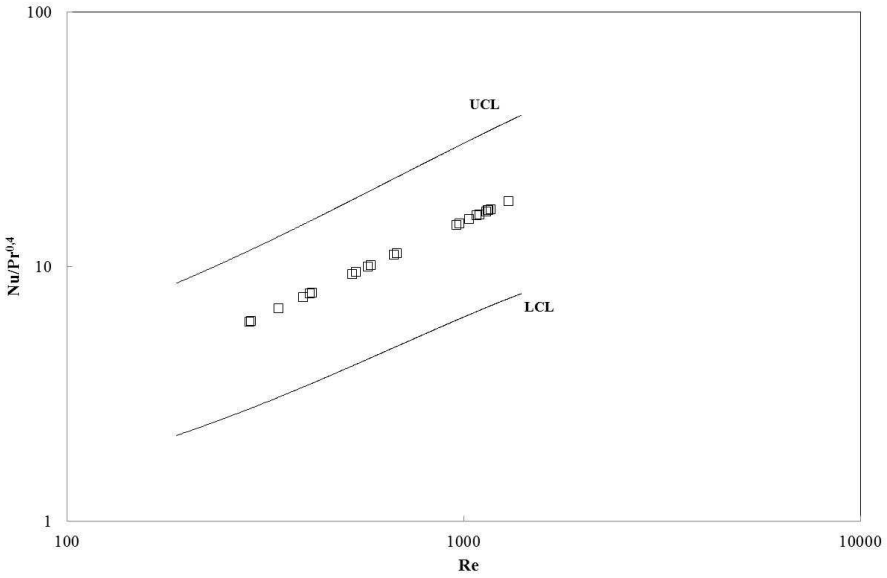


Figure 4.4- Thermal correlation for the mean convective heat transfer coefficient of the cooling water, as a function of the Reynolds number.

The correlation for the determination of the mean convective heat transfer coefficient of the cooling water was obtained by nonlinear regression analysis to determine the values of constants C_1 and b in the following equation (equation 3.37, section 3.8.1.):

$$\frac{1}{U} = \frac{1}{C_1 \cdot \mathrm{Re}_{cw}^{b}} + \frac{1}{C_1 \cdot K \cdot \frac{\mathrm{Pr}_{hw}^{c}}{\mathrm{Pr}_{cw}^{c'}} \cdot \mathrm{Re}_{hw}^{b}} + \frac{x_p}{\lambda_p}$$

The statistical parameters obtained from nonlinear regression analysis are presented in Table 4.2. The values obtained for constant C_1 were applied in equation (3.32) in order to obtain the value of constant *a*. These values were applied in equation (3.22), defined as follows:

$$Nu = aRe^{b}Pr^{c}$$

Table 4.2- Statistical parameters obtained by nonlinear regression analysis.

Parameter	**Estimate**	**Standard error**	**95% confidence interval**	
			lower bound	**upper bound**
C_1	15.718	2.895	9.697	21.739
b	0.728	0.027	0.673	0.784

Thus, the experimental data were correlated according to the following equation:

$$Nu = 0.0979 \cdot Re^{0.728} \cdot Pr^{0.4}, \quad r^2 = 0.979 \tag{4.1}$$

In Figure 4.4, the confidence limits slopes obtained by nonlinear regression analysis are shown. The confidence interval obtained for the constant *a* in equation (3.22) is 0.0604-0.1355 (P<0.05). For Reynolds number exponent, on obtained a lower (LCL) and upper (ULC) confidence limits (P<0.05) of 0.673 and 0.784, respectively.

In Figure 4.5 is shown a comparison between the correlation obtained experimentally for cooling water and other published correlations (Delplace, 1995; Afonso *et al.*, 2003; Gut *et al.*, 2004; Durmuş *et al.*, 2009).

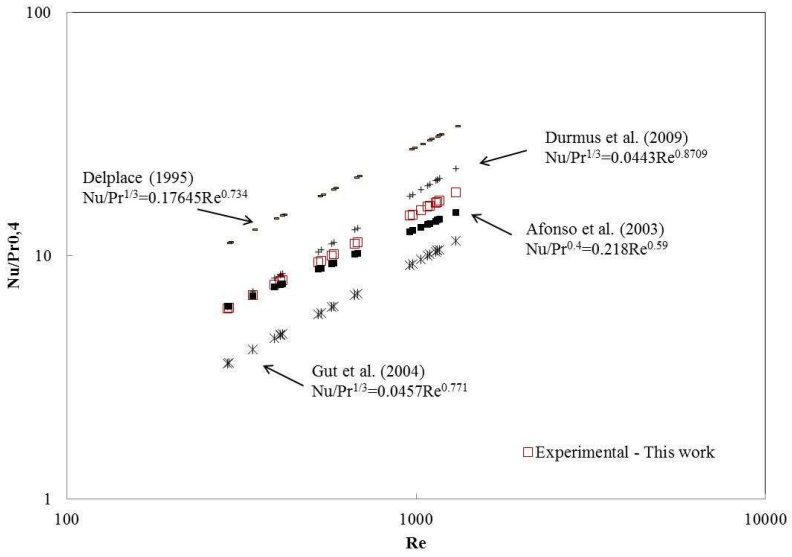


Figure 4.5- Comparison among obtained and published thermal correlations.

The reference correlations used in the comparison were obtained using plate heat exchangers using water as working fluids, countercurrent flow conditions. The plate geometry used in those studies varied from flat (Gut *et al.*, 2004), corrugated (Durmuş *et al.*, 2009) and chevron type (Delplace, 1995; Afonso *et al.*, 2003).

The correlation obtained for cooling water is similar to correlations found for turbulent flow in PHE in which the Reynolds number exponent varied in the range of 0.65-0.85, for water-like fluids (Kuppan, 2000). Due to corrugations, the flow turbulence and the heat transfer coefficients are increased and therefore increased, even for Reynolds numbers lower than 2000. Several authors mentioned that the corrugations

not only promote flow turbulence but also reduce the critical Reynolds number to values in the range 10-400 (Leuliet *et al.*, 1987; Kuppan, 2000; Li *et al.*, 2010).

The plots of experimental and predicted overall heat transfer coefficients as function of Reynolds number are presented in Figure 4.6.

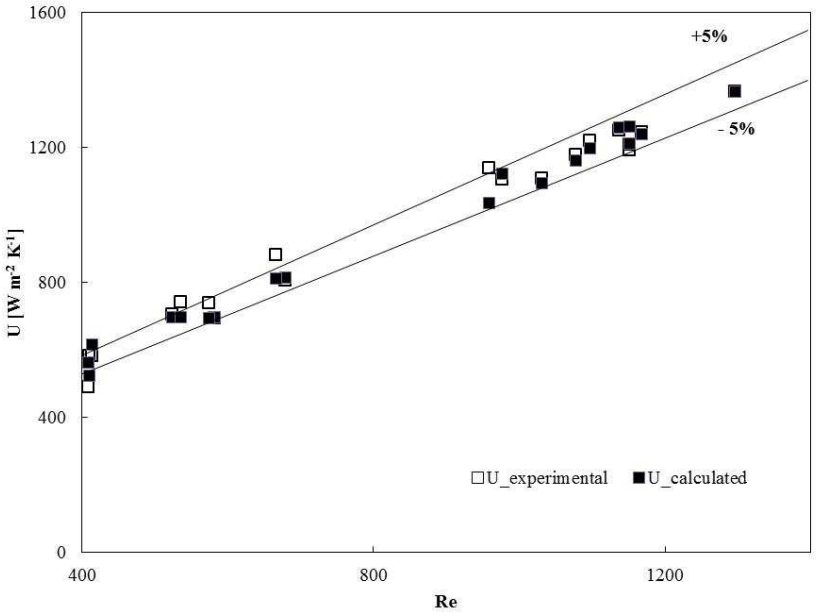


Figure 4.6- Experimental and predicted overall heat transfer coefficients as a function of Reynolds number of cooling water.

From Figure 4.6 it is possible to observe that an accurate correlation for the determination of mean heat transfer coefficients of cooling water was obtained once the predicted overall heat transfer coefficients were calculated with a mean relative error of less than 5%.

The correlation obtained can be applied in further studies using this plate heat exchanger with these flow arrangements.

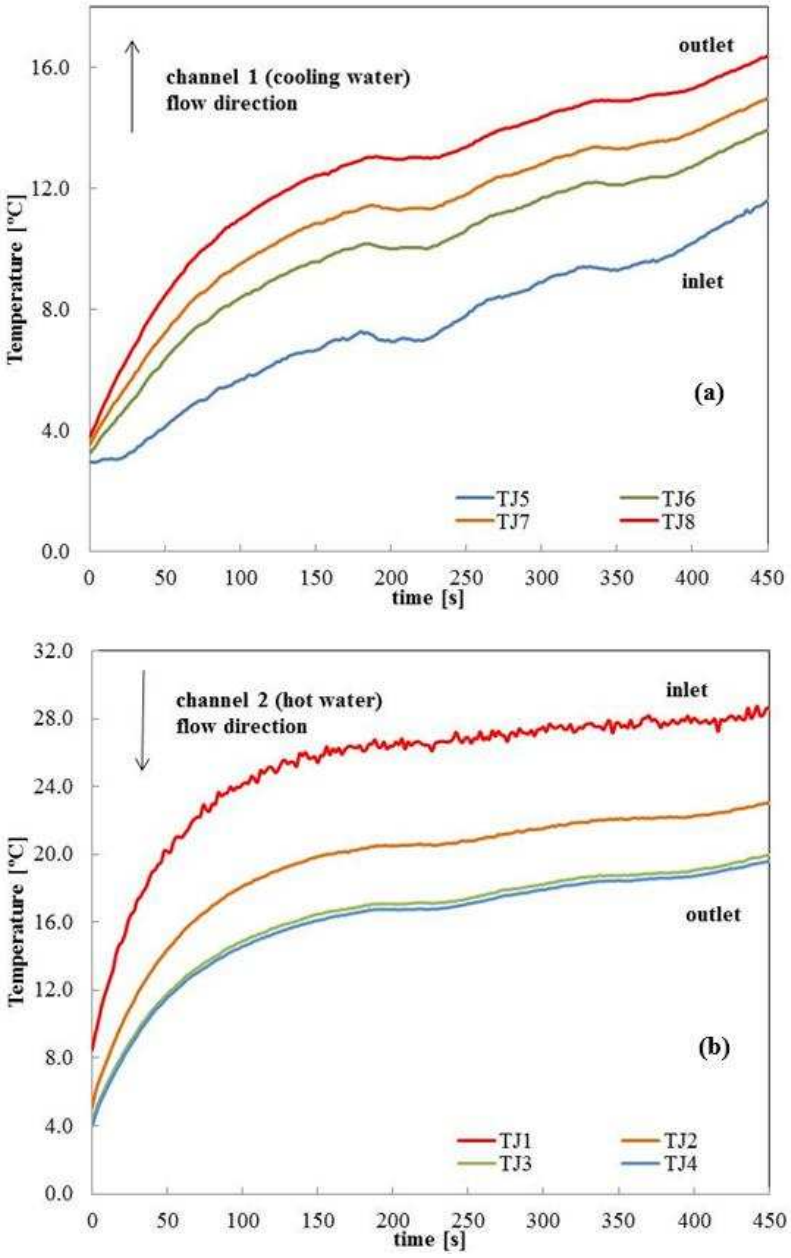
4.3.2. Determination of local convective heat transfer coefficients of cooling water

As previously mentioned, one plate and two adjacent channels in each pass of the PHE were assembled with temperature probes in order to obtain the temperature profiles of the working fluids along the PHE channels and wall temperatures along the PHE monitored plates. In each channel, four temperature probes were positioned in four sub-

sections, allowing the monitoring of fluid and wall temperatures variation along the channel length, during the time of the heat transfer experiment.

In Figure 4.7 it is possible to observe the temperature profiles of cooling water (Figure 4.7a) and hot water (Figure 4.7b) along the monitored channels in section 1 of PHE, corresponding to channel 1 and channel 2, respectively. These temperature profiles were obtained in the water-water heat experiment with a mean Reynolds number of 289, for cooling water. Temperature profiles similar to these ones were obtained for every heat exchanger experiment. Small differences were obtained in the profiles depending on the operating conditions, namely fluids inlet temperatures and flow rates. Nevertheless, the temperature profiles shown in Figure 4.7 are representative of the temperature variation along the PHE channels. The initial abrupt variation observed in the temperature profiles until 150 to 200 s corresponded to the transient period after the heat experiment start.

The wall temperature profiles measured on both sides of plate 2 are shown in Figure 4.8.a and b, for cooling water side and hot water side, respectively. In both figures, it is possible to observe that the wall temperature varied considerably along the plate length. Major temperature differences are observed between the inlet and outlet of channels, in both sides of the plate, and small fluctuations are detected in middle sections; this happened occasionally and no factor was identified as a possible cause.



c

Figure 4.7- Temperature profiles of working fluids ((a) cooling water channel, (b) hot water channel) along the PHE section 1 channels, as a function of time.

The wall temperature differences and those between the working fluids at the channels inlet and outlet can be observed in Figure 4.9a and b as a function of time. From Figure 4.9 it is possible to observe that the average temperature difference between the hot water entrance and cooling water exit is around 10-12ºC, for the operating conditions of the example presented. Similar average temperature difference

between the hot water exit and cooling water entrance is observed, as expected since the PHE operated in a countercurrent flow.

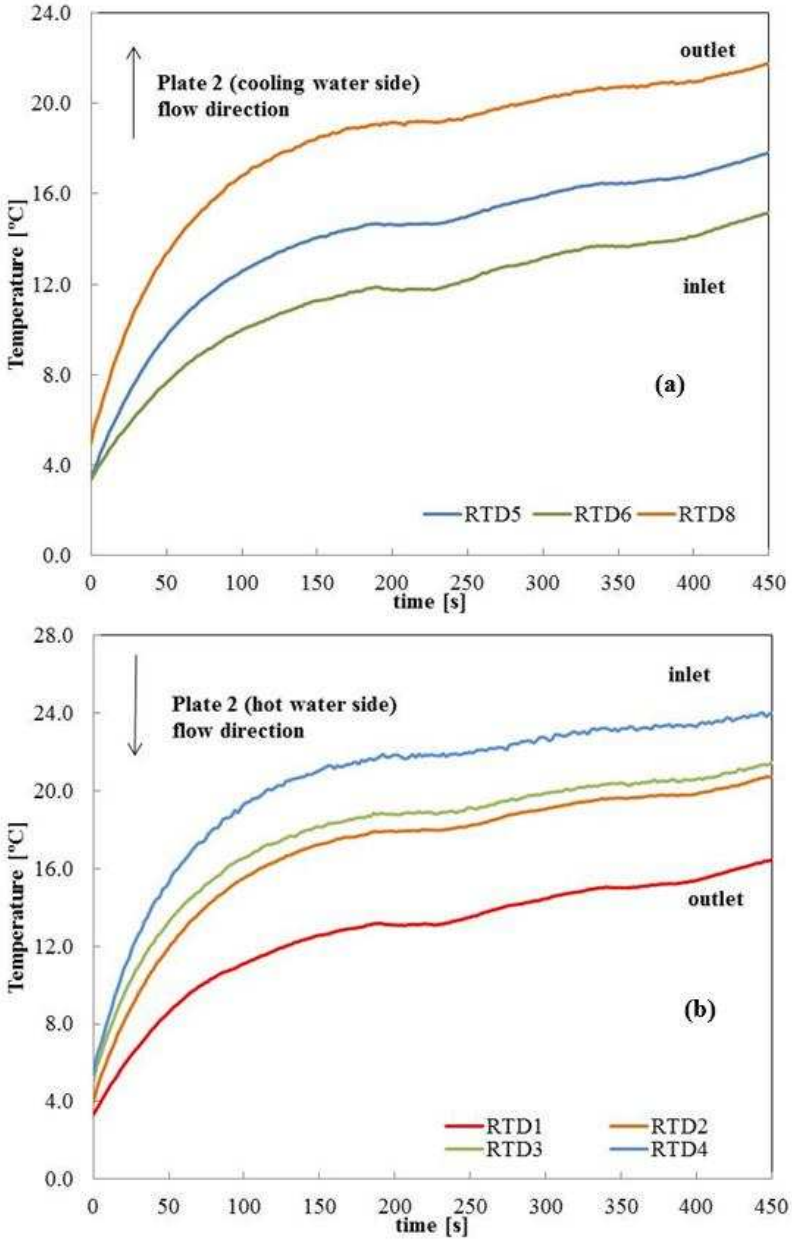


Figure 4.8- Wall temperature profiles along plate 2 ((a) cooling water side, (b) hot water side), as a function of time.

Although temperature differences between working fluids exhibit a constant range (10-12ºC, in the present example) at channels inlet and outlet, the heat flow rate through

the plate wall is not expected to have a constant value since the thermophysical properties of the fluids are temperature-dependent, varying along the channels length.

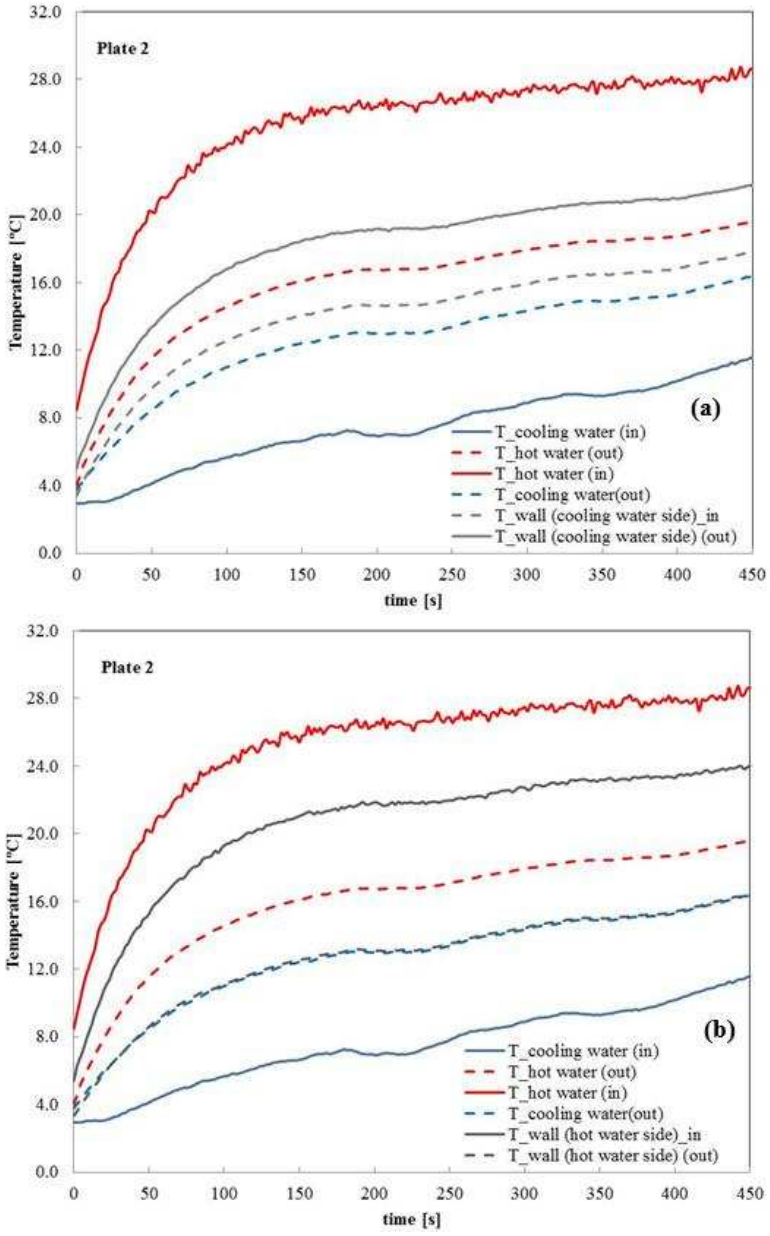


Figure 4.9- Wall temperatures (Plate 2) and working fluids temperatures at channels inlet and outlet ((a) cooling water side, (b) hot water side), as a function of time.

The temperature profiles of cooling water and hot water along the controlled channels in section 2 of PHE, corresponding to channel 7 and channel 8, are shown in Figure 4.10a and b, respectively. The temperature profiles presented in Figure 4.10 were

obtained in the water-water heat experiment with a mean Reynolds number of 289, for cooling water.

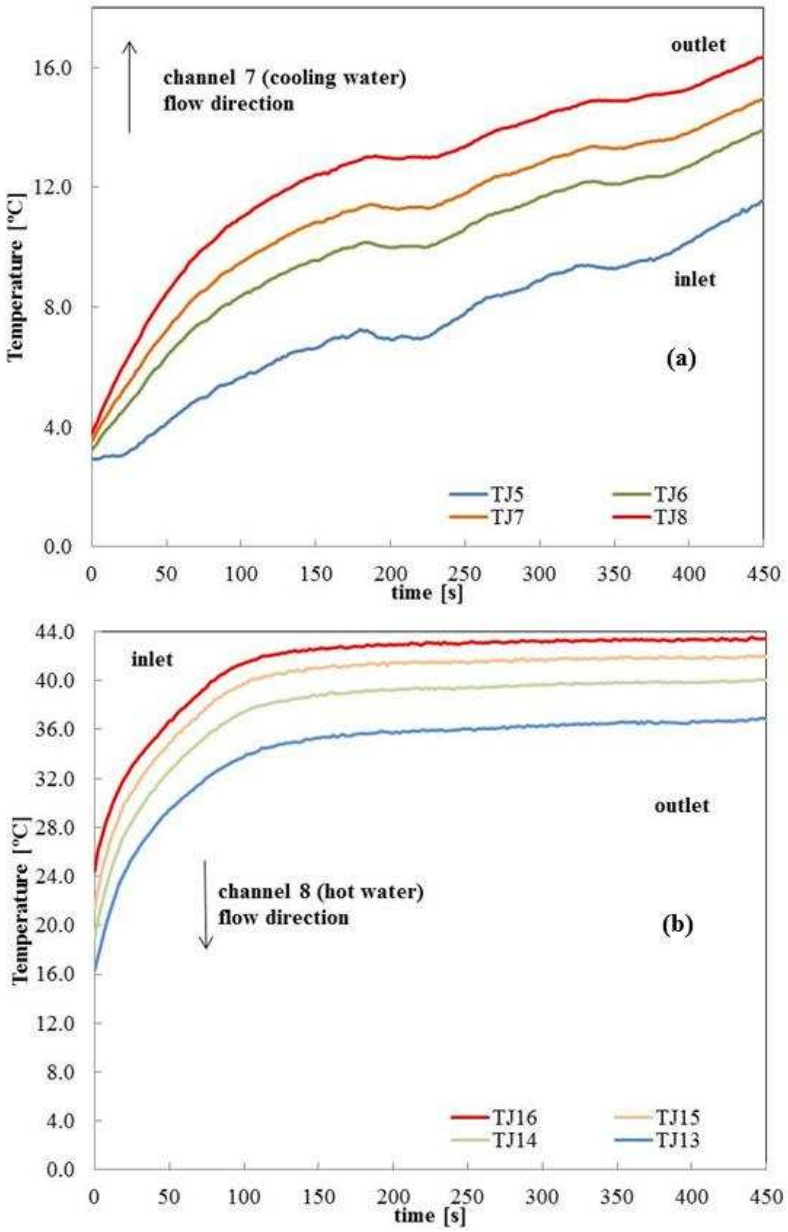


Figure 4.10- Temperature profiles of working fluids ((a) cooling water channel, (b) hot water channel) along the PHE section 2 channels, as a function of time.

Similarly to section 1, in section 2 it is also possible to observe the temperature variation of each fluid through the channel length. Comparing the temperature ranges in sections 1 and 2 it is possible to observe that the hot water suffered a temperature decrease of 44ºC to 34ºC, whereas in channel 2, the temperature decreased from 28 to

17ºC, in this water-water heat transfer experiment. That is, this flow arrangement (2×2/ 2×2)

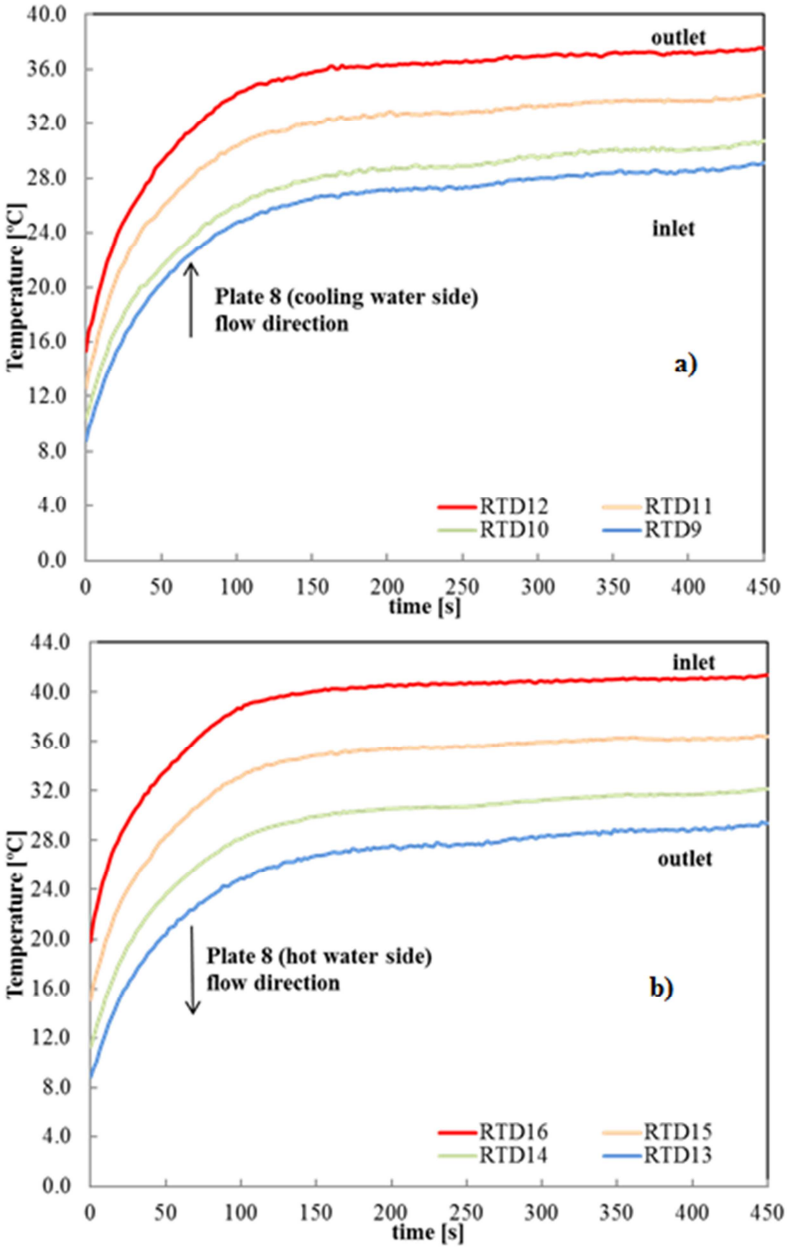


Figure 4.11- Wall temperature profiles along plate 8 ((a) cooling water side, (b) hot water side), as a function of time.

generates two distinct cooling zones, with quite different temperature ranges. These differences were observed in all experiments performed with the PHE.

The wall temperature profiles measured on both sides of plate 8 are shown in Figure 4.11.a and b, for cooling water side and hot water side, respectively. In both figures it is possible to observe that the wall temperature varied considerably along the plate length.

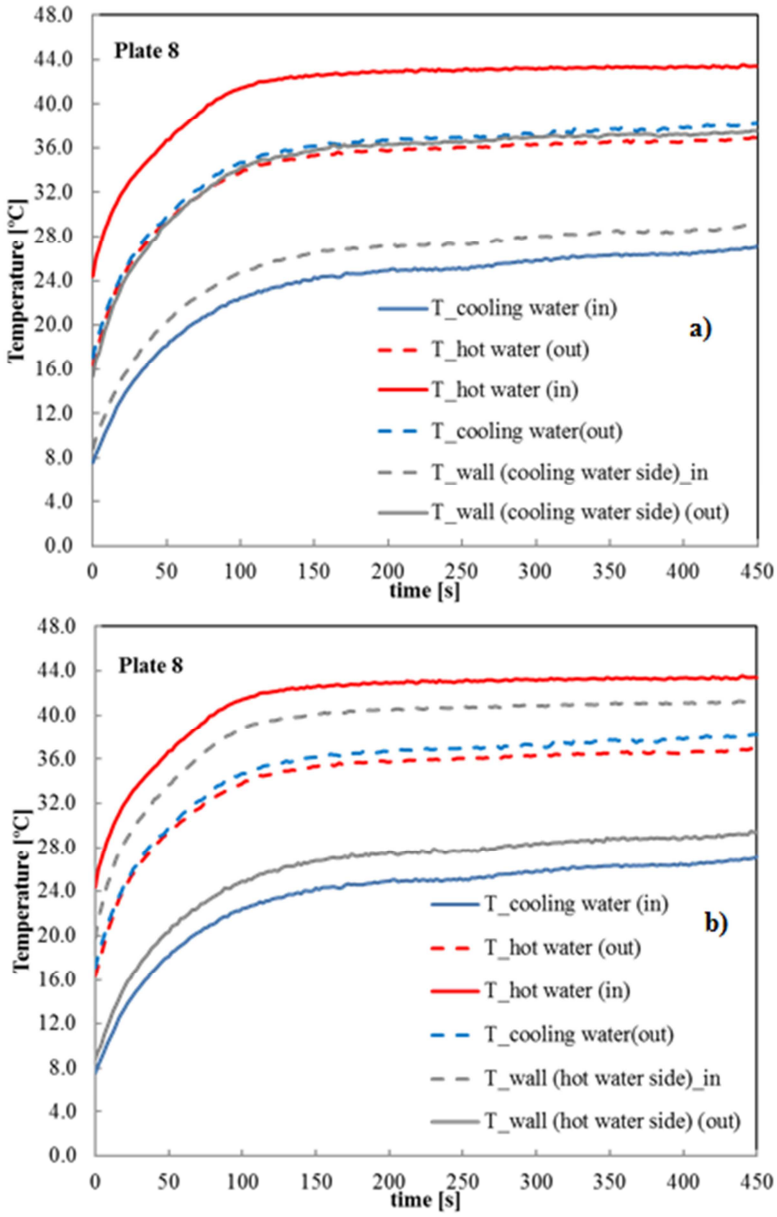


Figure 4.12- Wall temperatures (Plate 8) and working fluids temperatures at channels inlet and outlet ((a) cooling water side, (b) hot water side), as a function of time.

The wall temperature differences and those between the working fluids at the channels inlet and outlet can be observed in Figure 4.12a and b as a function of time. Such as it was observed in section 1, the temperature difference between working fluids has an approximately constant range (10-12ºC, in the present example) at channels inlet

and outlet, although the temperature ranges were quite different. Considering the temperature profiles and the temperature dependence of the thermophysical properties of the fluids, it is not expected the heat flow rate through the plate wall to be constant, neither the overall heat transfer coefficient.

In order to evaluate the fluids temperature variation along the channel length, for several experiment times, the temperature data was plotted versus the position of each temperature probe along the channel length, for section 1 and 2 as it is shown in Figures 4.13 and 4.14, respectively.

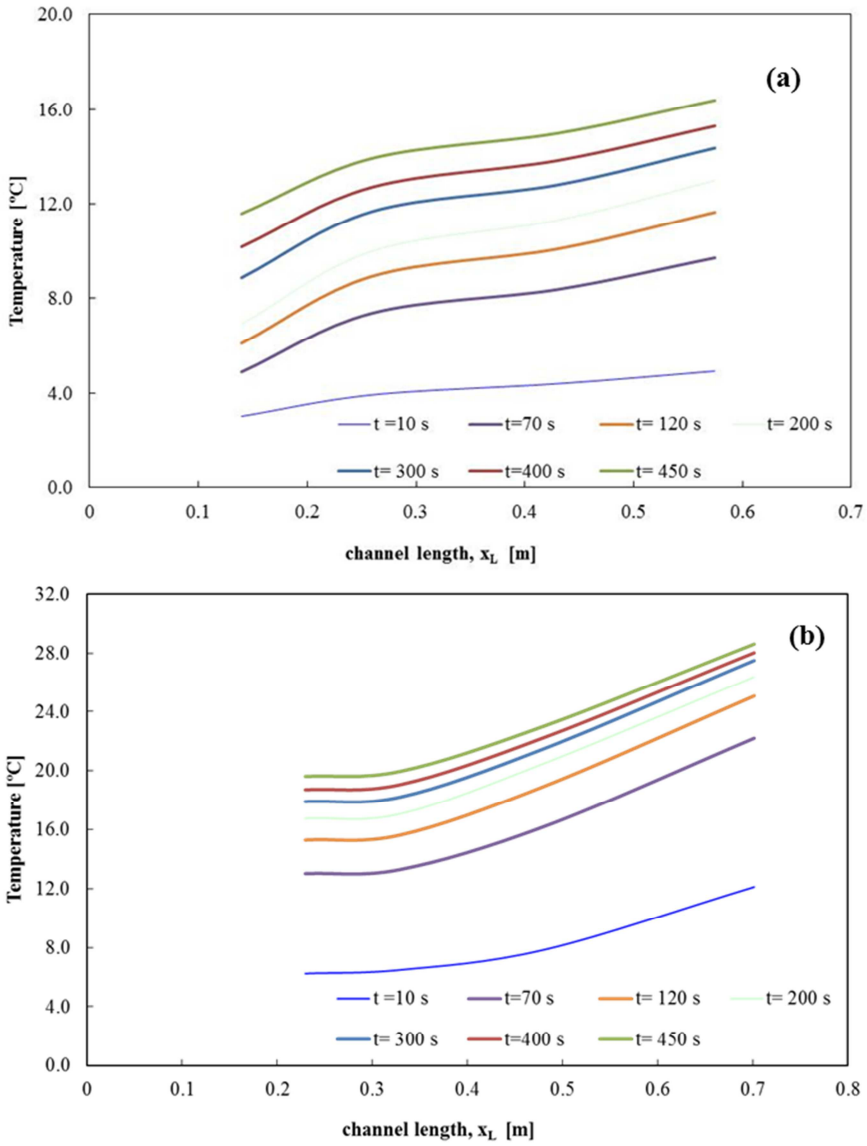


Figure 4.13- Working fluids temperatures along channels 1 and 2 corrugated zone, for different times ((a) cooling water channel, (b) hot water channel).

In both figures it is possible to observe that the temperature profiles along the channel length have an almost linear tendency. In these profiles, only the corrugated region of the plate was taken into consideration for calculation purposes. In all the water-water heat transfer experiments, this tendency was observed allowing the determination of temperature in several intermediate points in the plate length.

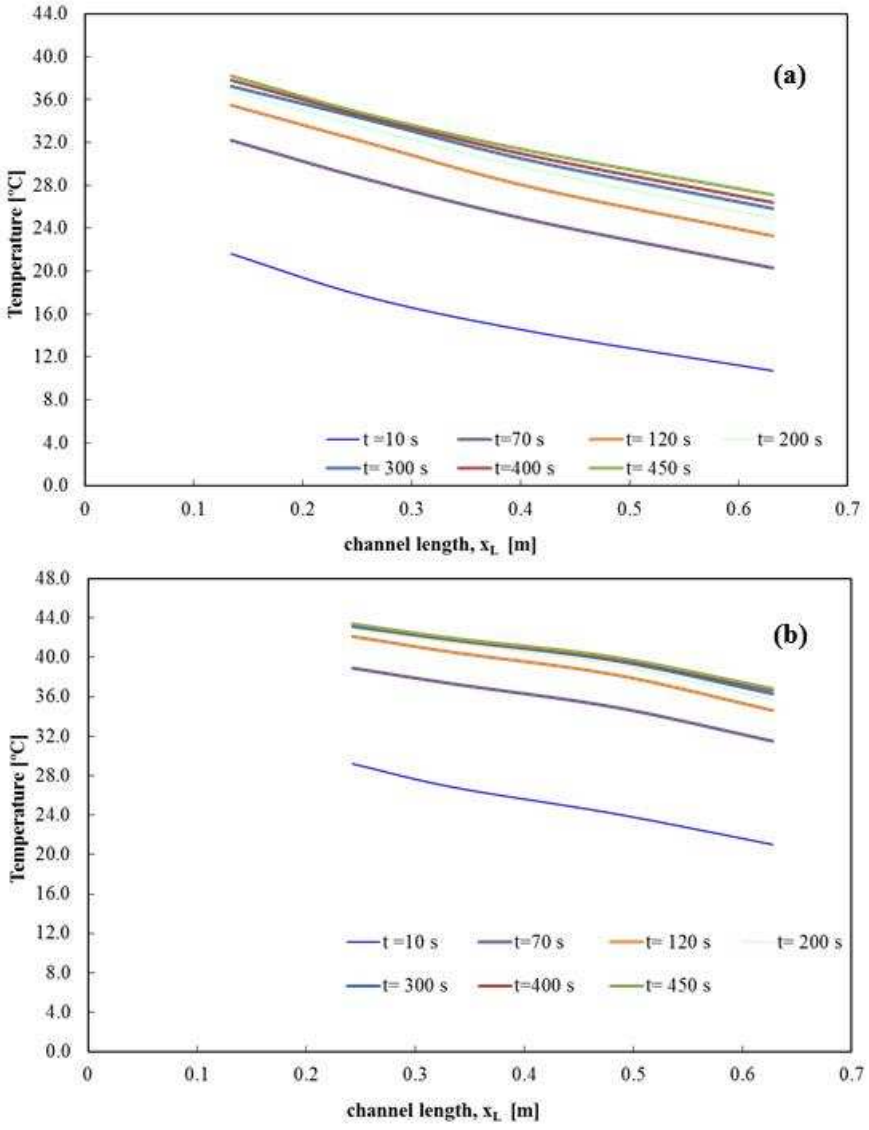


Figure 4.14- Working fluids temperatures along channels 7 and 8 corrugated zone, for different times ((a) cooling water channel, (b) hot water channel).

Following the calculation procedure described in section 3.8.2., four local overall heat transfer coefficients were calculated for each PHE section studied. Thus, it was possible to verify how local overall heat transfer coefficients vary along the plate length.

As mentioned previously, in all the calculations the temperature-dependence of the thermophysical properties of water (thermal conductivity, specific heat, density and viscosity) was taken into account.

Table 4.3 shows the values of local Reynolds numbers and local overall heat transfer coefficients for the four sub-sections analysed in section 1.

Considering the distribution of the overall heat transfer coefficients along section 1 as represented in Figure 3.12a (section 3.8.2.) and the results presented in Table 4.3, it is possible to observe that the overall heat transfer coefficient decreased in the direction of the cooling water flow, *i.e.*, following the increase in the cooling water temperature, reflected in the increase of local Reynolds number values.

In most of the works published in open the literature on simulation, modelling and optimization of PHE, the overall heat transfer coefficient was considered constant along the heat exchanger because this assumption brings a great mathematical simplification (e.g. (McKillop and Dunkley, 1960; Gut *et al.*, 2004; Fernandes *et al.*, 2006). Gut and Pinto (2001) studied the distribution of the overall heat transfer coefficients along the PHE, testing and comparing with the assumption of constant U. These authors observed little influence over the main simulation results for heat exchange (deviation < 1,5% for exchanger.

From the analysis of the distribution of overall heat transfer coefficients values in section 1 it was observed that the mean relative variation of U, varied from 3.2% in sub-section 2, 24.2% in sub-section 3 and 32.1% in sub-section 4. So, one can conclude that the mean relative variation of U for section 1 was 32.1%, comparing the U values between the inlet and outlet of section 1.

Similar analysis was carried out for section 2, as shown in Table 4.4 in which the values of local Reynolds number and local overall heat transfer coefficients are presented for the four sub-sections analysed in section 2.

Table 4.3- Average values of and local overall heat transfer coefficients (U_{ij}) and local Reynolds number (Re_{ij}) of cooling water for the four sub-sections analysed in section 1, for each experiment.

Experiment ID	**Re_{11} [-]**	**U_{11}, [$Wm^{-2}K^{-1}$]**	**Re_{12} [-]**	**U_{12}, [$Wm^{-2}K^{-1}$]**	**Re_{13} [-]**	**U_{13}, [$Wm^{-2}K^{-1}$]**	**Re_{14} [-]**	**U_{14}, [$Wm^{-2}K^{-1}$]**
1	734	1967	755	1878	797	1549	819	1417
2	298	1223	325	1315	335	1056	344	973
3	298	1316	326	1335	335	1039	345	931
4	433	1497	446	1450	458	1110	471	1035
5	872	2098	897	2001	922	1680	974	1530
6	900	2195	925	2053	951	1748	977	1590
7	194	1220	212	1257	224	902	237	785
8	210	1118	229	1167	235	836	242	727
9	887	2080	912	1925	938	1573	964	1406
10	857	2001	904	1961	927	1632	951	1490
11	840	2014	886	1860	886	1522	910	1358
12	516	1727	547	1617	563	1238	579	1093
13	258	1448	274	1312	282	882	291	747
14	316	1803	334	1406	334	890	344	727
15	311	1603	320	1319	329	878	339	731
16	872	2136	897	1994	922	1706	947	1531
17	862	2168	912	2068	938	1746	964	1574
18	999	2245	1056	2128	1085	1854	1114	1676
19	535	1902	567	1911	583	1540	599	1386
20	420	1654	444	1730	457	1320	470	1215
21	773	2257	795	2223	818	1827	841	1623
22	508	1719	520	1785	520	1346	532	1203
23	498	1587	523	1769	523	1335	536	1231

Having in consideration the distribution of the overall heat transfer coefficients along section 2, as represented in Figure 3.12b (section 3.8.2.) and the results presented in Table 4.4 on can observe that the U decreased in the direction of the hot water flow, i.e., in the direction of the decreasing of hot water temperature, *i.e.*, in the direction of the

increasing of cooling water temperature as reflected in the increasing of local Reynolds number values.

Table 4.4- Average values of and local overall heat transfer coefficients (U_{ij}) and local Reynolds number (Re_{ij}) of cooling water for the four sub-sections analysed in section 2, for each experiment.

Experiment ID	**Re_{21} [-]**	**U_{21}, [$Wm^{-2}K^{-1}$]**	**Re_{22} [-]**	**U_{22}, [$Wm^{-2}K^{-1}$]**	**Re_{23} [-]**	**U_{23}, [$Wm^{-2}K^{-1}$]**	**Re_{24} [-]**	**U_{24}, [$Wm^{-2}K^{-1}$]**
1	1271	2531	1219	2372	1145	2202	1047	2095
2	511	1137	488	1031	467	923	434	866
3	545	1572	523	1424	489	1275	457	1220
4	650	1654	622	1530	593	1392	565	1336
5	1460	2685	1399	2522	1309	2350	1222	2245
6	1464	2547	1403	2404	1313	2249	1226	2154
7	412	1192	388	1124	357	1007	327	1010
8	393	1162	369	1080	347	943	324	944
9	1413	2524	1384	2399	1295	2276	1209	2203
10	1449	2895	1392	2686	1284	2467	1204	2347
11	1212	2356	1185	2227	1133	2115	1082	2035
12	859	1776	822	1697	767	1622	714	1576
13	443	1070	424	1038	396	951	368	982
14	525	1286	502	1259	469	1183	425	1208
15	517	1246	494	1204	462	1130	419	1149
16	1301	2374	1244	2258	1188	2129	1132	2043
17	1383	2482	1323	2357	1237	2213	1180	2125
18	1625	2780	1557	2624	1457	2443	1393	2340
19	827	1743	809	1631	754	1528	718	1445
20	678	1537	648	1426	620	1300	577	1234
21	1161	2250	1110	2135	1058	2009	1008	1919
22	648	1498	634	1392	621	1253	595	1193
23	667	1598	653	1450	640	1271	613	1189

From the analysis of the distribution of overall heat transfer coefficients values in section 2 it was observed that the mean relative variation of U, varied from 6.0% in sub-

section 2, 13.3% in sub-section 3 and 16.0% in sub-section 4. Comparing the U values between the inlet and outlet of section 2 one can conclude that the mean relative variation of U for section 2 was 16.0%,

From the analysis of results presented in Table 4.3 and Table 4.4, it is possible to observe that, in general, section 2 has higher U values, mainly due to the higher temperature ranges this section exhibited and, consequently, the effects on thermophysical properties.

Although section 1 exhibited, in general, lower values of U, this section showed higher mean relative variation of U, almost twofold the values observed in section 2.

Following the calculation procedures described in section 3.8.2, for each sub-section, the thermal correlation for the determination of local convective heat transfer coefficient of the cooling water was obtained by nonlinear regression analysis to determine the values of constants C_1 and b in the following equation (equation 3.46):

$$\frac{1}{U_{ij}} = \frac{1}{C_{1,ij} \cdot \mathrm{Re}_{cw,ij}^{b,ij}} + \frac{1}{C_{1,ij} \cdot K_{ij} \cdot \frac{\mathrm{Pr}_{hw,ij}^{c,ij}}{\mathrm{Pr}_{cw,ij}^{c,ij'}} \cdot \mathrm{Re}_{hw,ij}^{b,ij}} + \frac{x_p}{\lambda_p}$$

The statistical parameters obtained from nonlinear regression analysis, applied to the four sub-sections analysed of section 1, are presented in Table 4.5.

Table 4.5- Statistical parameter obtained by nonlinear regression analysis, for the four sub-sections analysed in section 1.

Sub-section	**Parameter**	**Estimate**	**Standard error**	**95% confidence interval**	
				lower bound	**upper bound**
1	C_1	439.94	111.80	207.45	672.44
	b	0.360	0.039	0.279	0.441
2	C_1	433.04	91.71	242.32	623.76
	b	0.353	0.032	0.286	0.420
3	C_1	136.04	32.57	68.30	203.77
	b	0.491	0.036	0.416	0.565
4	C_1	106.57	28.84	46.60	166.54
	b	0.508	0.040	0.424	0.592

The values obtained for constants $C_{1,ij}$ were applied in equation (3.32) in order to obtain the value of constant a. The constants values were applied in equation (3.22), defined as follows:

$$Nu = aRe^{b}Pr^{c}$$

For section 1, four thermal correlations were obtained, one for each sub-section defined. Thus, the experimental data were correlated according to the following equations:

$$Nu = 2.519 \cdot Re^{0.36} \cdot Pr^{0.4}, \quad r^{2} = 0.82 \tag{4.2}$$

obtained for sub-section 1, with 194<*Re*<999 and 6.6<*Pr*<10.8;

$$Nu = 2.522 \cdot Re^{0.353} \cdot Pr^{0.4}, \quad r^{2} = 0.81 \tag{4.3}$$

obtained for sub-section 2, with 212<*Re*<1056 and 6.5<*Pr*<9.8;

$$Nu = 0.799 \cdot Re^{0.491} \cdot Pr^{0.4}, \quad r^{2} = 0.91 \tag{4.4}$$

obtained for sub-section 3, with 224<*Re*<1085 and 6.5<*Pr*<9.5;

$$Nu = 0.632 \cdot Re^{0.508} \cdot Pr^{0.4}, \quad r^{2} = 0.88 \tag{4.5}$$

obtained for sub-section 4, with 237<*Re*<1114 and 6.3<*Pr*<9.2.

Analysing the Reynolds number exponent in equations (4.2), (4.3), (4.4) and (4.5) it is possible to observe that the exponent increased along the channel length, *i.e.*, varying from 0.36 to 0.508, for sub-section 1 and 4, respectively. The variation of the Reynolds number exponent can be explained by the increase of Reynolds number values with the rise of cooling water temperature and consequent increase of turbulence along the channel length.

Comparing the correlations obtained in section 1 with the ones presented in the published literature for laminar and turbulent flow in plate heat exchanger (Edwards, Changal Vaie *et al.*, 1974; Muley and Manglik, 1999; Kakaç and Liu, 2002; Prabhakara Rao, Krishna Kumar *et al.*, 2002), which reported values of the exponent of Reynolds number from 0.32 to 0.73, one can verify that the exponents obtained in section 1 were within the range reported.

The variation of the value of the exponent of Reynolds number along the channel length in section 1 may be explained by entrance effects, since this section is the one nearest of the entrance port of cooling water in the PHE. The exponent of Reynolds number varied from 0.36 to 0.51 at the channel inlet and outlet, respectively. These results combined with the values of Prandtl number (Pr> 1) may indicate a developing thermal boundary layer.

Following the calculation procedure described in section 3.8.2, equations (4.2) to (4.5) were used in the determination of local convective heat transfer coefficients of CMC solutions and stirred yoghurt (see Chapters 6 and 7).

Similar analysis was performed for section 2 of the PHE. The statistical parameters obtained from nonlinear regression analysis, applied for the four sub-sections analysed in section 2, are presented in Table 4.6.

Table 4.6- Statistical parameter obtained by nonlinear regression analysis, for the four sub-sections analysed in section 2.

Sub-section	**Parameter**	**Estimate**	**Standard error**	**95% confidence interval**	
				lower bound	**upper bound**
1	C_1	42.24	7.62	26.39	58.08
	b	0.680	0.025	0.627	0.733
2	C_1	39.87	6.76	25.82	53.92
	b	0.683	0.024	0.633	0.733
3	C_1	31.78	6.05	19.20	44.36
	b	0.709	0.027	0.653	0.766
4	C_1	38.10	8.84	19.73	56.48
	b	0.683	0.033	0.614	0.753

For section 2, four thermal correlations were obtained, one for each sub-section defined. Thus, the experimental data were correlated according to the following equations:

$$Nu = 0.284 \cdot Re^{0.68} \cdot Pr^{0.4}, \quad r^2 = 0.98 \tag{4.6}$$

obtained for sub-section 1, with 393<*Re*<1625 and 4.6<*Pr*<6.8;

$$Nu = 0.264 \cdot Re^{0.683} \cdot Pr^{0.4}, \ r^2 = 0.98 \quad (4.7)$$

obtained for sub-section 2, with 369<*Re*<1557 and 4,8<*Pr*<6.3;

$$Nu = 0.207 \cdot Re^{0.709} \cdot Pr^{0.4}, \ r^2 = 0.98 \quad (4.8)$$

obtained for sub-section 3, with 347<*Re*<1457 and 5.3<*Pr*<6,6;

$$Nu = 0.243 \cdot Re^{0.683} \cdot Pr^{0.4}, \ r^2 = 0.96 \quad (4.9)$$

obtained for sub-section 4, with 324<*Re*<1393 and 5.5<*Pr*<7.2.

Analysing the Reynolds number exponent in equations (4.6), (4.7), (4.8) and (4.9) it is possible to observe that the Reynolds number exponent exhibited an approximate value of 0.68 along the channel length, by contrast with the variable value obtained in section 1. The correlations obtained in section 2 were similar to the ones published in the open literature, namely Cooper (1974), Kakaç and Liu (2002) and Gherasim et al (2009) for PHE channels in turbulent flow:

$$Nu = 0.3 \cdot Re^{0.663} \cdot Pr^{\frac{1}{3}} \left(\frac{\eta}{\eta_w}\right)^{0.17}, Re > 100 \quad (4.10)$$

The results obtained in section 2 show a turbulent flow heat transfer enhanced by higher temperature ranges that influenced the thermophysical properties of the cooling water and consequently the heat transfer and flow regime.

In order to gather more information concerning local convective heat transfer coefficients, the local Nusselt number versus channel length was plotted, for several Reynolds, for section 1 and 2, as shown in Figures 4.15 and 4.16, respectively. The experimental data used for this analysis is shown in Table A.3 and A.4 (Annex A).

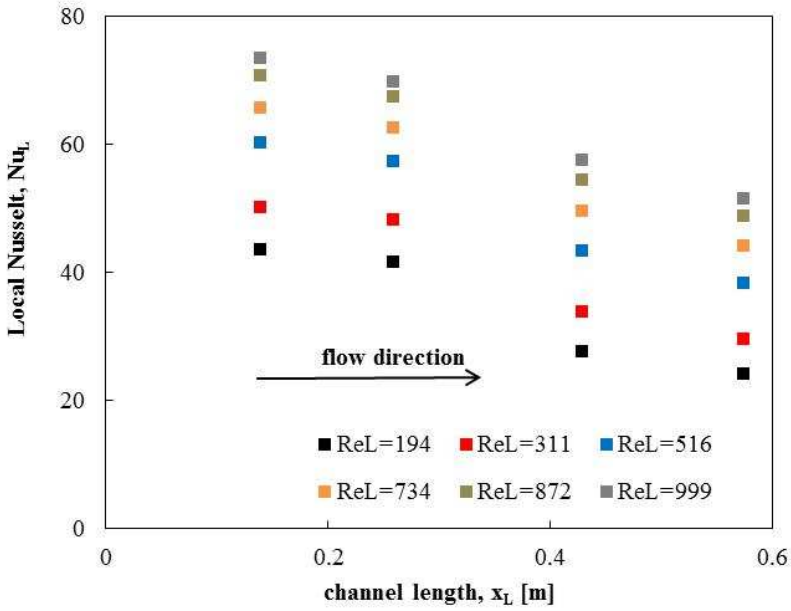


Figure 4.15- Cooling water local Nusselt number variation along channel length (channel 1, section 1), for several Reynolds numbers.

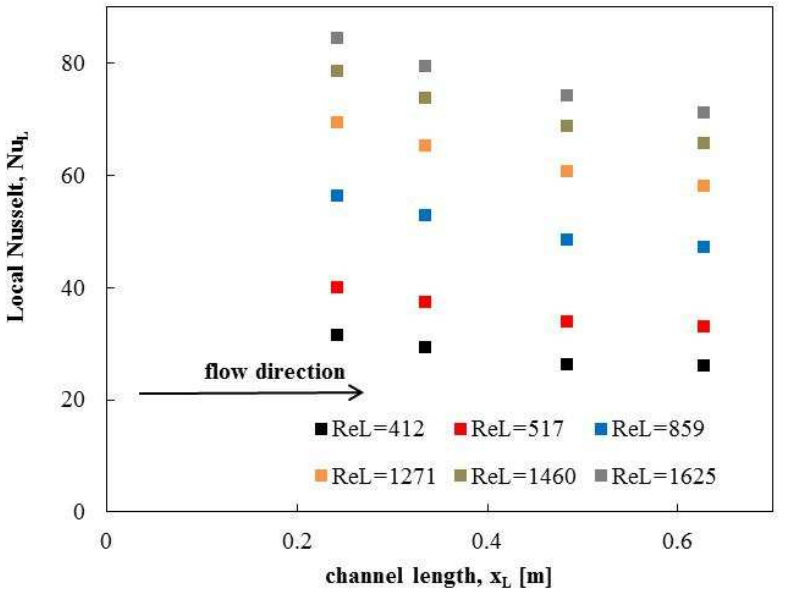


Figure 4.16- Cooling water local Nusselt number variation along channel length (channel 7, section 2), for several Reynolds numbers

From the analysis of Figures 4.15 and 4.16 it is possible to observe that local Nusselt numbers decreased along the channel length in the flow direction, for every Reynolds

numbers analysed. Comparing Figure 4.15 and 4.16 one can observe that in section 1 the decrease of local Nusselt number was more accentuated than in section 2, corroborating the supposition of the existence of a developing thermal boundary layer in section 1.

In section 1, the relative variation of the local Nusselt number between the channel inlet and outlet was 30 to 45%, to higher and lower value of Reynolds number, respectively. Whereas, in section 2, the relative variation of local Nusselt number between the channel inlet and outlet exhibited almost constant value of 17%.

The correlations obtained for local Nusselt number as a function of channel length, for several Reynolds number, in sections 1 and 2, are presented in Table 4.7.

Table 4.7- Local thermal correlation as a function of channel length, for several local Reynolds numbers, in channels 1 and 7.

Channel	**Local Reynolds number, Re [-]**	**Thermal correlations**
1	194	$Nu_L = 19.58 \cdot \mathrm{x}_L^{-0.445},\ r^2 = 0.876$
	311	$Nu_L = 24.73 \cdot \mathrm{x}_L^{-0.394},\ r^2 = 0.878$
	516	$Nu_L = 33.07 \cdot \mathrm{x}_L^{-0.332},\ r^2 = 0.894$
	734	$Nu_L = 38.83 \cdot \mathrm{x}_L^{-0.291},\ r^2 = 0.901$
	872	$Nu_L = 43.35 \cdot \mathrm{x}_L^{-0.27},\ r^2 = 0.905$
	999	$Nu_L = 46.25 \cdot \mathrm{x}_L^{-0.254},\ r^2 = 0.913$
7	412	$Nu_L = 23.05 \cdot \mathrm{x}_L^{-0.217},\ r^2 = 0.961$
	517	$Nu_L = 29.65 \cdot \mathrm{x}_L^{-0.208},\ r^2 = 0.978$
	859	$Nu_L = 42.59 \cdot \mathrm{x}_L^{-0.196},\ r^2 = 0.989$
	1271	$Nu_L = 52.89 \cdot \mathrm{x}_L^{-0.192},\ r^2 = 0.999$
	1460	$Nu_L = 60.14 \cdot \mathrm{x}_L^{-0.187},\ r^2 = 0.999$
	1625	$Nu_L = 65.22 \cdot \mathrm{x}_L^{-0.181},\ r^2 = 0.998$

The thermal correlations obtained in channel 1 (section 1) exhibited a power law dependence on the channel length, the values of the length exponent being in the same

range of those published in the open literature for thermally developing flow (~1/3) (Kakaç and Liu, 2002; Bejan and Kraus, 2003).

In channel 7 (section 2), the values of the length exponent were lower than those obtained in section 1 and varied in a range smaller than in section 1.

Although the former thermal correlations revealed the dependencies of local Nusselt number with the channel length for several Reynolds numbers, the flow effects were not taken into account in those correlations. Therefore, in order to have a proper characterisation of the heat transfer in developing flow along the PHE channels, the local Nusselt number of cooling water was plotted versus the Graetz number (*Gz*), the nondimensional inverse form of axial distance, in the representation of entrance effects on laminar flow heat transfer (Hewitt, Shires *et al.*, 1994b), defined as follows:

$$Gz = \frac{\dot{m} \cdot c_p}{x_L \cdot \lambda} \tag{4.11}$$

where $\dot{m}$, is the mass flow rate, c_p is the specific heat, λ is the thermal conductivity and x_L is the axial distance along the duct.

For the plate heat exchanger channels, the Graetz number was defined as follows:

$$Gz = \frac{w}{2x_L} \cdot Re_L \cdot Pr_L \tag{4.12}$$

where, w is the plate width and x_L is the axial distance along the PHE channel.

The variation of local Nusselt number with Graetz number for cooling water in channel 1 (section 1) is presented in Figures 4.17.

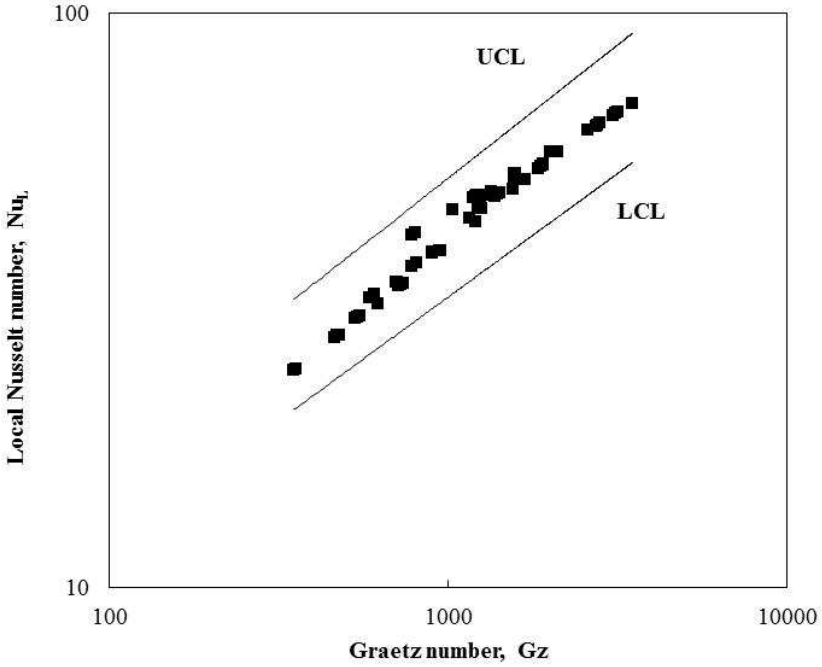


Figure 4.17- Cooling water local Nusselt number versus Graetz number (channel 1, section 1).

Statistical parameters obtained from nonlinear regression analysis carried out in order to obtain the constants C and b in equation (4.13), defined as follows:

$$Nu_L = \mathrm{C} \cdot Gz^b \tag{4.13}$$

The statistical parameters obtained are presented in Table 4.8.

Table 4.8- Statistical parameters obtained by nonlinear regression analysis for channel 1 (section 1).

Parameter	**Estimate**	**Standard error**	**95% confidence interval**	
			lower bound	**upper bound**
C	1.875	0.115	1.644	2.105
b	0.447	0.008	0.430	0.464

Thus, the experimental data, for channel 1 were correlated according to the following equation:

$$Nu_L = 1.875 \cdot Gz^{0.447}, \;\; r^2 = 0.979 \tag{4.14}$$

for 351< *Gz* <3498.

In Figure 4.18 is presented the variation of local Nusselt number with Graetz number for cooling water in channel 7 (section 2).

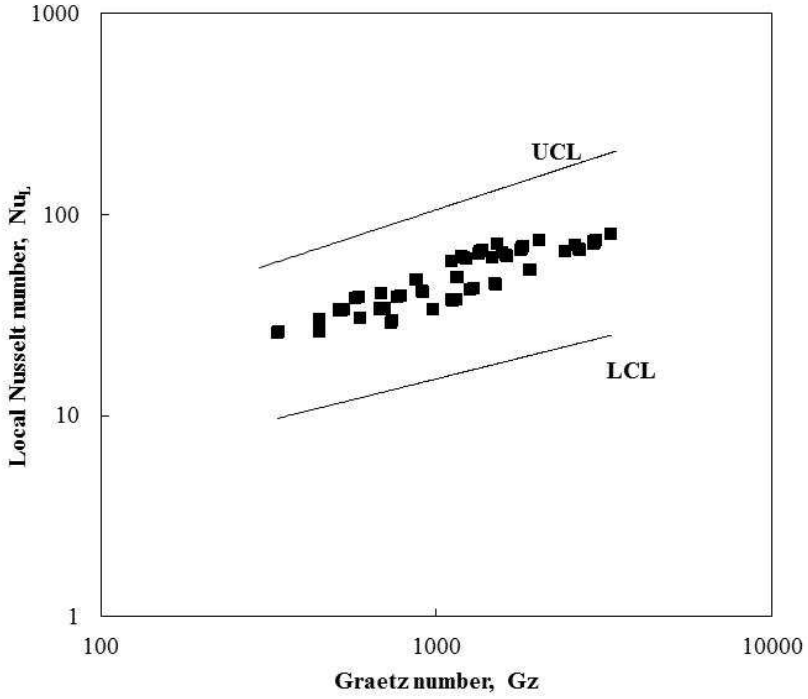


Figure 4.18- Cooling water local Nusselt number versus Graetz number (channel 7, section 2).

Statistical parameters obtained from nonlinear regression analysis carried out with experimental data from channel 7 are presented in Table 4.9.

Table 4.9- Statistical parameters obtained by nonlinear regression analysis for channel 7 (section 2).

Parameter	**Estimate**	**Standard error**	**95% confidence interval**	
			lower bound	**upper bound**
C	1.652	0.394	0.865	2.439
b	0.48	0.032	0.415	0.545

Thus, the experimental data, for channel 7 were correlated according to the following equation:

$$Nu_L = 1.652 \cdot Gz^{0.48}, \quad r^2 = 0.785 \tag{4.15}$$

for 338< *Gz* <3331.

Comparing equations (4.14) and (4.15) one can observe that the thermal correlations obtained for both studied channels are quite similar, although the correlation in channel 7 is not so strong (r^2=0.785), possibly due to more significant turbulence effect that may cause more perturbation in the temperature probes.

Figure 4.19 shows a comparison between the correlations obtained experimentally and correlations published in open literature for thermal entrance region of a parallel-plate channel with Hagen–Poiseuille flow (Bejan and Kraus, 2003; Shah and Sekuli, 2003).

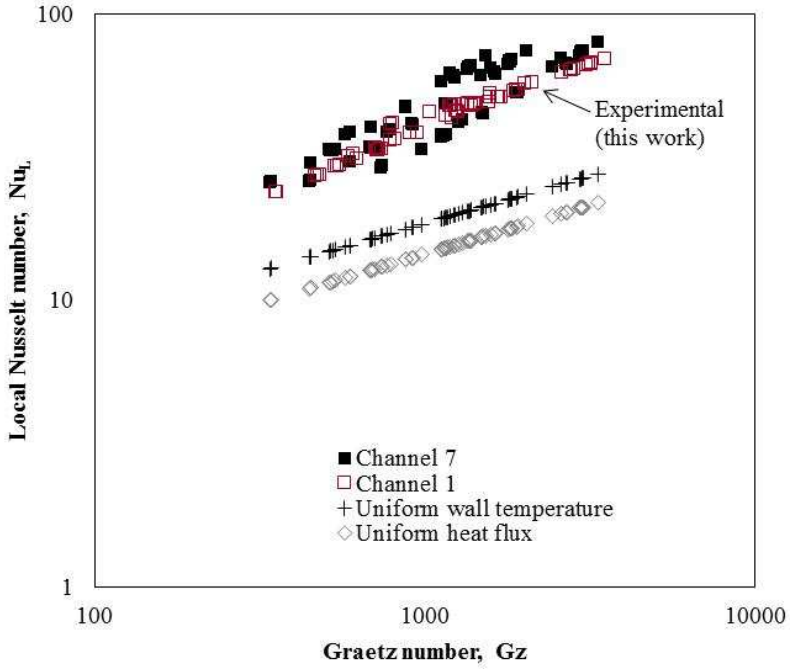


Figure 4.19- Comparison of local heat transfer correlations in the thermal entrance region obtained in the present work and in published in the open literature.

From Figure 4.19 it is possible to confirm what was stated previously regarding to the similarity of the correlations obtained experimentally. Comparing the results obtained with the published correlations for parallel-plate channels, one can observe that the present experimental results have higher values, as expected due to the heat transfer enhancement by the plate corrugations. The published correlations represented two boundary conditions generally used in studies of internal forced convection in ducts: uniform wall temperature and uniform heat flux. These correlations are represented by the following equations:

- uniform wall temperature:

$$Nu_L = 1.849 \cdot Gz^{\frac{1}{3}}, \quad Gz > 2000 \tag{4.16}$$

- uniform heat flux:

$$Nu_L = 1.490 \cdot Gz^{\frac{1}{3}} - 0.40, \quad Gz < 5000 \tag{4.17}$$

The main difference that can be notice between equations (4.16), (4.17) and the equations obtained in the present work is the exponent of the Graetz number that exhibited a value higher than the published ones (1/3) for thermal developing flow. As mentioned previously, higher heat transfer coefficients are obtained in the PHE channels due to channels geometrical effects when compared with flat parallel-plate channels, but also the boundary conditions have an important role. In fact, the boundary conditions in the PHE channel are not typical conditions since both heat flux and wall temperature varied along the channel length.

Notwithstanding the numerous studies carried out with corrugated channels and plate heat exchangers regarding heat transfer, no simplified correlations were reported concerning thermally developing flow in PHE channels.

This experimental study highlighted the effect of variable thermophysical properties usually assumed as constant. The majority of published correlations include a correction factor for constant property correlations in order to comprise the temperature effect on fluid properties. Typically the correction factor consists of a property ratio (usually a viscosity ratio) between the property evaluated at bulk mean temperature and the property evaluated at wall temperature.

The empirical correlations obtained for the determination of local convective heat transfer coefficients of cooling water obtained with variable thermophysical properties, hence no correction factor was included.

4.3.3. Determination of Fanning friction factor correlations

In addition the measurements of fluids and wall temperatures along the plate heat exchanger channels, and fluids temperature at PHE inlets and outlets, the total pressure drop was determined experimentally using pressure transmitters located at both hot and cold fluid sides of the PHE inlet and outlet.

Figure 4.20 presents the friction factors of cooling water and hot water as a function of mean Reynolds number.

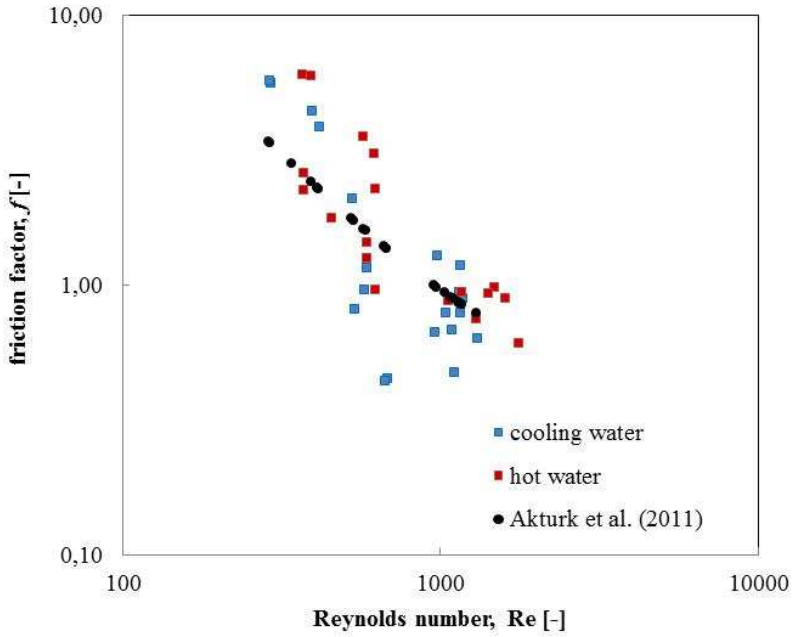


Figure 4.20- Friction factor versus Reynolds number, for cooling water and hot water.

From Figure 4.20 it possible to observe that, despite the data dispersion, the friction factor values of cooling water exhibited the same general tendency of those of hot water. Thus, increasing Reynolds number results in lower friction factor values. The increase of Reynolds number was achieved with higher flow rates which consequently increased pressure drop more than friction factor, due to the power relation with the fluid velocity through the channel more than friction factor, as also remarked by Aktur, Gulben et al. (2011).

The experimental data for cooling water were correlated according to the following equation:

$$f = 9370 \cdot Re^{-1.346}, \ r^2 = 0.741 \quad (4.18)$$

For hot water the experimental data were correlated as follows:

$$f = 1558 \cdot Re^{-1.041}, \ r^2 = 0.657 \quad (4.19)$$

The correlations obtained for Fanning friction factor were compared with correlations published in the open literature for heat exchangers with chevron plates (e.g. (Rene *et al.*, 1991a; Muley and Manglik, 1999; Kakaç and Liu, 2002; Wang and Sundén, 2003)) and a wide range of correlations were observed including effects of corrugations angle, surface enlargement factor. The applicability of these correlations, like the thermal correlations, is limited to the specific parameters and operational conditions.

Figure 4.20 also shows the friction factor values obtained by Aktur, Gulben et al. (2011) with water-water experiments in a PHE with chevron plates (β=30º) which had 0.1416 m^2 expanded heat transfer surface area and related as follows:

$$f = 4291 \cdot Re^{-1.278} + 0.3343 \quad (4.20)$$

The experimental friction factor correlations exhibited similar tendency as the correlation obtained by Aktur, Gulben et al. (2011), as shown in Figure 4.20. These correlations are quite different from those published by (e.g.):

- (Edwards *et al.*, 1974): $f = 34 \cdot Re^{-1.0} + 0.8$ (4.21)
- (Cooper, 1974): $f = 2.5 \cdot Re^{-0.30}$ (4.22)
- (Kakaç and Liu, 2002): $f = \begin{cases} \frac{24}{Re} & Re \leq 2000 \\ 0.1268 Re^{-0.3} & Re > 2000 \end{cases}$ (4.23)

As one can see from the previous examples, the differences observed between correlations are related with geometrical aspects of the chevron plates, the flow arrangement of the heat exchanger, the hydrodynamic regime and fluid properties.

The results obtained enhance the importance of the knowledge of design and operating conditions used in the production of empirical correlations in order to allow a more accurate selection of proper correlations in the analysis of the thermal and hydrodynamic performance of PHEs.

4.4 Conclusions

From the water-water heat transfer experiments results, the following conclusions were drawn:

a) the correlation obtained for the mean convective heat transfer coefficients of cooling water is similar to previous correlations found for turbulent flow in PHE for water-like fluids, and this similarity seems independent of the multipass arrangement, since the dependency of mean Nusselt number on Reynolds number, expressed by Reynolds number exponent is within the range 0.65-0.85 observed for different PHE arrangements with water-like fluids.

b) the fluids and wall temperature profiles along the PHE channels, in both passes of the heat exchanger provide valuable information regarding differentiated local heat transfer in PHE with a multipass arrangement.

c) due to temperature profiles along the PHE channels, the local thermal correlations obtained are variable-property correlations taking into account the temperature effect on the transport properties of the fluids, reducing the errors introduced by the constant – property assumption.

d) the overall heat transfer coefficient varied along the PHE channels, more significantly in section 1 (mean relative variation of U for section 1 was 32.1%), which is the section in the neighbourhood of cooling water inlet in the PHE, where the temperature ranges of both fluids are smaller. In section 2, the section in the neighbourhood of hot water inlet in the PHE, the mean relative variation was 16.0%. One can conclude that not only the overall heat transfer coefficient varies along the PHE but also the U variation is significantly different on both PHE pass.

e) the correlations obtained for the determination of convective heat transfer coefficients of cooling water for each sub-section along the PHE channel reflected the change of flow regime along the PHE. In the correlations obtained, the exponent of Reynolds number increased along the channel length, evidencing the transition to turbulent flow when cooling water flows through PHE from section 1 to section 2.

f) the results of local Nusselt number variation along the channel length highlighted the thermally developing flow along the PHE channels. The Nu-Gz correlations obtained

for both sections of the PHE were similar, exhibiting a higher value of the exponent of the Graetz number than the ones published for thermal developing flow.

g) regarding Fanning friction factor correlations, comparison of the experimental correlations with the available literature showed fair agreement, at least as regards the general trends reported in literature. Discrepancies may be due to differences in compared channels geometries and uncertainties in measurements.

5. DETERMINATION OF MEAN AND LOCAL CONVECTIVE HEAT TRANSFER COEFFICIENTS OF NEWTONIAN AND NON-NEWTONIAN FLUIDS IN A PLATE HEAT EXCHANGER

5.1 Introduction

The improvement of industrial design and optimization of plate heat exchangers is considerable, particularly in food industry domains in which heating and cooling of viscous and non-Newtonian fluids are usual operations, namely in dairy processes.

Fluid foodstuffs are complex in nature and structure and commonly exhibit a non-Newtonian behaviour. In order to gather information concerning heat transfer and hydrodynamic behaviour of non-Newtonian, several studies have been conducted, in the last decades, using different model fluids such as carboxymethylcellulose (CMC), sucrose, sodium alginate, guar-gum and glycerol solutions (e.g. (Metzner, Vaughn *et al.*, 1957; Mahalingam, Tilton *et al.*, 1975; Leuliet *et al.*, 1987; Sourlier, Devienne *et al.*, 1987; Rene *et al.*, 1991a; Carezzato *et al.*, 2007)). These fluids meet a set of criteria needed in heat transfer and hydrodynamic studies such as a wide range of non-Newtonian behaviour, transparency and stability during the thermomechanical treatments (Sourlier *et al.*, 1987).

In particular, research work with non-Newtonian fluids in different types of heat exchangers was carried out in order to study the efficiency of heat transfer, flow resistance, and the pressure capacity (e.g. (Jackson and Troupe, 1964; Edwards *et al.*, 1974; Leuliet *et al.*, 1987; Maingonnat, Leuliet *et al.*, 1987; Edwards, 1988; Leuliet *et al.*, 1990a; Rene *et al.*, 1991a; Leuliet and Maingonnat, 1992; Fernandes *et al.*, 2005b; Carezzato *et al.*, 2007; Fernandes *et al.*, 2008)).

In the present study, heat transfer experiments were conducted using water and aqueous solutions of CMC as working fluid in cold and hot sides of the plate heat exchanger, respectively. The heat experiments were carried out in order to obtain empirical thermal correlations for the determination of mean and local convective heat transfer coefficients for aqueous solutions of CMC with rheological behaviour varying

from viscous Newtonian fluids to non-Newtonian pseudoplastic fluids, obtained by preparation of aqueous solutions of CMC with different concentrations.

5.2 Experimental methodology

This chapter presents all the results obtained in the CMC/ water heat transfer experiments conducted in order to obtain accurate thermal correlations for the determination of both mean and local heat transfer coefficients of CMC aqueous solutions in a PHE with chevron plate (β=35º/35º) with a multipass configuration 2×2/2×2 in countercurrent.

The CMC solutions (CMC WALOCEL CRT 1000 GA from Wolff Cellulosics GmbH & Co, Germany) were prepared following the procedure described in section 3.7.2. The concentrations studied were 0.25, 1.0 and 2.0% (w/w).

5.2.1 Thermophysical properties

The rheology of 0.25% (w/w) CMC solution was determined by viscometry following the procedure described in section 3.5.2, since this solution was a water-like solution. The temperature dependence of the dynamic viscosity of this solution was evaluated by measuring the viscosity at different temperatures between 20-45ºC. The experiments were performed using a FUNGILAB S.A. VISCO STAR Plus L viscometer using spindle PA.

The rheological properties of 1.0% and 2.0% CMC solutions were determined by oscillatory shear rheometry (section 3.5.1), performing frequency sweeps in the 0.01-10 Hz range and the oscillation stress was fixed at 1.0 Pa. The temperature dependence of dynamic viscosity was determined by steady shear (shear stress and shear rate) data were obtained over the shear rate range of 0.001–100 s^{-1} at different temperatures (20–40ºC). The experiments were performed using a TA Instruments AR-G2 StressTech controlled-stress rheometer with 40 mm diameter parallel plate geometry (P 40 ETC) at 1.0 mm measuring gap distance.

The temperature dependence of the density at different concentration of CMC solution was determined by means of the empirical model developed by Cancela, Álvarez et al. (2005).

The temperature dependence of the specific heat at different concentration of CMC solution was determined by means of the empirical model developed by Semmar, Tanguier et al. (2003).

For the thermal conductivity, the temperature dependence at different concentration of CMC solutions was determined taking into account the data published in the open literature (Rohsenow, Hartnett *et al.*, 1998; Carezzato *et al.*, 2007).

5.2.2 Heat transfer experiments

The heat experiments in the plate heat exchanger with CMC solutions were carried out according to the procedures described in sections 3.7.1 and 3.7.2.

In the experiments, the CMC solutions flow rate varied between 0.03 kg/s and 0.17 kg/s, for 0.25% CMC solutions, between 0.04 and 0.27 kg/s for 1.0% CMC solutions and between 0.05 and 0.11 kg/s for 2.0% CMC solutions. The cooling water flow rate varied in the range of 0.18 and 0.28 kg/s.

The inlet cold water temperature varied between 10-25ºC and those of CMC solutions entries between 45-20ºC (mean ranges).

Table 5.1 shows the ranges of Reynolds and Prandtl numbers used for each set of CMC concentration.

Table 5.1- Reynolds number and Prandtl number ranges of CMC solutions and cooling water, for each concentration used.

% CMC	**CMC Reynolds number range [-]**	**CMC Prandtl number range [-]**	**Cooling water Reynolds number range [-]**	**Cooling water Prandtl number range [-]**
0.25	2.6-19.6	294-374	662-1115	7.6-12.5
1.0	4.0-37.3	219-402	955-1300	7.0-9.5
2.0	1.2-4.0	878-1423	1285-1321	7.4-7.6

The mean heat transfer coefficients of CMC solutions were calculated according to procedures described in section 3.8.1., having in consideration the following assumptions: average constant thermal properties (thermal conductivity and specific heat) and convective heat transfer coefficients along the heat exchanger, negligible internal heat generation, negligible axial convection or conduction and negligible free convection. Nonlinear regression analysis was performed using the Levenberg–Marquardt method for minimizing the sum of squared residuals function (section 3.9) in order to obtain a thermal correlation.

The local heat transfer coefficients of CMC solution were calculated according to procedures described in section 3.8.2., considering the experimentally two monitored sections of the PHE. Each section was divided in four sub-sections in order to determine four local overall heat transfer coefficients along the PHE controlled plates. Therefore, the variation of the local overall heat transfer coefficients as well as of the local convective heat transfer coefficients of the CMC solution along the PHE was determined, considering the temperature effect on the thermophysical properties of both fluids. The local heat transfer coefficients were calculated from the four correlations obtained by nonlinear regression analysis, as referred to section 3.9.

5.3 Results and Discussion

5.3.1. Rheological behaviour

Newtonian fluids

Figure 5.1 shows the viscometry data obtained for 0.25% CMC solution, at a constant spindle speed rotation (12 rpm), for different fluid temperatures.

From the analysis of Figure 5.1, one can observe that the 0.25% CMC solution exhibited a non-time-dependent rheological behaviour and an approximately constant viscosity for each temperature. At 20ºC, the 0.25% CMC solution exhibited an average viscosity of 50.3 mPa.s, 45.2 mPa.s at 30ºC, 40.3 mPa.s at 40ºC and 38.3 mPa.s at 45ºC. The results are in agreement with reported Newtonian behaviour of low concentrations CMC solutions evaluated by Béreiziat and Devienne (1999). The viscosity values of 0.25% CMC solutions are up to 10 times higher than the viscosity of water, at different temperatures.

It is here assumed that the temperature dependence of the viscosity of 0.25% CMC solution follows an Arrhenius temperature model, in which the apparent viscosity decreases exponentially with temperature:

$$\boldsymbol{\eta = A \cdot e^{E/RT}} \tag{5.1}$$

where η is the viscosity (Pa s), A a constant (Pa s), T the absolute temperature (K), R the gas constant (8.3144 J/mol K) and E the activation energy (J mol-1).

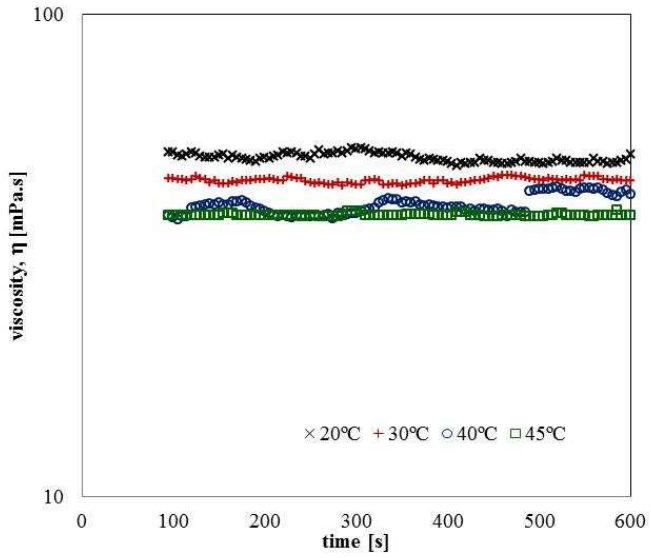


Figure 5.1- Viscosity data obtained of 0.25% CMC solution, at a constant spindle speed rotation (12 rpm), for different fluid temperatures.

The study of the temperature influence on the viscosity of 0.25% CMC solution was based on the method previously reported (see details in (Afonso *et al.*, 2003)), which follows the method proposed by Mendelson to predict the flow behaviour, at different temperatures. The displacement factor is mathematically defined as:

$$a_T = \frac{\eta(reference)}{\eta\,(T)} \tag{5.2}$$

where η(reference) is viscosity at a reference temperature and η(T) is the viscosity at a determined temperature. The displacement factor dependency on temperature can be observed in Figure 5.2 for temperatures within the range studied (20-45ºC), the activation energy is 8524 $Jmol^{-1}$. This energy value measures the material´s sensitivity to temperature changes (Afonso and Maia, 1999).

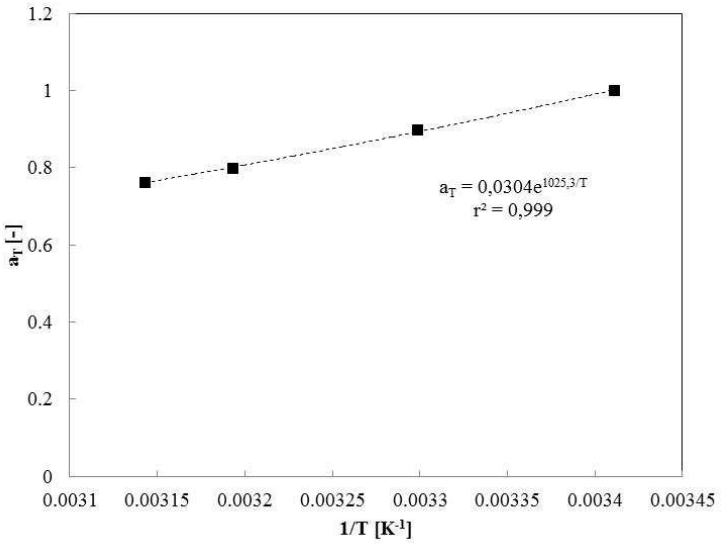


Figure 5.2- Displacement factor dependency on temperature of the 0.25% CMC solution.

These results were applied in the heat transfer analysis of CMC solutions cooling the PHE set-up.

The CMC solution viscosity at a determined temperature can be calculate as follows:

$$\eta(T) = \eta(reference) \cdot e^{\frac{E}{R}\left(\frac{1}{T}-\frac{1}{Tref}\right)} \quad (5.3)$$

where T_{ref} is the reference temperature defined as 20ºC in this experiments set.

Non-Newtonian fluids

Figure 5.3 shows the viscometry data obtained for 1.0% CMC solution, at a constant spindle speed rotation (12 rpm), for different fluid temperatures.

In Figure 5.3, one can observe that the 1.0 % CMC solution exhibited a non-time-dependent rheological behaviour and an approximately constant viscosity for each temperature. At 20ºC, the 0.25% CMC solution exhibited an average viscosity of 113.3 mPa.s, 90.52 mPa.s at 30ºC and 38.77 mPa.s at 40ºC.

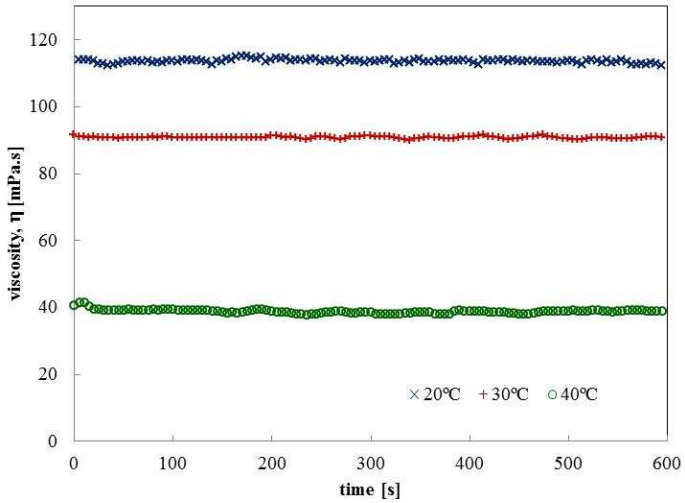


Figure 5.3- Viscosity data obtained of 1.0% CMC solution, at a constant spindle speed rotation (12 rpm), for different fluid temperatures.

Following the same procedure described for 0.25% CMC solution, the temperature dependence of the displacement factor was determined as shown in Fig. 5.4. For temperatures within the range studied (20-40ºC), the activation energy is 40650 $Jmol^{-1}$.

Further tests were performed in order to characterise the rheological behaviour of the 1.0% CMC solution, since the solution exhibited some thickening and the viscous Newtonian behaviour was not in agreement with the results obtained by Béreiziat and Devienne (1999) and Carezzato, Alcantara et al. (2007) that observed a non-Newtonian and pseudoplastic behaviour for 1.0% CMC solutions. Therefore, frequency sweeps were performed in order to gather more information concerning fluid structure.

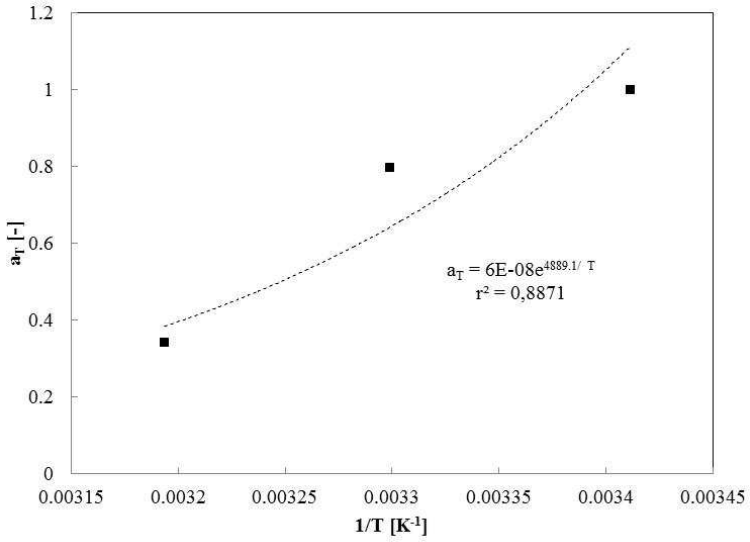


Figure 5.4- Displacement factor dependency on temperature of the 1.0% CMC solution.

Figure 5.5 shows the mechanical spectrum for 1.0% CMC solution at 20ºC in the linear domain (τ=1.0 Pa).

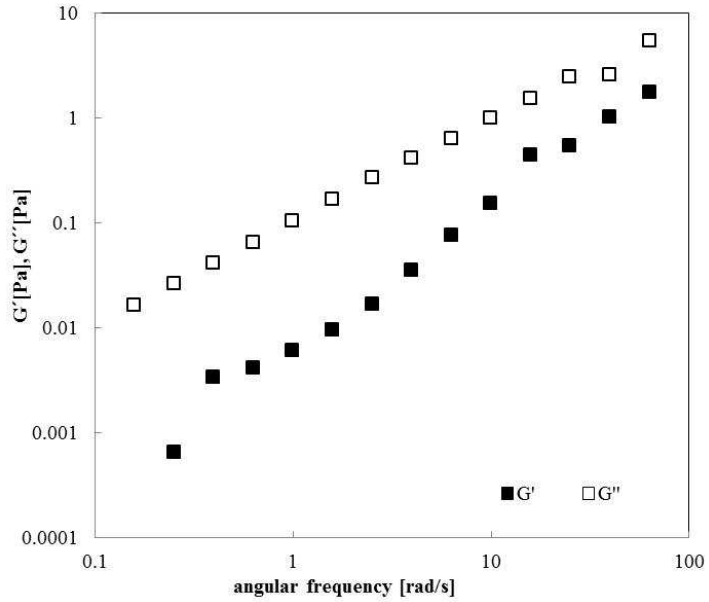


Figure 5.5- Mechanical spectrum for 1.0% CMC solution in the linear domain (τ=1.0 Pa), at 20ºC.

In the mechanical spectrum presented in Figure 5.5 one can observe that the magnitudes of storage modulus (G´) and loss modulus (G´´) increased with the increase in angular frequency($\dot{\omega}$). The loss modulus (G´´) which describes the viscous properties of the fluid is much higher than the storage modulus (G´) which indicates that the 1.0 % CMC solution behaves like a viscous liquid. These results are in good agreement with the ones obtained by Benchabane and Bekkour (2008) in their work with CMC solutions with a concentration range from 0.2 to 7.0% (wt) which revealed that at low CMC concentrations, the viscous properties were dominant compared to the elastic ones, i.e. G´´>G´. This is also in some extent in agreement with the results obtained by Bayarri, González-Tomás et al. (2009) in the study of influence of added CMC solutions in the viscoelastic properties of aqueous and milk systems.

From the oscillatory shear experiments, the dynamic viscosity (η´) was obtained, shown in Figure 6.6 and defined as follows (Chhabra and Richardson, 2008):

$$\eta' = \frac{G''}{\omega} \tag{5.4}$$

where G'' (Pa) is the loss modulus and ($\dot{\omega}$) is the angular frequency (rad s^{-1}).

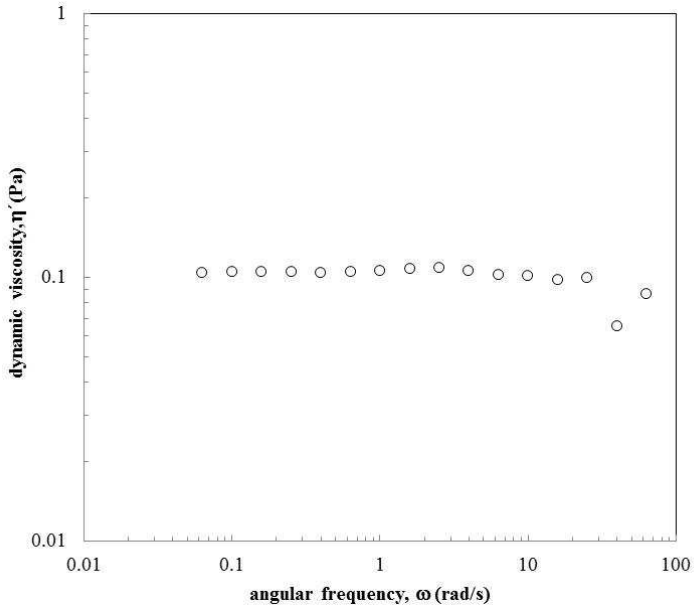


Figure 5.6- Dynamic viscosity as a function of angular frequency, at 20ºC, for 1.0% CMC solution.

From Figure 5.6 it is possible to verify that the dynamic viscosity exhibited almost no variation with the angular frequency corroborating the results obtained by viscometry. Fitting a power law equation to the plotted results the following equation was obtained:

$$\eta' = 0.103 \cdot \dot{\omega}^{-0.03} \tag{5.5}$$

where 0.103 is the value of the consistency index, k (Pa s^n) and (-0.03) is the value of (n-*1*), as written in equation:

$$\eta' = k \cdot \dot{\omega}^{n-1} \tag{5.6}$$

where n represents the flow behaviour index (-). Therefore, for 1.0% CMC solution the structure index has a value of 0.97, evidencing a very weak shear-thinning behaviour, as reported by Béreiziat and Devienne (1999), Ghannam and Esmail (1997) and Cancela, Álvarez et al. (2005), in which the flow behaviour index varied in the range of 0.84 to 0.95 and the consistency index varied between 0.05 to 0.08. Carezzato, Alcantara et al. (2007) in their study with heat transfer with non-Newtonian fluids using CMC solutions as test fluids reported 1.0% CMC solution with a strong shear-thinning behaviour ($n<0.4$ at 20ºC), these differences in the rheological behaviour can be explained by distinct degrees of polymerization (average number of anhydroglucose units per molecule) and degrees of substitution (average number of carboxymethyl groups per anhydroglucose unit) closely related to state of aggregation or molecular structure of CMC, which is reflected in the rheological behaviour of its solutions (Elliot and Ganz, 1974).

For 2.0% CMC solutions a similar rheological characterisation was carried out although the temperature dependence of dynamic viscosity was determined by steady shear rheometry.

In Figure 5.7 are shown the flow curves of 2.0% at different temperatures, where it is possible to observe that the apparent viscosity decreased with increasing temperature. For all temperatures the 2.0% CMC solution exhibited a non-Newtonian and shear-thinning behaviour. Applying the shear rate-temperature superposition method (see, for example, (Macosko, 1994)), whereby a correspondence between data obtained under certain experimental conditions, i.e., certain shear rate and temperature ranges, can be

used to predict the flow behaviour of the material at other equivalent ones, at the same shear stress (Afonso and Maia, 1999).

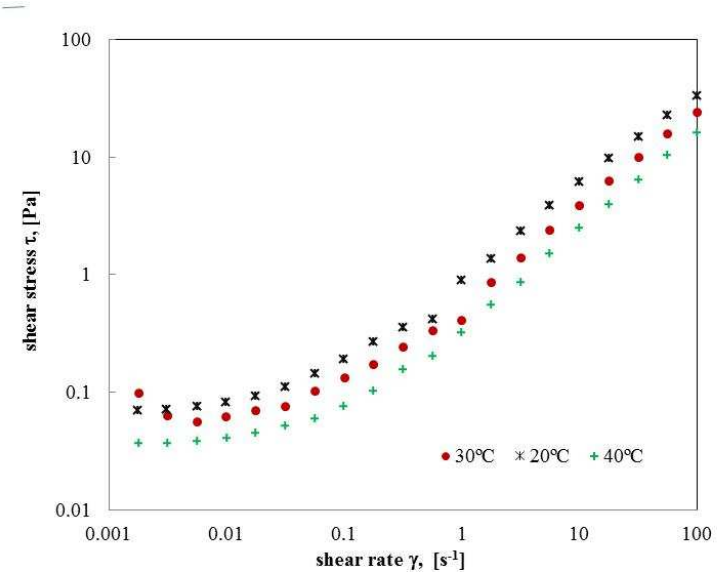


Figure 5.7- Flow curves of the 2.0% CMC solution, as a function of temperature.

The displacement factor is mathematically defined as:

$$a_T = \frac{\dot{\gamma}(reference)}{\gamma(\dot{T})} \tag{5.7}$$

where $\dot{\gamma}(reference)$ is the shear rate at the reference temperature, at a defined shear stress and $\dot{\gamma}(T)$ is the shear rate at a determined temperature T, at the same shear stress.

The displacement factor dependency on temperature can be observed in Figure 5.8. For temperatures within the range studied (20-40ºC), the activation energy is 47180 $Jmol^{-1}$. The material´s sensitivity to temperature changes for 2.0% CMC solution is identical to the one observed with a concentration of 1.0%.

Figure 5.9 shows the mechanical spectrum for 2.0% CMC solution at 20ºC in the linear domain (τ=1.0 Pa).

In the mechanical spectrum presented in Figure 5.9 one can notice the strong frequency dependence of dynamic moduli, the magnitudes of storage modulus (G´) and loss modulus (G´´) increased with the increase in angular frequency($\dot{\omega}$), as previously observed with 1.0% CMC solution.

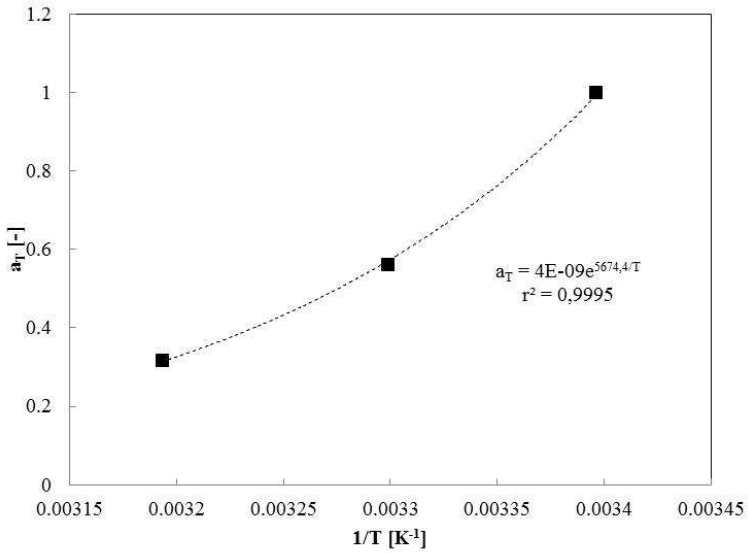


Figure 5.8- Displacement factor dependency on temperature of the 2.0% CMC solution.

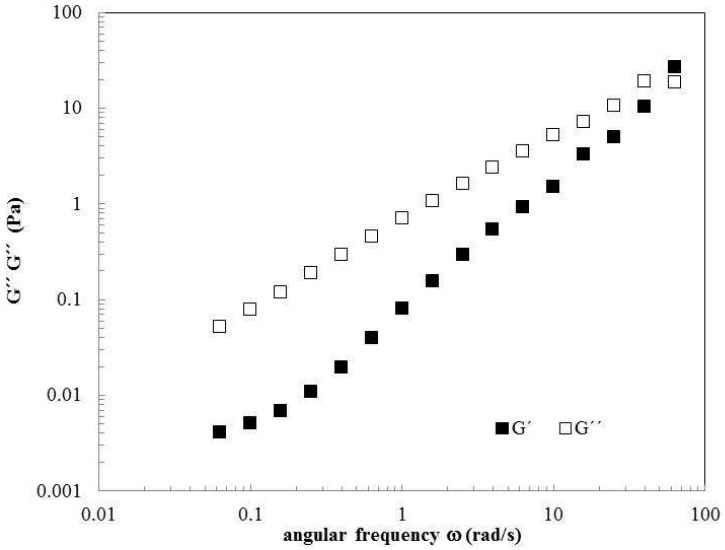


Figure 5.9- Mechanical spectrum for 2.0% CMC solution in the linear domain (τ=1.0 Pa), at 20ºC.

In the whole frequency range scanned, it is observed that viscous component exceeded the elastic one indicating that the CMC solution behaved as an entangled polysaccharide solution. These results corroborate the ones obtained by Florjancic, Zupancic et al. (2002) in their study on the evaluating of synergistic/non-synergistic effects of mixed compatible biopolymers systems, using CMC and xanthan.

At higher oscillation frequencies it is observed a shift in the relation between the viscous and the elastic moduli, in which the G´ became slightly higher than G´´, behaving like a viscous solid. Benchabane and Bekkour (2008) in their study on the rheological properties of CMC solutions noticed that CMC solutions exhibited concentration-dependent viscoelastic properties, with a dominant viscous behaviour at lower CMC concentrations and dominant elastic behaviour at CMC concentrations higher than 2.5% wt.

Figure 5.10 shows the frequency dependence of dynamic viscosity (η´) of 2.0% CMC solution, at 20ºC.

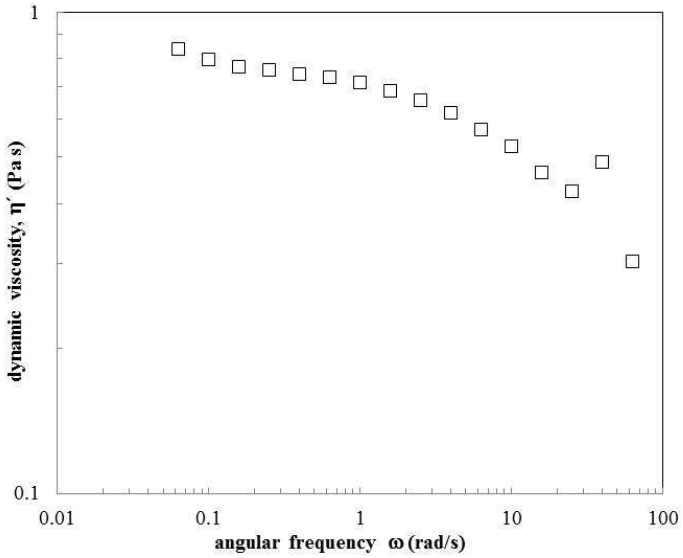


Figure 5.10- Dynamic viscosity as a function of angular frequency, at 20ºC, for 2.0% CMC solution.

From Figure 5.10 one can verify that the dynamic viscosity decreased with increasing of the angular frequency corroborating the results obtained by steady shear rheometry, in which the shear-thinning was evidenced. Fitting a power law equation to the plotted results the following equation was obtained:

$$\eta' = 0.660 \cdot \dot{\omega}^{-0.121} \tag{5.8}$$

where 0.660 is the value of the consistency index, *k* (Pa s^n) and (-0.121) is the value of (*n-1*). Thus, for 2.0% CMC solution the flow behaviour index has a value of 0.879, evidencing a shear-thinning behaviour, as reported by Béreiziat and Devienne (1999), Ghannam and Esmail (1997) and Cancela, Álvarez et al. (2005), in which the flow

behaviour index varied in the range of 0.69 to 0.85 and the consistency index varied between 0.45 and 1.23.

With the results obtained from steady shear and oscillatory shear rheometry it was verified the applicability of the Cox-Merz empirical rule, presented in Figure 5.11.

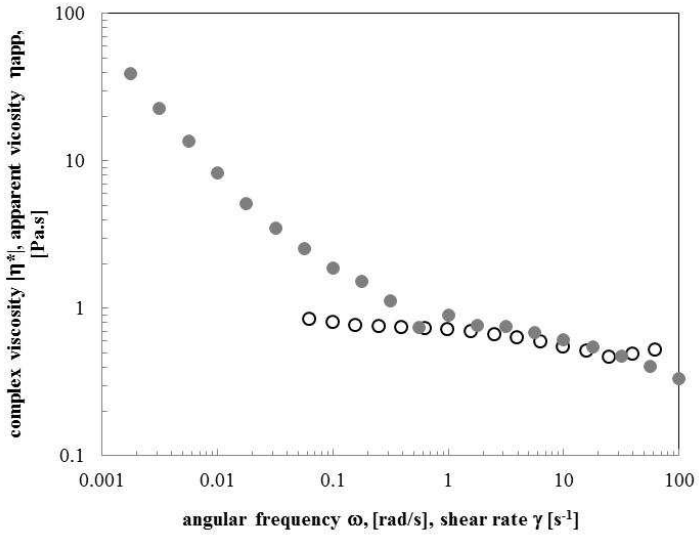


Figure 5.11- The Cox-Merz superposition of shear viscosity versus shear rate and complex viscosity versus oscillation frequency for 2.0% CMC solution, at 20ºC (closed symbol: η_{app}, open symbol: η*).

The theoretical basis of Cox-Merz rule is that the dynamic viscosity and the steady state viscosity are related in the low frequency and shear rate limits (Malkin and Isayev, 2006):

$$\dot{\eta}(\omega)|_{\omega\to 0} = \eta(\dot{\gamma})|_{\gamma\to 0} \tag{5.9}$$

where $\dot{\eta}$ is defined by equation 5.4. At low frequencies, the elastic contribution of η´(ω) disappears and equation (5.9) can be rewritten as:

$$\eta^*(\omega)|_{\omega\to 0} = \eta(\dot{\gamma})|_{\gamma\to 0} \tag{5.10}$$

where η* is the complex viscosity defined as follows:

$$\eta^* = \eta'(\omega) - i\eta''(\omega) \tag{5.11}$$

where $\eta''(\omega)$ is out-of-phase viscosity, or imaginary part of the complex viscosity (Malkin and Isayev, 2006).

From Figure 5.11 one can observe that the 2.0 % CMC solution obeys the Cox-Merz rule as observed for entanglement polymer solutions and verified by other authors (Florjancic *et al.*, 2002; Kim and Yoo, 2006).

The Cox-Merz rule can be used to compare and predict the steady shear properties of a material from the dynamic rheological properties obtained without extensive alteration of structures (Kim and Yoo, 2006).

5.3.2. Determination of the mean convective heat transfer coefficients of CMC solutions

Newtonian behaviour

As previously mentioned, for each heat experiment, temperatures of both hot and cold fluid sides of the PHE inlet and outlet were monitored and registered as mentioned in section 3.2.2.

Figure 5.12 shows an example of PHE inlet and outlet temperatures during an CMC/ water experiment carried out with a 0.25% CMC solution, in which it is possible to observe that temperatures became steady about one to two minutes after the beginning of the heat transfer experiment. Such as in water/ water experiments, the transient period observed in the temperature profiles was neglected for calculation purposes.

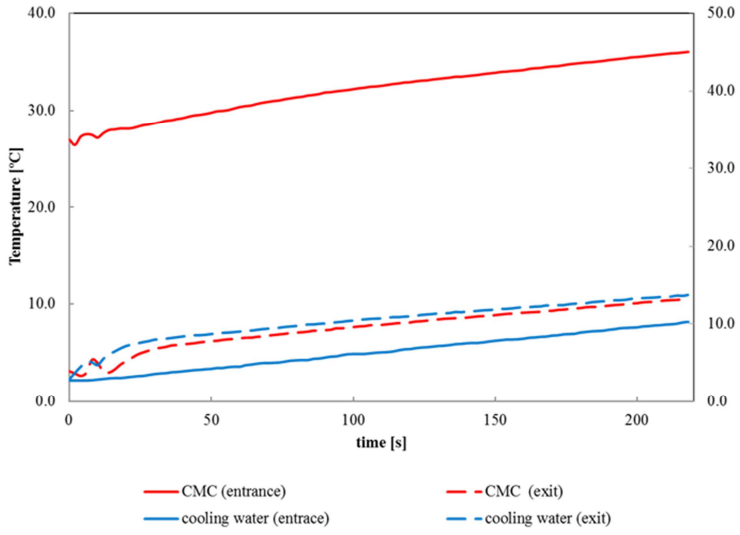


Figure 5.12- PHE ports temperatures (entrance/exit) along experiment time of each fluid, in 0.25%CMC solution / water experiment (Re_{CMC}=2.56).

From the experimental data (temperatures of both CMC and cold water sides of the PHE inlet and outlet, mass flow rates of both fluids) the heat flow transferred to cooling water and the heat flow transferred from warm CMC solution was determined. In these experiments the flow rate of cooling water was kept almost constant at maximum power of the centrifuge pump used in the set-up. Different process conditions were obtained by varying temperature of the inlet fluids and the flow rate of CMC solution. The criterion of data acceptance used in water/ water experiments was applied in this set of experiments. Thus, data were accepted only if the deviation between heat transfer rates from the hot and cold sides were less than 20%.

Table 5.2 shows the values of the heat transfer rates in each experiment for different Reynolds numbers. Differences between the rates of heat transfer to the cold water and from the warm 0.25% CMC solution can be observed in Table 5.2, evidencing the existence of some heat exchange with the surrounding air. The mean value of heat losses percentage was 11%.

Table 5.2- Average values of heat transfer rate transferred to cooling water (Q_{cw}), heat transfer rate transferred from CMC solution (Q_{CMC}) and Reynolds numbers of 0.25% CMC solution (Re_{CMC}), for each experiment.

% CMC solution	**Reynolds number, Re_{CMC} [-]**	**Heat transfer rate, Q_{cw} [W]**	**Heat transfer rate, Q_{CMC} [W]**
0.25	2.9	3685	4097
	4.3	4825	5360
	7.0	9611	10816
	6.8	9248	10467
	2.6	3225	3632
	10.2	11357	12878
	19.6	17817	21562
	2.7	3220	3341
	6.2	5893	6390
	14.7	8904	10161

As previously discussed for water/ water experiments, due to the differences observed in the heat rates exchanged between the two fluids, a criterion was established so that the overall heat transfer coefficients were determined from the data measured on the cooling water side. The overall heat transfer coefficients were obtained by equation 3.9 (section 3.8.1.).

From the results presented in Table 5.2 and Table A.5 (Annex A), by following the calculation procedures described in section 3.8.1., it was obtained the relation between the mean Nusselt number and Reynolds number for 0.25% CMC solution, as shown in Figure 5.13.

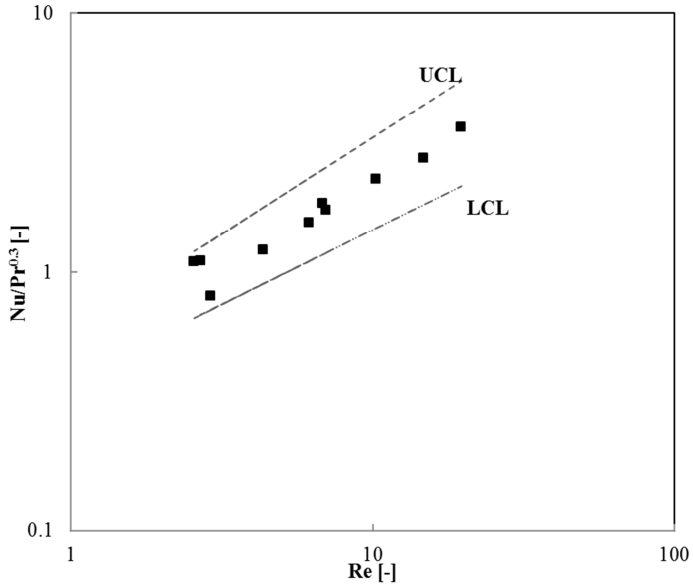


Figure 5.13- Thermal correlation for the mean convective heat transfer coefficient of the 0.25% CMC solution, as a function of the Reynolds number.

The statistical parameters obtained from nonlinear regression analysis are presented in Table 5.3. The values obtained were applied in equation (3.22), defined as follows:

$$Nu = aRe^{b}Pr^{c}$$

Table 5.3- Statistical parameters obtained by nonlinear regression analysis.

Parameter	**Estimate**	**Standard error**	**95% confidence interval**	
			lower bound	**upper bound**
a	0.493	0.045	0.389	0.596
b	0.661	0.037	0.575	0.746

Therefore, the experimental data were correlated according to the following equation:

$$Nu = 0.493 \cdot Re^{0.661} \cdot Pr^{0.3}, \quad r^{2} = 0.978 \tag{5.12}$$

for 2.6<*Re*<19.6 and 294<*Pr*<374.

The temperature dependence of the viscosity was taken into account in the calculation of the Reynolds and Prandtl number, replacing the viscosity term by equation (5.3).

In Figure 5.13, the confidence limits slopes obtained by nonlinear regression analysis are shown. The confidence interval obtained for the constant *a* in equation (3.22) is 0.389-0.596 ($P<0.05$). For Reynolds number exponent, on obtained a lower (LCL) and upper (ULC) confidence limits ($P<0.05$) of 0.575 and 0.746, respectively.

In Figure 5.14 is shown a comparison between the correlation obtained experimentally for 0.25% CMC solution with a viscous Newtonian behaviour and other published correlations for Newtonian and non-Newtonian fluids, e.g. (Edwards, 1988; Rene *et al.*, 1991a; Warnakulasuriya and Worek, 2008).

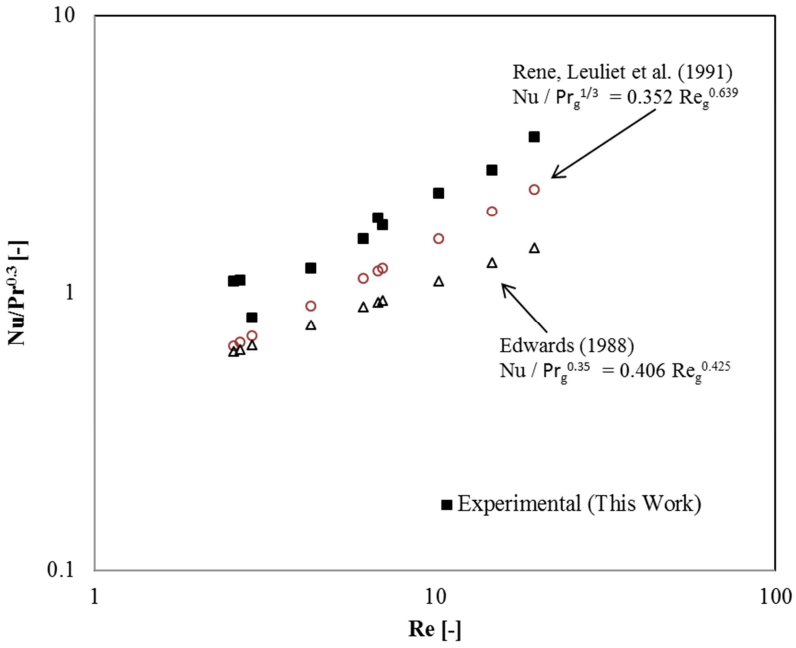


Figure 5.14- Comparison among obtained and published thermal correlations, for viscous Newtonian fluids.

The reference correlations used in the comparison were obtained in plate heat exchangers with water and sucrose solutions as Newtonian fluids , and CMC, sodium alginate solutions as non-Newtonian fluids, countercurrent flow condition, with chevron type plates.

The correlation obtained here for 0.25% CMC solution is similar to correlations found for turbulent flow in PHE in which the Reynolds number exponent approaches value of about 2/3, which is typical of most typical of most turbulent flows even at relatively low Reynolds numbers (Edwards, 1988; Rene *et al.*, 1991a). The plate corrugations induce turbulence at low values of the Reynolds number compared to pipe flow (Edwards *et al.*, 1974; Kuppan, 2000).

Figure 5.15 shows the plots of experimental and predicted overall heat transfer coefficients as function of Reynolds number of 0.25% CMC solution.

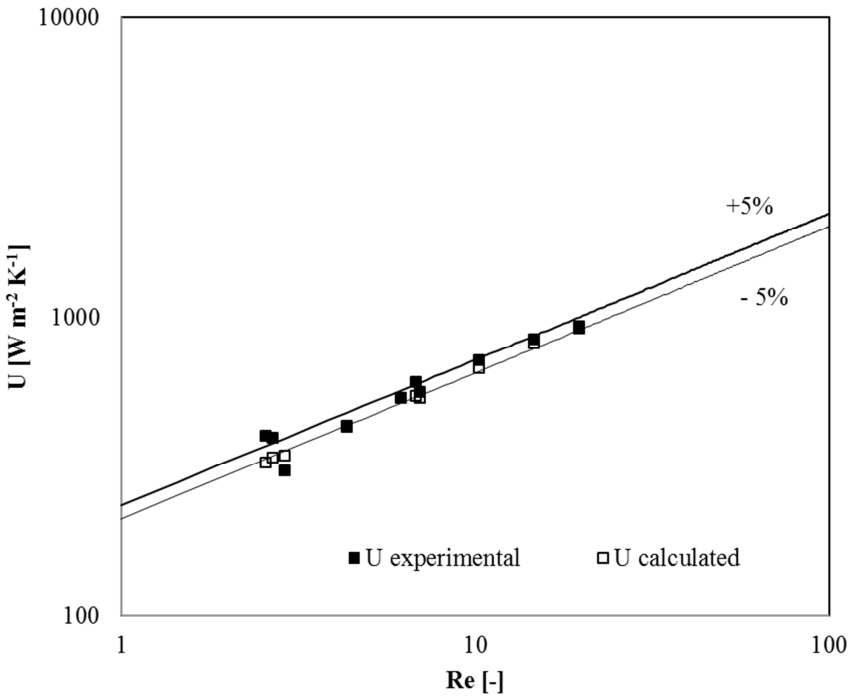


Figure 5.15- Experimental and predicted overall heat transfer coefficients as a function of Reynolds number of 0.25% CMC solution.

From Figure 5.15 it is possible to observe that an accurate correlation for the determination of mean heat transfer coefficients of 0.25% CMC solution, representative of viscous Newtonian fluids, was obtained since the predicted overall heat transfer coefficients were calculated with a mean relative error of less than 7%.

The correlation obtained can be applied in further studies of the heat transfer using viscous Newtonian fluids in this plate heat exchanger with these flow arrangements.

Non-Newtonian behaviour

The CMC/ water heat transfer experiments, accomplished with CMC solutions with concentrations of 1.0% and 2.0% (w/w), were carried out following the same procedures previously mentioned for the Newtonian 0.25% CMC solution.

Figures 5.16 and 5.17 show an example of PHE inlet and outlet temperatures during a CMC/ water experiments carried out with a 1.0% and 2.0% CMC solutions, respectively.

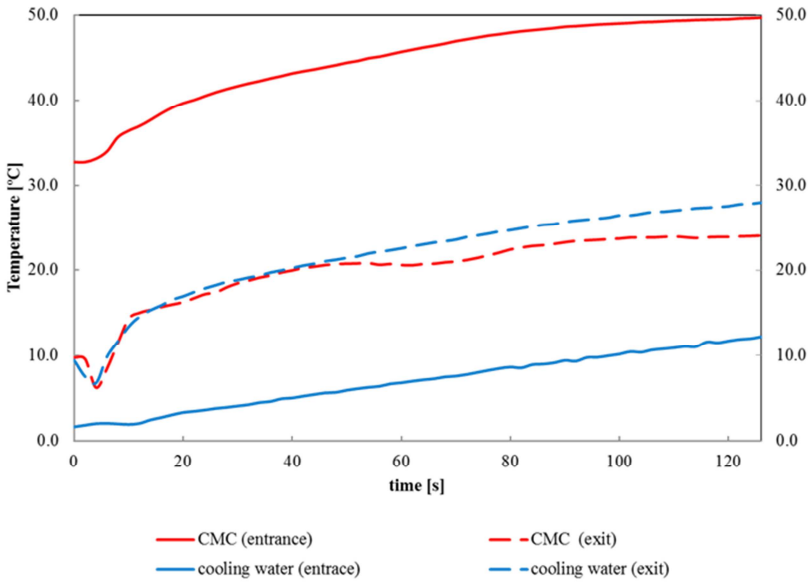


Figure 5.16- PHE ports temperatures (entrance/exit) along experiment time of each fluid, in 1.0% CMC solution / water experiment (Re_{CMC}=23.5).

In Figures 5.16 and 5.17 it is possible to observe that temperatures became steady about one minute after the beginning of the heat transfer experiment. Such as in water/ water experiments, the transient period observed in the temperature profiles was neglected for calculation purposes.

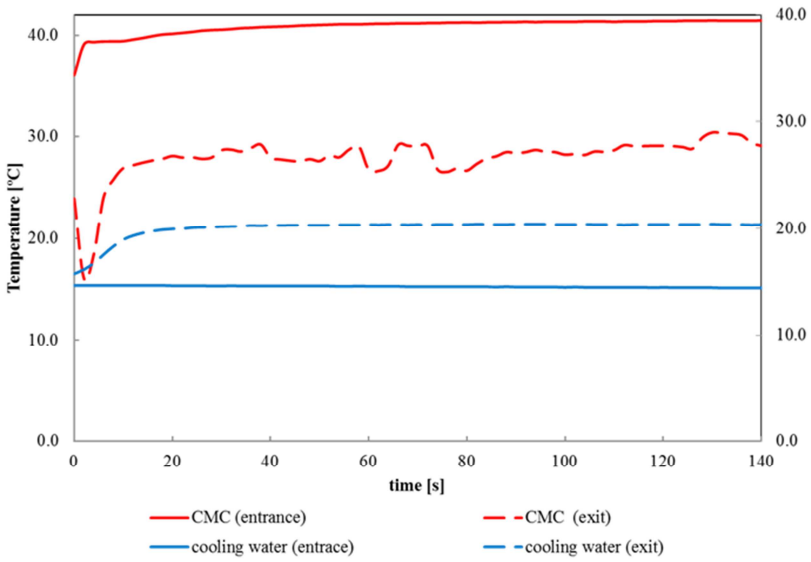


Figure 5.17- PHE ports temperatures (entrance/exit) along experiment time of each fluid, in 2.0% CMC solution / water experiment (Re_{CMC}= 4.0).

From the experimental data it was determined the heat flow transferred to cooling water and the heat flow transferred from warm CMC solutions. Data were accepted only if the deviation between heat transfer rates from hot and cold sides were less than 20%.

Table 5.4 shows the values of the heat transfer rates in each experiment for different Reynolds numbers, for 1.0% and 2.0% CMC solutions.

Differences between the rates of heat transfer to the cold water and from the warm 1.0% and 2.0% CMC solutions can be observed in Table 5.4, evidencing the existence of some heat exchange with the surrounding air. The mean value of heat losses percentage was 17% and 13% for 1.0% CMC and 2.0% CMC heat experiments, respectively.

From the results presented in Table 5.4 and Table A.5 (Annex A), by following the calculation procedures described earlier, it was possible to obtain the relation between the mean Nusselt number and Reynolds number for CMC solution, as shown in Figure 5.18 and Figure 5.19 for 1.0% CMC and 2.0% CMC solutions, respectively.

Table 5.4- Average values of heat transfer rate transferred to cooling water (Q_{cw}), heat transfer rate transferred from CMC solution (Q_{CMC}) and Reynolds numbers of CMC solution (Re_{CMC}), for each experiment at different % CMC solution.

% CMC solution	Reynolds number, Re_{CMC} [-]	Heat transfer rate, Q_{cw} [W]	Heat transfer rate, Q_{CMC} [W]
1.0	4.7	7029	8675
	15.1	11237	13761
	6.3	7953	10923
	12.4	10168	12722
	20.4	10899	13815
	23.5	16635	19241
	26.4	16183	17201
	37.3	18070	21199
	35.3	20626	23352
2.0	1.5	2907	4090
	2.5	3767	5365
	4.0	6029	5512
	1.2	3136	2546
	1.9	4055	3609
	2.4	4607	4301
	3.1	5184	4673

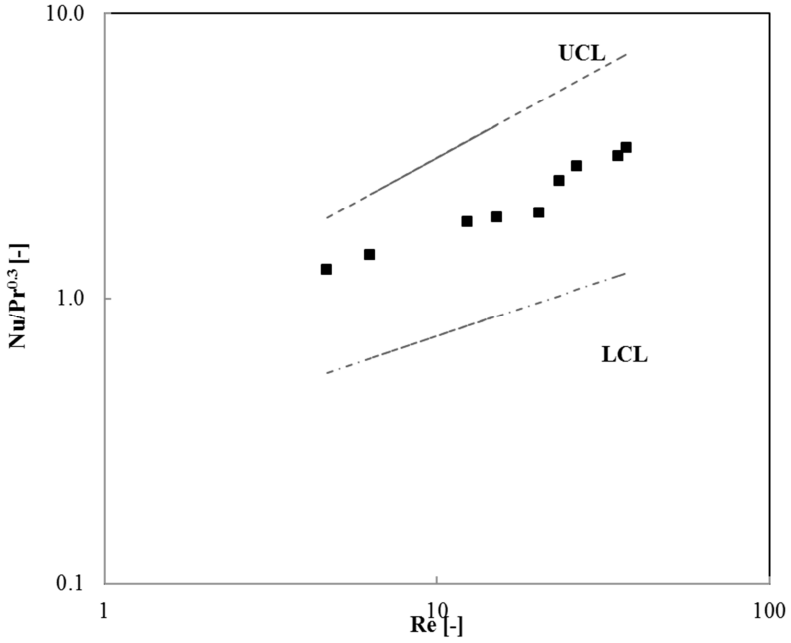


Figure 5.18- Thermal correlation for the mean convective heat transfer coefficient of the 1.0% CMC solution, as a function of the Reynolds number.

The statistical parameters obtained from nonlinear regression analysis of 1.0% CMC experimental data are presented in Table 5.5.

Considering the non-Newtonian, shear-thinning behaviour of the CMC solutions used in these experiments, the temperature dependence of the viscosity was taken into account in the calculation of the Reynolds and Prandtl number, replacing the viscosity term by equation (3.41) and equations (5.5) and (5.8) for 1.0% CMC and 2.0% CMC solutions, respectively. Accordingly, the values obtained from statistical analysis were applied in equation (3.38), defined as follows:

$$Nu = aRe_g^b Pr_g^c$$

Table 5.5- Statistical parameters obtained by nonlinear regression analysis of 1.0% CMC experimental data.

Parameter	**Estimate**	**Standard error**	**95% confidence interval**	
			lower bound	**upper bound**
a	0.508	0.087	0.302	0.714
b	0.513	0.054	0.387	0.640

Therefore, the experimental data obtained in 1.0% CMC experiments were correlated according to the following equation:

$$Nu = 0.508 \cdot Re_g^{0.513} \cdot Pr_g^{0.3}, \;\; r^2 = 0.945 \qquad (5.13)$$

for 4.7<*Re*< 37.3 and 219<*Pr*<402.

In Figure 5.18, the confidence limits slopes obtained by nonlinear regression analysis are shown. The confidence interval obtained for the constant *a* in equation (3.38) is 0.302-0.714 (P<0.05).). As regards the Reynolds number exponent, lower (LCL) and upper (ULC) confidence limits (P<0.05) of 0.387 and 0.640 were obtained, respectively.

The statistical parameters obtained from nonlinear regression analysis of 2.0% CMC experimental data are presented in Table 5.6. The same calculation and analysis procedures were followed as regards to the shear-thinning behaviour reported in section 5.3.1.

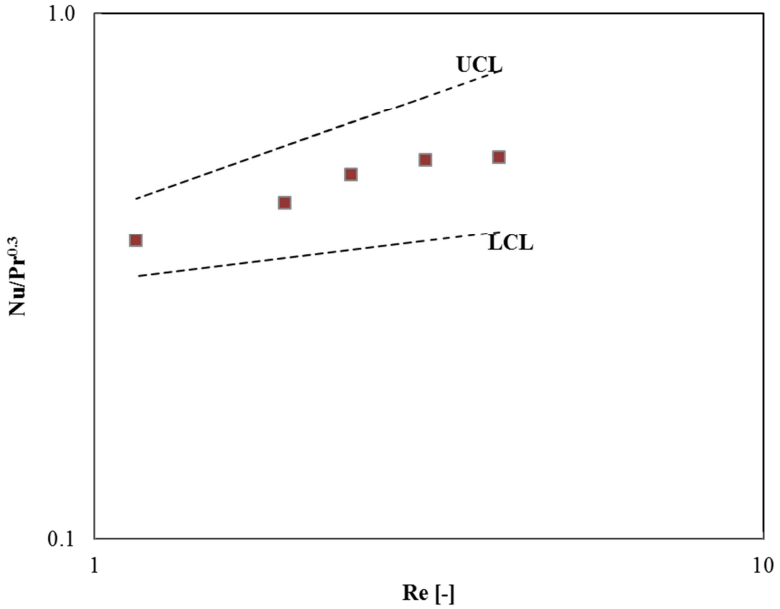


Figure 5.19- Thermal correlation for the mean convective heat transfer coefficient of the 2.0% CMC solution, as a function of the Reynolds number.

Table 5.6- Statistical parameters obtained by nonlinear regression analysis of 2.0% CMC experimental data.

Parameter	**Estimate**	**Standard error**	**95% confidence interval**	
			lower bound	**upper bound**
a	0.364	0.017	0.310	0.419
b	0.300	0.046	0.155	0.446

The experimental data obtained in 2.0% CMC experiments were correlated as follows:

$$Nu = 0.364 \cdot Re_g^{0.300} \cdot Pr_g^{0.3}, \;\; r^2 = 0.940 \qquad (5.14)$$

for 1.2<*Re*< 4.0 and 878<*Pr*<1423.

In Figure 5.19, the confidence limits slopes obtained by nonlinear regression analysis are shown. The confidence interval obtained for the constant *a* in equation (3.38) is

0.310-0.419 (P<0.05). For Reynolds number exponent, lower (LCL) and upper (ULC) confidence limits (P<0.05) of 0.155 and 0.446 were obtained, respectively.

Figure 5.20 shows a comparison between the correlations obtained experimentally for 1.0% CMC and 2.0% CMC solutions with a shear-thinning, power-law behaviour and other published correlations for Newtonian and non-Newtonian fluids (Edwards, 1988; Rene *et al.*, 1991a; Carezzato *et al.*, 2007).

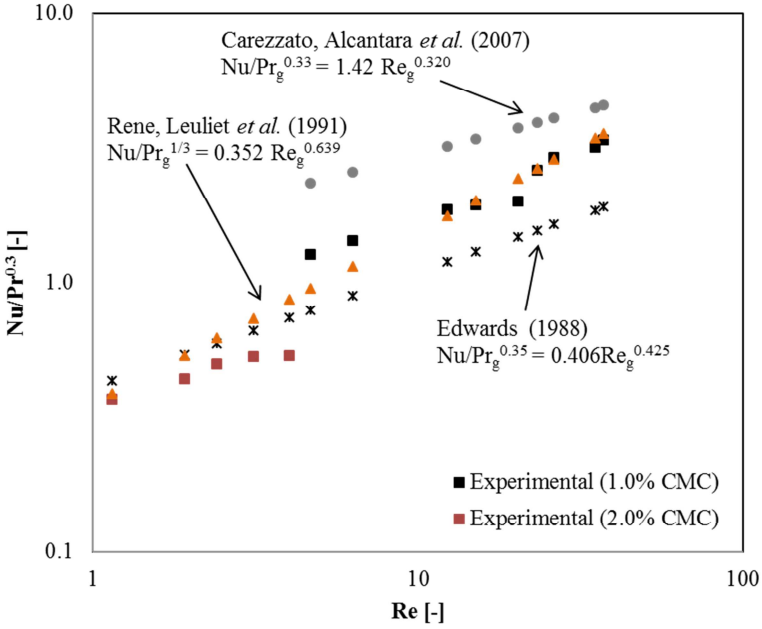


Figure 5.20- Comparison among obtained and published thermal correlations, for non-Newtonian fluids.

The published correlations used in the comparison were obtained in plate heat exchangers using as working fluids CMC, sodium alginate solutions and guar-gum as pseudoplastic, power-law non-Newtonian fluids, in countercurrent flow conditions, with chevron type plates (Edwards, 1988; Rene *et al.*, 1991a; Carezzato *et al.*, 2007).

From Figure 5.20, one can compare the Reynolds number ranges obtained for each CMC solution studied. In fact, the higher the concentration of the CMC solution, stronger shear-thinning behaviour was observed, and consequently, lower values of Reynolds number were obtained, due to the significant effect of apparent viscosity.

For 1.0% CMC solution, with weak shear-thinning behaviour (n=0.97), the correlation obtained is similar to the correlations found for turbulent flow in PHE (Rene

et al., 1991a; Warnakulasuriya and Worek, 2008). Notwithstanding, the experimental data obtained for this CMC solution, followed the same tendency as the thermal correlations published by Edwards (1988) in which the Reynolds number exponent varied from 0.379 to 0.425, for Reynolds number lower than 50. This range of values for Reynolds number exponent is lower than those observed for turbulent flows at high Reynolds numbers (n>0.6).

Carezzato, Alcantara et al. (2007) in their study of non-Newtonian heat transfer for different PHE configurations, using CMC solutions as test fluid, obtained a thermal correlation, valid for Reynolds number values lower than 27.5 (and high Prandtl number, Pr>81) with a Reynolds number exponent typical of most laminar flows compared to pipe flow. The mean Nusselt numbers obtained are higher than those obtained in this work. This evidenced the fact that at low Reynolds numbers, even if the flow is laminar, still the plate corrugations may induce secondary flows, boundary layer separation, etc, leading to good heat transfer conditions (Edwards, 1988).

The results obtained with 2.0% CMC solutions evidenced what has been mentioned previously, since for very low values of the Reynolds number the correlation obtained has a Reynolds number exponent typical of most laminar flows (n=1/3). Nevertheless, this correlation has a similar tendency of those obtained by Edwards (1988) and Rene, Leuliet et al. (1991a) for turbulent flow.

Figure 5.21 shows the plots of experimental and predicted overall heat transfer coefficients as function of Reynolds number of 1.0% and 2.0% CMC solutions.

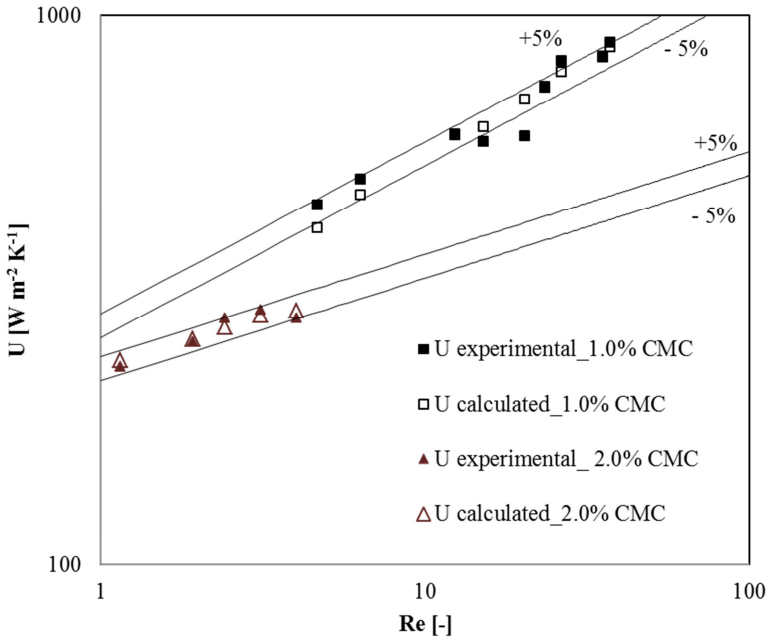


Figure 5.21- Experimental and predicted overall heat transfer coefficients as a function of Reynolds number of 1.0% CMC and 2.0% CMC solutions.

From Figure 5.21 it is possible to observe that accurate correlations for the determination of mean convective heat transfer coefficients 1.0% and 2.0% CMC solution, representative of shear-thinning, power-law non-Newtonian fluids, were obtained, since the predicted overall heat transfer coefficients were calculated with a mean relative error of less than 13%.

The correlations obtained can be applied in further studies of the heat transfer using viscous Newtonian and power-law non-Newtonian fluids in this type of plate heat exchanger with this multipass arrangement.

5.3.3. Determination of the local convective heat transfer coefficients of CMC solutions

As previously mentioned for water/ water heat transfer experiments, one plate and two adjacent channels in each pass of the PHE were instrumented with temperature probes in order to obtain the temperature profiles of the working fluids along the PHE channels and wall temperatures along the PHE monitored plates. In each channel, the fluid and wall temperatures variation along the channel length were monitored in each

of the four sub-sections defined previously, during the time of the heat transfer experiment.

Newtonian fluids

In Figure 5.22 it is possible to observe the temperature profiles of cooling water (Figure 5.22a) and warm CMC solution (0.25% w/w) (Figure 5.22b) along the controlled channels in section 1 of PHE, corresponding to channel 1 and channel 2, respectively. These temperature profiles were obtained in the 0.25% CMC-water heat transfer experiment with a mean Reynolds number of CMC solution of 2.56.

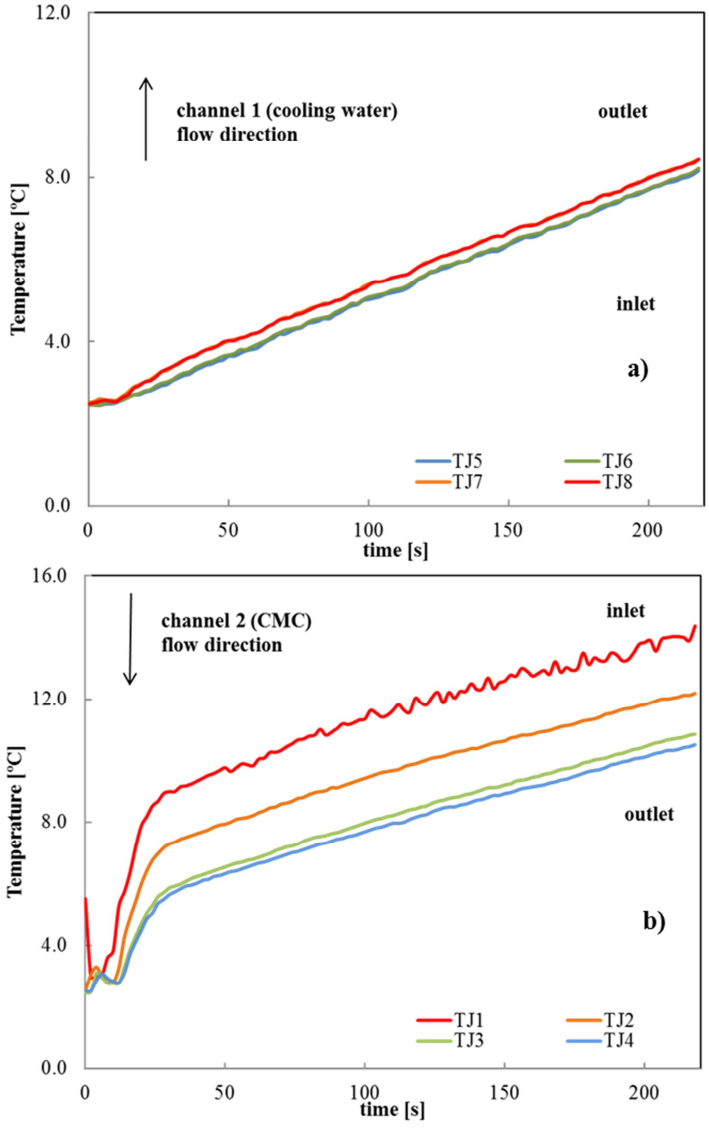


Figure 5.22- Temperature profiles of working fluids ((a) cooling water channel, (b) warm CMC channel) along the PHE section 1 channels, as a function of time, for 0.25% CMC solution (Re=2.56).

Temperature profiles similar to these ones were obtained for every heat exchange experiment. Small differences were obtained in the profiles depending on the operating conditions, namely fluids inlet temperatures and flow rates. Nevertheless, the temperature profiles shown in Figure 5.22 are representative of the temperature variation along the PHE channels.

The wall temperature profiles measured on both sides of plate 2 are shown in Figure 5.23.a and b, for cooling water side and warm CMC side, respectively.

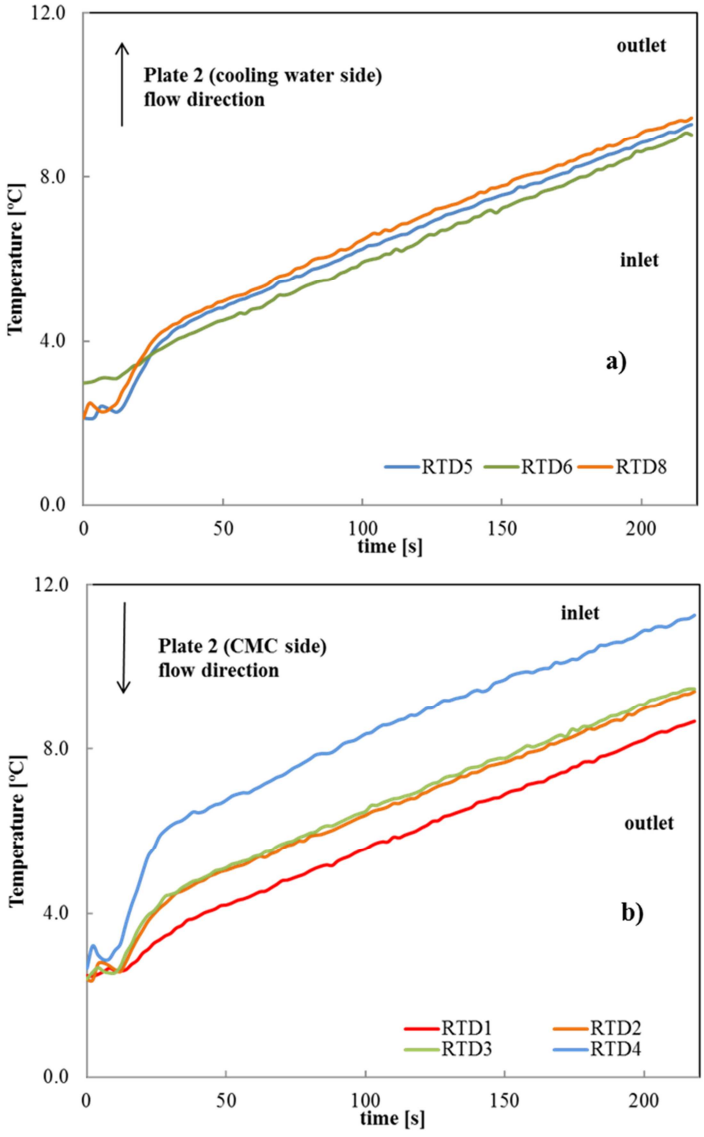


Figure 5.23- Wall temperature profiles along plate 2 ((a) cooling water side, (b) warm CMC side), as a function of time, for 0.25% CMC solution (Re=2.56).

In Figure 5.23a, it is possible to observe that the in the cooling water side the wall temperature exhibited very small variations along the plate length. On the other wall side (Figure 5.23b), major temperature differences are observed between the inlet and outlet of warm CMC channel. The wall temperature differences and those between the fluids at the channels inlet and outlet can be observed in Figure 5.24a and b as a function of time.

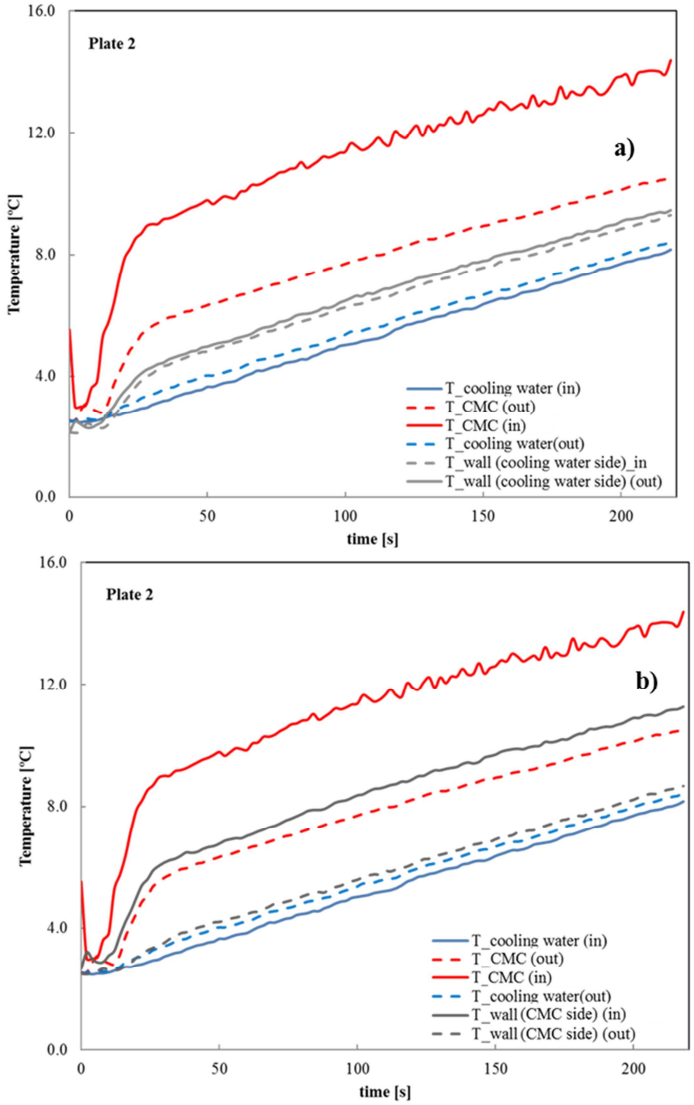


Figure 5.24- Wall temperatures (Plate 2) and working fluids temperatures at channels inlet and outlet ((a) cooling water side, (b) warm CMC side), as a function of time, for 0.25% CMC solution.

Oppositely to what was noticed in water/ water heat experiments, in which it was observed an approximately similar temperature differences at the two extremes of the heat exchanger, here, for the operating conditions of the example presented, one can observe significant changes between the average temperature differences at the inlet zones of both working fluids.

Similarly to section 1, the temperature profiles of cooling water and warm CMC along the monitored channels in section 2 of PHE (channels 7 and 8) are shown in Figure 5.25a and b.

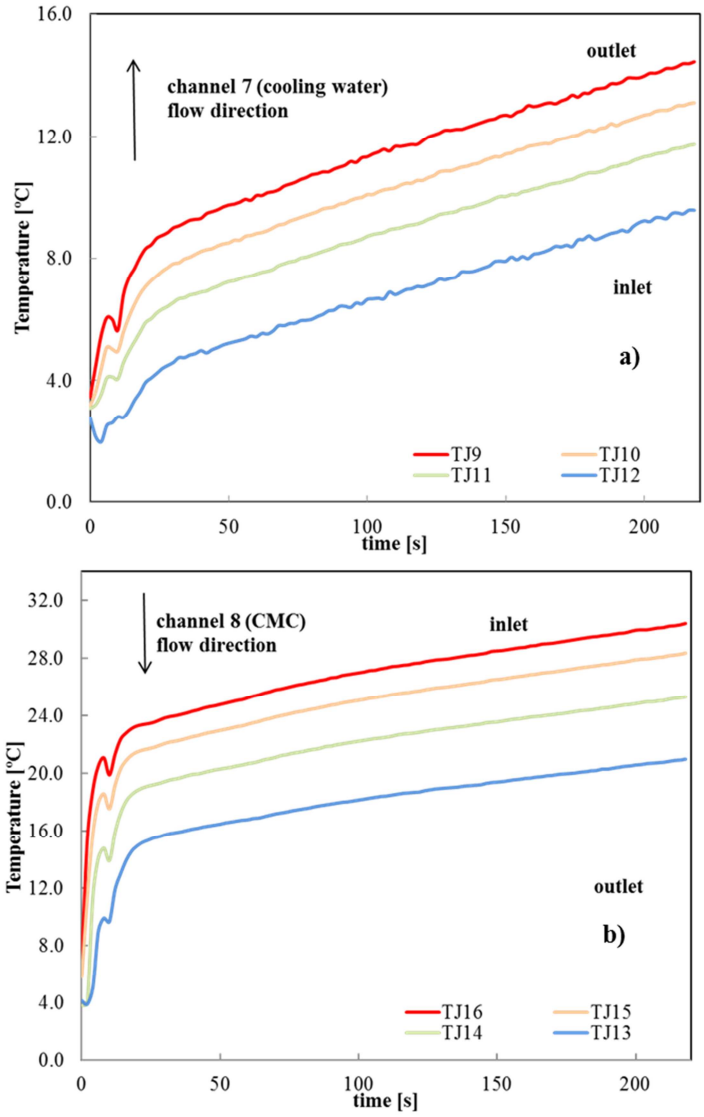
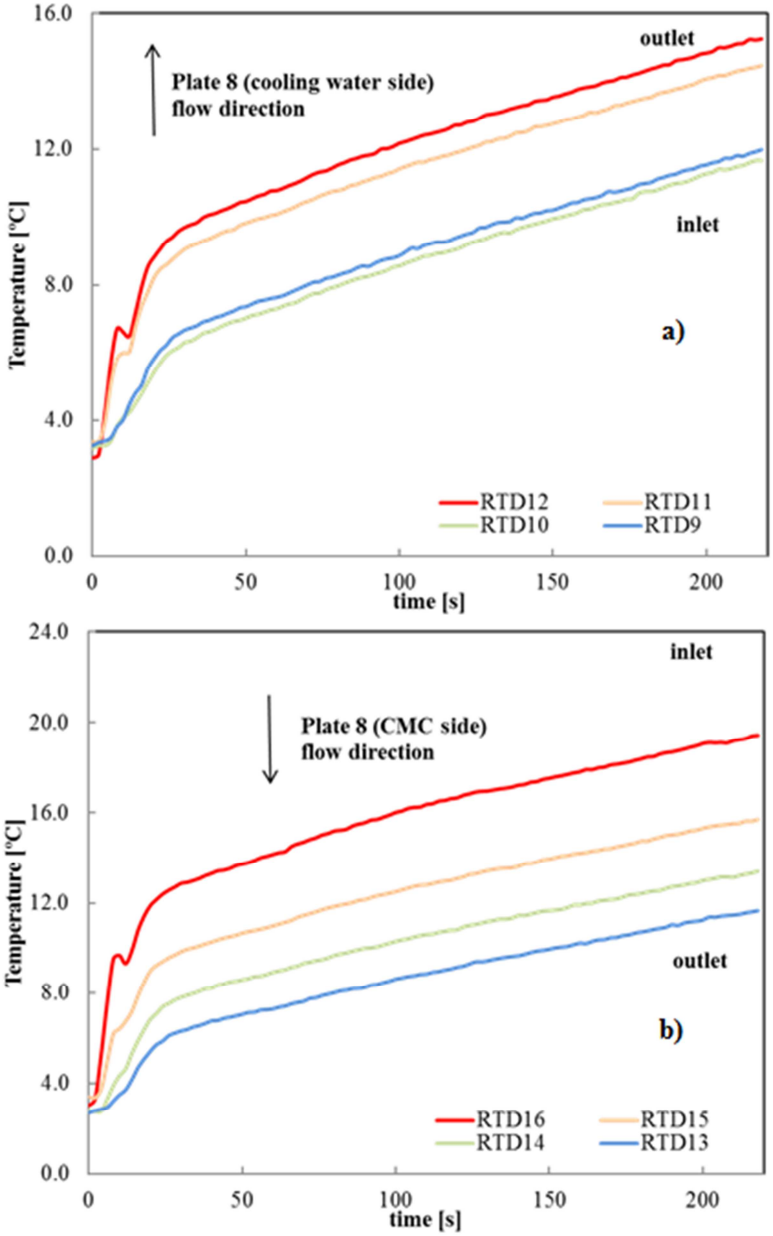


Figure 5.25- Temperature profiles of working fluids ((a) cooling water channel, (b) warm CMC channel) along the PHE section 2 channels, as a function of time, for 0.25% CMC solution.

Likewise to section 1, in section 2 it is also possible to observe the temperature variation of each fluid through the channel length. In section 2, the cooling water exhibited more significant temperature variations along the channel length, most probably related to higher temperature differences between the two fluids and due to the proximity of warm CMC PHE inlet.



o

Figure 5.26- Wall temperature profiles along plate 8 ((a) cooling water side, (b) warm CMC side), as a function of time, for 0.25% CMC solution.

The wall temperature profiles measured on both sides of plate 8 are shown in Figure 5.26.a and b, for cooling water side and warm CMC side, respectively. Similarly to what was observed for the fluids temperatures, the wall temperatures varied more significantly along the plate length. These differences observed are strongly related to the temperature dependence of thermophysical properties of CMC, namely the viscosity that exhibited an exponential relationship with temperature, and consequently a more pronounced effect on the fluid hydrodynamic behaviour.

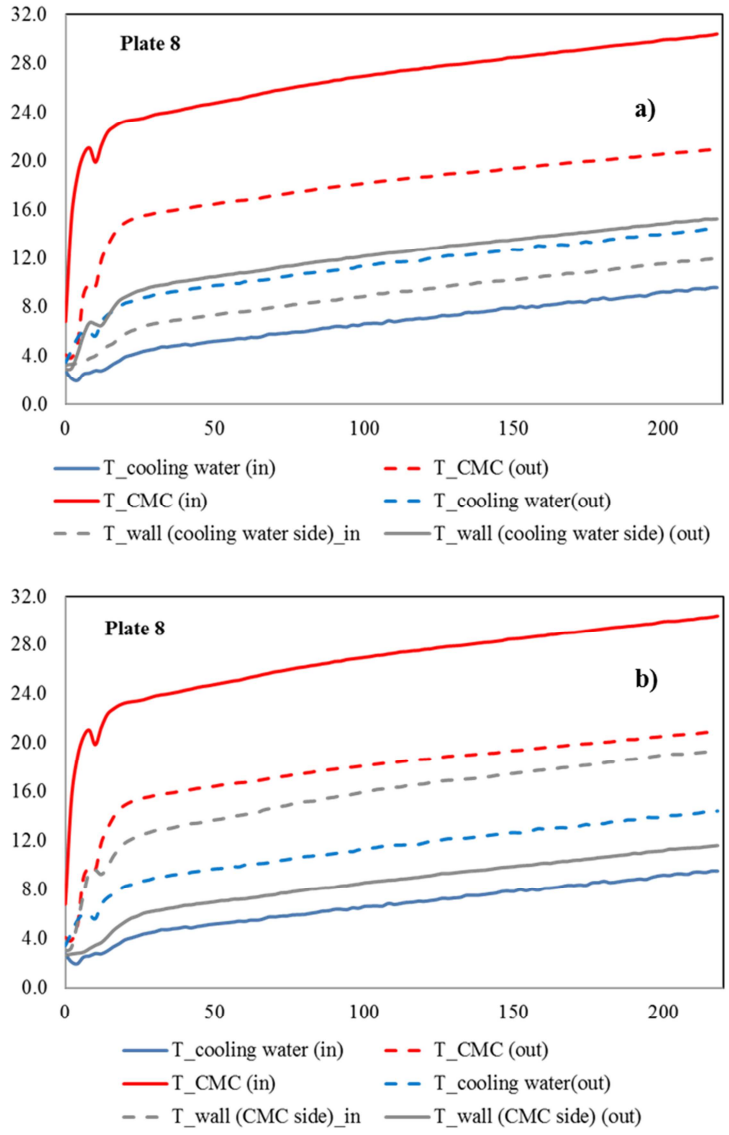


Figure 5.27- Wall temperatures (Plate 8) and working fluids temperatures at channels inlets ((a) cooling water side, (b) CMC side), as a function of time, for 0.25% CMC solution.

The wall temperature differences and those between the working fluids at the channels inlet and outlet can be observed in Figure 5.27a and b as a function of time. Such as it was observed in section 1, the temperature difference between working fluids has an approximately constant range (10-16ºC, in the present example) at channels inlet and outlet, although the temperature ranges were quite different.

In order to evaluate the fluids temperature variation along the channel length, for several experiment times, the temperature data was plotted versus the position of each temperature probe along the channel length, for section 1 and 2 as it is shown in Figures 5.28 and 5.29, respectively.

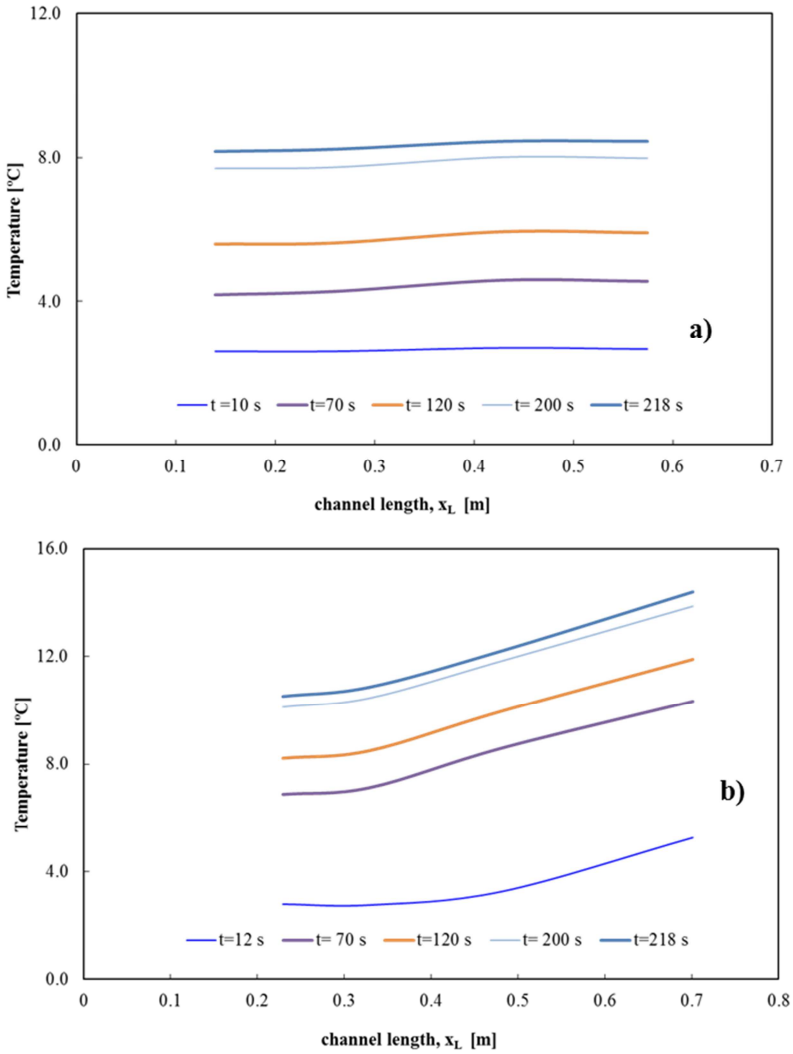


Figure 5.28- Working fluids temperatures along channels 1 and 2 corrugated zone, for different times ((a) cooling water channel, (b) warm CMC channel), for 0.25% CMC solution.

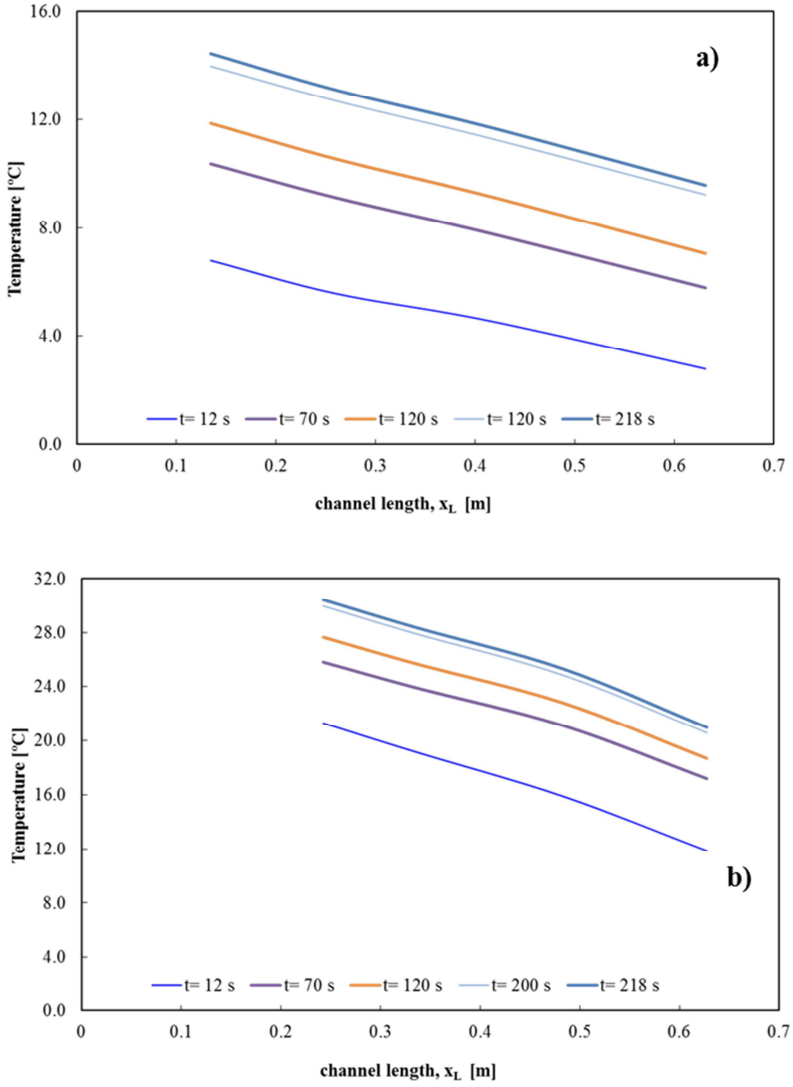


Figure 5.29- Working fluids temperatures along channels 7 and 8 corrugated zone, for different times ((a) cooling water channel, (b) warm CMC channel), for 0.25% CMC solution.

In both figures it is possible to observe that the temperature profiles along the channel length have an almost linear tendency. In Figure 5.28a one can observe that, in section 1, the cooling water kept a nearly constant temperature along the channel length whereas in section 2 exhibited an almost linear increasing along the channel length.

As previously mentioned, only the corrugated region of the plate was considered in the calculation procedures. During the accomplishment of the analysis of the experimental data, some sporadic problems related to local data temperature acquisition were spotted which were not detected during the experimental work. In this set of

experiments, the experimental data produced for PHE section 2 was not consistent. Thus, the local heat transfer analysis of section 2 will not be presented.

Table 5.7 shows the values of local Reynolds numbers of 0.25% CMC and cooling water and local overall heat transfer coefficients for the four sub-sections analysed in section 1.

Table 5.7- Average values of and local overall heat transfer coefficients (U_{ij}) and local Reynolds number (Re_{ij}) of 0.25% CMC solution for the four sub-sections analysed in section 1, for each experiment.

Experiment ID	**Re_{11} [-]**	**U_{11}, [$Wm^{-2}K^{-1}$]**	**Re_{12} [-]**	**U_{12}, [$Wm^{-2}K^{-1}$]**	**Re_{13} [-]**	**U_{13}, [$Wm^{-2}K^{-1}$]**	**Re_{14} [-]**	**U_{14}, [$Wm^{-2}K^{-1}$]**
1	2.3	1665	2.3	862	2.3	522	2.3	375
2	3.5	1561	3.6	825	3.6	502	3.7	369
3	5.8	1126	5.9	874	6.1	656	6.2	538
4	5.8	1294	5.9	973	6.0	730	6.1	597
5	2.2	2086	2.2	741	2.2	415	2.3	284
6	8.9	1634	9.1	1236	9.4	909	9.7	741
7	17.2	1621	17.8	1464	18.4	1145	19.0	984
8	2.2	2539	2.2	1226	2.2	769	2.2	550
9	5.2	1344	5.3	852	5.4	592	5.5	458
10	13.1	1738	13.2	1405	13.5	1147	13.7	967

The statistical parameters obtained from nonlinear regression analysis, applied to the four sub-sections of section 1, are presented in Table 5.8.

Table 5.8- Statistical parameter obtained by nonlinear regression analysis, for the four sub-sections analysed in section 1, for 0.25% CMC solution.

Sub-section	**Parameter**	**Estimate**	**Standard error**	**95% confidence interval**	
				lower bound	**upper bound**
1	a	2.355	0.687	0.447	4.264
	b	0.374	0.126	0.024	0.725
2	a	1.017	0.174	0.533	1.501
	b	0.595	0.071	0.399	0.791
3	a	0.644	0.147	0.235	1.053
	b	0.656	0.092	0.400	0.912
4	a	0.459	0.113	0.145	0.774
	b	0.704	0.098	0.433	0.975

The values obtained for constants $C_{1,ij}$ were applied in equation (3.32) in order to obtain the value of constant *a*. Following the procedures described in sections 3.8.1 and 3.8.2, the constants values were applied in equation (3.22), defined as follows:

$$Nu = aRe^{b}Pr^{c}$$

For section 1, four thermal correlations were obtained, one for each sub-section defined. Thus, the experimental data were correlated according to the following equations:

$$Nu = 2.355 \cdot Re^{0,374} \cdot Pr^{0,3}, \;\; r^{\,2} = 0.69 \qquad (5.15)$$

obtained for sub-section 1, with 2.2<*Re*<17.1 and 351<*Pr*<480;

$$Nu = 1.017 \cdot Re^{0.595} \cdot Pr^{0.3}, \;\; r^{\,2} = 0.94 \qquad (5.16)$$

obtained for sub-section 2, with 2.2<*Re*<17.8 and 335<*Pr*<471;

$$Nu = 0.644 \cdot Re^{0,656} \cdot Pr^{0.3}, \;\; r^{\,2} = 0.92 \qquad (5.17)$$

obtained for sub-section 3, with 2.2<*Re*<18.4 and 321<*Pr*<471;

$$Nu = 0.459 \cdot Re^{0.704} \cdot Pr^{0.3}, \;\; r^{\,2} = 0.923 \qquad (5.18)$$

obtained for sub-section 4, with 2.2<*Re*<19.0 and 307<*Pr*<471.

In channel 2, the CMC solution enters the channel in sub-section 4 and exits the channel in sub-section 1. Considering the flow direction, this viscous Newtonian CMC solution and observing the Reynolds number exponent equations 5.15, 5.16, 5.17 and 5.18, one can observe that in sub-sections 4 (CMC channel inlet) and 3 the values of Reynolds number exponent are within the reference range for turbulent flow, e.g. (Jackson and Troupe, 1964; Edwards *et al.*, 1974; Rene *et al.*, 1991a). Along the channel length the value of Reynolds exponent decreased until values denoted as transitional to laminar flow. This thermal behaviour may be explained by the more pronounced cooling of the CMC solution, since in this section the cooling water temperature is lower than in section 2, and consequently a more markedly increase on the viscosity values and its effect on the hydrodynamic behaviour are obtained (lower Reynolds numbers in sub-section1).

In order to gather more information concerning local convective heat transfer coefficients, the local Nusselt number versus channel length was plotted, for several Reynolds, for section 1, as it is shown in Figure 5.30. The experimental data that used for this analysis is shown in Table A.6 (Annex A).

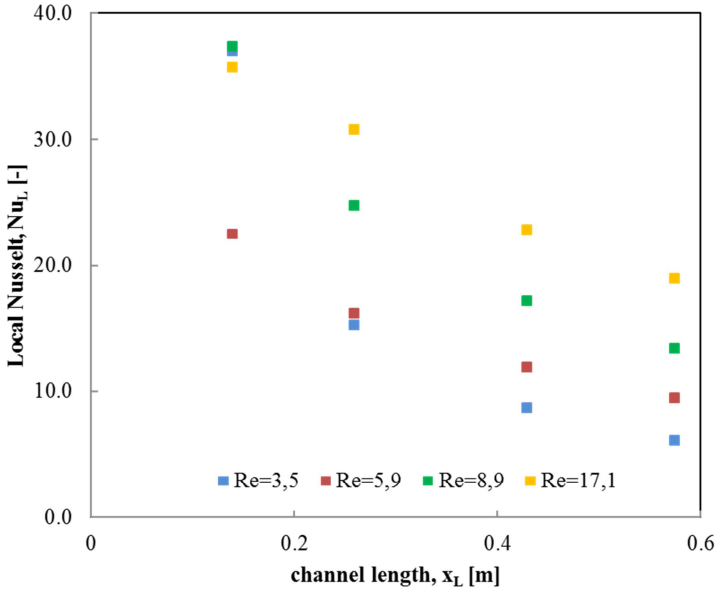


Figure 5.30- CMC solution (0.25%) local Nusselt number variation along channel length (channel 2, section 1), for several Reynolds numbers.

The correlations obtained for the local Nusselt number as a function of channel length, for several Reynolds numbers, in section 1, are presented in Table 5.9.

Table 5.9- Local thermal correlation as a function of channel length, for several local Reynolds numbers of 0.25% CMC solution, in channel 2.

Channel	**Local Reynolds number, Re [-]**	**Thermal correlations**
2	3.5	$Nu_L = 2.963 \cdot x_L^{-1.264}$, $r^2 = 0{,}997$
	5.9	$Nu_L = 6.936 \cdot x_L^{-0.608}$, $r^2 = 0{,}994$
	8.9	$Nu_L = 9.205 \cdot x_L^{-0.719}$, $r^2 = 0{,}998$

The local thermal correlations evidence not only the variation of local Nusselt number with the channel length (x_L) but also with the Reynolds number, as indicated by

the variation of the constant value. In order to obtain a more explanatory correlation of the effects mentioned previously, the variation of local Nusselt number with Graetz number for 0.25% CMC solution in channel 2 (section 1) is presented in Figure 5.31.

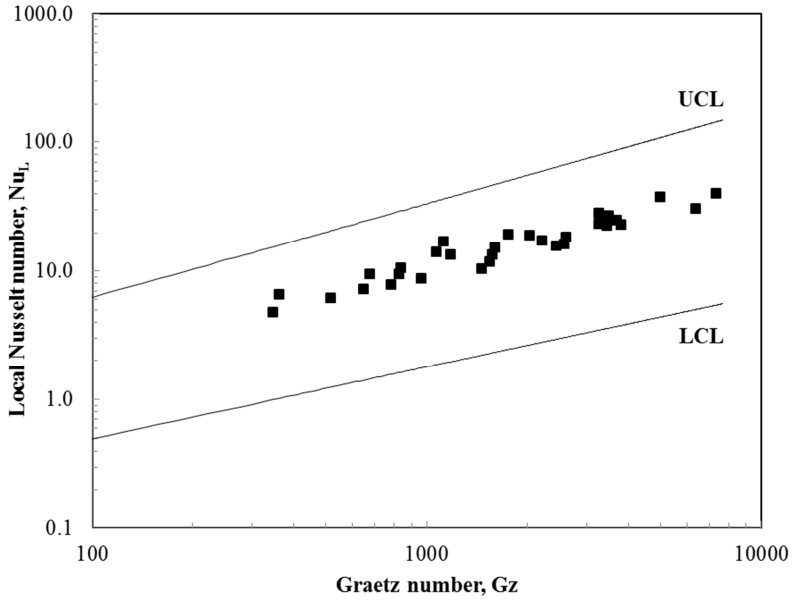


Figure 5.31- CMC solution (0.25%) local Nusselt number versus Graetz number (channel 2, section 1).

Table 5.10 presents the statistical parameters obtained from the nonlinear regression analysis applied to the heat transfer experiments carried out with 0.25% CMC. This analysis led to the determination of constants C and b in equation (5.19):

$$Nu_L = \mathrm{C} \cdot Gz^b \tag{5.19}$$

The parameters obtained from experimental data of 0.25% CMC heat experiments are presented in Table 5.10.

Table 5.10- Statistical parameters obtained by nonlinear regression analysis for channel 2 (section 1).

Parameter	**Estimate**	**Standard error**	**95% confidence interval**	
			lower bound	**upper bound**
C	0.128	0.044	0.038	0.218
b	0.643	0.042	0.556	0.729

Thus, the experimental data for channel 2 were correlated according to the following equation:

$$Nu_L = 0.128 \cdot Gz^{0.643}, \quad r^2 = 0.905 \tag{5.20}$$

for 347< *Gz* <7354.

Figure 5.32 shows a comparison between the correlations obtained in this work (Channel 2) and those published in the open literature, for the thermal entry region of a parallel-plate channel with Hagen–Poiseuille flow (Bejan and Kraus, 2003; Shah and Sekuli, 2003).

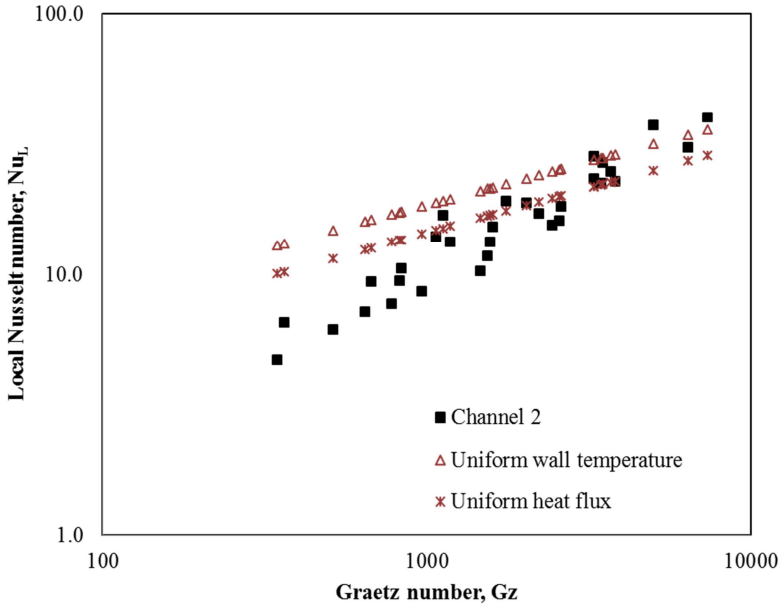


Figure 5.32- Comparison of local heat transfer correlations in the thermal entry region obtained in the present work (0.25% CMC solution) and those published in the open literature.

Matching the results obtained here with the published correlations for parallel-plate channels, one can observe that the present values of the local Nusselt numbers are slightly lower, mainly due to viscous effects.

By comparison of equation 5.20 with equation 4.15 obtained in this work for water (see chapter 4) the main difference that can be notice d in these equations is the value of the exponent of Graetz number, which was lower in water (0.48), although water Nu-Gz correlation has a higher value of the correlation constant (1.652). The higher values of Prandtl number observed in this set of experiments with viscous Newtonian fluids, suggested more significant entrance effects.

The published correlations used in this analysis embodied two boundary conditions generally used in studies of internal forced convection in ducts: uniform wall temperature and uniform heat flux, represented by equations (4.16) and (4.17) (see Chapter 4).

Differences can be signalised between the thermal correlation obtained in the present work and those published for thermal developing flow in flat parallel-plate channels, for the two boundary conditions: constant wall temperature and constant heat flux, represented by equations (4.16), (4.17) . The main difference both for Newtonian (water) and viscous Newtonian fluids (0.25% CMC solution), is the Graetz number exponent with a value higher than the published ones (1/3). Although, the boundary conditions in the PHE channel are not typical conditions, since both heat flux and wall temperature varied along the channel length, from Figure 5.32 one can observe that the absolute results are quite approximated.

Considering the viscous Newtonian behaviour of the test fluid, the correlation obtained in this work was compared with the numerical solution proposed by Metzner, Vaughn et al. (1957) for plug-flow given by:

$$Nu_L = \frac{8}{\pi} + \frac{4}{\pi} \cdot Gz^{1/2} \tag{5.21}$$

The correlation obtained in this set of heat experiments has an exponent of the Graetz number with a value higher than the one published by Metzner, Vaughn et al. (1957) for plug-flow. Nevertheless, the local Nusselt numbers obtained experimentally are still lower than those obtained by equation 5.21. In fact, due to plate geometrical characteristics, the plug-flow assumption is not realistic since in the PHE corrugated channels, even at low Reynolds numbers in which flow will be mostly laminar, the secondary flow effects caused by corrugations will promote the heat transfer and some flow perturbations (Edwards, 1988; Galeazzo *et al.*, 2006).

Non-Newtonian fluids

As the temperature profiles obtained with both non-Newtonian CMC solutions (with different concentrations) revealed an identical tendency, it only will be presented the

channel and plate temperature profiles of 2.0% CMC solution, chosen due to its more pronounced shear-thinning behaviour.

In Figure 5.33 it is possible to observe the temperature profiles of cooling water (Figure 5.33a) and warm CMC solution (2.0% w/w) (Figure 5.33b) along the monitored channels in section 1 of PHE, corresponding to channel 1 and channel 2, respectively. These temperature profiles were obtained in the 2.0% CMC-water heat transfer experiment with a mean Reynolds number of CMC solution of 4.02.

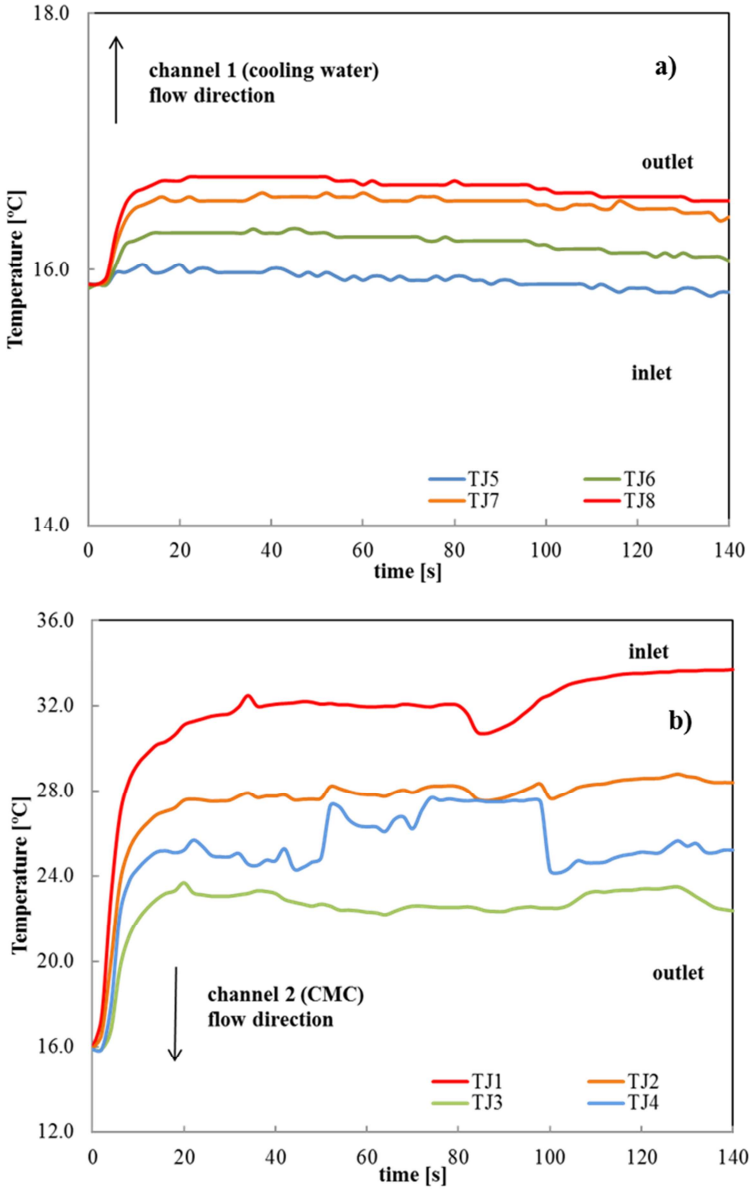


Figure 5.33- Temperature profiles of working fluids ((a) cooling water channel, (b) warm CMC channel) along the PHE section 1 channels, as a function of time, for 2.0% CMC solution (Re=4.02).

Temperature profiles similar to these ones were obtained for every heat transfer experiment. Small differences were detected in the profiles depending on the operating conditions, namely fluids inlet temperatures and flow rates. The temperature profiles shown in Figure 5.33 are illustrative of the temperature variation along the PHE channels.

The wall temperature profiles obtained on both sides of plate 2 are shown in Figure 5.34.a and b, for cooling water side and warm CMC side, respectively.

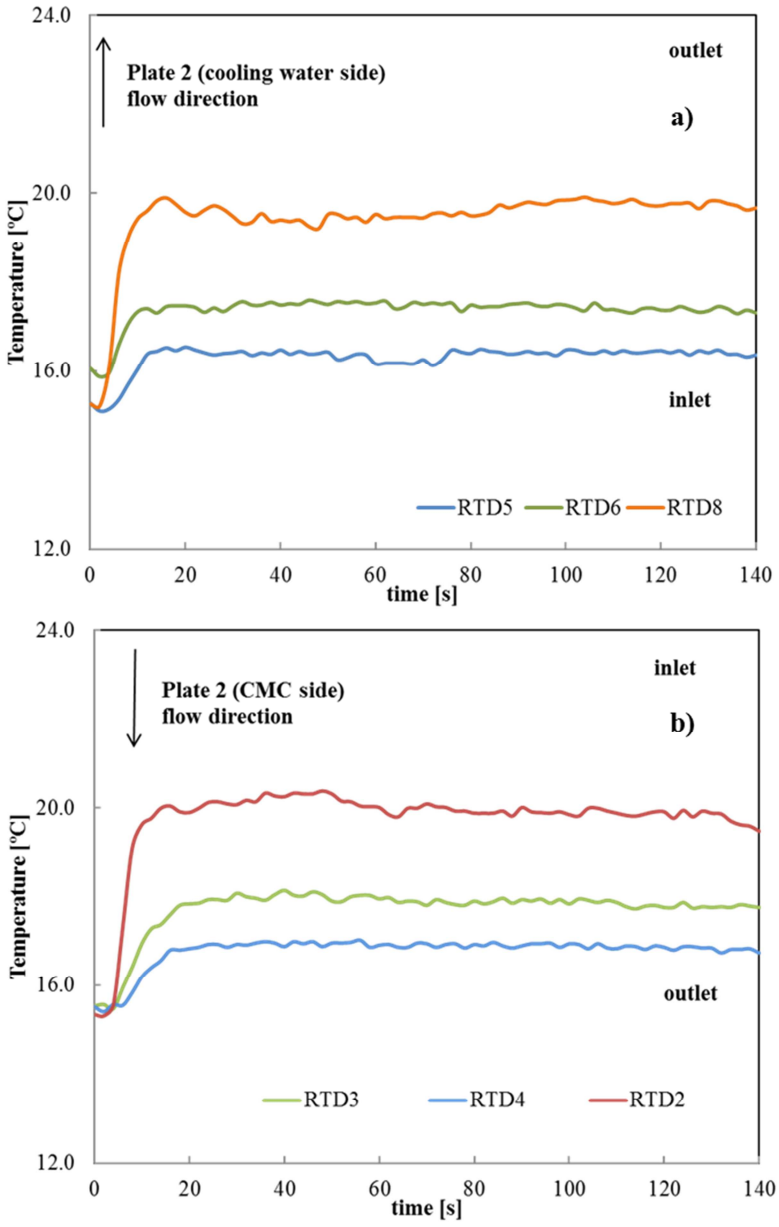


Figure 5.34- Wall temperature profiles along plate 2 ((a) cooling water side, (b) warm CMC side), as a function of time, for 2.0% CMC solution (Re= 4.02).

In Figures 5.34a and b, it is possible to observe that on both working fluids sides the wall temperature exhibited significant variations along the plate length. The wall temperature differences and those between the fluids at the channels inlet and outlet can be observed in Figure 5.35a and b as a function of time.

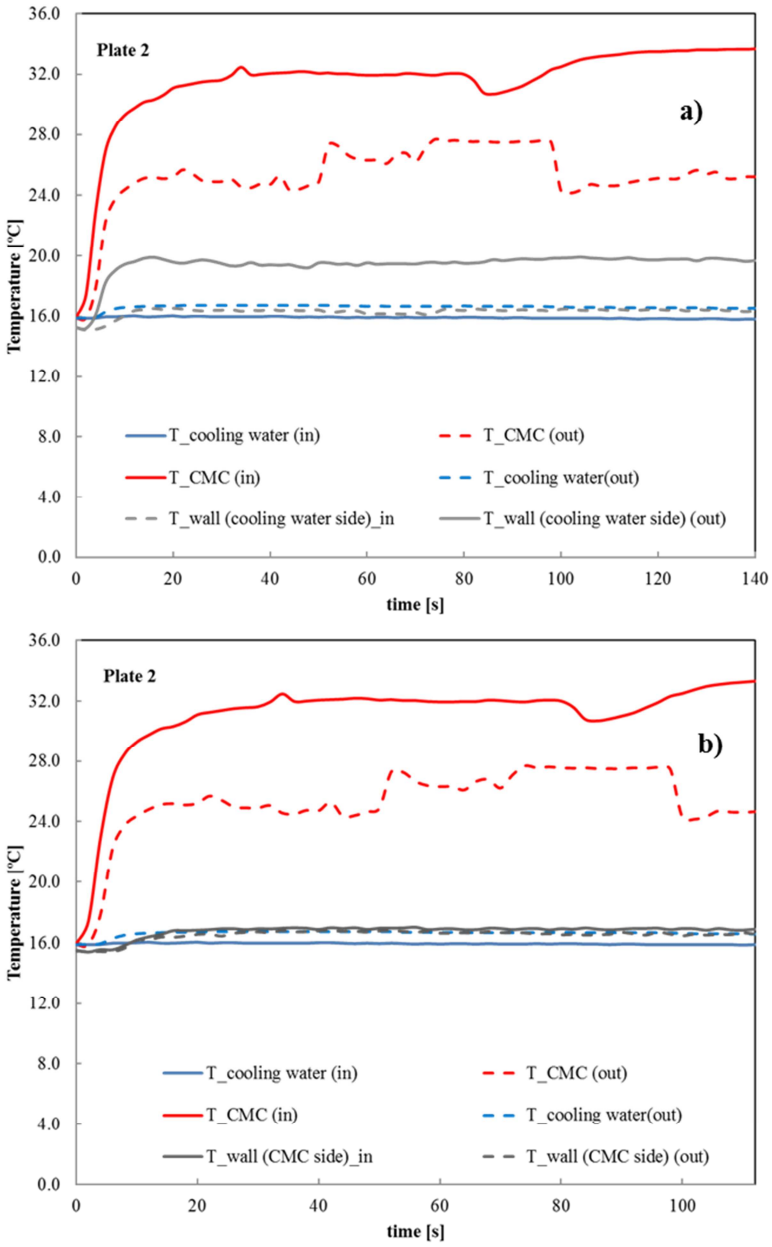


Figure 5.35- Wall temperatures (Plate 2) and working fluids temperatures at channels inlet and outlet ((a) cooling water side, (b) warm CMC side), as a function of time, for 2.0% CMC solution (Re=4.02).

The results are in opposition to water/ water heat experiments, in which it was observed an approximately constant temperature difference between the hot water

entrance and cooling water. Likewise, in 0.25% CMC /water experiments, for the operating conditions of the example presented, one can only observe such significant deviations on the average temperature differences between inlets of CMC solution. These dissimilarities in average temperature differences between inlets on both working fluids are due to the flowrates differences between the two fluids, the cooling water flowrates being much higher than those of CMC solutions, whereas in water/water experiments the flowrates were kept almost equals.

Similarly to section 1, the temperature profiles of cooling water and warm CMC along the monitored channels in section 2 of PHE (channels 7 and 8) are shown in Figure 5.36a and b.

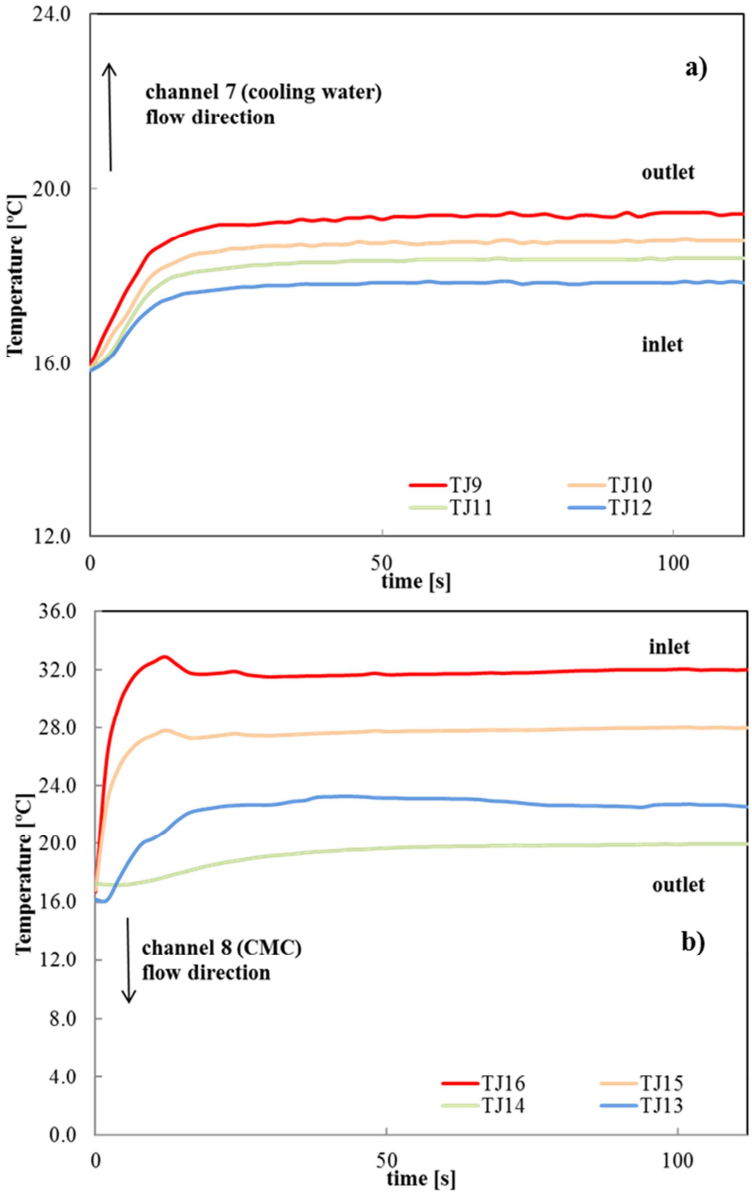


Figure 5.36- Temperature profiles of working fluids ((a) cooling water channel, (b) warm CMC channel) along the PHE section 2 channels, as a function of time, for 2.0% CMC solution.

Similarly to section 1, in section 2 it is also possible to observe the temperature variation of each fluid through the channel length. In section 2, the CMC solution exhibited a more significant temperature variation along the channel length than the cooling water temperature variation, most probably related to the flow rate differences between the working fluids.

In Figures 5.37a and b, it is possible to observe that on both working fluids sides the wall temperature exhibited significant variations along the plate length.

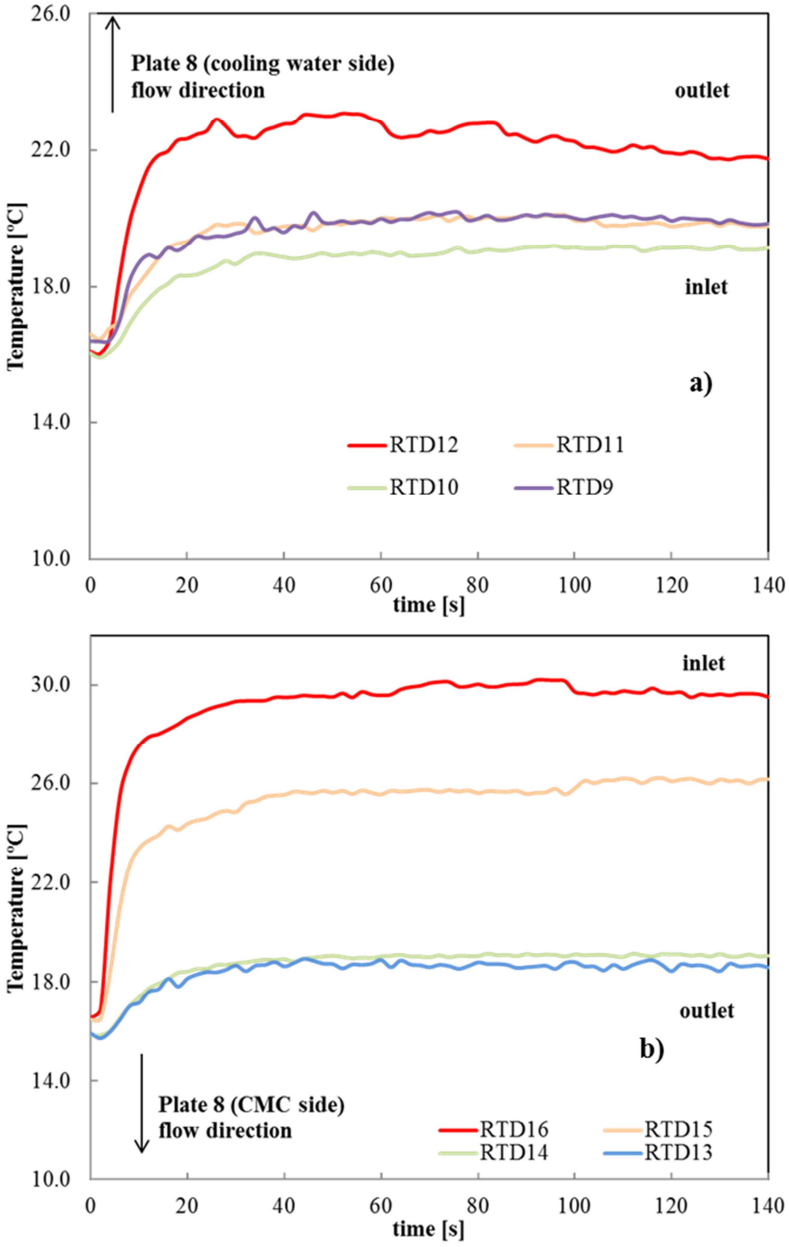


Figure 5.37- Wall temperature profiles along plate 8 ((a) cooling water side, (b) warm CMC side), as a function of time, for 2.0% CMC solution.

In Figure 5.37a one can observe the perturbation caused by the viscous fluid in the temperature acquisition systems. These perturbations were more frequent when the working fluid had a pronounced viscous behaviour as compared to “water-like” fluids.

The wall temperature differences and those between the fluids at the channels inlet and outlet can be observed in Figure 5.38a and b as a function of time.

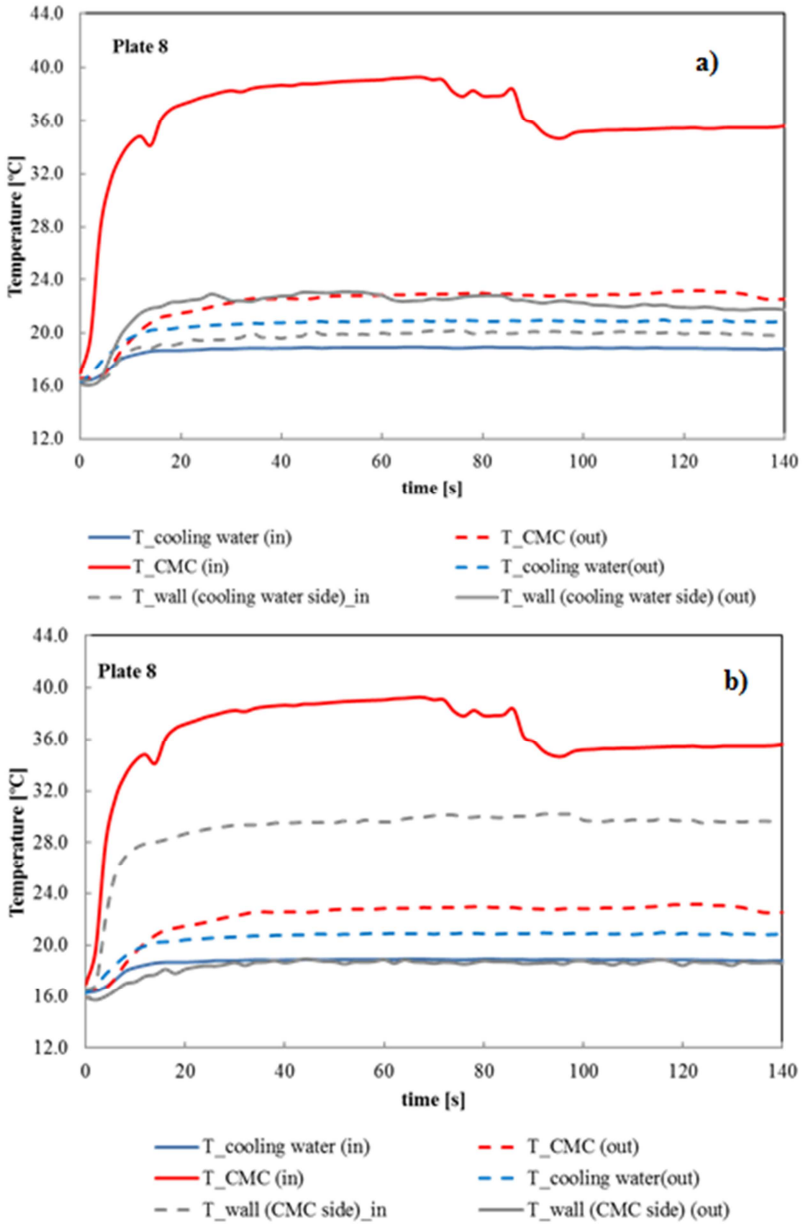


Figure 5.38- Wall temperatures (Plate 8) and working fluids temperatures at channels inlet and outlet ((a) cooling water side, (b) warm CMC side), as a function of time, for 2.0% CMC solution (Re=4.02).

Similarly to section 1, in Figures 5.38a and b, one can only observe the significant differences between the average temperature differences between inlets of CMC solution and very small differences between cooling water inlets. The differences between the flowrates of the two fluids are most probably the cause of these temperature differences.

Table 5.11 shows the values of local Reynolds numbers of both 1.0% and 2.0% CMC and local overall heat transfer coefficients for the four sub-sections analysed in section 1.

Table 5.11- Average values of and local overall heat transfer coefficients (U_{ij}) and local Reynolds number (Re_{ij}) of 1.0% and 2.0% CMC solutions for the four sub-sections analysed in section 1, for each experiment.

% CMC	Re_{11} [-]	U_{11}, [$Wm^{-2}K^{-1}$]	Re_{12} [-]	U_{12}, [$Wm^{-2}K^{-1}$]	Re_{13} [-]	U_{13}, [$Wm^{-2}K^{-1}$]	Re_{14} [-]	U_{14}, [$Wm^{-2}K^{-1}$]
1.0	1.4	2124	1.5	1116	1.7	696	1.8	517
	6.4	1266	7.2	1011	8.5	797	9.7	663
	2.1	2144	2.4	1089	2.9	672	3.3	498
	6.2	1231	6.8	1017	7.9	845	8.9	714
	11.4	1036	12.3	954	13.8	868	15.2	774
	11.9	1110	13.1	1067	14.9	965	16.7	877
	15.7	1130	16.7	1135	18.3	1073	19.7	1003
	22.4	1205	24.1	1234	26.8	1150	29.2	1075
	18.5	1162	20.1	1161	22.7	1089	25.2	1017
2.0	1.8	819	2.1	618	2.5	460	2.9	383
	0.6	749	0.7	596	0.7	443	0.8	380
	1.0	753	1.1	628	1.2	506	1.3	443
	1.2	892	1.3	748	1.4	611	1.5	537
	1.5	949	1.6	744	1.8	573	2.0	488

The statistical parameters obtained from nonlinear regression analysis, applied to the four sub-sections of section 1 for 1.0% CMC solution, are presented in Table 5.12.

Considering the non-Newtonian, shear-thinning behaviour of the CMC solutions used in these experiments, the temperature dependence of the viscosity was taken into account in the calculation of the local Reynolds and Prandtl numbers, replacing the viscosity term by equation (3.41) and equations (5.5) and (5.8) for 1.0% CMC and 2.0% CMC solutions, respectively. Accordingly, the values obtained from statistical analysis were applied in equation (3.38), defined as follows:

$$Nu = aRe_g^b Pr_g^c$$

Table 5.12- Statistical parameter obtained by nonlinear regression analysis, for the four sub-sections analysed in section 1, for 1.0% CMC solution.

Sub-section	**Parameter**	**Estimate**	**Standard error**	**95% confidence interval**	
				lower bound	**upper bound**
1	a	2.384	0.375	1.421	3.348
	b	0.117	0.061	-0.041	0.275
2	a	2.171	0.229	1.630	2.712
	b	0.146	0.042	0.046	0.246
3	a	1.012	0.111	0.751	1.274
	b	0.395	0.039	0.302	0.488
4	a	0.596	0.087	0.390	0.803
	b	0.539	0.050	0.422	0.657

For section 1, four thermal correlations were obtained, one for each sub-section defined. Thus, the experimental data were correlated according to the following equations:

$$Nu = 2.384 \cdot Re^{0,117} \cdot Pr^{0,3}, \;\; r^2 = 0.419 \tag{5.22}$$

obtained for sub-section 1, with 1.4<*Re*<22.4 and 414<*Pr*<1380;

$$Nu = 2.171 \cdot Re^{0.146} \cdot Pr^{0.3}, \;\; r^2 = 0.639 \tag{5.23}$$

obtained for sub-section 2, with 1.5<*Re*<24.1 and 383<*Pr*<1268;

$$Nu = 1.012 \cdot Re^{0,395} \cdot Pr^{0.3}, \;\; r^2 = 0.952 \tag{5.24}$$

obtained for sub-section 3, with 1.5<*Re*<26.8 and 343<*Pr*<1124;

$$Nu = 0.596 \cdot Re^{0.539} \cdot Pr^{0.3}, \;\; r^2 = 0.963 \tag{5.25}$$

obtained for sub-section 4, with 1.8<*Re*<29.2 and 313<*Pr*<1014.

The statistical parameters obtained from nonlinear regression analysis of 2.0% CMC experimental data are presented in Table 5.13. The same calculation and analysis procedures were followed as regards to the shear-thinning behaviour.

Table 5.13- Statistical parameter obtained by nonlinear regression analysis, for the four sub-sections analysed in section 1, for 2.0% CMC solution.

Sub-section	**Parameter**	**Estimate**	**Standard error**	**95% confidence interval**	
				lower bound	**upper bound**
1	a	1.321	0.072	1.093	1.549
	b	0.235	0.139	-0.209	0.679
2	a	1.048	0.030	0.951	1.144
	b	0.347	0.088	0.067	0.628
3	a	0.706	0.079	0.453	0.958
	b	0.603	0.291	-0.323	1.529
4	a	0.570	0.102	0.244	0.896
	b	0.248	0.269	-0.608	1.105

For section 1, four thermal correlations were obtained, one for each sub-section defined. Thus, the experimental data were correlated according to the following equations:

$$Nu = 1.321 \cdot Re^{0,235} \cdot Pr^{0,3}, \;\; r^{\,2} = 0.503 \tag{5.26}$$

obtained for sub-section 1, with 0.6<*Re*<1.8 and 2065<*Pr*<2692;

$$Nu = 1.048 \cdot Re^{0.347} \cdot Pr^{0.3}, \;\; r^{\,2} = 0.839 \tag{5.27}$$

obtained for sub-section 2, with 0.7<*Re*<2.1 and 1784<*Pr*<2532;

$$Nu = 0.706 \cdot Re^{0,603} \cdot Pr^{0.3}, \;\; r^{\,2} = 0.599 \tag{5.28}$$

obtained for sub-section 3, with 0.7<*Re*<2.5 and 1454<*Pr*<2326;

$$Nu = 0.570 \cdot Re^{0.248} \cdot Pr^{0.3}, \;\; r^{\,2} = 0.223 \tag{5.29}$$

obtained for sub-section 4, with 0.8<*Re*<2.9 and 1224<*Pr*<2164.

As mentioned previously, in channel 2 the CMC solutions enter the channel in sub-section 4 and exit the channel in sub-section 1.

Considering the flow direction of this non-Newtonian, shear-thinning CMC solution (1.0% w/w) and observing the Reynolds number exponent equations 5.22, 5.23, 5.24 and 5.25, one can conclude that in sub-sections 4 (CMC channel inlet) the value of

Reynolds number exponent is the within the reference range for transitional to turbulent flow, e.g. (Jackson and Troupe, 1964; Edwards *et al.*, 1974; Rene *et al.*, 1991a).

Along the channel length the value of Reynolds exponent decreased until values denoted as laminar flow, as observed by several authors in their studies of heat transfer of non-Newtonian fluids in PHE, using CMC solutions as test fluid, e.g. (Rene *et al.*, 1991a; Galeazzo *et al.*, 2006). This thermal behaviour, observed in the set of heat transfer experiments with 0.25% CMC solution, may also be explained by the more pronounced cooling of the CMC solution in section 2 that contribute to the increase of the viscosity values against the shear rate effect on the viscosity. Consequently, the increased apparent viscosity of CMC solution influences the hydrodynamic behaviour (lower Reynolds numbers in sub-section1).

In the 2.0% CMC/ water heat transfer experiment, carried out with a CMC solution with a stronger shear-thinning behaviour, the same tendency of decrease of Reynolds number exponent was observed when comparing equations 5.26, 5.27, 5.28 and 5.29. At the channel inlet (sub-section 4), a fluctuation of Reynolds number can be observed probably due to entrance effects.

In order to gather more information concerning local convective heat transfer coefficients, the local Nusselt number versus channel length was plotted, for several Reynolds, for section 1, as it is shown in Figures 5.39 and 5.40 for 1.0% and 2.0% CMC solutions, respectively. The experimental data that used for this analysis are shown in Tables A.7 and A.8 (Annex A).

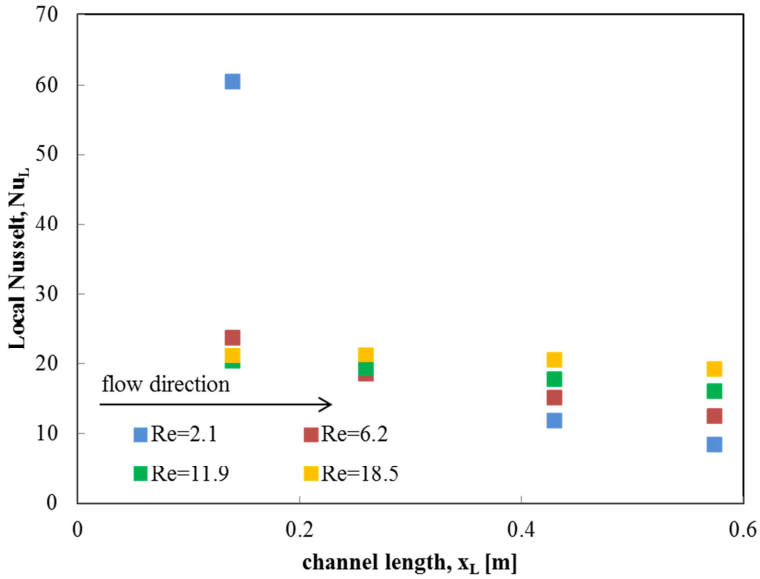


Figure 5.39- CMC solution (1.0%) local Nusselt number variation along channel length (channel 2, section 1), for several Reynolds numbers.

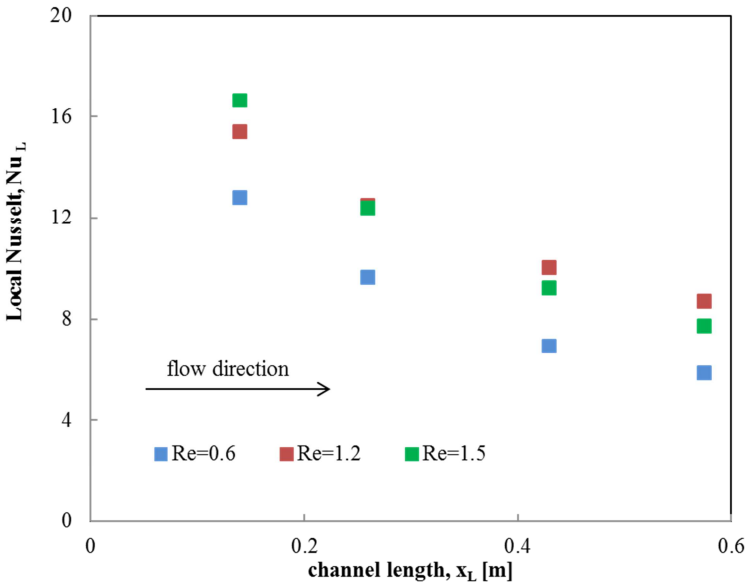


Figure 5.40- CMC solution (2.0%) local Nusselt number variation along channel length (channel 2, section 1), for several Reynolds numbers.

The correlations obtained for local Nusselt number of 1.0% and 2.0% CMC as a function of channel length, for several Reynolds number, in section 1, are presented in Table 5.14.

Table 5.14- Local thermal correlation as a function of channel length, for several local Reynolds numbers of both 1.0% and 2.0% CMC solution, in channel 2.

% CMC	**Local Reynolds number, Re [-]**	**Thermal correlations**
1.0	2.1	$Nu_L = 3.623 \cdot x_L^{-1.386},\ r^2 = 0.990$
	6.2	$Nu_L = 10.082 \cdot x_L^{-0.444},\ r^2 = 0.994$
	11.9	$Nu_L = 15.149 \cdot x_L^{-0.162},\ r^2 = 0.909$
	18.5	$Nu_L = 19.126 \cdot x_L^{-0.061},\ r^2 = 0.656$
2.0	0.6	$Nu_L = 4.368 \cdot x_L^{-0557},\ r^2 = 0.994$
	1.2	$Nu_L = 7.086 \cdot x_L^{-0.401},\ r^2 = 0.994$
	1.5	$Nu_L = 5.825 \cdot x_L^{-0.541},\ r^2 = 0.997$

The local thermal correlations evidence not only the variation of local Nusselt number with the channel length (x_L) but also with Reynolds number noticed by the variation of the constant value.

From Figure 5.39 and 5.40 one can verify that the local Nusselt number has more pronounced variation along the channel length for 2.0% CMC solution most probably due to the more pronounced shear-thinning behaviour and temperature dependence of viscosity as reported in section 5.3.1.

In order to obtain a more clarifying correlation of the effects mentioned previously, the variation of local Nusselt number with Graetz number for both 1.0% and 2.0% CMC solution in channel 2 (section 1) is presented in Figure 5.41.

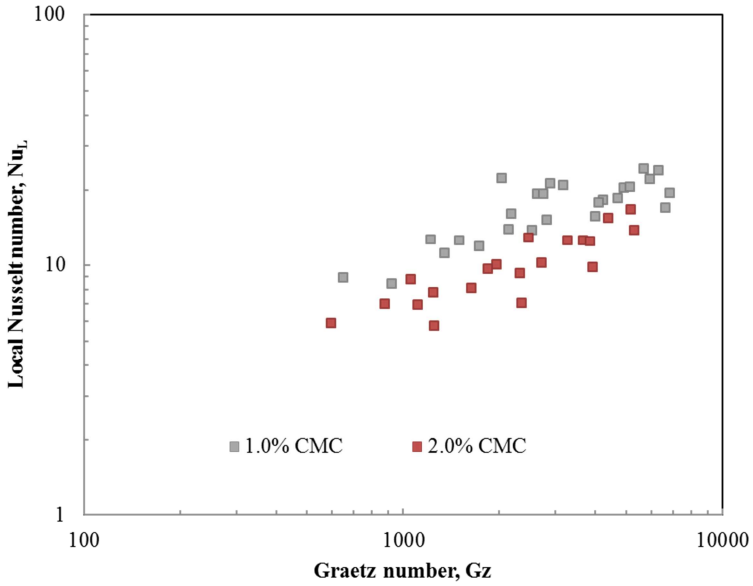


Figure 5.41- CMC solutions (1.0% and 2.0%) local Nusselt number versus Graetz number (channel 2, section 1).

The statistical parameters obtained from nonlinear regression analysis for both non-Newtonian CMC solutions are presented in Table 5.15.

Table 5.15- Statistical parameters obtained by nonlinear regression analysis for channel 2 (section 1).

% CMC	Parameter	Estimate	Standard error	95% confidence interval	
				lower bound	upper bound
1.0	C	1.260	0.607	0.008	2.512
	b	0.325	0.059	0.204	0.446
2.0	C	0.271	0.139	-0.021	0.562
	b	0.466	0.064	0.331	0.601

Thus, the experimental data, for channel 2 were correlated according to the following equations:

$$Nu_L = 1.260 \cdot Gz^{0.325}, \quad r^2 = 0.608 \tag{5.30}$$

for 1.0% CMC solution in the range 653< *Gz* <6844.

For 2.0% CMC solution the correlation obtained is:

$$Nu_L = 0.271 \cdot Gz^{0.466}, \quad r^2 = 0.767 \tag{5.31}$$

for 596< *Gz* <5310.

Figure 5.42 shows a comparison between the correlations obtained in this work (1.0% and 2.0% CMC) and those published in the open literature for thermal entrance region of a parallel-plate channel with Hagen–Poiseuille flow (Bejan and Kraus, 2003; Shah and Sekuli, 2003) and plug-flow (Metzner *et al.*, 1957).

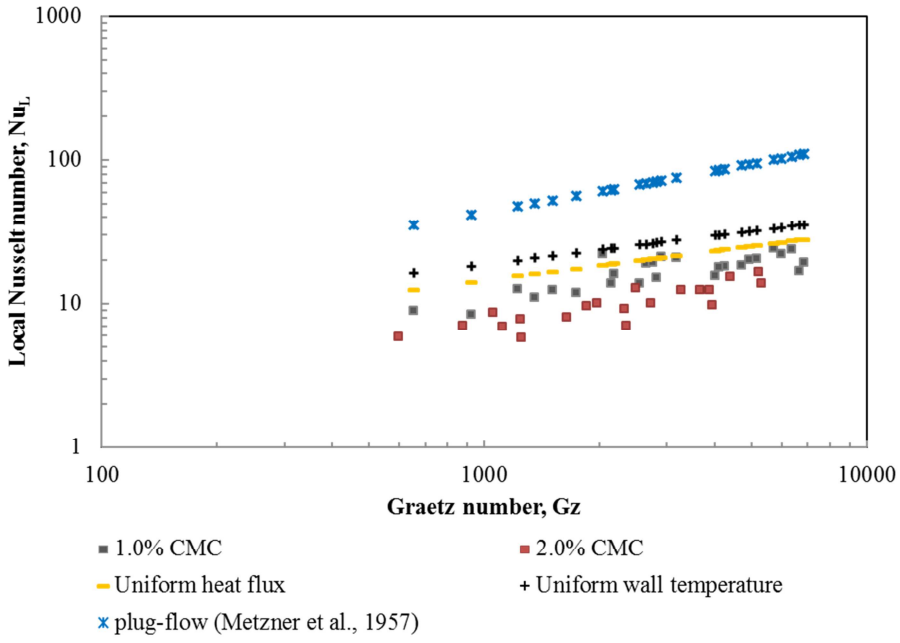


Figure 5.42- Comparison of local heat transfer correlations in the thermal entrance region obtained in the present work (1.0% and 2.0% CMC solutions) and those published in the open literature.

Comparing the results obtained in the present work for different concentrations of CMC and therefore for different non-Newtonian, shear-thinning behaviour fluids, one can notice that for both CMC solutions the Nu-Gz correlations exhibit values of Graetz number exponent typical of thermally developing flows (~1/3).

When comparing the empirical correlations here obtained with those previously published for thermal developing flow in flat parallel-plate channels (for uniform wall temperature and uniform heat flux), as shown in Figure 5.41, the present ones exhibited slightly lower convective heat transfer coefficients, that may be explained by the non-

Newtonian characteristics of the tested fluids and the temperature dependence of their thermophysical properties.

The correlations obtained in this set of heat experiments were also compared with the one published by Metzner, Vaughn et al. (1957) for plug-flow in parallel plates, being observed that local Nusselt numbers determined here were lower than those calculated with equation 5.21. However, the empirical correlations are in good agreement with the correlations proposed by Sourlier, Devienne et al.(1987) for heat transfer of pseudoplastic fluid in parallel plaques in laminar flow, using CMC solutions as test fluid¸ in which Graetz number exponents varied from 0.26 to 0.43.

This experimental study highlighted the effect of the non-Newtonian behaviour on the thermal performance of the PHE. The experimental data obtained in this study is of major importance for the proper design and optimization of PHE, in order to ensure the best thermal performance when used in heat transfer operations with complex fluids such as non-Newtonian food fluids.

5.3.4. Determination of Fanning friction factor correlations

Additionally to the measurement of fluids and wall temperatures along the plate heat exchanger channels, and fluids temperature at PHE inlets and outlets, the overall pressure drop was determined experimentally using pressure transmitters located at both hot and cold fluid sides of the PHE inlet and outlet, as mentioned in section 3.7.2.

Figure 5.43 shows the overall pressure drop on the warm CMC solution side of the PHE as a function of the mean Reynolds number, for different CMC concentrations.

In this Figure, it is possible to observe the effect of CMC concentration in the overall pressure drop, directly related to the viscous Newtonian or non-Newtonian of the CMC solutions tested. Thus, increasing the CMC concentration results in the increase of the overall pressure drop, this effect being more pronounced for the 2.0% CMC solution, due to its the stronger viscous non-Newtonian behaviour. This is also related to the low Reynolds number range observed for the 2.0% CMC solution.

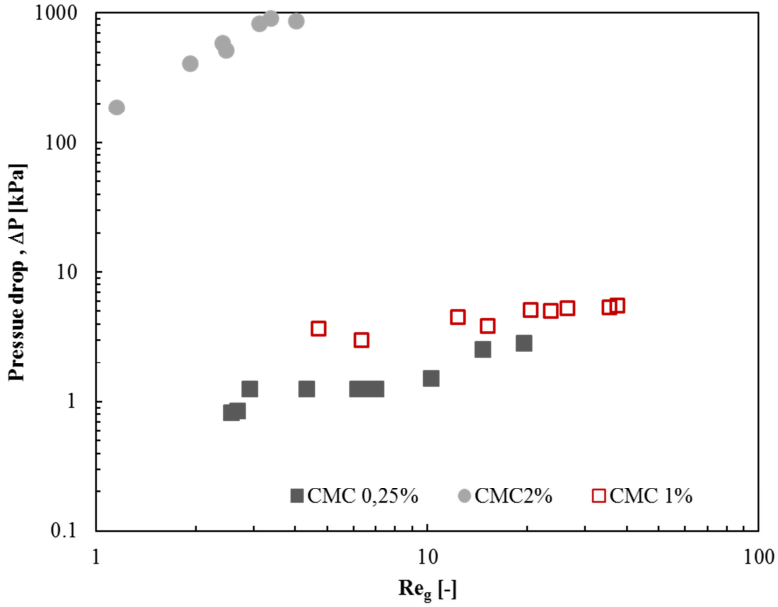


Figure 5.43- Overall pressure drop versus Reynolds number of different CMC solutions.

Figure 5.44 presents the friction factors as a function of the mean Reynolds number of CMC solutions in the present work and those obtained from correlations published in the open literature (Edwards *et al.*, 1974; Leuliet, Maingonnat *et al.*, 1990b; Warnakulasuriya and Worek, 2008).

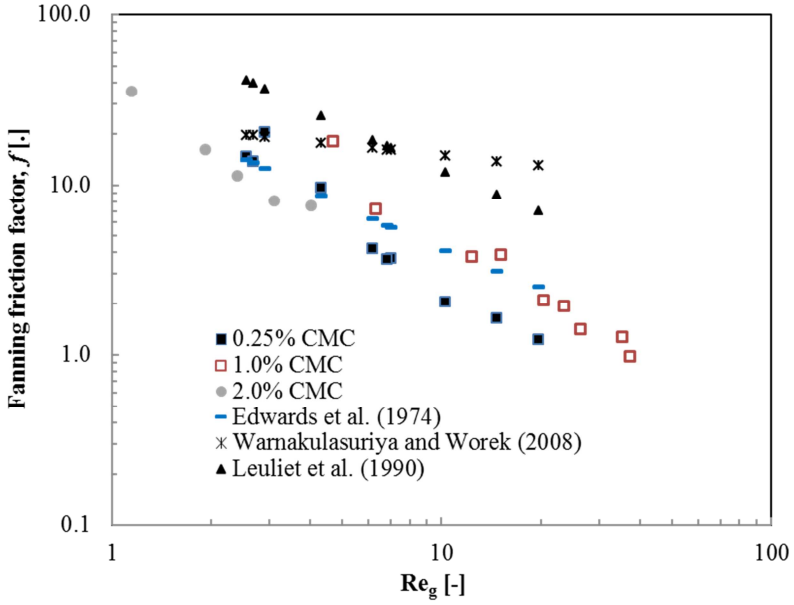


Figure 5.44- Fanning friction factor versus Reynolds number, comparison of correlations obtained in the present work and those published in the open literature.

From Figure 5.44, it possible to observe that the friction factor values of CMC solutions exhibited the same general tendency, noticing a small shift in the friction factor of 0.25% CMC solution due to the fact that the Reynolds number range is slightly higher for this viscous Newtonian solution.

The friction factor values of the 2.0% CMC solution are the highest due to the lower range of Reynolds number of this non-Newtonian solution, which as mentioned before exhibited the stronger shear-thinning behaviour.

The experimental data for the different CMC solutions were correlated according to the following equations:

$$f = 60.538 \cdot Re^{-1,344}, \ r^2 = 0.877 \tag{5.32}$$

for the 0.25% CMC solution;

$$f = 87.973 \cdot Re^{-1,230}, \ r^2 = 0.818 \tag{5.33}$$

for the 1.0% CMC solution;

$$f = 42.629 \cdot Re^{-1.442}, \ r^2 = 0.992 \tag{5.34}$$

for the 2.0% CMC solution.

The correlations obtained for Fanning friction factor were compared with correlations published in the open literature for heat exchangers with chevron plate. In Figure 5.44, it can be observed that the correlations obtained in this work exhibited similar tendency as the previous correlations.

The friction factor correlation obtained by Leuliet, Maingonnat et al. (1990a) in their research on heat transfer to viscous Newtonian and pseudplastic fluids in a plate heat exchanger with chevron plates (β=35º) ranging from laminar to turbulent flow is:

$$\frac{f}{2} = \frac{50}{Re} + \frac{1.30}{Re^{0.10}} \tag{5.35}$$

Edwards, Changal Vaie et al. (1974), in their study of heat transfer and pressure drop of a PHE using Newtonian and non-Newtonian liquids, reported the following correlation:

$$f = \frac{34}{Re} + 0.8 \tag{5.36}$$

referring to the term $\frac{34}{Re}$ as the laminar contribution to pressure drop, which dominates at low values of Reynolds number (Re<10), while 0.8 is the turbulent contribution which becomes important at higher Reynolds number (Re>10) (Edwards *et al.*, 1974). The correlations obtained in the present work for 0.25% and 1.0% CMC solution are in good agreement with this correlation as shown in Figure 5.44.

Warnakulasuriya and Worek (2008), in their study on the heat transfer and pressure drop of high viscous solutions in a single-pass cross-corrugated plate heat exchanger, obtained the following correlation:

$$f = \frac{23.8}{Re^{0.205}} \tag{5.37}$$

In Figure 5.44, one can observe that this correlation does not represent the experimental data, mainly due to the effect of different plate geometrical features that influence the hydrodynamic performance of the PHEs.

5.4 Conclusions

From the CMC-water heat transfer experiments results, the following conclusions were drawn:

a) the correlations obtained for the mean convective heat transfer coefficients of warm CMC solutions are highly dependent on the rheological properties of the fluid. Thus, for low CMC concentration solution (0.25% w/w), the fluid exhibits a viscous Newtonian behaviour dependent on temperature, and the thermal correlation has a Reynolds number exponent within the range 0.65-0.85, typical turbulent flow in PHE for water-like fluids, even at low Reynolds number. As the CMC concentration increased, the rheological behaviour of solutions changed to a shear-thinning non-Newtonian behaviour, exhibiting a more pronounced temperature dependence of the apparent viscosity, evidenced by higher activation energies. Thus, as the CMC concentration increased the Reynolds number exponent decreases to 0.51 for 1.0% CMC solution (flow behaviour index, n=0.97) and to 0.30 for 2.0% CMC solution (n=0.879). The Nusselt-Prandtl-Reynolds correlation obtained for the 2.0% CMC solution has a Reynolds number exponent typical of laminar flow. The stronger the shear-thinning

behaviour, expressed by low flow behaviour index (n<1) and higher consistency index, the lower the Reynolds number ranges.

b) the fluids and wall temperature profiles along the PHE channels, in both passes of the heat exchanger, provided valuable information regarding differentiated local heat transfer in a PHE with a multipass arrangement. The CMC-water experiments corroborated the results obtained in water-water experiments and also provide important information concerning local heat transfer dominances along the heat exchanger.

c) as in water-water experiments, due to temperature profiles along the PHE channels, the local thermal correlations obtained are variable-property correlations that take into account the temperature effects on the transport properties of the fluids, reducing the errors introduced by the constant –property assumption. This is quite important when the fluids exhibit different sensitivities to temperature changes evidenced by different activation energies, influencing the rheological behaviour of the fluids and consequently the local hydrodynamics and heat transfer process.

d) CMC-water heat transfer experiments confirmed that the overall heat transfer coefficient varied along the PHE channels, more significantly in section 1, as mentioned previously. In section 1, the local overall heat transfer coefficient values varied within the ranges 284-2539 for 0.25% CMC experiments, 498-2144 for 1.0% CMC experiments and 380-949 for 2.0% CMC experiments. These data evidence the decreasing of local overall heat transfer coefficients due to the decrease of local convective heat transfer coefficients of CMC solution as consequence of lower Reynolds number caused by the increase of the shear-thinning non-Newtonian behaviour.

e) the correlations obtained for the local convective heat transfer coefficients of each CMC, for every single sub-section along the PHE channel reflected the change of flow regime along the PHE. For the studied section (section 1), the exponent of the Reynolds number decreased along the channel length, as the fluid was cooled down, evidencing turbulent to laminar flow when the warm CMC solution flows through PHE from section 2 to section 1. The changes in the Reynolds number exponent are more pronounced for CMC non-Newtonian solutions. For CMC viscous Newtonian solution, the exponent of Reynolds number decreased progressively along the channel length, as

the fluid was cooled down, evidencing turbulent, transition and laminar flow along PHE section 1.

f) the local Nusselt number variation along the channel length highlighted the thermally developing flow along the PHE channels. The Nu-Gz correlations obtained for section 1 of the PHE were similar to ones published for thermal developing flow, for the non-Newtonian CMC solutions, and exhibited a higher value of the exponent of the Graetz number for the viscous Newtonian CMC solution.

g) concerning Fanning friction factor correlations, comparison of the experimental correlations with the available literature showed good agreement, at least as regards the general trends reported. As regards to the CMC concentration effect, the study evidenced, as expected, that increasing the CMC concentration results in the increase of the overall pressure drop, this effect is more pronounced for the 2.0% CMC solution, due to the stronger viscous non-Newtonian behaviour when compared with the other solutions tested. Discrepancies may be due to differences in the compared channels geometries and uncertainties in measurements.

6. DETERMINATION OF MEAN AND LOCAL CONVECTIVE HEAT TRANSFER COEFFICIENTS OF STIRRED YOGHURT COOLING IN A PLATE HEAT EXCHANGER

6.1 Introduction

Yoghurt is a dairy food with a complex theology that depends on some physical properties of the milk-base such as solids concentration, the physical state of fats and proteins and presence of thickening and type of starter culture (ropy/ non-ropy strains) all together with processing conditions such as heat treatment and post-incubation conditions as cooling and packaging conditions (Fangary, Barigou *et al.*, 1999; Tamime and Robinson, 1999; Afonso *et al.*, 2003).

The knowledge and understanding of the rheological properties of yoghurt are of major importance to texture, stability and process design and optimisation in order to obtain a product with the desired sensory attributes, particularly with the well-defined texture which is a key quality attribute for consumer acceptability (Fangary *et al.*, 1999).

Food processing conditions can bring about irreversible changes in the product texture and sensory attributes. In stirred yoghurt production, the post-incubation processes as cooling in a plate heat exchanger, pumping and flowing in a pipeline are responsible for viscosity decay and partial or complete structure breakdown of the product (Maia, Nóbrega *et al.*, 2007).

The industrial development of plate heat exchangers was considerable in recent years, particularly in the food industry for viscous food fluids, but the information available for the design of plate heat exchangers is scanty and continues to be proprietary, particularly using real food fluids.

In order to gather information concerning heat transfer and hydrodynamic behaviour of Newtonian and non-Newtonian food fluids in heat exchangers, very few studies have been conducted in the last years, using real food fluids such as milk (Delplace, 1995; Zettler and Müller-Steinhagen, 2001), stirred yoghurt (Afonso *et al.*, 2003; Fernandes, Dias *et al.*, 2005a; Fernandes *et al.*, 2006), orange juice (Kim, Tadini *et al.*, 1999),

pineapple juice and banana puree (Tadini, Badolato *et al.*, 2000; Ditchfield, Tadini *et al.*, 2007; Cabral, Gut *et al.*, 2010; Cabral, Gut *et al.*, 2011) and liquid egg yolk (Bernardi, Silveira Jr. *et al.*, 2009) and pasteurisation processes (Gut and Pinto, 2003b).

Heat transfer experiments were conducted using water and stirred yoghurt as working fluid in cold and hot sides of the plate heat exchanger, respectively.

The heat experiments were carried out in order to obtain empirical thermal correlations for the determination of mean and local convective heat transfer coefficients for stirred yoghurt with different rheological properties obtained by preparation and production stirred yoghurt with different total solids concentrations.

6.2 Experimental methodology

In this chapter are presented all the results obtained in the stirred yoghrt/ water heat transfer experiments conducted in order to obtain accurate thermal correlations for the determination of both mean and local vaconvective heat transfer coefficients of stirred yoghurt during cooling in a PHE with chevron plate (β=35º/35º) with a multipass configuration 2×2/2×2 in countercurrent.

Stirred yoghurt was produced in the test facility following the procedure described in section 3.3.2. Products with different rheological properties were produced by varying the type of starter culture and total solids content following the blending described for each formulation as presented in Table 6.1.

Table 6.1- Stirred yoghurt formulations used in heat transfer experiments

Formulation ID	**Starter Culture**	**MSNF (%)**	**SMP (%)**	**SMP HP50 (%)**	**CMC (%)**	**Sweet Whey (%)**	**Total Solids (%)**
12% TS-YF (F1)	YF–L812	12	0	0	0	0	12
13% TS-YF (F2)		12	1	0	0	0	13
13% TS-HP50 (F8)		12	0	1	0	0	13
13% TS-HWC (F43)		12	0.625	0.125	0.125	0.125	13
13% TS-YC (F17)	YC-380	12	0	0	0	0	13

6.2.1 Thermophysical properties

The rheological properties of stirred yoghurt were determined by oscillatory shear rheometry (section 3.5.1), performing frequency sweeps in the 0.01-10 Hz range and the oscillation stress was fixed at 1.0 Pa. The temperature dependence of dynamic viscosity was determined by steady shear (shear stress and shear rate) data were obtained over the shear rate range of 0.001–100 s^{-1} at different temperatures (20–45ºC). The experiments were performed using a TA Instruments AR-G2 StressTech controlled-stress rheometer with 40 mm diameter parallel plate geometry (P 40 ETC) at 1.0 mm measuring gap distance.

The density of stirred yoghurt in kg/m^3, as a function of temperature was determined by mean of the following empirical model (Toledo, 2007):

$$\boldsymbol{\rho} = \frac{\mathbf{1}}{[\sum(\mathbf{X_i}/\boldsymbol{\rho_i})]} \tag{6.1}$$

where X_i is the individual mass fraction of each food component considered and ρ_i is the individual density of the component.

The individual densities, ρ_i, were calculated at the temperature T, in ºC, using the following equations for water (ρ_w) and protein (ρ_p), the individual components considered in this study (Toledo, 2007):

$$\rho_w = 997.18 + 0.0031439 \cdot T - 0.0037574 \cdot T^2 \tag{6.2}$$

$$\rho_p = 1329.9 - 0.51814 \cdot T \tag{6.3}$$

The specific heat of stirred yoghurt, in J/(kg K), as a function of temperature was determined by mean of the following empirical model (Toledo, 2007):

$$c_p = \sum(X_i \cdot C_{p,i}) \tag{6.4}$$

where X_i is the individual mass fraction of each food component considered and $c_{p,i}$ is the individual specific heat of the component.

The individual specific heat, $c_{p,i}$, were calculated at the temperature T, in ºC, using the following equations for water $(c_{p,w})$ and protein $(c_{p,p})$, the individual components considered in this study (Toledo, 2007):

$$c_{p,w} = 4176.2 - 9.0864 \times 10^{-5} \cdot T + 5473.1 \times 10^{-6} T^2 \quad (6.5)$$

$$c_{p,p} = 2008.2 - 1208.9 \times 10^{-3} \cdot T + 1312.9 \times 10^{-6} T^2 \quad (6.6)$$

The thermal conductivity of stirred yoghurt, W/(m K) , as a function of temperature was determined by mean of the following empirical model (Toledo, 2007):

$$\lambda = \sum(\lambda_i \cdot X_i) \quad (6.7)$$

where X_i is the individual mass fraction of each food component considered and λ_i is the individual thermal conductivity of the component.

The individual thermal conductivity, λ_i, were calculated at the temperature T, in ºC, using the following equations for water (λ_w) and protein (λ_p), the individual components considered in this study (Toledo, 2007):

$$\lambda_w = 0.57109 + 0.0017625 \cdot T - 6.7306 \times 10^{-6} \cdot T^2 \quad (6.8)$$

$$\lambda_p = 0.1788 + 0.0011958 \cdot T - 2.7178 \times 10^{-6} \cdot T^2 \quad (6.9)$$

6.2.2 Structure analysis by CryoSEM

The Cryo-Scanning Electron Microscopy observations (CryoSEM) were performed in the Materials Center of University of Porto (CEMUP) with a JEOL JSM-6301F microscopy coupled with the micro-analysis system OXFORD INCA/ENERGY 350.

The yoghurt samples analysis were carried out following the procedure described in section 3.6.2.

6.2.3 Heat transfer experiments

The heat experiments in the plate heat exchanger with stirred yoghurt were carried out according to the procedures described in sections 3.7.1 and 3.7.2.

In Table 6.2 it is presented the flow rates of stirred yoghurt and cooling water for each set of heat transfer experiments with a different yoghurt formulation.

.

Table 6.2- Flow rates ranges of stirred yoghurt and cooling water, for each yoghurt formulation tested.

Formulation ID	**Yoghurt flow rate range [kg/s]**	**Cooling water flow rate range [kg/s]**
12% TS-YF	0.06 – 2.8	1682 - 9351
13% TS-YC	0.05 - 0.68	3284 - 10379
13% TS-YF	0.07 - 0.84	4226 - 12574
13%TS-HP50	0.34 - 2.10	2005 - 4537
13%TS-HMC	0.18 - 1.04	3411 - 7670

The cooling water temperature at the PHE inlets varied among 10-22ºC and the stirred yoghurt entries among 43-20ºC (mean ranges).

In Table 6.3 are presented the Reynolds number and Prandtl number ranges used for each stirred yoghurt formulation heat experiments set.

Table 6.3- Reynolds number and Prandtl number ranges of stirred yoghurt and cooling water, for each yoghurt formulation tested.

Formulation ID	**Yoghurt Reynolds number range [-]**	**Yoghurt Prandtl number range [-]**	**Cooling water Reynolds number range [-]**	**Cooling water Prandtl number range [-]**
12% TS-YF	0.06 – 2.8	1682 - 9351	979 - 1473	6.5 - 9.8
13% TS-YC	0.05 - 0.68	3284 - 10379	869 - 1255	7.6 - 11.2
13% TS-YF	0.07 - 0.84	4226 - 12574	1198 - 1478	6.5 - 8.1
13%TS-HP50	0.34 - 2.10	2005 - 4537	1019 - 1338	7.2 - 9.8
13%TS-HMC	0.18 - 1.04	3411 - 7670	1079 - 1316	7.4 - 9.2

The mean convective heat transfer coefficients of stirred yoghurt formulations were calculated according to procedures described in section 3.8.1, having in consideration the following assumptions: average constant thermal properties (thermal conductivity and specific heat) and convective heat transfer coefficients along the heat exchanger, negligible internal heat generation, negligible axial convection or conduction and

negligible free convection. Nonlinear regression analysis was performed using the Levenberg–Marquardt method for minimizing the sum of squared residuals function (section 3.9) in order to obtain a thermal correlation.

The local convective heat transfer coefficients of stirred yoghurt formulations were calculated according to procedures described in section 3.8.2., considering the experimentally two monitored sections of the PHE. Each section was divided in four sub-sections in order to determine four local overall heat transfer coefficients along the PHE controlled plates. Therefore, the variation of the local overall heat transfer coefficients as well as the local convective heat transfer coefficients of stirred yoghurt along the PHE was determined, considering the temperature dependence of the thermophysical properties of both fluids. The local convective heat transfer coefficients were calculated from the four correlations obtained by nonlinear regression analysis as referred in section 3.9.

6.3 Results and Discussion

6.3.1 Rheological characterisation

In Table 6.4 are presented the main operating conditions of stirred yoghurt for all the formulation sets used in the yoghurt/water heat transfer experiments.

Table 6.4- Yoghurt production conditions, pH of milk before innoculation, fermentation temperature and pH variation (mean values).

Formulation ID	**milk pH before innoculation**	**Fermentation temperature [°C]**	**Fermentation**	
			pH (t=0h)	**pH (t=3-3.5h)**
12% TS-YF	6.52 ±0.05	42.9±0.6	6.42±0.05	4.72±0.06
13% TS-YC	6.60 ±0.08	42.6±0.9	6.39±0.05	4.83±0.06
13% TS-YF	6.50 ±0.10	43.3±0.6	6.39±0.07	4.83±0.09
13%TS-HP50	6.43 ±0.04	42.5±0.7	6.36±0.0	4.83±0.03
13%TS-HMC	6.53 ±0.16	42.0±0.0	6.41±0.08	4.84±0.01

In Table 6.4 one can observe that the pH of milk blending before the addition of starter culture didn´t varied significantly with the formulation used. The fermentation temperature was kept around 43ºC, though small variations were observed. The fermentation temperature was in the range (35-45ºC) recommended for the starter cultures used in this study: a ropy starter culture YF-L812 (CHR-HANSEN, 2003) and a non-ropy starter culture YC-380 (CHR-HANSEN, 2004).

The profile of pH reduction during the fermentation process was similar for both starter cultures, as shown in Figure 6.1 in which the time-course of pH change during fermentation is presented for both lactic acid cultures used.

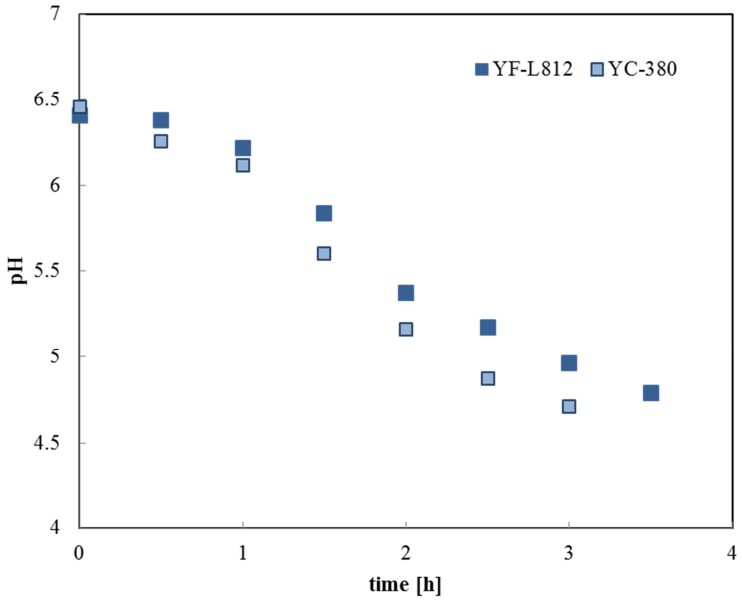


Figure 6.1- Time-course of pH reduction during fermentation for both starter culture used in this study.

Although the profiles of pH reduction were similar, in Figure 6.1 one can observe that after 1.0 h of fermentation, the starter culture YC-380 exhibited a the rate of pH reduction higher than those of YF-L812, reaching the desired pH 0.5 h earlier. This was observed in all the experiments.

In Table 6.5 are shown the main composition parameters of stirred yoghurt, for each formulation tested.

Table 6.5- Composition parameters of stirred yoghurt for each formulation tested (mean values).

Formulation ID	Total solids content (%)	Fat content (%)	Protein content (%)
12% TS-YF	11.31±0.51	0	5.04±1.38
12% TS-YC	11.07±0.64	0	4.38±0.47
13% TS-YF	11.83±0.69	0	6.32±1.10
13%TS-HP50	11.83±0.03	0	7.56±0.64
13%TS-HMC	13.45±1.25	0	6.48±1.15

The values obtained for the main composition parameters are within the range observed in published literature for skimmed and fatty-free yoghurts, which usually contained higher protein content (>4.0%; (w/w),. e.g. (Alakali, Okonkwo *et al.*, 2008; Chryssanthopoulos and Maridaki, 2010).

The formulation 13%TS-HP50 exhibits higher protein content explained not only by a high total solids content but also by the blending characteristics. This blending included skim milk powder and high protein content skim milk powder (HP50) that contributed for this high parameter(Mistry and Hassan, 1992).

Oscillatory shear rheometry procedures were run for all the formulations tested.in order to characterise the rheological behaviour of the stirred yoghurt produced,

Dynamic stress sweeps were performed prior to frequency sweeps in order to characterise the materials stability by identifying the limits of linear viscoelastic region.

Figure 6.2 shows a variation of storage (G´) and loss (G``) moduli obtained during a stress sweep procedure for the formulation 13%ST-YF. This is representative of the spectra obtained with the other stirred yoghurt samples.

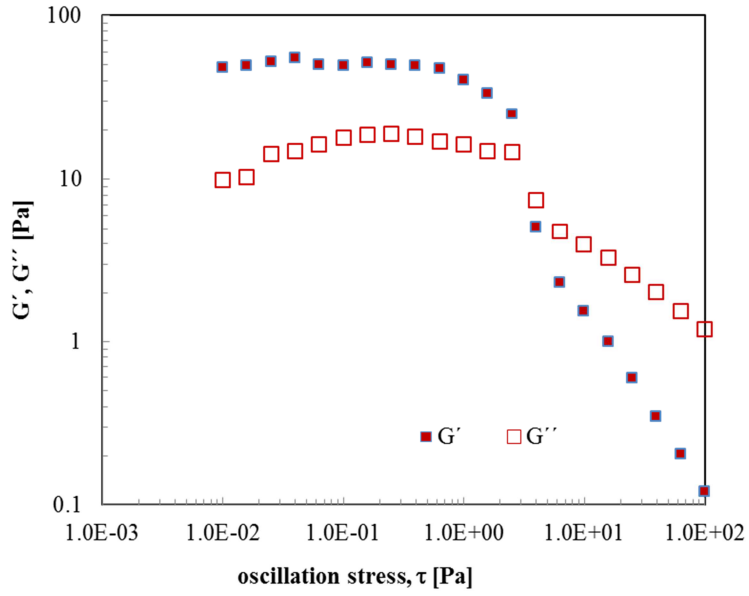


Figure 6.2- Storage and loss moduli as a function of oscillation stress of stirred yoghurt in fermentation tank (13%ST-YF).

From Figure 6.2 one can observe that the linear region until an oscillation stress around 1.5 Pa after which the gel exhibits an abrupt change in its structure, this is typical of weak gels (Steffe, 1996). Thus, it is possible verify that at oscillation stress higher than 1.5 Pa, further than this linear region, the elastic structure begins partially to breakdown, when G' < G", the material undergoes change from a predominantly elastic to a viscous structure. These results are corroborated by former studies accomplished by the author (Afonso and Maia, 1999) and by other authors, e.g. (Benezech and Maingonnat, 1994; Tunick, 2000; Lee and Lucey, 2006), regarding the weak gel behaviour at small stress amplitudes.

Figure 6.3 shows the mechanical spectra, at 20ºC, of the stirred yoghurt collected in the fermentation tank after stirring, for the different formulations used in these experiments.

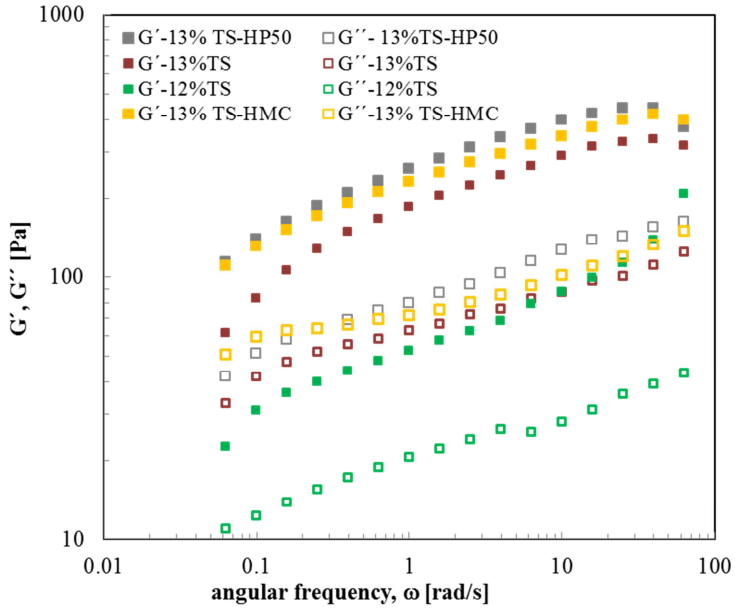


Figure 6.3- Comparison of the mechanical spectra of the stirred yoghurt in the fermentation tank for all the formulations.

From Figure 6.3 one can observe that for all the stirred yoghurt formulations analysed the storage (elastic) modulus is higher than the loss (viscous) modulus in all the range of angular frequency sweep, evidencing the elastic structure of the disrupted protein network of stirred yoghurt.

Comparing the mechanical spectra of the 12% TS–YF and 13% TS stirred yoghurts on can verify that the stirred yoghurt with higher total solids content (13% TS – YF) exhibited in all the frequency range an G´ and G´´ values three times higher than those of 12% TS–YF. Thus, the higher the total solid content the stronger is the elastic structure of the disrupted protein network. It is well reported the effect of total solids content in the firmness and viscosity of yoghurt, relating high solids content with higher viscosities and firmness (Lucey and Singh, 1997; Tamime and Robinson, 1999).

Figure 6.4 shows the variation of complex viscosity (η^*) and tan δ (=G´´/G´), at 20ºC, for the different stirred yoghurt formulations.

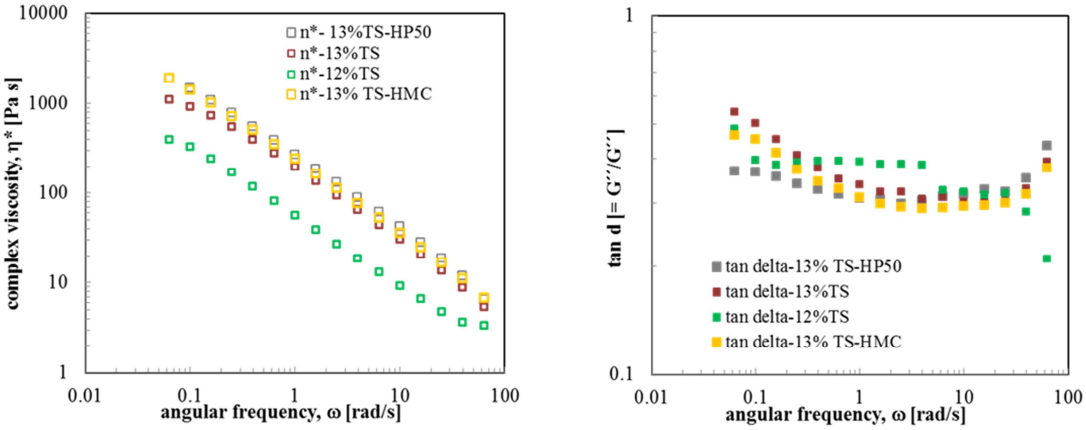


Figure 6.4- Complex viscosity (η*) and tan δ, at 20ºC, for the different stirred yoghurt formulations.

From Figure 6.4 one can confirm that the higher the total solids contents the higher the firmness of stirred yoghurt, since the complex viscosity values are higher in all the stirred yoghurt formulations with 13% TS content when compared with 12% TS–YF.

From all the mechanical spectra shown in Figures 6.3 and 6.4 one can observe that all the stirred yoghurt exhibited a typical behaviour of weak gel in which tan δ <1 (G´>G´´) for the angular frequencies range applied.

For angular frequencies higher than 6.283 rad/s, the 12% TS–YF stirred yoghurt exhibited a decrease of tan δ, due to some structure rearrangement mainly caused by some wheying off, a problem that frequently occurs in set yoghurt.

Comparing the stirred yoghurt formulations with 13% TS and different blends, one can verify in Figure 6.4 that no significant differences are observed in complex viscosity and tan δ values. In Figure 6.3 it is shown that 13% TS stirred yoghurt with no further addition besides skim milk powder has G´ values lower than the other formulation. Hence, 13% TS stirred yoghurt protein network is weaker gel than those obtained when high protein skim milk powder is added or when it is also added a thickening agent (CMC). These results are in agreement with the work carried out by Moddler et al. (1983) in the determination of the influence of various milk-based protein additives in physical-chemical and sensory properties of yoghurt, observing an increase of yoghurt firmness with the increase of protein content as well as a decrease on syneresis.

In Figure 6.5 is presented a comparison between the mechanical spectra of 13% TS content stirred yoghurt produced with different starter cultures in order to evaluate the effect of starter culture in the mechanical spectrum of stirred yoghurt.

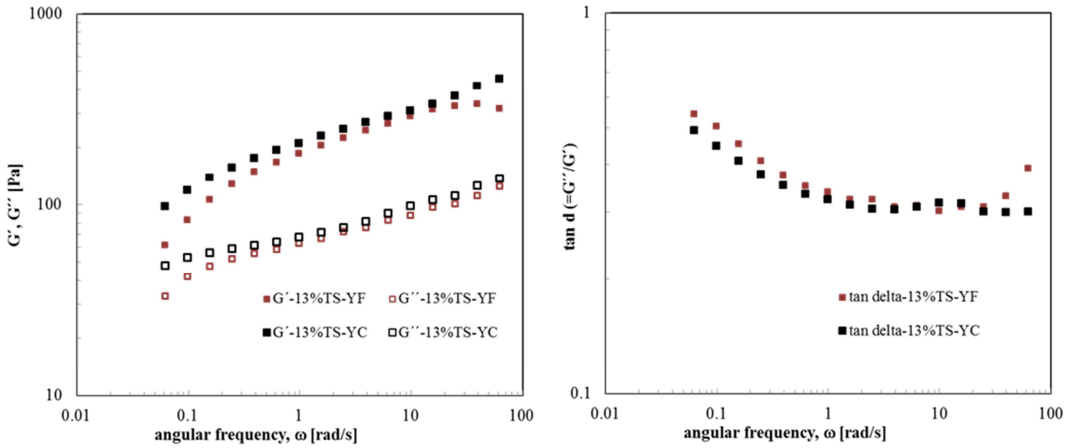


Figure 6.5- Effect of the starter culture in the mechanical spectra of the stirred yoghurt produced.

From Figure 6.5 one can observe that the stirred yoghurt produced with ropy strains starter cultures (13%TS-YF) exhibited slightly lower values of G´ and G´´, resulting in less firm yoghurt, this may be explained by the influence of exopolysaccharides produced by ropy bacteria in the protein matrix, these results are in agreement with those reported by Hassan et al. (1996b) in their study on the effects of encapsulated strains of lactic acid bacteria on the textural properties of yoghurt. Tunick (2000) in his review on the rheology of dairy foods that gel, stretch, and fracture referred that more viscous yoghurts are produced with longer fermentation times and more ropy strains, but less firm products are obtained when ropy strains are used.

In Table 6.6 are presented the physical and rheological parameters obtained for each formulation of stirred yoghurt.

The effect of total solids content in the occurrence of syneresis is evidenced from the results in Table 6.6. Thus, low total solids content are related with higher syneresis values, as one can verify when comparing 12%TS-YF and 13% TS-YF stirred yoghurts. These results are in good agreement with results published in open literature (Lucey and Singh, 1997; Penna, Converti *et al.*, 2006).

The rheological parameters were determined following the same calculation procedure described in section 5.3.1 for the non-Newtonian CMC solutions, in which from the oscillatory shear experiments it was obtained the dynamic viscosity (η') as a function of the angular frequency. The curve was fitted with a power law equation, written as follows (Rohm and Kovac, 1995) :

$$\eta' = k \cdot \dot{\omega}^{n-1} \tag{6.10}$$

where *k* is the consistency (Pa s^n) and *n* represents the flow behaviour index (-).

Regarding the rheological parameter, one can observe that increasing the total solids content the consistency value will increase while the flow index behaviour decrease. This was also observed by Penna et al. (2006) when studying the simultaneous effects of total solids content, milk base and heat treatment temperature on the rheological properties of stirred yoghurt. The density values determined using a pycnometer were not in accordance with the expected ones, since no clear tendency is observed between the increase of total solids content and the expected density increasing.

Table 6.6- Physical and rheological parameter of stirred yoghurt, for each formulation (mean values).

Formulation ID	**Syneresis (fermentation tank) (%)**	**Density [g/ cm^3]**	**Consistency, K [Pa s^n]**	**flow behaviour index, n [-]**
12% TS-YF	76.63±4.79	1.039±0.023	27.45	0.197
13% TS-YC	74.73±7.17	1.035±0.002	35.34	0.176
13% TS-YF	72.80±4.36	1.027±0.004	62.07	0.185
13%TS-HP50	73.67±1.72	1.035±0.002	39.26	0.167
13%TS-HMC	79.29±0.63	1.047±0.003	75.57	0.139

As regards the effect of starter culture one can verify that the use of EPS-producing strains reduced the % syneresis as reported by Tunick (2000) and Hassan et al. (1996b). The use of ropy strains resulted in stirred yoghurts with higher consistency and no significant effect is observed in the flow behaviour, these results are in good agreement with those obtained by Hassan et al. (1996a) in their study on the rheological properties of yoghurt produced with ropy cultures, ropy encapsulated cultures and nonropy

unencapsulated cultures in which they had produced higher consistency yoghurts with ropy strains compared with those of products produced using encapsulated and unencapsulated nonropy strains.

Oscillatory time sweeps were carried out in order to evaluate the occurrence of possible macro- or micro-structural rearrangements with time that may influence rheological behaviour of stirred yoghurt. Time sweeps were performed in the linear viscoelastic region.

Figure 6.6 shows the G´ and G´´ values as a function of time. The plots shown for 13%ST-YF stirred yoghurt collected in the fermentation tank after stirring and after cooling in the PHE are representative of the behaviour observed in the others formulations of stirred yoghurt.

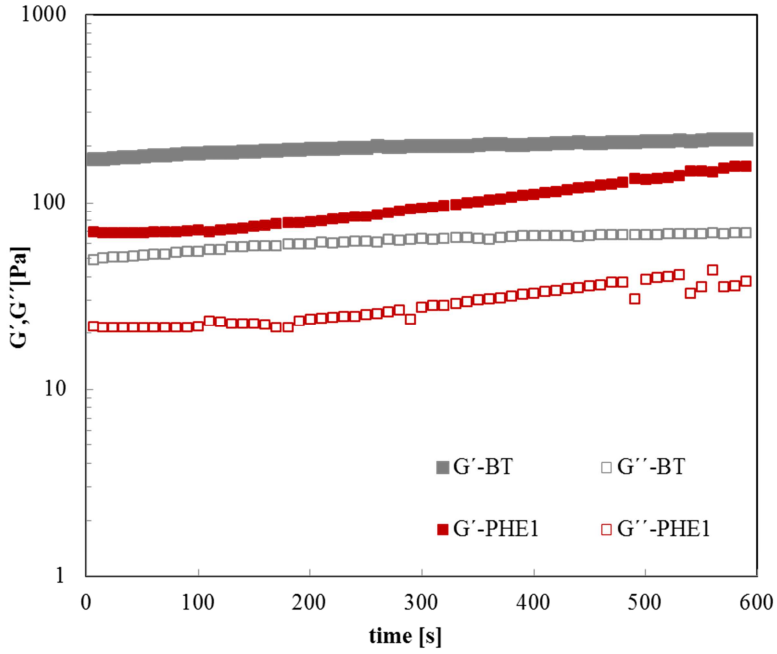


Figure 6.6- Storage and loss moduli of stirred yoghurt as function of time (BT-sample collected in the fermentation tank; PHE- sample collected after cooling in the PHE).

From the analysis of Figure 6.6 one can verify that the stirred yoghurt sample collected after stirring in the fermentation tank exhibited a steady weak gel structure (G´>G´´). The stirred yoghurt sample collected after cooling in the PHE exhibited a gel

structure weaker than the stirred sampled collected in the fermentation tank, as expected since the product during cooling in the PHE were submitted to high shear stress that contributed to further structure breakdown.

6.3.2 Temperature dependence

The evaluation of the temperature dependence of the apparent viscosity of the stirred yoghurt samples was carried out by oscillation procedure with a temperature ramp from 20 to 45ºC at an angular frequency of 6.283 rad/s and an oscillation stress of 1 Pa.

In Figures 6.7 and 6.8 are shown the logarithmic dynamic viscosity as a function of the inverse of the absolute temperature, for the stirred yoghurt samples collected in the fermentation tank and after cooling in the PHE, respectively.

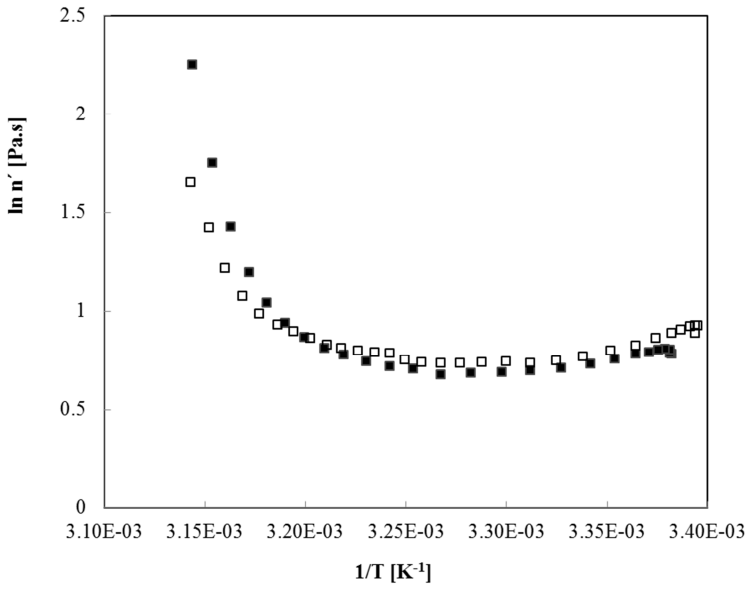


Figure 6.7- Temperature dependence, stirred yoghurt in the fermentation tank (13%ST-YF).

From Figure 6.7 one can observe that the stirred yoghurt collected in the fermentation tank exhibited an inflection in the temperature dependence at a temperature around 30ºC, evidencing the existence of two different regions that express different temperature dependencies. The existence of stirred yoghurt flow behaviour with different temperature dependencies was already been described by Afonso and

Maia (1999) and Afonso et al. (2003) in their stirred yoghurt rheology and heat transfer studies. These authors reported that for temperatures below 25°C, the stirred yoghurt showed activation energy values rather lower than those for temperatures above 25°C.

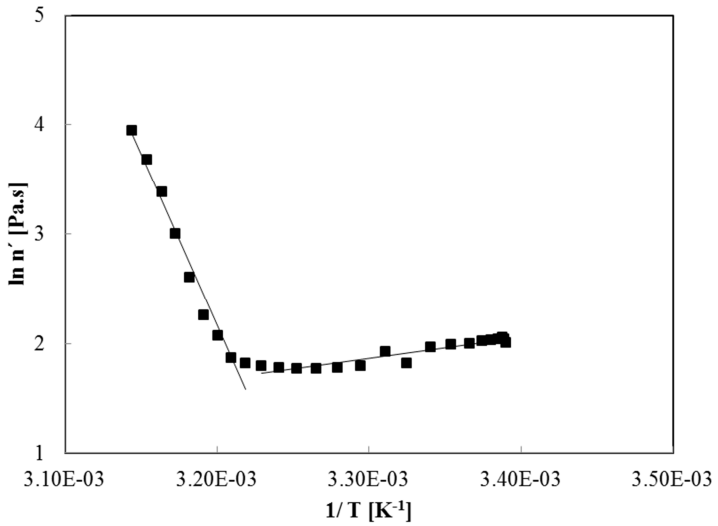


Figure 6.8- Temperature dependence, stirred yoghurt after cooling stage (13%ST-YF).

In Figure 6.8 one can verify that the stirred yoghurt collected after cooling in the PHE exhibited a similar behaviour with temperature, although a more pronounced the transition in the temperature dependence is observed at 35-40ºC.

Assuming that the temperature dependency of the apparent viscosity can be characterised by the Arrhenius-type equation ($\eta = A \cdot e^{E/RT}$), the activation energy values were determined, as shown in Table 6.7, as a function of total solids content.

Table 6.7- Energy activation values, at constant oscillation stress, stirred yoghurt with 12% and 13% total solids content (TS%).

TS [%]	**Temperature range [ºC]**	**Slope [K]**	**Activation energy, Ea [J/mol]**
12%	20 – 30 30 - 45	2113 4469	17564 37159
13%	20 – 30 30 - 45	1438 6463	11957 53733

The activation energy values were determined for all the stirred yoghurt formulations samples collected in the fermentation tank due to the interest of these values to be included in the heat transfer analysis of the yoghurt/ water experiments. The activation energy values obtained are similar to those obtained by Afonso and Maia (1999) using yoghurt samples collected along the an industrial production line and by Afonso et al. (2003) with yoghurt samples produced in a stirred yoghurt production pilot facility.

6.3.3. Determination of the mean convective heat transfer coefficients of stirred yoghurt

For each heat experiment, temperatures of both hot and cold fluid sides of the PHE inlet and outlet were monitored and registered as mentioned in section 3.2.2.

Figure 6.9 shows an example of PHE inlet and outlet temperatures during an stirred yoghurt/ water experiment carried out with a stirred yoghurt with 12% total solids content, in which it is possible to observe that temperatures became steady less than one minute after the beginning of the heat transfer experiment. Such as in water/ water experiments, the transient period observed in the temperature profiles was neglected for calculation purposes.

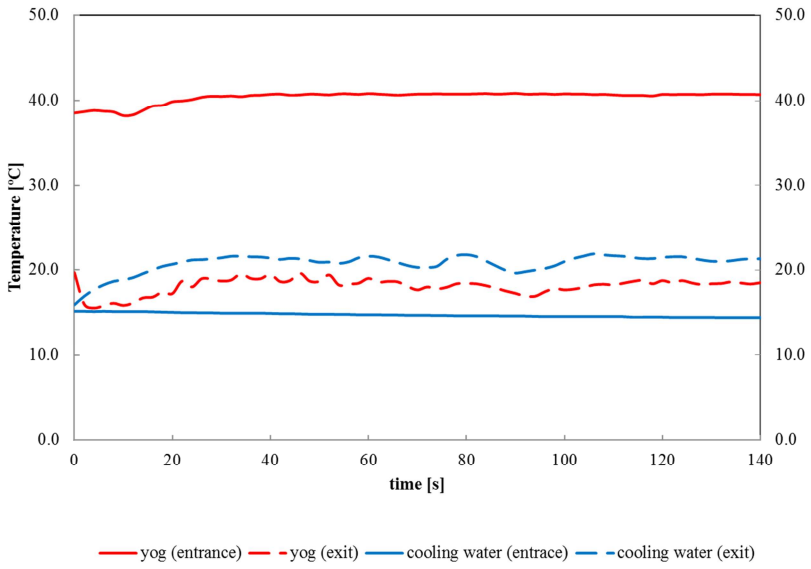


Figure 6.9- PHE ports temperatures (entrance/exit) along experiment time of each fluid, in 12%TS stirred yoghurt / water experiment (Re_{YOG}=1.10).

From the experimental data (temperatures of both stirred yoghurt and cold water sides of the PHE inlet and outlet, mass flow rates of both fluids) the heat flow transferred to cooling water and the heat flow transferred from the warm stirred yoghurt was determined.

In these experiments the flow rate of cooling water was kept almost constant at maximum power of the centrifuge pump used in the set-up. Different process conditions were obtained by varying temperature of the inlet fluids and flow rate of CMC solution. The criterion of data acceptance used in water/ water experiments was applied in this set of experiments. Thus, data were accepted only if the deviation between heat transfer rates from hot and cold sides were less than 20%.

Table 6.8 shows the values of the heat transfer rates in each experiment for different generalised Reynolds numbers of stirred yoghurt and different yoghurt formulations.

Differences between the rates of heat transfer to the cold water and from the warm stirred yoghurt can be observed in Table 6.8, evidencing the existence of some heat exchange with the surrounding air. The mean value of heat losses percentage was within the range of 5 to 14%.

Likewise in the former heat transfer experiments, due to the differences observed in the heat rates exchanged between the two fluids, a criterion was established so that the overall heat transfer coefficients were determined from the data measured on the cooling water side. The overall heat transfer coefficients were obtained by equation 3.9 (section 3.8.1).

Table 6.8- Average values of heat transfer rate transferred to cooling water (Q_{cw}), heat transfer rate transferred from stirred yoghurt (Q_{yog}) and generalised Reynolds numbers of stirred yoghurt (Re_{yog}), for each yoghurt formulation tested.

Formulation ID	**Reynolds number, Re_{YOG} [-]**	**Heat transfer rate, Q_{cw} [W]**	**Heat transfer rate, Q_{YOG} [W]**
12% TS-YF	0.59	8097	8671
	0.61	7717	6500
	0.06	1817	1802
	0.92	8129	8666
	0.16	3894	3190
	0.45	6009	5541
	1.00	7860	7561
	0.72	6420	6155
	1.10	7297	7718
	1.72	9669	9156
	1.37	8904	8131
	2.75	10155	10241
	1.72	8978	8960
	0.96	7463	6818
13% TS-YC	0.07	2793	2996
	0.45	5437	7389
	0.68	6877	7311
	0.18	4131	4528
	0.44	5977	6151
	0.05	1975	1911
	0.66	5667	5604
	0.61	6661	6672
	0.30	4760	4564
	0.48	6605	6163
13% TS-YF	0.17	5778	5134
	0.69	9287	9568
	0.07	2828	2445
	0.84	8368	7958
	0.45	5913	5405
	0.72	7962	7829
	0.84	8642	8132
13% TS-HP50	0.34	4501	4130
	0.64	5903	5711
	0.90	6655	6202
	1.90	8038	7850
	1.34	7694	7705
	1.90	8827	8492
	2.10	8742	8176
13% TS-HMC	0.55	4918	5443
	0.32	5948	5085
	0.18	4294	3668
	0.42	5812	5309
	1.04	7564	8296

From the results presented in Table 6.8 and Table A.9 (Annex A), by following the calculation procedures described in section 3.8.1, it were obtained the relations between the mean Nusselt number and generalised Reynolds number of stirred yoghurt for all the formulations tested, as shown in Figure 6.10.

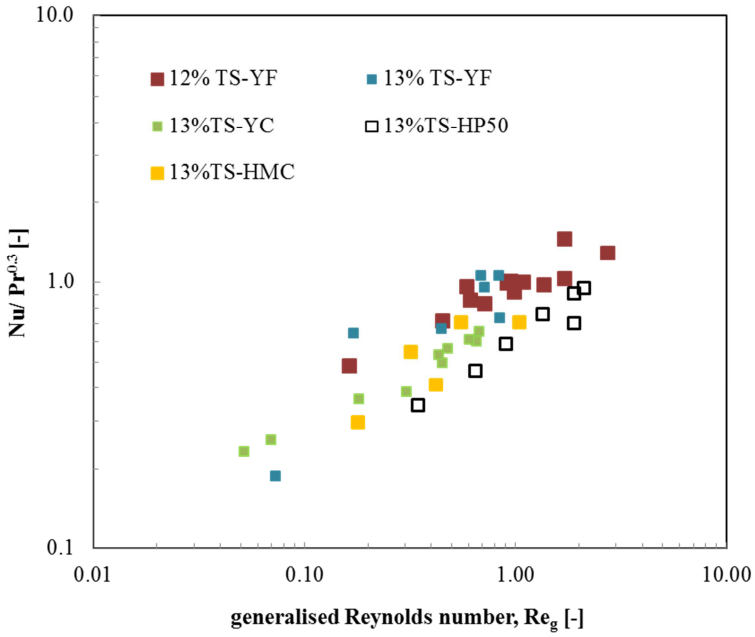


Figure 6.10- Thermal correlation for the mean convective heat transfer coefficient of the stirred yoghurt, as a function of the Reynolds number, for all the formulations tested.

From Figure 6.10 one can verify that the thermal correlations obtained for the different formulations of stirred yoghurt exhibited a similar tendency.

The statistical parameters obtained from nonlinear regression analysis of the experimental data obtained in all stirred yoghurt/ water heat transfer experiments, for all formulations tested, are presented in Table 6.9.

Considering the non-Newtonian, shear-thinning behaviour of the stirred yoghurt, the temperature dependence of the viscosity was taken into account in the calculation of the generalised Reynolds and Prandtl numbers, replacing the viscosity term by equation (3.41) and equations (6.10), substituting the rheological parameters and activation energy values presented in Table 6.6 and 6.7, respectively. Accordingly, the values obtained from statistical analysis were applied in equation (3.38), defined as follows:

$$Nu = aRe_g^b Pr_g^c$$

Table 6.9- Statistical parameters obtained by nonlinear regression analysis of stirred yoghurt experimental data, for all formulations tested.

Formulation ID	**Parameter**	**Estimate**	**Standard error**	**95% confidence interval**	
				lower bound	**upper bound**
12% TS-YF	a	0.971	0.034	0.896	1.046
	b	0.356	0.053	0.240	0.472
13% TS-YC	a	0.736	0.025	0.678	0.794
	b	0.421	0.036	0.339	0.504
13% TS-YF	a	1.051	0.115	0.756	1.347
	b	0.435	0.158	0.030	0.840
13% TS-HP50	a	0.611	0.035	0.520	0.701
	b	0.523	0.095	0.279	0.767
13% TS-HMC	a	0.743	0.102	0.419	1.067
	b	0.412	0.169	-0.126	0.950

Therefore, the experimental data obtained in stirred yoghurt/ water experiments, for each formulation tested, were correlated according to the following equations:

- 12% TS-YF:

$$Nu = 0.971 \cdot Re_g^{0.356} \cdot Pr_g^{0.3}, \;\; r^2 = 0.849 \tag{6.11}$$

for $0.16<Re_g<2.8$ and $1682<Pr_g<9351$.

- 13% TS-YC:

$$Nu = 0.736 \cdot Re_g^{0.421} \cdot Pr_g^{0.3}, \;\; r^2 = 0.965 \tag{6.12}$$

for $0.07<Re_g<0.68$ and $3284<Pr_g<9029$.

- 13% TS-YF

$$Nu = 1.051 \cdot Re_g^{0.435} \cdot Pr_g^{0.3}, \;\; r^2 = 0.741 \tag{6.13}$$

for $0.07<Re_g<0.84$ and $4226<Pr_g<8574$.

- 13% TS-HP50

$$Nu = 0.611 \cdot Re_g^{0.523} \cdot Pr_g^{0.3}, \;\; r^2 = 0.895 \tag{6.14}$$

for $0.34<Re_g<2.10$ and $2005<Pr_g<4537$.

- 13% TS-HMC

$$Nu = 0.743 \cdot Re_g^{0.412} \cdot Pr_g^{0.3}, \quad r^2 = 0.687 \tag{6.15}$$

for $0.18 < Re_g < 1.04$ and $3411 < Pr_g < 7670$.

From the analysis of the equation (6.11) to (6.15) it is possible to verify that the generalised Reynolds number exponent varied within the range of 0.356 to 0.523, with very low Reynolds number (Re<2.80). The values of the Reynolds number exponent obtained are strongly related to the pronounced shear-thinning behaviour exhibited by stirred yoghurt.

Figure 6.11 shows a comparison between the correlations obtained experimentally for stirred yoghurt with a shear-thinning, power-law behaviour and other published correlations for Newtonian and non-Newtonian food fluids (Rene *et al.*, 1991a; Afonso *et al.*, 2003; Warnakulasuriya and Worek, 2008; Cabral *et al.*, 2011)

It should be stated that the information concerning heat transfer in plate heat exchangers is scanty, particularly experimental studies using real food fluids.

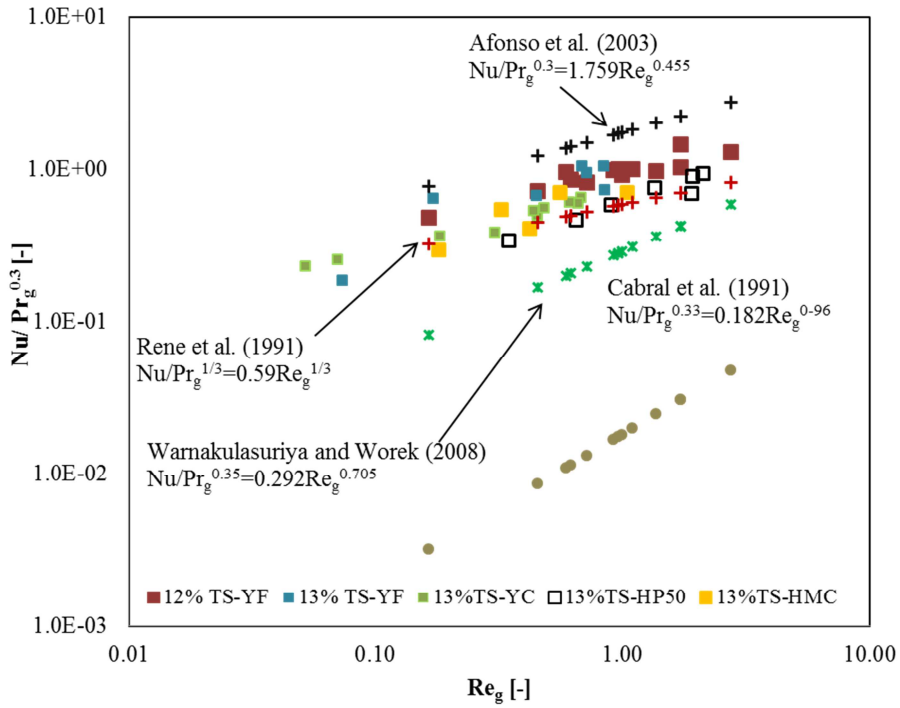


Figure 6.11- Comparison among obtained and published thermal correlations, for non-Newtonian fluids.

The published correlations used in the comparison were obtained in plate heat exchangers using as working fluids stirred yoghurt (Afonso *et al.*, 2003), CMC, sodium alginate solutions, guar-gum (Rene *et al.*, 1991a), pineapple juice (Cabral *et al.*, 2011) as pseudoplastic, power-law non-Newtonian fluids and water (Warnakulasuriya and Worek, 2008), in countercurrent flow conditions, with chevron type plates.

The experimental data obtained for the different formulation of stirred yoghurt tested, followed the same tendency as the thermal correlations published by Edwards (1988) in which the generalised Reynolds number exponent varied from 0.379 to 0.425, for Reynolds number lower than 50. As mentioned before for the non-Newtonian CMC solutions, the range of values for generalised Reynolds number exponent is lower than those observed for turbulent flows at high Reynolds numbers (n>0.6). So, most likely one can consider a laminar flow regime although not fully developed, since the very high Prandtl number values indicate the existence of a thermally developing flow.

The correlations obtained for stirred yoghurt are good agreement with those proposed by Rene et al.(1991a) non-Newtonian food fluids (flowing in a PHE in laminar regime Re_g<5.5).

The correlations for stirred yoghurt obtained in this study are in in good agreement with those obtained by Afonso et al. (2003) in their study on stirred yoghurt cooling in a PHE. The mean convective heat transfer coefficients of the stirred yoghurt obtained by these authors are slightly higher than those obtained in this work, this difference can be explained by the short length of the PHE used in the former study, which was almost three times shorter than the plates used in the present work. Combining the effects of high Prandtl numbers and the short length of the plates a thermal boundary layer was far from being fully developed. The differences in the flow arrangement can also influence the heat transfer coefficients values.

The correlations obtained were compared to the correlation obtained by Cabral et al. (2011) in their study on non-Newtonian flow and heat transfer of pineapple juice in a plate heat exchanger. The results obtained in this study were much higher although they followed a similar tendency. The temperature ranges used in the study performed by these authors can explained the differences in the flow regime, for Re<3.56, since the

high temperatures have a great influence in the decrease of consistency and flow behaviour index values of this non-Newtonian fluid.

The mean relative error of the Nusselt number predicted using the correlations obtained in the present work, varied between 6% and 25% for the experiments carried out with 13%TS-YC and13%TS-YF stirred yoghurt, respectively.

The correlations obtained can be applied in further studies of the heat transfer using power-law non-Newtonian food fluids in this type of plate heat exchanger with this multipass arrangement. Nevertheless, this type of thermal correlations should be applied cautiously since were achieved considering specific rheological behaviour of the fluid tested.

6.3.4. Determination of the local convective heat transfer coefficients of stirred yoghurt

As previously mentioned for water/ water heat transfer experiments, in each channel, the fluid and wall temperatures variation along the channel length were monitored in each of the four sub-sections defined previously, during the time of the heat transfer experiment.

In Figure 6.12 it is possible to observe the temperature profiles of cooling water (Figure 6.12a) and warm stirred yoghurt (Figure 6.12b) along the controlled channels in section 1 of PHE, corresponding to channel 1 and channel 2, respectively. These temperature profiles were obtained in the 12% TS-YF stirred yoghurt -water heat transfer experiment with a mean Reynolds number of stirred yoghurt of 1.10.

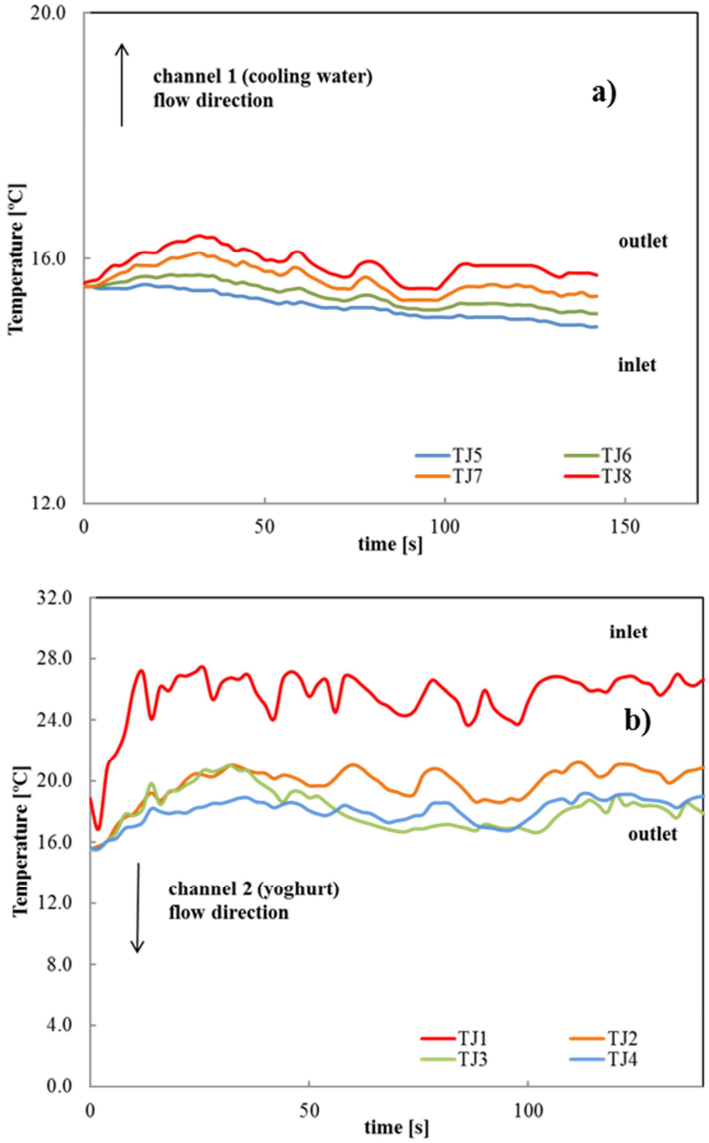


Figure 6.12- Temperature profiles of working fluids ((a) cooling water channel, (b) warm stirred yoghurt) along the PHE section 1 channels, as a function of time, for 12% TS-YF stirred yoghurt (Re=1.10).

Temperature profiles similar to these ones were obtained for every heat transfer experiment. Small differences were obtained in the profiles depending on the operating conditions, namely fluids inlet temperatures and flow rates. Nevertheless, the temperature profiles shown in Figure 6.12 are representative of the temperature variation along the PHE channels.

In Figure 6.12 b) in channel 2 it is possible to observe, for this Reynolds number, that the temperature probes suffered a great perturbation with the flow of such a viscous fluid. This mean Reynolds number value is high considering the maximum value (*Re*=2.80) obtained in the yoghurt/ water heat transfer experiments.

The wall temperature profiles measured on both sides of plate 2 are shown in Figure 6.13.a and b, for cooling water side and warm stirred yoghurt, respectively.

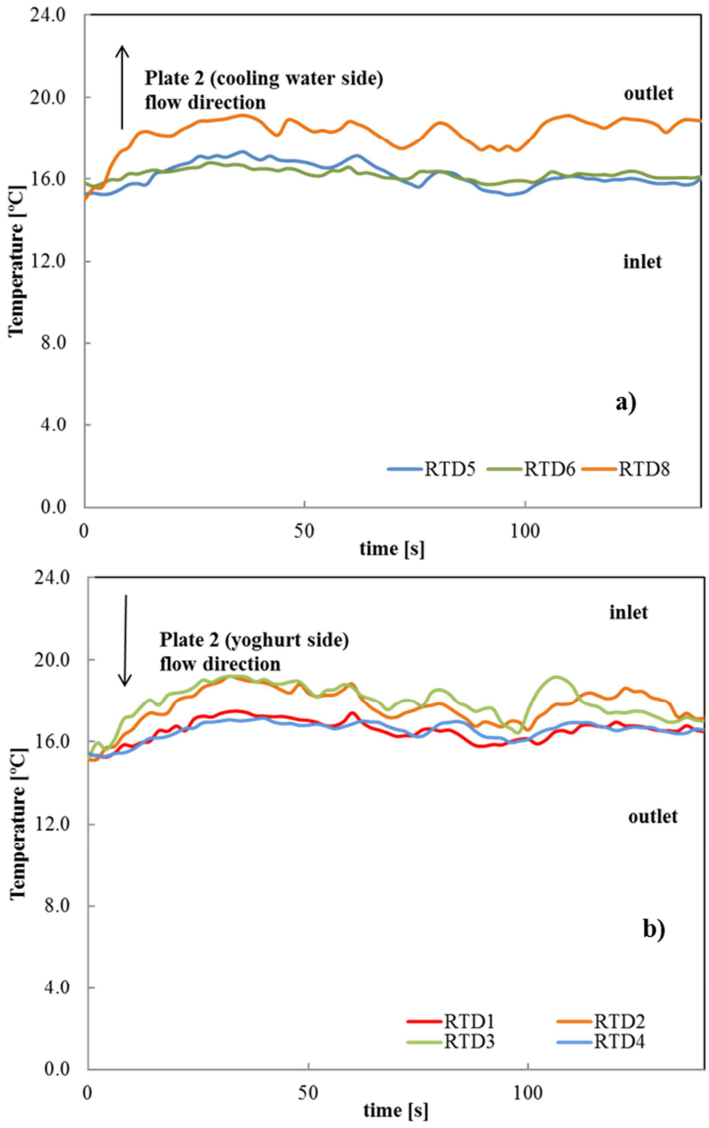


Figure 6.13- Wall temperature profiles along plate 2 ((a) cooling water side, (b) warm stirred yoghurt), as a function of time, for 12%TS-YF stirred yoghurt (Re=1.10).

In Figure 6.13a, it is possible to observe that in both yoghurt and cooling water side the wall temperature exhibited a constant perturbation along the plate length, during all the experiment time. The yoghurt flow introduced some perturbations in the temperature measurement systems due to its high viscous flow.

The wall temperature differences and those between the fluids at the channels inlet and outlet can be observed in Figure 6.14a and b as a function of time.

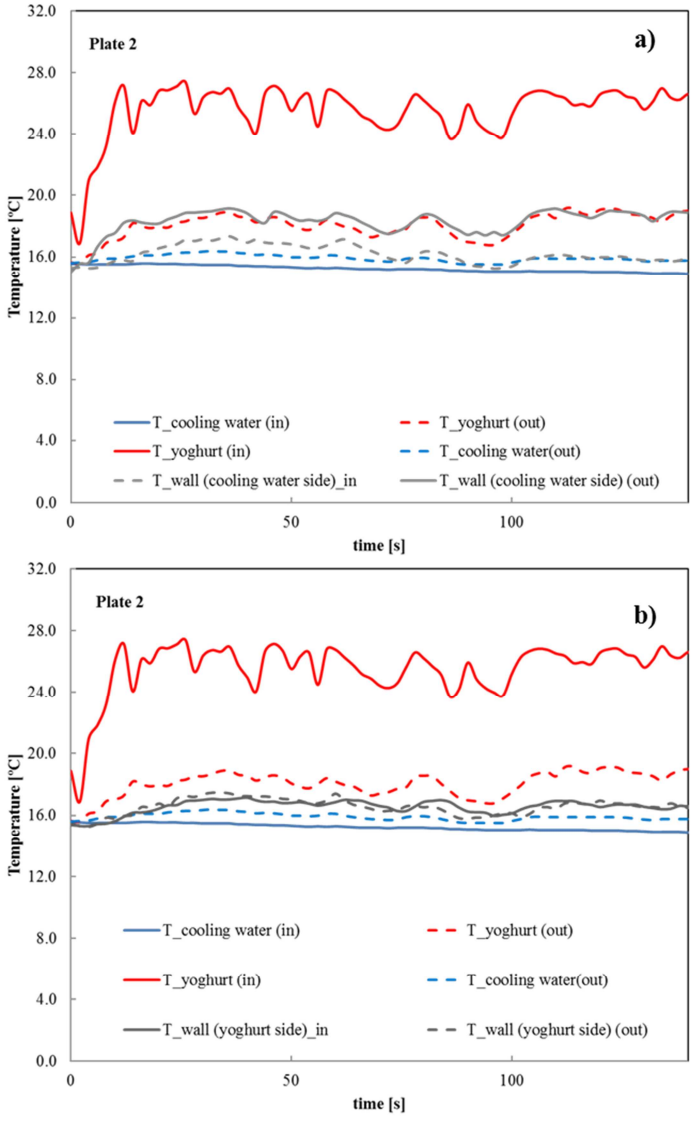


Figure 6.14- Wall temperatures (Plate 2) and working fluids temperatures at channels inlet and outlet ((a) cooling water side, (b) warm stirred yoghurt), as a function of time, for 12%TS-YF stirred yoghurt (Re=1.10).

In opposition to what was noticed in water/ water heat experiments, in which it was observed an approximately similar temperature differences at the two extremes of the PHE channel, here, for the operating conditions of the example presented, one can only observe the significant differences between the average temperature differences at the inlets of stirred yoghurt. These dissimilarities in average temperature differences between inlets on both working fluids are due to the flow rates differences between the two fluids, being the cooling water flow rate much higher than those of stirred yoghurt, whereas in water/water experiments the flow rates were kept almost equals.

Similarly to section 1, the temperature profiles of cooling water and stirred yoghurt along the controlled channels in section 2 of PHE (channels 7 and 8) are shown in Figure 6.15a and b.

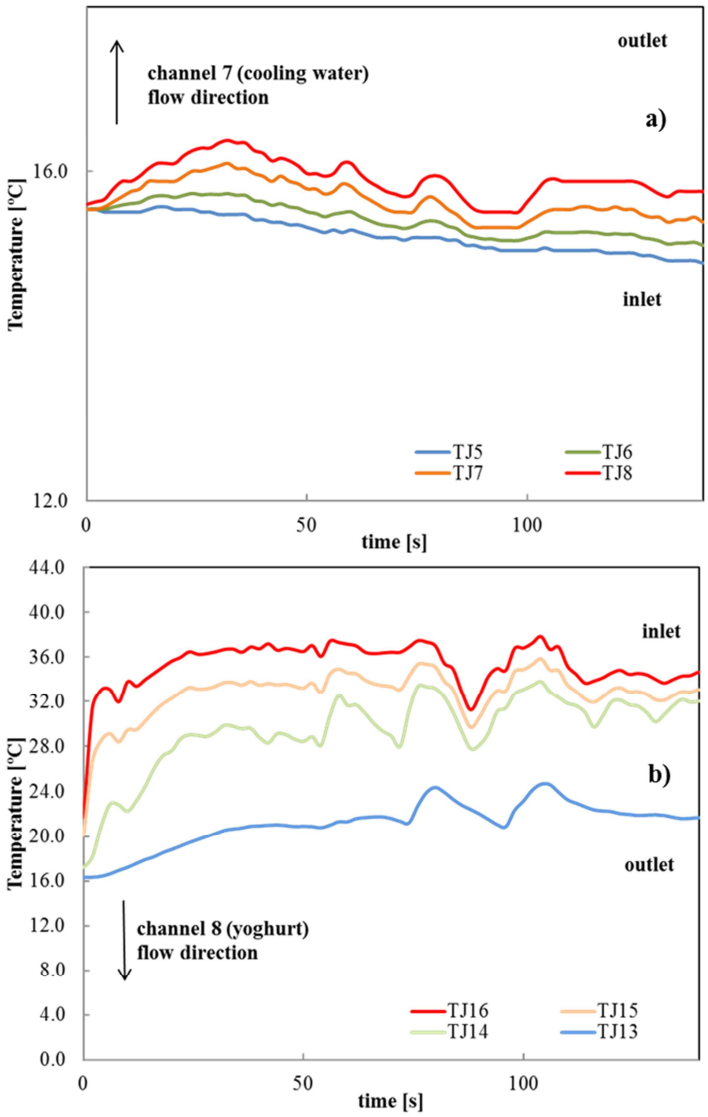


Figure 6.15- Temperature profiles of working fluids ((a) cooling water channel, (b) warm stirred yoghurt channel) along the PHE section 2 channels, as a function of time, for 12%TS-YF stirred yoghurt (Re=1.10).

Likewise to section 1, in section 2 it is also possible to observe the temperature variation of each fluid through the channel length. Again, some temperature perturbations can be noticed in section 2, those are much less than the observed in section 1. This is most probably related to the higher temperature ranges observed in this section due to the proximity of warm stirred yoghurt PHE inlet, and the higher temperature differences between the two fluids.

The wall temperature profiles measured on both sides of plate 8 are shown in Figure 6.16 a and b, for cooling water side and warm stirred yoghurt, respectively.

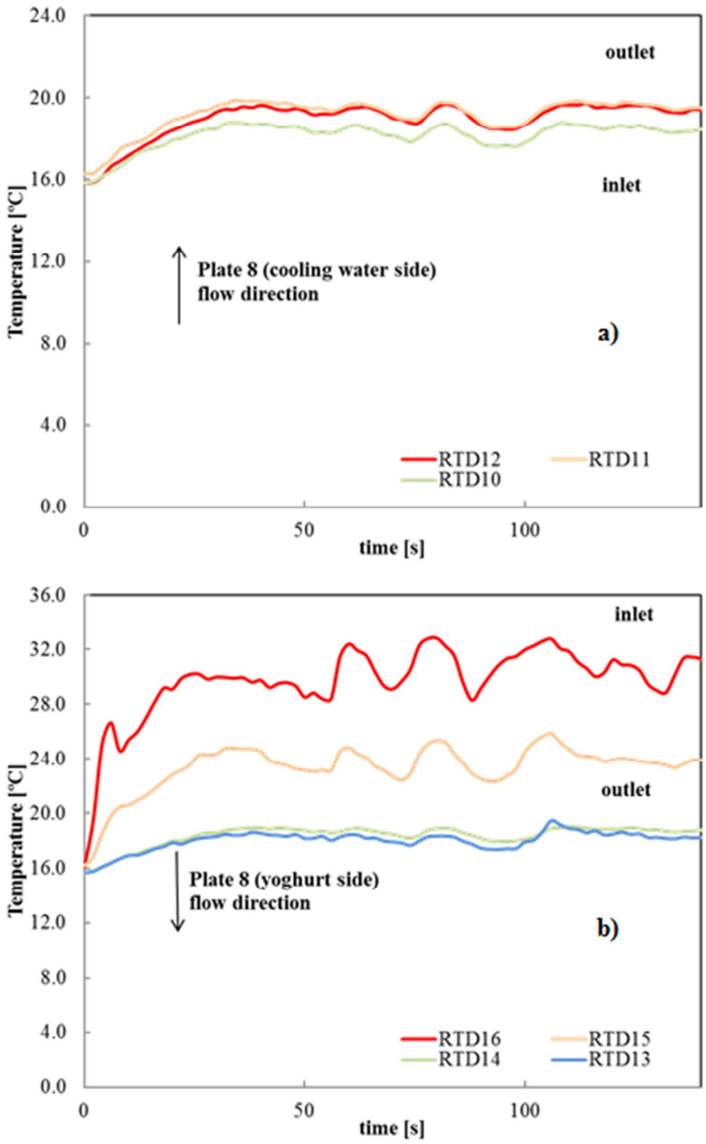


Figure 6.16- Wall temperature profiles along plate 8 ((a) cooling water side, (b) warm stirred yoghurt side), as a function of time, for 12%TS-YF stirred yoghurt (Re=1.10).

Similarly to what was observed for the fluids temperatures, the wall temperatures varied more significantly in the cooling water side along the plate length. These differences observed are strongly related to the temperature dependence of thermophysical properties of stirred yoghurt, namely the viscosity that exhibited an exponential relationship with temperature, and consequently a more pronounced effect

on the fluid hydrodynamic behaviour. As regards to water flow behaviour, in previous experiments it was observed that in this section cooling water exhibits a typical turbulent flow.

The wall temperature differences and those between the working fluids at the channels inlet and outlet can be observed in Figure 6.17a and b as a function of time.

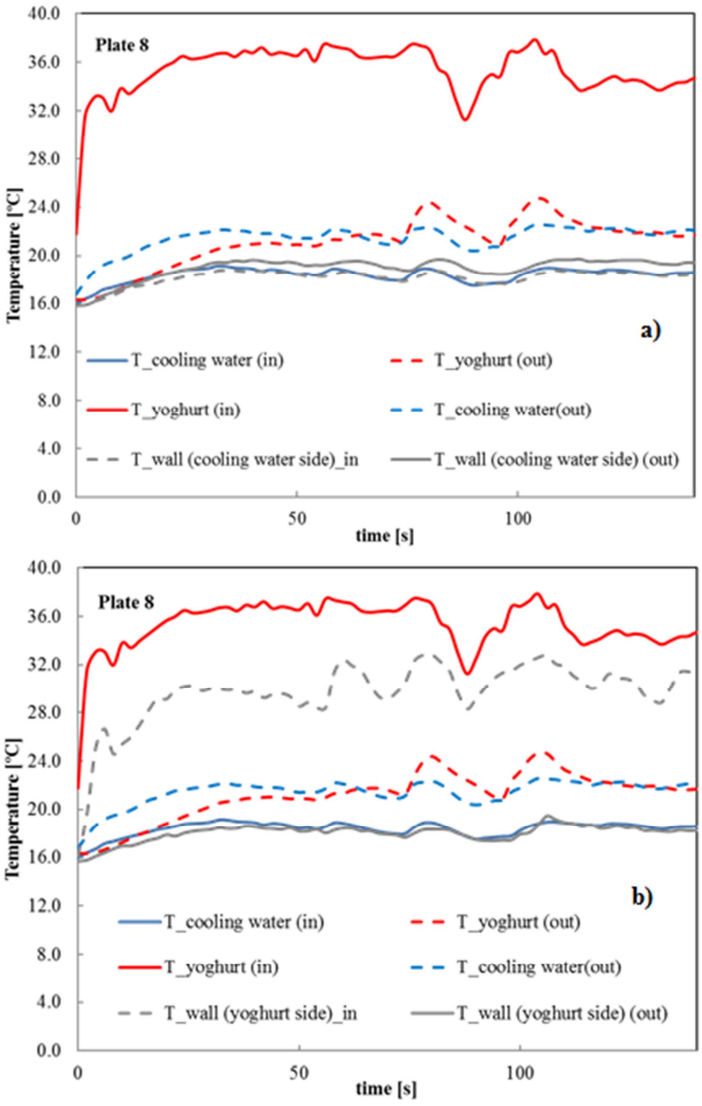


Figure 6.17- Wall temperatures (Plate 8) and working fluids temperatures at channels inlets ((a) cooling water side, (b) warm stirred yoghurt side), as a function of time, for 12%TS-YF stirred yoghurt (Re=1.10).

Like in section 1, the temperature difference between working fluids has an approximately constant range (6-16ºC, in the present example) at channels inlet and outlet, although the temperature ranges were quite different.

In order to evaluate the fluids temperature variation along the channel length, for several experiment times, the temperature data was plotted versus the position of each temperature probe along the channel length, for section 1 and 2 as it is shown in Figures 6.18 and 6.19, respectively.

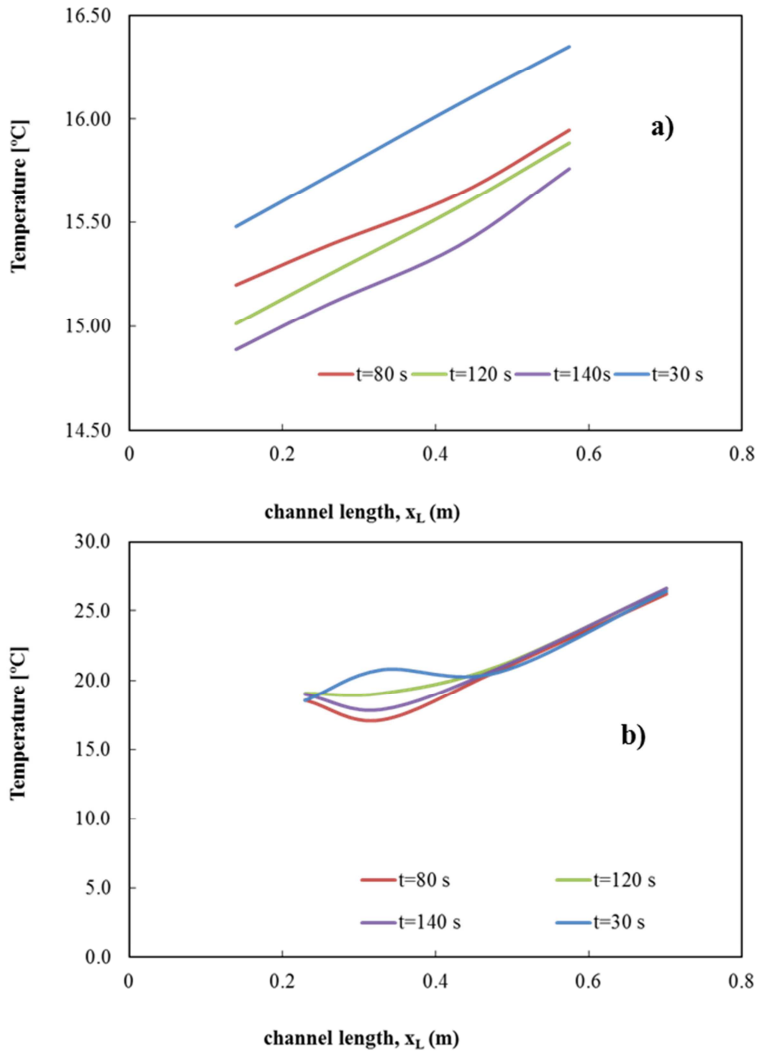


Figure 6.18- Working fluids temperatures along channels 1 and 2 corrugated zone, for different times ((a) cooling water channel, (b) warm stirred yoghurt channel), for 12%TS-YF stirred yoghurt (Re=1.10).

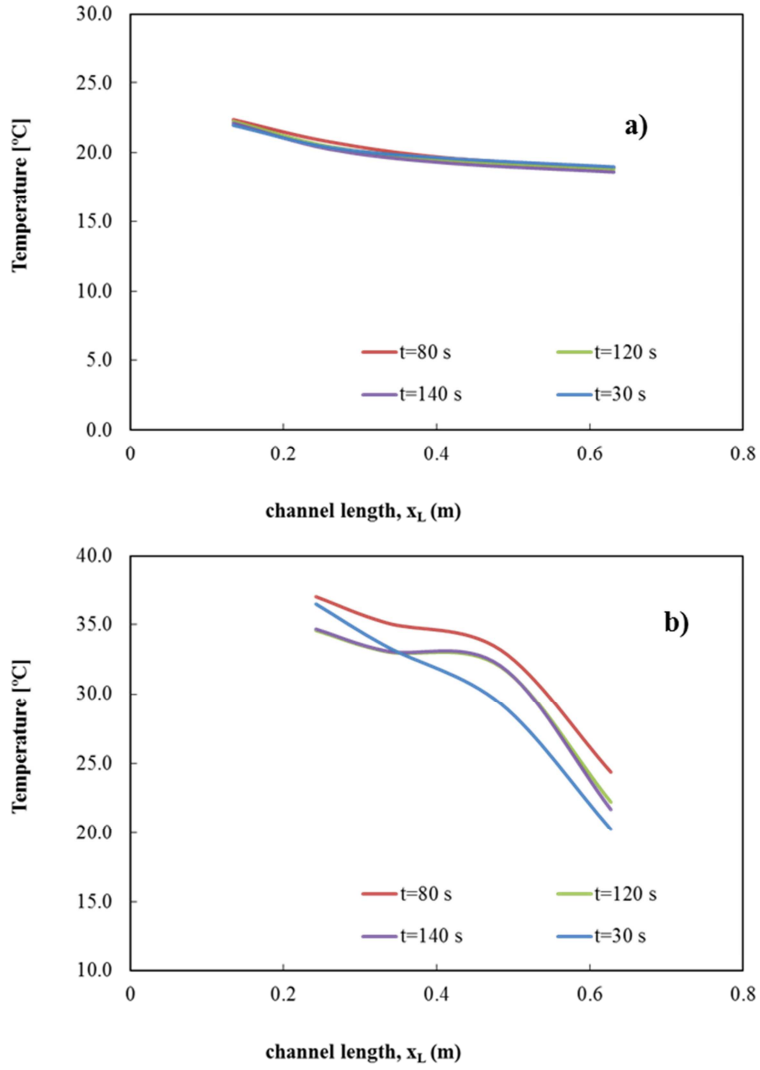


Figure 6.19- Working fluids temperatures along channels 7 and 8 corrugated zone, for different times ((a) cooling water channel, (b) warm stirred yoghurt channel), for 12%TS-YF stirred yoghurt (Re=1.10).

In both figures it is possible to observe that the temperature profiles along the channel length have an almost linear tendency. In Figure 7.18a one can observe that, in section 1, the cooling water exhibited a linear increasing along the channel length whereas in section 2, the cooling water kept a nearly constant temperature .

As stated for the previous heat transfer experiments, only the corrugated region of the plate was considered in calculation procedures. During the accomplishment of the analysis of the experimental data, some sporadic problems related to local data temperature acquisition were spotted which were not detected during the experimental work. In this set of experiments, the experimental data produced for PHE section 1 was not consistent, due to local perturbation in the temperature probes. Thus, the local heat transfer analysis of section 1 will not be presented.

In the analysis of the local heat transfer along the PHE channel, it will be only presented two different stirred yoghurt formulations, considering the effect of total solids content in the rheological behaviour and the experimental data validated.

Table 6.10 shows the values of local generalised Reynolds numbers of the 12%TS-YF stirred yoghurt and local overall heat transfer coefficients for the four sub-sections analysed in section 2.

Table 6.10- Average values of and local overall heat transfer coefficients (U_{ij}) and local Reynolds number (Re_{ij}) of 12% TS-YF stirred yoghurt for the four sub-sections analysed in section 2, for each experiment.

Formulation ID	**Re_{21} [-]**	**U_{21}, [$Wm^{-2}K^{-1}$]**	**Re_{22} [-]**	**U_{22}, [$Wm^{-2}K^{-1}$]**	**Re_{23} [-]**	**U_{23}, [$Wm^{-2}K^{-1}$]**	**Re_{24} [-]**	**U_{24}, [$Wm^{-2}K^{-1}$]**
12% TS-YF	1.72	662	0.49	966	0.52	1164	0.59	2363
	2.55	635	2.09	720	0.66	929	0.70	909
	0.10	249	0.11	306	0.12	526	0.12	864
	0.62	261	0.41	271	0.42	291	0.42	309
	2.28	824	1.81	996	0.61	1440	0.69	4873
	3.21	919	2.81	1013	2.44	1113	1.04	3263
	6.98	985	5.41	1192	4.67	1282	1.52	2314
	5.39	1364	2.47	1587	2.58	2778	2.52	1314
	3.13	622	1.55	738	1.63	1577	1.55	544

The statistical parameters obtained from nonlinear regression analysis of the experimental data obtained for 12%TS-YF stirred yoghurt/ water heat transfer experiments are shown in Table 6.11.

Similarly to the conditions taking into account in the calculation of the mean convective heat transfer coefficient of stirred yoghurt: non-Newtonian, shear-thinning behaviour of the stirred yoghurt, the temperature dependence of the viscosity was considered in the calculation of the generalised Reynolds and Prandtl numbers, replacing the viscosity term by equation (3.41) and equations (6.10), substituting the rheological parameters and activation energy values presented in Table 6.6 and 6.7, respectively. Accordingly, the values obtained from statistical analysis were applied in equation (3.38), defined as follows:

$$Nu = aRe_g^b Pr_g^c$$

Table 6.11- Statistical parameter obtained by nonlinear regression analysis, for the four sub-sections analysed in section 2, for 12%TS-YF stirred yoghurt.

Sub-section	**Parameter**	**Estimate**	**Standard error**	**95% confidence interval**	
				lower bound	**upper bound**
1	a	0.776	0.199	0.307	1.246
	b	0.673	0.168	0.276	1.069
2	a	1.274	0.249	0.686	1.861
	b	0.530	0.165	0.141	0.920
3	a	2.545	0.917	0.376	4.714
	b	0.479	0.325	-0.289	1.246
4	a	2.409	0.731	0.612	4.369
	b	0.584	0.330	-0.264	1.431

For section 2, four thermal correlations were obtained, one for each sub-section defined. Thus, the experimental data were correlated according to the following equations:

$$Nu = 0.776 \cdot Re^{0.673} \cdot Pr^{0,3}, \quad r^2 = 0.812 \tag{6.16}$$

obtained for sub-section 1, with 0.10<*Re*<6.98 and 1892<*Pr*<7990;

$$Nu = 1.274 \cdot Re^{0..530} \cdot Pr^{0.3}, \quad r^2 = 0.718 \tag{6.17}$$

obtained for sub-section 2, with 0.11<*Re*<5.41 and 2671<*Pr*<7777;

$$Nu = 2.545 \cdot Re^{0.479} \cdot Pr^{0.3}, \quad r^2 = 0.603 \tag{6.18}$$

obtained for sub-section 3, with 0.12<*Re*<4.67 and 3110<*Pr*<7171;

$$Nu = 2.409 \cdot Re^{0.584} \cdot Pr^{0.3}, \quad r^2 = 0.491 \tag{6.19}$$

obtained for sub-section 4, with 0.12<*Re*<2.52 and 3330<*Pr*<6803.

Table 6.12 shows the values of local generalised Reynolds numbers of the 13%TS-YC stirred yoghurt and local overall heat transfer coefficients for the four sub-sections analysed in section 2.

Table 6.12- Average values of and local overall heat transfer coefficients (U_{ij}) and local Reynolds number (Re_{ij}) of 13% TS-YC stirred yoghurt for the four sub-sections analysed in section 2, for each experiment.

Formulation ID	**Re_{21} [-]**	**U_{21}, [$Wm^{-2}K^{-1}$]**	**Re_{22} [-]**	**U_{22}, [$Wm^{-2}K^{-1}$]**	**Re_{23} [-]**	**U_{23}, [$Wm^{-2}K^{-1}$]**	**Re_{24} [-]**	**U_{24}, [$Wm^{-2}K^{-1}$]**
13% TS-YC	0.06	194	0.07	213	0.07	235	0.08	590
	0.78	483	0.44	1003	0.45	1048	0.47	1222
	1.51	627	0.63	1255	0.66	1700	0.66	1620
	0.79	494	0.41	822	0.43	1125	0.44	1377
	0.16	346	0.17	428	0.19	742	0.20	963
	0.05	186	0.05	240	0.05	496	0.06	785
	1.61	702	0.56	889	0.61	1752	0.67	1931
	2.02	720	1.36	986	1.23	1048	0.61	5056
	0.54	496	0.22	676	0.24	728	0.44	3359
	2.40	787	1.78	934	0.46	3335	0.49	7423

The statistical parameters obtained from nonlinear regression analysis of the experimental data obtained for 13%TS-YC stirred yoghurt/ water heat transfer experiments are shown in Table 6.13.

Table 6.13- Statistical parameter obtained by nonlinear regression analysis, for the four sub-sections analysed in section 2, for 13%TS-YC stirred yoghurt.

Sub-section	Parameter	Estimate	Standard error	95% confidence interval	
				lower bound	upper bound
1	a	0.619	0.038	0.531	0.708
	b	0.896	0.024	0.841	0.951
2	a	1.621	0.138	1.304	1.938
	b	0.467	0.102	0.232	0.703
3	a	2.688	0.493	1.521	3.854
	b	0.492	0.213	-0.011	0.996
4	a	4.769	0.635	3.137	6.402
	b	0.765	0.180	0.323	1.247

For section 2, four thermal correlations were obtained, one for each sub-section defined. Thus, the experimental data were correlated according to the following equations:

$$Nu = 0.619 \cdot Re^{0.896} \cdot Pr^{0,3}, \quad r^2 = 0.987 \tag{6.20}$$

obtained for sub-section 1, with 0.05<*Re*<2.40 and 750<*Pr*<9886;

$$Nu = 1.621 \cdot Re^{0..467} \cdot Pr^{0.3}, \quad r^2 = 0.803 \tag{6.21}$$

obtained for sub-section 2, with 0.05<*Re*<1.78 and 1019<*Pr*<9602;

$$Nu = 1.688 \cdot Re^{0.492} \cdot Pr^{0.3}, \quad r^2 = 0.571 \tag{6.22}$$

obtained for sub-section 3, with 0.05<*Re*<1.23 and 1715<*Pr*<9297;

$$Nu = 4.769 \cdot Re^{0..785} \cdot Pr^{0.3}, \quad r^2 = 0.897 \tag{6.23}$$

obtained for sub-section 4, with 0.06<*Re*<0.67 and 3350<*Pr*<9866.

In channel 8, the stirred yoghurt enters the channel in sub-section 1 and exits the channels in sub-section 4. Considering the flow direction, this non-Newtonian food fluids and observing the Reynolds number exponent in equations 6.16, 6.17, 6.18 and 6.19, for the 12%TS-YF stirred yoghurt, one can observe that in sub-section 1 (yoghurt inlet) the value of Reynolds exponent is within the range for turbulent flow, e.g. (Edwards, 1988; Rene *et al.*, 1991a).

Along the channel length the value of Reynolds exponent decreased until values denoted as transitional to laminar. A deviation on this tendency is observed in sub-section 4 (yoghurt exit) probably due to end effects that can introduced some perturbation in the flow. Nevertheless, it is evident a clear tendency on the flow regime that prevails in this section. This thermal behaviour may be explained by the high temperature ranges in this section, in which its effects on the thermophysical properties of the yoghurt are more pronounced in the proximity of the stirred yoghurt inlet. Thus, along the channel the stirred yoghurt is cooled down and consequently the viscosity values will increase and its effect on the hydrodynamic behaviour are obtained (lower Reynolds number in sub-section 4).

A similar analysis can be performed for the 13%TS-YC stirred yoghurt. Thus, observing the Reynolds number exponent in equations 6.20, 6.21, 6.22 and 6.23, one can notice that in sub-section 1 (yoghurt inlet) the value of Reynolds exponent (0.896) is within the range for turbulent flow (0.65-0.85). Along the channel length the value of Reynolds exponent decreased until values denoted as laminar. Again, at the channel exit (sub-section 4) is observed a deviation on this tendency, this may be due to end effect or most probably due to the perturbations in the temperature probes, since this effect was only observed in the stirred yoghurt/water experiments.

In order to gather more information concerning local convective heat transfer coefficients, the local Nusselt number versus channel length was plotted, for several Reynolds, for section 2, as it is shown in Figures 6.20 and 6.21 for stirred yoghurt with 12%TS-YF and 13%TS-YC, respectively. The experimental data that used for this analysis are shown in Tables A.10 and A.11 (Annex A).

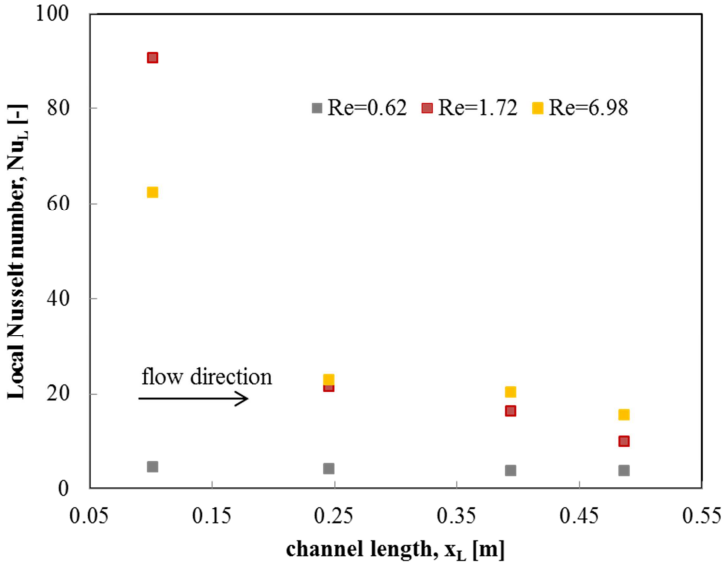


Figure 6.20- Stirred yoghurt (12%TS-YF) local Nusselt number variation along channel length (channel 8, section 2), for several Reynolds numbers.

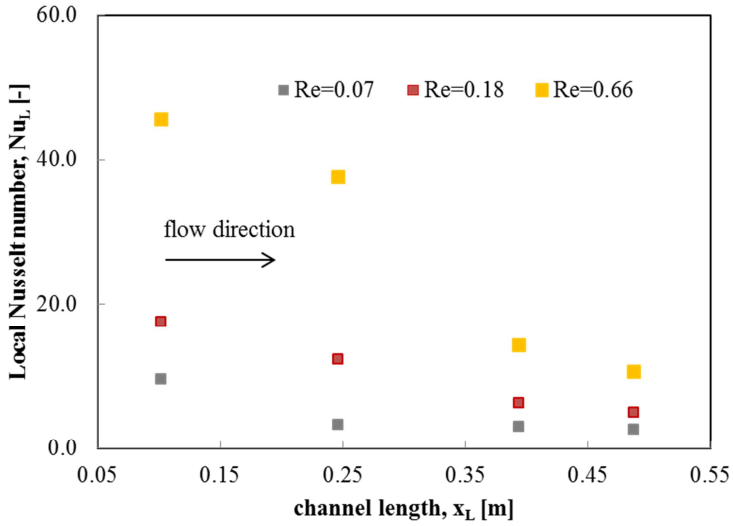


Figure 6.21- Stirred yoghurt (13%TS-YC) local Nusselt number variation along channel length (channel 8, section 2), for several Reynolds numbers.

The correlations obtained for the local Nusselt number of the stirred yoghurts with 12%TS-YF and 13%TS-YC as a function of channel length, for several Reynolds number, in section 2, are presented in Table 6.14.

Table 6.14- Local thermal correlation as a function of channel length, for several local Reynolds numbers of both stirred yoghurts 12%TS-YF and 13%TS-YC, in channel 8.

Formulation ID	**Local Reynolds number, Re [-]**	**Thermal correlations**
12%TS-YF	0.62	$Nu_L = 3.403 \cdot x_L^{-0.124},\ r^2 = 0.945$
	1.72	$Nu_L = 3.915 \cdot x_L^{-1.35},\ r^2 = 0.974$
	6.98	$Nu_L = 8.293 \cdot x_L^{-0.855},\ r^2 = 0.957$
13%TS-YC	0.07	$Nu_L = 1.364 \cdot x_L^{-0.81},\ r^2 = 0.925$
	0.18	$Nu_L = 3.114 \cdot x_L^{-0.801},\ r^2 = 0.912$
	0.66	$Nu_L = 6.496 \cdot x_L^{-0.934},\ r^2 = 0.822$

The local thermal correlations evidence not only the variation of local Nusselt number with the channel length (x_L) but also with the Reynolds number, as indicated by the variation of the constant value. In order to obtain a more illustrative correlation of the effects mentioned previously, the variation of local Nusselt number with Graetz number for both stirred yoghurt 12%TS-YF and 13%TS-YC in channel 8 (section 2) is presented in Figure 6.22.

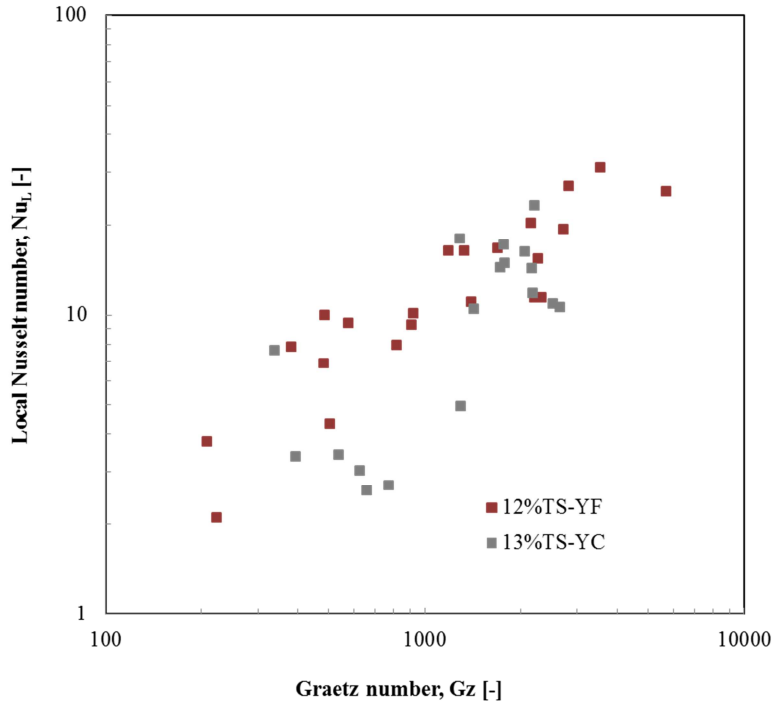


Figure 6.22- Stirred yoghurt (12%TS-YF and 13%TS-YC) local Nusselt number versus Graetz number (channel 8, section 2).

Table 6.15 shows the statistical parameters obtained from nonlinear regression analysis applied to the heat transfer experiments of both stirred yoghurt formulation.

Table 6.15- Statistical parameters obtained by nonlinear regression analysis for channel 8 (section 2).

Formulation ID	**Parameter**	**Estimate**	**Standard error**	**95% confidence interval**	
				lower bound	**upper bound**
12%TS-YF	C	0.219	0.136	-0.064	0.501
	b	0.570	0.080	0.403	0.736
13%TS-YC	C	0.057	0.103	-0.160	0.275
	b	0.720	0.238	0.215	1.225

Thus, the experimental data, for channel 8 were correlated according to the following equations:

$$Nu_L = 0.219 \cdot Gz^{0.57}, \quad r^2 = 0.763 \tag{6.24}$$

for 12%TS-YF stirred yoghurt in the range 209< *Gz* <5715.

$$Nu_L = 0.057 \cdot Gz^{0.720}, \quad r^2 = 0.506 \tag{6.25}$$

for 13%TS-YC stirred yoghurt in the range 340< *Gz* <2662.

Figure 6.23 shows a comparison between the correlations obtained in the present work (12%TS-YF and 13%TS-YC) and those published in the open literature for the thermal entry region of a parallel-plate channel with Hagen–Poiseuille flow (Bejan and Kraus, 2003; Shah and Sekuli, 2003) and plug-flow (Metzner *et al.*, 1957).

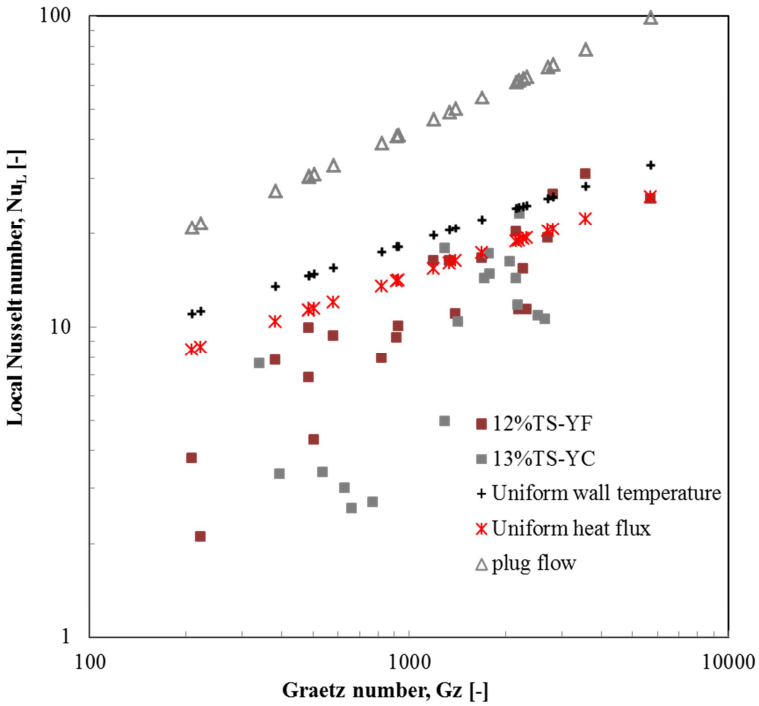


Figure 6.23- Comparison of local heat transfer correlations in the thermal entrance region obtained in the present work (12%TS-YF and 13%TS-YC stirred yoghurt) and published in the open literature.

Comparing the results obtained in the present work for the two formulations of stirred yoghurt analysed and therefore for different non-Newtonian, shear-thinning behaviour fluids, one can verify that for both stirred yoghurt formulations the Nu-Gz correlations exhibit values of Graetz number exponent higher than those typical of

thermally developing flow. However the very high values of Prandlt number suggested more significant entrance effects.

When comparing the empirical correlations here obtained with those published for the thermal developing flow in a flat parallel-plate channels for the two boundary conditions analysed (uniform wall temperature and uniform heat flux) as shown in Figure 6.23, the present one exhibited slightly lower convective heat transfer coefficients, for higher Graetz number value, that may be explained by the non-Newtonian characteristics of the tested fluids and the temperature dependence of the thermophysical properties. Differences were more pronounced for lower Graetz number values of the 13%TS-YC stirred yoghurt, which has not only higher consistency index but also higher activation energy values, therefore more pronounced sensitivity to temperature changes.

The empirical correlations obtained in this set of experiments were also compared with the correlations for plug-flow in parallel-plates published by Metzner e al. (1957), being noticed that the local Nusselt numbers determined here were much lower than those calculated with equation 5.21.

Regarding the non-Newtonian characteristics of the tested fluids and the temperature dependence of the thermophysical properties, the empirical correlations obtained here were compared with the computed solutions obtained using the numerical approach developed by Afonso, Cruz et al. (2008) in order to obtained simplified numerical solutions for thermally developing region of non-Newtonian fluids whose rheological behaviour can be approximated by a temperature-dependent power-law equation (see Annex A2, for further details).

In Figure 6.24a and b shows the heat transfer data obtained numerically for parallel flat plates, for constant wall temperature and the empirical local thermal correlations obtained here for 12%TS-YF (a) and for 13%TS-YC (b) stirred yoghurts.

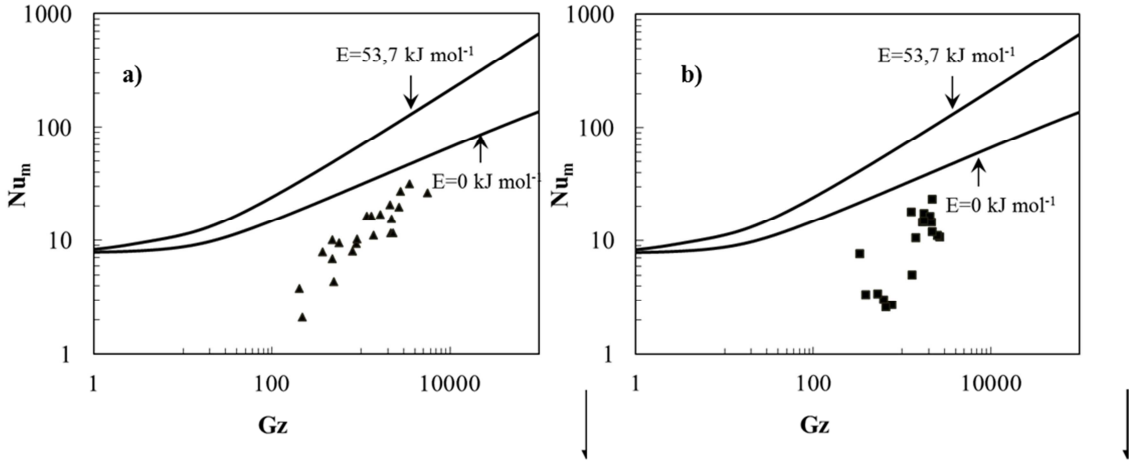


Figure 6.24- Computed average Nusselt number as a function of Graetz number and activation energy (E), for constant wall temperature boundary condition, for parallel flat plates. Comparison with empirical correlations obtained: a) 12%TS-YF and b) 13%TS-YC stirred yoghurt.

From Figure 6.24a and b one can observed that the thermal correlations obtained exhibited lower convective heat transfer coefficients when compared with the computed solutions that take into account the rheological behaviour and its temperature-dependence (solutions computed for zero activation energy (E = 0) and for activation energy of 53,78 kJ/mol).

From Figure 6.24 it is possible to observe that the experimental correlations are located in the non-developed thermal flow, far from the constant heat transfer coefficients region, characteristic of fully developed flow.

This experimental study highlighted the effect of the non-Newtonian behaviour on the thermal performance of the PHE when applied to food fluids.

The experimental data obtained in this study is of major importance not only for the PHE design engineers but also for food industries particularly for dairy processors.

6.3.5. Determination of Fanning friction factor correlations

Additionally to the measurement of fluids and wall temperatures along the plate heat exchanger channels, and fluids temperature at PHE inlets and outlets, the overall

pressure drop was determined experimentally using pressure transmitters located at both hot and cold fluid sides of the PHE inlet and outlet, as mentioned in section 3.7.2.

Figure 6.25 shows the overall pressure drop of warm stirred yoghurt PHE side as a function of mean Reynolds number, for the different formulations tested.

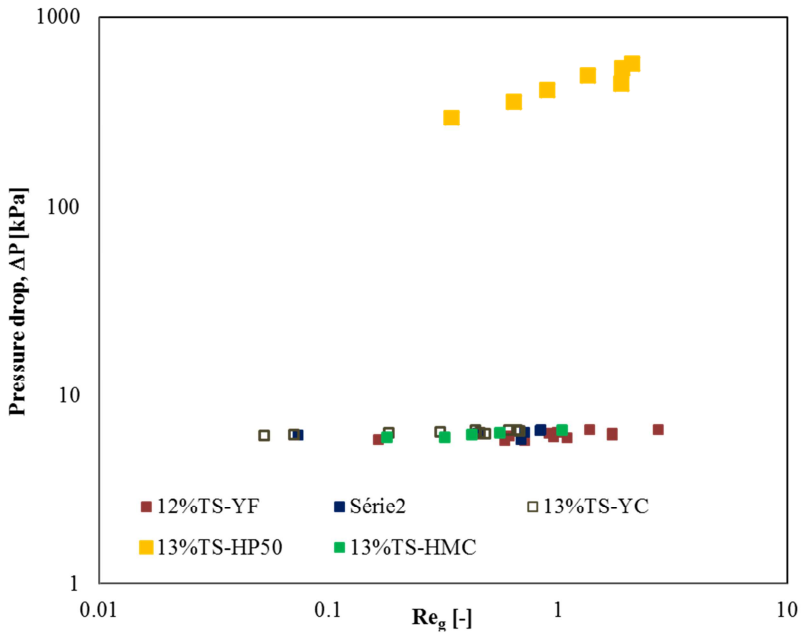


Figure 6.25- Overall pressure drop versus generalised Reynolds number of different stirred yoghurt formulations.

In Figure 6.25 it is possible to observe the effect of stirred yoghurt formulations in the overall pressure drop, directly related to the non-Newtonian behaviour of the stirred yoghurt formulations tested.

Apparently no significant effect was evidenced by the increase of total solids content of stirred yoghurt. However, a significant effect is observed when the stirred yoghurt formulation included an increase of its protein content, by fortification with a high protein skim milk powder. This increase in the overall pressure drop cannot be explained by a significant increase of the stirred yoghurt apparent viscosity since the rheological parameters such as consistency index and flow behaviour index have similar magnitude of others formulation tested.

Figure 6.26 presents the friction factors as a function of mean Reynolds number of stirred yoghurt formulations obtained in the present work and those published in the open literature (Edwards *et al.*, 1974; Rene *et al.*, 1991a; Cabral *et al.*, 2010).

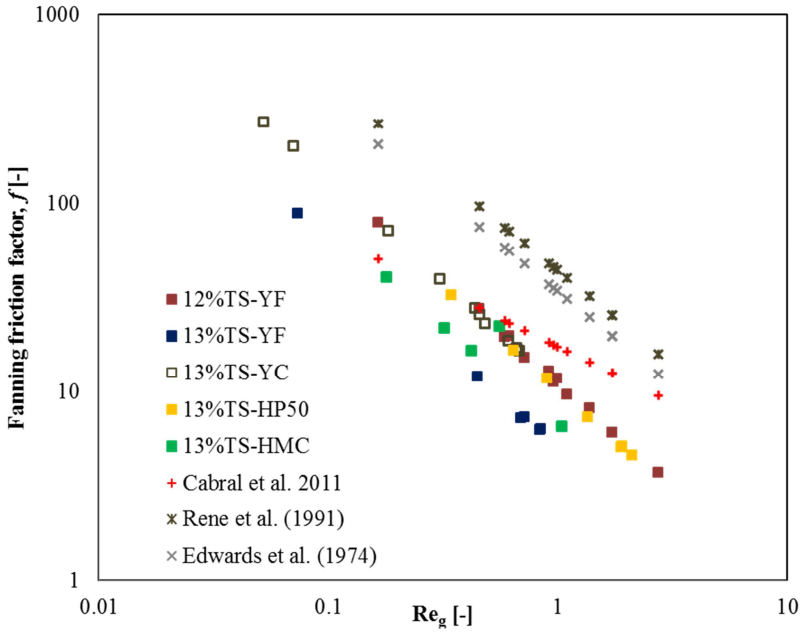


Figure 6.26- Fanning friction factor versus generalised Reynolds number, comparison of correlations obtained in the present work and those published in the open literature.

From Figure 6.26, it possible to observe that the friction factor values of all the formulations of stirred yoghurt tested exhibited the same general tendency.

The experimental data for the different stirred yoghurt tested were correlated according to the following equations:

- 12%TS-YF:

$$f = 10.120 \cdot Re^{-1.158}, \; r^2 = 0.999 \tag{6.26}$$

- 13%TS-YC:

$$f = 11.169 \cdot Re^{-1.083}, \; r^2 = 1.000 \tag{6.27}$$

- 13%TS-YF:

$$f = 5.039 \cdot Re^{-1.102}, \; r^2 = 1.000 \tag{6.28}$$

- 13%TS-HP50:

- $f = 10.272 \cdot Re^{-1.071}, \ r^2 = 1.000$ (6.29)
- 13%TS-HMC:
- $f = 9.287 \cdot Re^{-0.843}, \ r^2 = 0.889$ (6.30)

The correlations obtained for Fanning friction factor were compared with correlations published in the open literature for heat exchangers with chevron plate and one can observe in Figure 6.26 the correlations obtained in this work exhibited similar tendency as those referred correlations.

The friction factor correlation obtained by Cabral, Gut et al. (2010), in their study on the non-Newtonian flow and pressure drop of pineapple juice in a plate heat exchanger with 50º chevron plates, for parallel/ side plate and laminar flow (Reg≤300), is:

- $f = \frac{17.3}{Re_g^{0.593}}$ (6.31)

In Figure 6.26, one can observe that this correlation does not fully represent the experimental data, mainly due to the effect of different plate geometrical features and the fluids thermophysical properties, particularly the rheological properties and its effects in the Reynolds number values.

6.3.6. Effect of cooling stage in the structure of the stirred yoghurt

In order to gain some understanding of the structural changes caused by the cooling stage in the structure and rheological characteristics of stirred yoghurt, samples of stirred yoghurt were collected in different post-incubation stages. Thus, samples of undisturbed coagulum with a total solids content of 13% were collected directly from the incubation tank.

Oscillatory shear rheometry were performed in order to obtain the mechanical spectrum of the coagulum and evaluate its structure.

Figure 6.27 shows the mechanical spectrum of yoghurt coagulum collected in the fermentation tank.

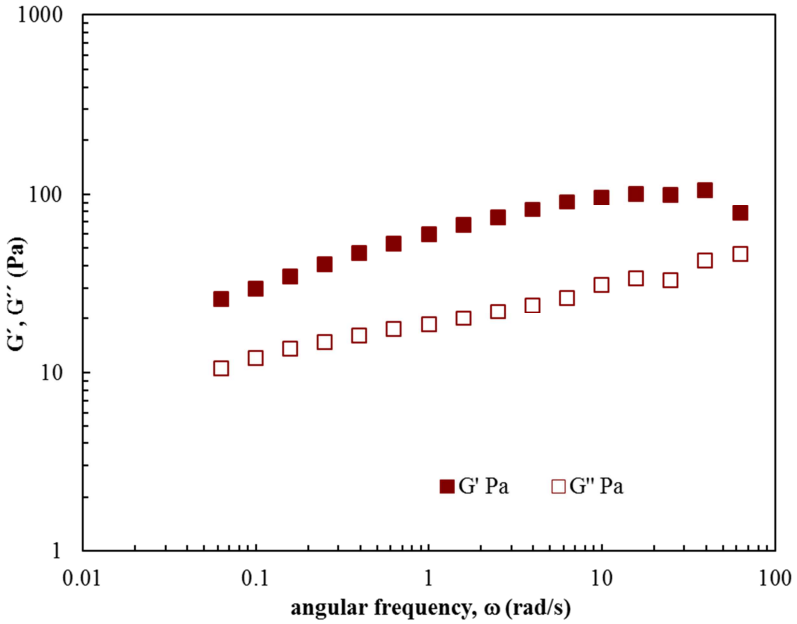


Figure 6.27- Mechanical spectrum of yoghurt coagulum in fermentation tank (13%ST-YF).

From Figure 6.27 one can observe that, in all the range of angular frequency used as mentioned in section 6.2.2., the storage modulus (G´) is higher than the loss modulus (G´´) revealing the weak elastic behaviour of the protein network, as frequently reported by several authors, e.g. (Benezech and Maingonnat, 1994; Lucey, 2002; Lee and Lucey, 2006).

At high angular frequencies, the G´ value decreased almost reaching the G´´ value, indicating occurrence of some structure rearrangement, probably due to the presence in the protein network of extraneous-polysaccharides produced the lactic acid bacteria used in this work. The occurrence of syneresis is another phenomenon very frequent in yoghurt coagulum caused in the majority of the cases by small stress that may disturb the protein network and promote the whey off.

In Figure 6.28 are presented the mechanical spectra the stirred yoghurt in fermentation tank and after cooling in the PHE at a certain flow rate ($\dot{\gamma} = 241\ s^{-1}$).

From Figure 6.28 one can observed that the weak gel structure is present in both samples of stirred yoghurt with different shear histories, since the yoghurt sample PHE2 not only was submitted to the stirring operation in which the yoghurt coagulum was

completely disrupted but also was submitted to high shear rates during the cooling stage in a PHE.

Comparing the mechanical spectra obtained for both yoghurt samples one can observe that they are very similar, indicating that, in fact, the stirring stage is critical for the loss of structure of the yoghurt. Some structure rearrangements are detected, at high angular frequencies, by the increase of the G´. In fact, this increase of G´ may be due to some whey off caused by some internal strength but also to temperature effect (essay performed at 20ºC).

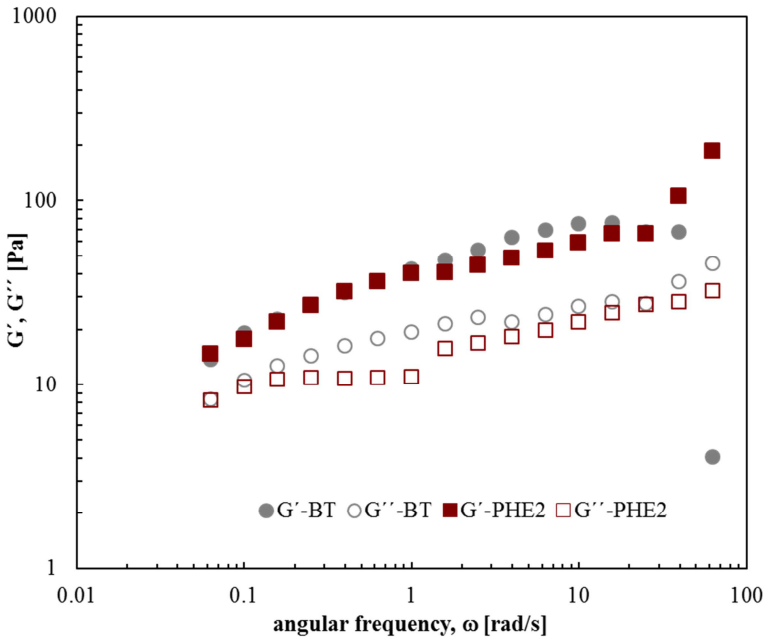


Figure 6.28- Comparison of mechanical spectra stirred yoghurt in fermentation tank and after cooling in the PHE at a shear rate (13%ST-YF).

From Figure 6.28 one can verify that the post-incubation stages have a great influence in the quality of the final product, since the coagulum disruption caused in these process stages may deeply affect the consumer acceptability of the product, strongly related to the product rheology (Fangary *et al.*, 1999).

In order to evaluate the impact of the cooling stage in the stirred yoghurt structure, the mechanical spectra of stirred yoghurt samples cooled at different flow rates are shown in Figure 6.29.

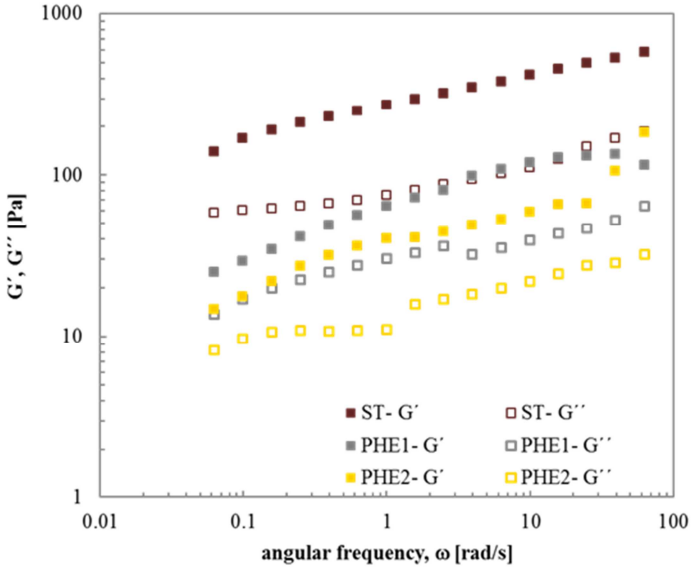


Figure 6.29- Comparison of mechanical spectra of the stirred yoghurt after cooling stage at different shear rates (13%ST-YF).

From Figure 7.29 one can observe that all the cooled samples were submitted at high shear rates during its cooling conditions comparing with the stirred yoghurt (ST) before the cooling stage. The yoghurt sample that was submitted to cooling conditions with higher shear rate ($\dot{\gamma} = 221$ s^{-1}) is sample PHE2, which exhibited lower values of G´ and G´´, even though G´>G´´. The yoghurt sample PHE1 was submitted to cooling at shear rate of ($\dot{\gamma} = 94$ s^{-1}).

These results evidence the importance of the selection of the proper cooling conditions, in order to minimise the impact of this production stage in the final quality of the yoghurt, since other operations like pumping, pipe flowing and filling the packaging stage are operations strongly related with high shear rates (Fangary *et al.*, 1999).

Figure 6.30 shows the microstructure and the mechanical spectra of the stirred yoghurt (with 12% total solids) collected in the fermentation tank (ST), after cooling stage in a PHE at different shear rates.

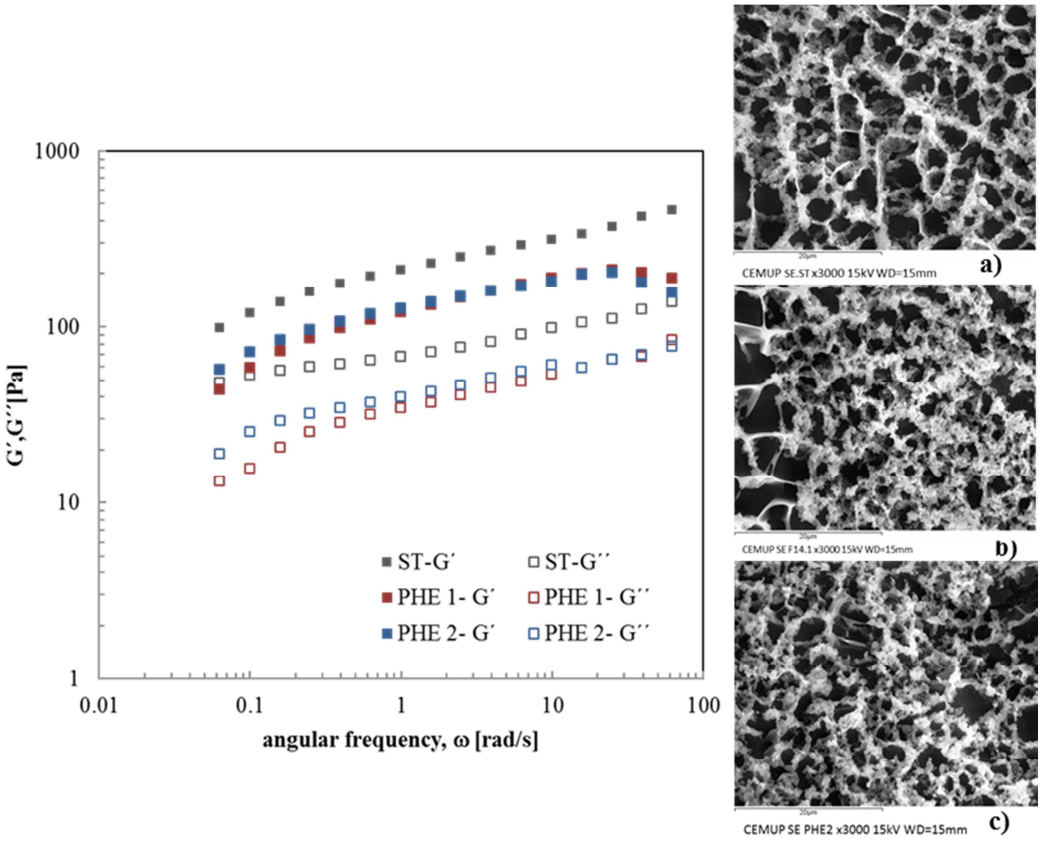


Figure 6.30- Microstructure and storage and loss moduli of stirred yoghurt (with 12% total solids) in the fermentation tank (ST), after cooling stage in a PHE at different shear rates: PHE1 ($\dot{\gamma}$=94 s^{-1}) and PHE 2 ($\dot{\gamma}$=158 s^{-1}).

From Figure 6.30 one can observe the differences between the two operating conditions used in the cooling stage and evaluate their impact on the yoghurt structure. It is noticed that no significant are detected between the two PHE samples, since their mechanical spectra almost superimposed. The weak gel-like structure is observed in all the stirred yoghurt samples.

As regards to the microstructure, small differences in the protein network are detected in between the samples collected after cooling stage. The sample PHE cooled at lower shear rate, exhibited a protein network more open (Figure 6.30b), even though

less "porous" than the microstructure of the yoghurt sample collected in the fermentation tank.

Figure 6.31 shows the microstructure and the mechanical spectra of the stirred yoghurt (with 13% total solids) collected in the fermentation tank (ST), after cooling stage in a PHE at different shear rates.

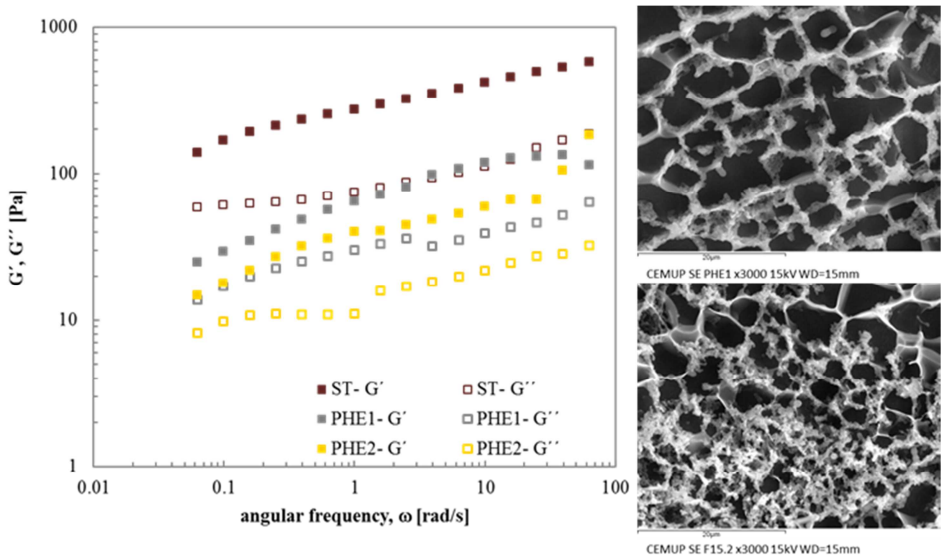


Figure 6.31- Microstructure and storage and loss moduli of stirred yoghurt (13% total solids with 1% HP50) in the fermentation tank (ST), after cooling stage in a PHE at different shear rates: PHE1 ($\dot{\gamma}$=113 s^{-1}) and PHE 2 ($\dot{\gamma}$=221 s^{-1}).

From Figure 6.31 one can detect the differences between the two cooled stirred yoghurt. The mechanical spectrum revealed the yoghurt submitted to a higher shear rate, has lower values of both G´, G´´ maintaining the weak gel-like behaviour and a denser protein network, as expected.

When comparing the results of Figures 6.30 and 6.31, one can observed that at the same, or approximately, the same shear rate value ($\dot{\gamma}$=113 s^{-1}), the impact of cooling is greater at a lower total solids content.

Structural and rheological changes that occurred during cooling stage were observed during the analysis of several yoghurt samples, indicating that at lower total solid

content the structure disruption was more severe, and almost no structure differences were observed by Cryo-SEM when shear rate conditions varied.

For stirred yoghurts containing higher total solids content a more compact microstructure was observed at higher shear rates, the effect of shear rate was evidenced.

Structure rebuilding after 2 hours of incubation at 43ºC

In order to minimise the impact of the physical, post-incubation processes in the texture and rheological properties of stirred yoghurt, the dairy processors used a set of strategies that may improve the quality of the yoghurt, namely its rheological properties and texture. Some dairy industries include an incubation stage post-cooling in order to promote some structure rebuilding, as reported by in several studied (Afonso and Maia, 1999; Anema, 2008).

Figure 6.32 shows the comparison between the mechanical spectrum of the cooled stirred yoghurt and those after an incubation stage post-cooling of 2 hours at 43ºC.

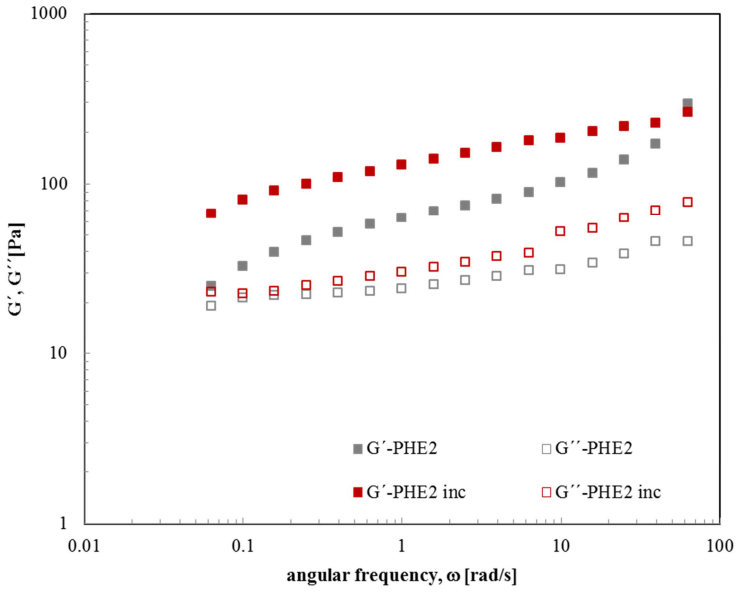


Figure 6.32- Comparison of mechanical spectra of the cooled stirred yoghurt and after an incubation stage post-cooling (13%ST-YF).

From Figure 6.32 one can observe that the incubation stage of 2 hour at 43ºC have a significant positive effect in the yoghurt structure, evidenced by the substantial increase of G´and G`` more pronounce in the elastic modulus.

6.4 Conclusions

From the stirred yoghurt/water heat transfer experiments results, the following conclusions were drawn:

a) the correlations obtained for the mean convective heat transfer coefficients of stirred yoghurt are dependent on the rheological properties of the fluid. Although, no significant dependence on the composition of stirred yoghurt was evidenced, namely on total solids content, type of protein added, presence of a thickening agent (CMC). The thermal correlations obtained have a Reynolds number exponent within the range 0.326-0.523, typical of laminar flow. All the yoghurt formulation exhibited a stronger shear-thinning behaviour, with a very low flow behaviour index that varied within the range 0.139-0.197. Therefore, the generalised Reynolds number values were very low, in all the experiments $Re_g<2.80$. Although no significant dependence on yoghurt formulation was evidence, one should notice that the thermal correlation with the lower value of the Reynolds number exponent was the correlation obtained in the heat transfer experiments carried out with the 12%TS-YF formulation, which has the lower consistency and higher value of flow behaviour index.

b) the fluids and wall temperature profiles along the PHE channels, in both passes of the heat exchanger, provided valuable information regarding differentiated local heat transfer in a PHE with a multipass arrangement. The stirred yoghurt-water experiments corroborated in some extent the results obtained in water-water experiments and CMC-water experiments, providing important information concerning local heat transfer dominances along the heat exchanger and the temperature dependence of the thermophysical of the fluids, particularly the rheological behaviour and its great influence in the hydrodynamics of thermal processes.

c) yoghurt-water heat transfer experiments evidenced the importance of including the fluids temperature dependence, particularly with complex fluids, as the stirred yoghurt that may exhibit different sensitivities to temperature changes evidenced by different

activation energies, influencing the rheological behaviour of the fluids and consequently the local hydrodynamics and heat transfer process

d) stirred yoghurt-water heat transfer experiments confirmed that the overall heat transfer coefficient varied along the PHE channels, more significantly in section 1, as mentioned previously. In this set of experiments, the section1 exhibited high perturbations due to the highly viscous behaviour of stirred yoghurt that reached high viscosity values in this section where the temperature range is low. This resulted in very low Reynolds number along the PHE.

e) the correlations obtained for the local convective heat transfer coefficients of each stirred yoghurt formulation tested, for every single sub-section along the PHE channel reflected the change of flow regime along the PHE. For the studied section (section 2), the exponent of the Reynolds number decreased along the channel length, as the fluid was cooled down, evidencing turbulent to laminar flow when the warm stirred yoghurt flows through PHE from section 2 to section 1. The changes in the Reynolds number exponent are more pronounced for stirred yoghurt with 13% of total solid content.

f) the local Nusselt number variation along the channel length highlighted the thermally developing flow along the PHE channels. The Nu-Gz correlations obtained for section 2 of the PHE were similar, at least have the same tendency, to ones published for thermal developing flow, though the values of local heat transfer coefficients were lower than those published. The local heat transfer coefficients were compared with a simplified numerical solution that accounts for the non-Newtonian behaviour and temperature dependence of the fluids like yoghurt. The results of local heat transfer coefficients were lower than the computed ones, however it was evidenced the thermally developed flows.

g) regarding Fanning friction factor correlations, comparison of the experimental correlations with the available literature showed good agreement, at least as regards the general trends reported. No relation between the Fanning friction factor and the stirred yoghurt composition was found. Discrepancies may be due to differences in the compared channels geometries and uncertainties in measurements.

h) the effect of the cooling stage in the structure of the stirred yoghurt was evaluated, and the results evidenced the importance of the selection of the proper cooling

conditions, particularly shear rate ranges, in order to minimise the impact of this production stage in the final quality of the yoghurt.

7. MAIN CONCLUSIONS AND SUGGESTIONS FOR FORTHCOMING WORK

7.1 Main conclusions

The main conclusion arising from the work presented in this thesis is the fact that a plate heat exchanger with a multipass arrangement exhibits a differentiated local heat transfer on both passes of the PHe, with completely different flow regimes depending on the proximity to the inlets of hot and cold fluids, since the temperature ranges with each pass are different.

The major implication of this differentiated local heat transfer is that not only the overall heat transfer coefficients vary along the plate heat exchanger but also the U variation is significantly different on both PHE pass. The implications of these facts are great when the thermophysical properties of the working fluids, particularly the rheological properties, exhibit high temperature dependence.

The experimental work produced a huge amount of data of the fluids and wall temperature profiles along the PHE channels, in both passes, providing valuable information for the determination of the local thermal variable-property correlations that take into account the temperature effects on the transport properties of the fluids, reducing the errors introduced by the constant –property assumption. This is quite important when the fluids exhibit different sensitivities to temperature changes evidenced by different activation energies, influencing the rheological behaviour of the fluids and consequently the local hydrodynamics and heat transfer process.

The experimental work comprised the study of heat transfer in a plate heat exchanger using working fluids with different flow behaviour from the Newtonian fluids (water), viscous Newtonian (0.25% CMC solution) and non-Newtonian, shear-thinning fluids (CMC solutions and stirred yoghurt) in order to obtain a set of local thermal correlations that could be applied in a large range of flow behaviour.

The results obtained for each set of heat transfer experiments, provided valuable information mainly in what non-Newtonian fluids are concerned.

The stirred yoghurt heat transfer experiments were accomplished for two purposes, one related to the determination of mean and local heat transfer coefficients for the optimisation of the cooling conditions and geometrical PHE configurations and the other related the processing conditions that minimise the negative effects on the yoghurt quality.

7.2 Forthcoming work

A confirmation of the achieved conclusions on the differentiated local heat transfer within the plate heat exchanger, as well as an insight on the role of different rheological behaviours on the hydrodynamic and heat transfer in the PHE should be investigated in further experiments.

Regarding to non-Newtonian food fluids exhibiting complex behaviour, such as stirred yoghurt, that exhibits shear-thinning, thixotropic, viscoelastic and yield stress properties, an insight on the influence these properties should be explored in further experiments.

A better understanding of the non-Newtonian flow and heat transfer in a plate heat transfer can be attained with the contribution of computer modelling and simulation.

BIBLIOGRAPHY

Abbasi, H., M. E. Mousavi, et al. (2009). "Influence of starter culture type and incubation temperatures on rheology and microstructure of low fat set yoghurt." International Journal of Dairy Technology **62**(4): 549-555.

Abu-Jdayil, B. (2003). "Modelling the time-dependent rheological behavior of semisolid foodstuffs." Journal of Food Engineering **57**(1): 97-102.

Afonso, I. M., P. Cruz, et al. (2008). "Simplified numerical simulation to obtain heat transfer correlations for stirred yoghurt in a plate heat exchanger." Food and Bioproducts Processing **86**(4): 296-303.

Afonso, I. M., L. Hes, et al. (2003). "Heat transfer and rheology of stirred yoghurt during cooling in plate heat exchangers." Journal of Food Engineering **57**(2): 179-187.

Afonso, I. M. and J. M. Maia (1999). "Rheological monitoring of structure evolution and development in stirred yoghurt." Journal of Food Engineering **42**(4): 183-190.

Aguirre-Mandujano, E., C. Lobato-Calleros, et al. (2009). "Microstructure and viscoelastic properties of low-fat yoghurt structured by monoglyceride gels." Lwt-Food Science and Technology **42**(5): 938-944.

Akturk, F., G. Gulben, et al. (2011). Experimental investigation of the characteristics of a chevron type gasketed -plate heat exchanger. 6th International Advanced Technologies Symposium (IATS'11). Elazığ, Turkey, University of Firat**:** 172-178.

Alakali, J. S., T. M. Okonkwo, et al. (2008). "Effect of stabilizers on the physico-chemical and sensory attributes of thermized yoghurt." African Journal of Biotechnology **7**(2): 158-163.

Amatayakul, T., A. L. Halmos, et al. (2006). "Physical characteristics of yoghurts made using exopolysaccharide-producing starter cultures and varying casein to whey protein ratios." International Dairy Journal **16**(1): 40-51.

Amatayakul, T., F. Sherkat, et al. (2006). "Syneresis in set yogurt as affected by EPS starter cultures

and levels of solids." International Journal of Dairy Technology **59**(3): 216-221.

Anema, S. G. (2008). "Effect of temperature and rate of acidification on the rheological properties of acid skim milk gels." Journal of Food Processing and Preservation **32**(6): 1016-1033.

Anema, S. G. and H. Klostermeyer (1997). "Heat-Induced, pH-Dependent Dissociation of Casein Micelles on Heating Reconstituted Skim Milk at Temperatures below 100 °C." Journal of Agricultural and Food Chemistry **45**(4): 1108-1115.

Baixauli, R., T. Sanz, et al. (2007). "Influence of the dosing process on the rheological and microstructural properties of a bakery product." Food Hydrocolloids **21**(2): 230-236.

Barnes, H. A., J. F. Hutton, et al. (1989). An introduction to rheology. Amsterdam, Elsevier Science Publishers.

Bassiouny, M. K. and H. Martin (1984a). "Flow distribution and pressure drop in plate heat exchangers--I U-type arrangement." Chemical Engineering Science **39**(4): 693-700.

Bassiouny, M. K. and H. Martin (1984b). "Flow distribution and pressure drop in plate heat exchangers--II Z-type arrangement." Chemical Engineering Science **39**(4): 701-704.

Bayarri, S., L. González-Tomás, et al. (2009). "Viscoelastic properties of aqueous and milk systems with carboxymethyl cellulose." Food Hydrocolloids **23**(2): 441-450.

Bejan, A. and A. D. Kraus (2003). Heat Transfer Handbook, John Wiley & Sons**:** 878-886.

Benchabane, A. and K. Bekkour (2008). "Rheological properties of carboxymethyl cellulose (CMC) solutions." Colloid & Polymer Science **286**(10): 1173-1180.

Benezech, T. and J. F. Maingonnat (1993). "Flow Properties of Stirred Yogurt - Structural Parameter Approach in Describing Time-Dependency." Journal of Texture Studies **24**(4): 455-473.

Benezech, T. and J. F. Maingonnat (1994). "Characterization of the Rheological Properties of Yogurt - a Review." Journal of Food Engineering **21**(4): 447-472.

Béreiziat, D. and R. Devienne (1999). "Experimental characterization of Newtonian and non-Newtonian fluid flows in corrugated channels." International Journal of Engineering Science **37**(11): 1461-1479.

Bernardi, M., V. Silveira Jr., et al. (2009). "Forced convection to laminar flow of liquid egg yolk in circular and annular ducts." Brazilian Journal of Chemical Engineering **26**: 287-298.

Bobbili, P. R., B. Sunden, et al. (2006). "An experimental investigation of the port flow maldistribution in small and large plate package heat exchangers." Applied Thermal Engineering **26**(16): 1919-1926.

Buffo, R. A. and G. A. Reineccius (2002). "Modeling the rheology of concentrated beverage emulsions." Journal of Food Engineering **51**(4): 267-272.

Buffo, R. A., G. A. Reineccius, et al. (2002). "Influence of time-temperature treatments on the emulsifying properties of gum acacia in beverage emulsions." Journal of Food Engineering **51**(4): 341-345.

Buonopane, R. A., R. A. Troupe, et al. (1963). "Heat Transfer Design method for plate heat exchangers." Chemical Engineering Progress **59**(7): 5.

Cabral, R. A. F., J. A. W. Gut, et al. (2010). "Non-newtonian flow and pressure drop of pineapple juice in a plate heat exchanger." Brazilian Journal of Chemical Engineering **27**: 563-571.

Cabral, R. A. F., J. A. W. Gut, et al. (2011). Non-Newtonian flow and heat transfer of pineapple juice in a plate heat exchanger. 11th International Congress on Engineering and Food, iCEF11 Congress Proceeding, Atenas.

Cancela, M. A., E. Álvarez, et al. (2005). "Effects of temperature and concentration on carboxymethylcellulose with sucrose rheology." Journal of Food Engineering **71**(4): 419-424.

Carezzato, A., M. R. Alcantara, et al. (2007). "Non-Newtonian Heat Transfer on a Plate Heat Exchanger with Generalized Configurations." Chemical Engineering & Technology **30**(1): 21-26.

Chakrabandhu, K. and R. K. Singh (2005). "Rheological properties of coarse food suspensions in tube flow at high temperatures." Journal of Food Engineering **66**(1): 117-128.

Chen, H.-H., H.-Y. Kang, et al. (2008). "The effects of ingredients and water content on the rheological properties of batters and physical properties of crusts in fried foods." Journal of Food Engineering **88**(1): 45-54.

Chen, J. and E. Dickinson (1998). "Viscoelastic properties of heat-set whey protein emulsion gels." Journal of Texture Studies **29**(3): 285-304.

Chhabra, R. P. and J. F. Richardson (2008). Non-Newtonian Flow and Applied Rheology - Engineering Applications (2nd Edition), Elsevier**:** 97-101.

CHR-HANSEN (2003). FD-DVS YF-L811 - Yo-Flex$^{(R)}$. Product information. Horsholm, Chr-Hansen. **EN FD-DVS YF-L811 -FD PI-0603:** 2.

CHR-HANSEN (2004). FD-DVS YC-380 - Yo-Flex$^{(R)}$ Product Information. FD-DVS YC-380 - Yo-Flex PI EN vs2 July 2004.doc/Jul 2004/1:2 Chr-Hansen. **FD-DVS YC-380 - Yo-Flex PI EN vs2:** 2.

Chryssanthopoulos, C. and M. Maridaki (2010). Nutritional Aspects of Yogurt and Functional Dairy Products. Development and manufacture of yogurt and other functional dairy products F. Yildiz. Boca Raton, Taylor and Francis Group, LLC**:** 39.

Cooper, A. (1974). "Recover more heat with plate heat echanger." The Chemical Engineer(May): 280-285.

Corrieu, G., Y. Noël, et al. (1985). "Liquides alimentaires complexes caractérisation rhéologique et traitement thermique." Revue Générale de Thermique **279**: 229–240.

Coulson, J. M., J. F. Richardson, et al. (1999). Coulson and Richardson's Chemical Engineering Volume 1 - Fluid Flow, Heat Transfer and Mass Transfer (6th Edition), Elsevier**:** 41-50.

Croce, G. and P. D'Agaro (2002). "Numerical analysis of forced convection in plate and frame heat exchangers." International Journal of Numerical Methods for Heat and Fluid Flow **12**(6): 756-771.

Cronin, K., J. Caro-Corrales, et al. (2010). "Heat transfer analysis of cheese cooling incorporating uncertainty in temperature measurement locations: Model development and validation." Journal of Food Engineering **99**(2): 175-183.

Delplace, F. (1995). Identification des échangeurs de chaleur à plaques: Application à l'étude de l'encrassement par produits laitiers. Nancy, Université Henri Poincaré. **PhD**.

Ditchfield, C., C. C. Tadini, et al. (2007). "Heat transfer during thermal processing of a temperature dependent non-Newtonian fluid in a tubular heat exchanger." Chemical Engineering and Processing **46**(5): 472-476.

Domagala, J., M. Sady, et al. (2005). "The influence of storage time on rheological properties and texture of yoghurts with the addition of oat-maltodextrin as the fat substitute." International Journal of Food Properties **8**(3): 439-448.

Domagata, J., M. Sady, et al. (2006). "Rheological properties and texture of yoghurts when oat-maltodextrin is used as a fat substitute." International Journal of Food Properties **9**(1): 1-11.

Durmuş, A., H. Benli, et al. (2009). "Investigation of heat transfer and pressure drop in plate heat exchangers having different surface profiles." International Journal of Heat and Mass Transfer **52**(5–6): 1451-1457.

Edwards, M. F. (1988). Heat transfer in plate heat exchangers at low Reynolds number. Low Reynolds number forced convection in channels and bundles applied to heat exchangers. S. Kakaç. Ankara, NATO Advanced Study Institute**:** 23-37.

Edwards, M. F., A. A. Changal Vaie, et al. (1974). "Heat transfer and pressure drop characteristics of a plate heat exchanger using Newtonian and non-Newtonian liquids." The Chemical Engineer(May): 286-288.

Elliot, J. and A. Ganz (1974). "Some rheological properties of sodium carboxymethylcellulose solutions and gels." Rheologica Acta **13**(4): 670-674.

Fangary, Y. S., M. Barigou, et al. (1999). "Simulation of yoghurt flow and prediction of its end-of-process properties using rheological measurements." Food and Bioproducts Processing **77**(C1): 33-39.

Fernandes, C. S. (2009). Optimização do projecto e desempenho de permutadores de calor de placas para fluidos alimentares. Departamento de Polímeros. Guimarães, Universidade do Minho. **Doctoral:** 184.

Fernandes, C. S., R. Dias, et al. (2005a). "Simulation of stirred yoghurt processing in plate heat exchangers." Journal of Food Engineering **69**(3): 281-290.

Fernandes, C. S., R. P. Dias, et al. (2006). "Thermal behaviour of stirred yoghurt during cooling in plate heat exchangers." Journal of Food Engineering **76**(3): 433-439.

Fernandes, C. S., R. P. Dias, et al. (2005b). Effect of corrugation angle on the hydrodynamic behaviour of power-law fluids during flow in plate heat exchanger. Fifth Conference on Enhanced, Compact and Ultra-Compact Heat Exchangers: Science, Engineering and Technology, Whistler, Canada, Engineering Conferences International.

Fernandes, C. S., R. P. Dias, et al. (2007). "Laminar flow in chevron-type plate heat exchangers: CFD analysis of tortuosity, shape factor and friction factor." Chemical Engineering and Processing **46**(9): 825-833.

Fernandes, C. S., R. P. Dias, et al. (2008). "Friction factors of power-law fluids in chevron-type plate heat exchangers." Journal of Food Engineering **89**(4): 441-447.

Florjancic, U., A. Zupancic, et al. (2002). "Rheological Characterization of Aqueous Polysaccharide Mixtures Undergoing Shear." Chem. Biochem. Eng. Q **16**(3): 105–118.

Fricke, B. A. and B. R. Becker (2002). "Calculation of heat transfer coefficients for foods." International Communications in Heat and Mass Transfer **29**(6): 731-740.

Galeazzo, F. C. C., R. Y. Miura, et al. (2006). "Experimental and numerical heat transfer in a plate heat exchanger." Chemical Engineering Science **61**(21): 7133-7138.

Ghannam, M. T. and M. N. Esmail (1997). "Rheological properties of carboxymethyl cellulose." Journal of Applied Polymer Science **64**(2): 289-301.

Gherasim, I., N. Galanis, et al. (2009). "Effects of dissipation and temperature-dependent viscosity on the performance of plate heat exchangers." Applied Thermal Engineering **29**(14–15): 3132-3139.

Gut, J. A. W. (2003). Configurações ótimas para trocadores de calor a placas. São Paulo, Escola Politécnica da Universidade de São Paulo. **PhD**.

Gut, J. A. W., R. Fernandes, et al. (2004). "Thermal model validation of plate heat exchangers with generalized configurations." Chemical Engineering Science **59**(21): 4591-4600.

Gut, J. A. W. and J. M. Pinto (2001). Modeling of the plate heat exchangers with generalized configurations. COBEM 2001 - 16th Brazilian Congress of Mechanical Engineering, Uberlândia (Br). .

Gut, J. A. W. and J. M. Pinto (2003a). "Modeling of plate heat exchangers with generalized configurations." International Journal of Heat and Mass Transfer **46**(14): 2571-2585.

Gut, J. A. W. and J. M. Pinto (2003b). "Selecting Optimal Configurations for Multisection Plate Heat Exchangers in Pasteurization Processes." Industrial & Engineering Chemistry Research **42**(24): 6112-6124.

Hamdami, N., J.-Y. Monteau, et al. (2004). "Thermophysical properties evolution of French partly baked bread during freezing." Food Research International **37**(7): 703-713.

Han, X.-H., L.-Q. Cui, et al. (2010). "A numerical and experimental study of chevron, corrugated-plate heat exchangers." International Communications in Heat and Mass Transfer **37**(8): 1008-1014.

Hassan, A. N., J. F. Frank, et al. (1996a). "Rheological Properties of Yogurt Made with Encapsulated Nonropy Lactic Cultures." Journal of Dairy Science **79**(12): 2091-2097.

Hassan, A. N., J. F. Frank, et al. (1996b). "Textural Properties of Yogurt Made with Encapsulated Nonropy Lactic Cultures." Journal of Dairy Science **79**(12): 2098-2103.

Heggs, P. J., P. Sandham, et al. (1997). "Local heat transfer coefficients in corrugated plate heat exchanger channels." Transactions of the Institution of Chemical Engineers **Part A**(75): 641-645.

Hewitt, G. F., G. L. Shires, et al. (1994a). Process Heat Transfer. Boca Raton, CRC Press LLC.

Hewitt, G. F., G. L. Shires, et al. (1994b). Process Heat Transfer. Boca Raton, CRC Press LLC.

International, A. (1995). Official Methods of Analysis of AOAC International. Ash of Dried Milk. Arlington,. **930.30**.

Jackson, B. W. and R. A. Troupe (1964). "Laminar flow in a plate heat exchanger. A correlation predicting the average film coefficient for heating or cooling at Reynolds numbers below 400." Chemical Engineering Progress **60**(7): 62-65.

Kakaç, S. and H. Liu (2002). Heat exchangers- selection, rating and thermal design. Boca Raton, CRC Press LLC.

Kalab, M., P. Allan-Wojtas, et al. (1983). "Development of microstructure in set-style nonfat yoghurt[mdash]a review." Food Microstruct. **2**: 51-66.

Kamizake, N. K. K., M. M. Gonçalves, et al. (2003). "Determination of total proteins in cow milk powder samples: a comparative study between the Kjeldahl method and spectrophotometric methods." Journal of Food Composition and Analysis **16**(4): 507-516.

Khalaf, W. G. and S. K. Sastry (1996). "Effect of fluid viscosity on the ohmic heating rate of solid-liquid mixtures." Journal of Food Engineering **27**(2): 145-158.

Kho, T. and H. Müller-Steinhagen (1999). "An experimental and numerical investigation of heat transfer fouling and fluid flow in flat plate heat exchangers." Transactions of the Institution of Chemical Engineers **Part A**(77): 124-130.

Kim, C. and B. Yoo (2006). "Rheological properties of rice starch–xanthan gum mixtures." Journal of Food Engineering **75**(1): 120-128.

Kim, H. B., C. C. Tadini, et al. (1999). "Heat transfer in a plate exchanger during pasteurization of orange juice." Journal of Food Engineering **42**(2): 79-84.

Kowalczyk, W., C. Hartmann, et al. (2005). "Determination of thermophysical properties of foods under high hydrostatic pressure in combined experimental and theoretical approach." Innovative Food Science & Emerging Technologies **6**(3): 318-326.

Kresic, G., V. Lelas, et al. (2008). "Influence of novel food processing technologies on the rheological and thermophysical properties of whey proteins." Journal of Food Engineering **87**(1): 64-73.

Kruger, N. J. (2002). The Bradford Method for Protein Quantitation

The Protein Protocols Handbook. J. M. Walker, Humana Press**:** 15-21.

Kuppan, T. (2000). Heat Exchanger Design Handbook. New Jersey, Marcel Dekker Inc.

Lee, W. J. and J. A. Lucey (2006). "Impact of Gelation Conditions and Structural Breakdown on the Physical and Sensory Properties of Stirred Yogurts." Journal of Dairy Science **89**(7): 2374-2385.

Leuliet, J.-C., J.-F. Maingonnat, et al. (1987). "Étude de la Perte de Charge dans des Échangeurs de Chaleur à Plaques Traitant des Produits Non-Newtoniens." Revue Générale de Thermique Française **308-309**: 445-450.

Leuliet, J.-C., J.-F. Maingonnat, et al. (1990a). "Écoulements et Transferts dans les Échangeurs à Plaques Traitant des Produits Visqueux Newtoniens et Pseudoplastiques." Canadian Journal of Chemical Engineering **68**: 220-229.

Leuliet, J. C. and J. F. Maingonnat (1992). Influence du seil d'ecoulement sur les performances thermiques d'echangeurs de caleur à plaques. Proceedings 5ème Colloque TIFAN, Strasbourg, France.

Leuliet, J. C., J. F. Maingonnat, et al. (1990b). "Écoulement et transfers de chaleur dansles échangeurs à plaques traitant des produits visqueux newtoniens et pseudoplastiques. 1. Modélisation des variations du diamètre hydraulique." The Canadian Journal of Chemical Engineering **68**(April): 220-229.

Li, X. W., J. A. Meng, et al. (2010). "An experimental study of the flow and heat transfer between enhanced heat transfer plates for PHEs." Experimental Thermal and Fluid Science **34**(8): 1194-1204.

Longo, G. A., A. Gasparella, et al. (2004). "Experimental heat transfer coefficients during refrigerant vaporisation and condensation inside herringbone-type plate heat exchangers with enhanced surfaces." International Journal of Heat and Mass Transfer **47**(19-20): 4125-4136.

Luan, Z. j., G. m. Zhang, et al. (2008). "Flow resistance and heat transfer characteristics of a new-type plate heat exchanger." Journal of Hydrodynamics **20**(4): 524-529.

Lucey, J. A. (2002). "Formation and Physical Properties of Milk Protein Gels." Journal of Dairy Science **85**(2): 281-294.

Lucey, J. A. and H. Singh (1997). "Formation and physical properties of acid milk gels: a review." Food Research International **30**(7): 529-542.

Lucey, J. A., M. Tamehana, et al. (1998). "Effect of interactions between denatured whey proteins and casein micelles on the formation and rheological properties of acid skim milk gels." J. Dairy Res. **65**: 555-567.

Lucey, J. A., C. T. Teo, et al. (1998). "Microstructure, permeability and appearance of acid gels made from heated skim milk." Food Hydrocolloids **12**: 159-165.

Macosko, C. W. (1994). Rheology - Principles, Measurements and Applications, John Wiley & Sons**:** 109-133.

Madigan, M. T., J. M. Mortinka, et al. (2009). Brock Biology of Microorganisms. San Francisco, Pearson Benjamin Cummings.

Mahalingam, R., L. O. Tilton, et al. (1975). "Heat transfer in laminar flow of non-Newtonian fluids." Chemical Engineering Science **30**(8): 921-929.

Maia, J. M., J. M. Nóbrega, et al. (2007). CFD simulation of stirred yoghurt processing in plate heat exchangers. Computational fluid dynamics in food processing D.-W. Sun, Taylor & Francis Group, LLC**:** 381-402.

Maingonnat, J. F., J. C. Leuliet, et al. (1987). "Modélisation de la vitesse de cisaillement apparente dans un échangeur de chaleur à surface raclée. Application aux performances thermiques avec des produits non-newtoniens." Révue Génerale de Thermique Française **306-307**(juin-juillet): 381-385.

Maingonnat, J. F., L. Muller, et al. (2005). "Modelling the build-up of a thixotropic fluid under viscosimetric and mixing conditions." Journal of Food Engineering **71**(3): 265-272.

Malkin, A. Y. and A. I. Isayev (2006). Rheology - Concepts, Methods, & Applications, ChemTec Publishing**:** 94-96.

McKillop, A. A. and W. L. Dunkley (1960). "Heat transfer (Plate heat exchangers)." Industrial and Engineering Chemistry **52**(9): 740-744.

Mehrabian, M. A. (2009). "Construction, performance, and thermal design of plate heat exchangers." Proceedings of the Institution of Mechanical Engineers, Part E: Journal of Process Mechanical Engineering **223**(3): 123-131.

Metzner, A. B., R. D. Vaughn, et al. (1957). "Heat transfer to non-Newtonian fluids." A.I.Ch.E. Journal **3**(1): 92-100.

Mistry, V. V. and H. N. Hassan (1992). "Manufacture of Nonfat Yogurt from a High Milk Protein Powder." Journal of Dairy Science **75**(4): 947-957.

Modler, H. W., M. E. Larmond, et al. (1983). "Physical and Sensory Properties of Yogurt Stabilized with Milk Proteins." Journal of Dairy Science **66**(3): 422-429.

Mortazavian, A. M., K. Rezaei, et al. (2009). "Application of Advanced Instrumental Methods for Yogurt Analysis." Critical Reviews in Food Science and Nutrition **49**(2): 153 - 163.

Muley, A. and R. M. Manglik (1999). "Experimental Study of Turbulent Flow Heat Transfer and Pressure Drop in a Plate Heat Exchanger With Chevron Plates." Journal of Heat Transfer **121**(1): 110-117.

Muley, A., R. M. Manglik, et al. (1999). "Enhanced heat transfer characteristics of viscous liquid flows in a chevron plate heat exchanger." Jounal of Heat Transfer **121**: 1011-1017.

Otero, L., B. Guignon, et al. (2010). "Modeling thermophysical properties of food under high pressure." Critical Reviews in Food Science and Nutrition **50**(4): 344-368.

Palm, B. and J. Claesson (2005). Plate heat exchangers, calculation methods for single- and two-phase flow, Toronto, ON.

Penna, A. L. B., A. Converti, et al. (2006). "Simultaneous Effects of Total Solids Content, Milk Base, Heat Treatment Temperature and Sample Temperature on the Rheological Properties of Plain Stirred Yogurt " Food Technology and Biotechnology **44**(4): 515-518.

Prabhakara Rao, B., P. Krishna Kumar, et al. (2002). "Effect of flow distribution to the channels on the thermal performance of a plate heat exchanger." Chemical Engineering and Processing: Process Intensification **41**(1): 49-58.

Qualidade, I.-I. P. d. (1982a). NP 701:1982 (2ª Edição) Iogurtes. Determinação da acidez. Lisboa, IPQ. **NP 701:1982**.

Qualidade, I.-I. P. d. (1982b). NP 703:1982 (Ed. 2). Iogurtes. Determinação do resíduo seco e resíduo seco isento de matéria gorda. **NP 703:1982 (Ed. 2).** .

Qualidade, I.-I. P. d. (1983). NP 469:1983 - Leites. Determinação do teor da matéria gorda. Técnica de Gerber. Processo de referência. Lisboa, IPQ. **NP 469:1983**.

QUALIDADE, I.-I. P. D. (1987). NP 1864 (1987) - Norma portuguesa : Microbiologia alimentar: Iogurte: Contagem da flora específica: Processo corrente e processo de referência. Lisboa : IPQ, OPQ**:** 10.

Qualidade, I.-I. P. d. (1991). NP 1986:1991 (1ª Edição). Leites Determinação do teor de proteína bruta. Técnica de Kjeldahl. Lisboa, IPQ. **NP 1986:1991**.

Raju, K. S. N. and J. C. Bansal (1986). Design of Plate Heat Exchangers. Heat Exchanger Sourcebook. J. W. Palen. Berlin, Springer- Verlag**:** 563-582.

Raudsepp, A., K. W. Feindel, et al. (2010). "Shear localisation in stirred yoghurt." Rheologica Acta **49**(4): 371-379.

Reddy, C. S. and A. K. Datta (1994). "Thermophysical properties of concentrated reconstituted milk during processing." Journal of Food Engineering **21**(1): 31-40.

Rene, F. and M. Lalande (1987). "Échangeur de chaleur à plaques et joints. Résolution numérique des équations d´échange thermique entre les différents canaux." Revue Générale Thermique Française **311**: 577-583.

Rene, F., J. C. Leuliet, et al. (1991a). "Heat transfer to Newtonian and non-Newtonian food fluids in plate heat exchangers. Experimental and numerical approaches." Food and Bioproducts Processing: Transactions of the Institution of of Chemical Engineers, Part C **69**(3): 115-126.

Rene, F., J. C. Leuliet, et al. (1991b). "Heat transfer to Newtonian and non-Newtonian food fluids in plate heat exchangers: experimental and numerical approaches." Transactions of the Institution of Chemical Engineers **Part C**(69): 115-126.

Rohm, H. and A. Kovac (1994). "Effects of starter cultures on lienar viscoelastic and physical properties of yogurt gels." Journal of Texture Studies **25**(3): 311-329.

Rohm, H. and A. Kovac (1995). "Effects of Starter Cultures on Small Deformation Rheology of Stirred Yogurt." Food Science and Technology-Lebensmittel-Wissenschaft & Technologie **28**(3): 319-322.

Rohsenow, W. M., J. P. Hartnett, et al. (1998). NonNewtonian Fluids. Handbook of heat transfer New York, McGraw Hill.

Sanz, T., A. Salvador, et al. (2008). "Yogurt enrichment with functional asparagus fibre. Effect of fibre extraction method on rheological properties, colour, and sensory acceptance." European Food Research and Technology **227**(5): 1515-1521.

Schwartzberg, H. G. (1976). "Effective heat capacities for the freezing and thawing of food." Journal of Food Science **41**(1): 152-156.

Semmar, N., J. L. Tanguier, et al. (2003). "Specific heat of carboxymethyl cellulose and Carbopol aqueous solutions." Thermochimica Acta **402**(1–2): 225-235.

Sesták, J., R. Zitný, et al. (1983). "Simple rheological models of food liquids for process design and quality assessment." Journal of Food Engineering **2**(1): 35-49.

Shah, R. K., Sekuli, et al. (2003). Fundamentals of Heat Exchanger Design, John Wiley & Sons**:** 23-29.

Shah, R. K. and D. P. Sekuli (2003). Fundamentals of Heat Exchanger Design, John Wiley & Sons**:** 244-258.

Shah, R. K. and D. P. Sekulic (2003). Fundamentals of Heat Exchanger Design. New Jersey, John Wiley & Sons, Inc.

Smyth, C., E. D. Kudryashov, et al. (2001). "High-frequency shear and volume viscoelastic moduli of casein particle gel." Colloids and Surfaces a-Physicochemical and Engineering Aspects **183**: 517-526.

Sodini, I., J. Mattas, et al. (2006). "Influence of pH and heat treatment of whey on the functional properties of whey protein concentrates in yoghurt." International Dairy Journal **16**(12): 1464-1469.

Sourlier, P., R. Devienne, et al. (1987). "Laminar Flow and Heat Transfer for a Pseudoplastic Fluid Between Two Planes Parallel, and Horizontal Plates." ECOULEMENT LAMINAIRE ET TRANSFERT DE CHALEUR POUR UN FLUIDE PSEUDOPLASTIQUE ENTRE DEUX PLAQUES PLANES PARALLELES ET HORIZONTALES. **26**(308-309): 432-439.

Steffe, J. F. (1996). Rheological Methods in Food Process Engineering. East Lansing, MI, USA, Freeman Press.

Tadini, C. C., G. G. Badolato, et al. (2000). Study of heat transfer of liquid foods using a plate heat exchanger. FoodSim2000.

Tamime, A. Y. and R. K. Robinson (1999). Yogurt- Science and Technology. Boca Raton, CRC Press LLC.

Tavman, I. H. and S. Tavman (1999). "Measurement of thermal conductivity of dairy products." Journal of Food Engineering **41**(2): 109-114.

Tavman, S., I. H. Tavman, et al. (1997). "Measurement of thermal diffusivity of granular food materials." International Communications in Heat and Mass Transfer **24**(7): 945-953.

Tetra Pak Processing Components AB (2000). Tetra Plex ^{R} - plate heat exchangers. Lund, Sweden. **Code PD 63504 en1 00-04**.

ThermExcel (2003, June 2003). "Physical characteristics of water (at the atmospheric pressure)." from http://www.thermexcel.com/english/tables/eau_atm.htm.

Thonon, B., S. Grandgeorge, et al. (1999). "Effect of Geometry and Flow Conditions on Particulate Fouling in Plate Heat Exchangers." Heat Transfer Engineering **20**: 12-24.

Toledo, R. T. (2007). Fundamentals of Food Process Engineering. New York, Springer Science+Business Media, LLC.

Torre, L. L., A. Y. Tamime, et al. (2003). "Rheology and sensory profiling of set-type fermented milks made with different commercial probiotic and yoghurt starter cultures." International Journal of Dairy Technology **56**(3): 163-170.

Tunick, M. H. (2000). "Rheology of Dairy Foods that Gel, Stretch, and Fracture." J. Dairy Sci. **83**(8): 1892-1898.

Vélez-Ruiz, J. F., G. V. B. Cánovas, et al. (1997). "Rheological properties of selected dairy products." Critical Reviews in Food Science and Nutrition **37**(4): 311 - 359.

Veloso, A. C. A., N. Teixeira, et al. (2001). "Metodologias de Doseamento das Proteínas do Leite." Boletim de Biotecnologia **69**: 17-31.

Wang, L. and B. Sundén (2003). "Optimal design of plate heat exchangers with and without pressure drop specifications." Applied Thermal Engineering **23**(3): 295-311.

Wang, Y., L.-J. Wang, et al. (2009). "Effects of drying methods on rheological properties of flaxseed gum." Carbohydrate Polymers **78**(2): 213-219.

Wang, Z. and S. Hirai (2011). "Modeling and estimation of rheological properties of food products for manufacturing simulations." Journal of Food Engineering **102**(2): 136-144.

Warnakulasuriya, F. S. K. and W. M. Worek (2008). "Heat transfer and pressure drop properties of high viscous solutions in plate heat exchangers." International Journal of Heat and Mass Transfer **51**(1-2): 52-67.

Welti-Chanes, J., F. Vergara-Balderas, et al. (2005). "Transport phenomena in food engineering: basic concepts and advances." Journal of Food Engineering **67**(1-2): 113-128.

Zettler, H. U. and H. Müller-Steinhagen (2001). The use of CFD for the interpretation of fouling data in PHEs. Heat Exchangers Fouling- Fundamental Approaches & Technical Solutions. I. UEF- United Engineering Foundation. Davos, UEF- United Engineering Foundation, Inc.

ANNEXES

ANNEX A1 - COMPLEMENTARY DATA AND RESULTS

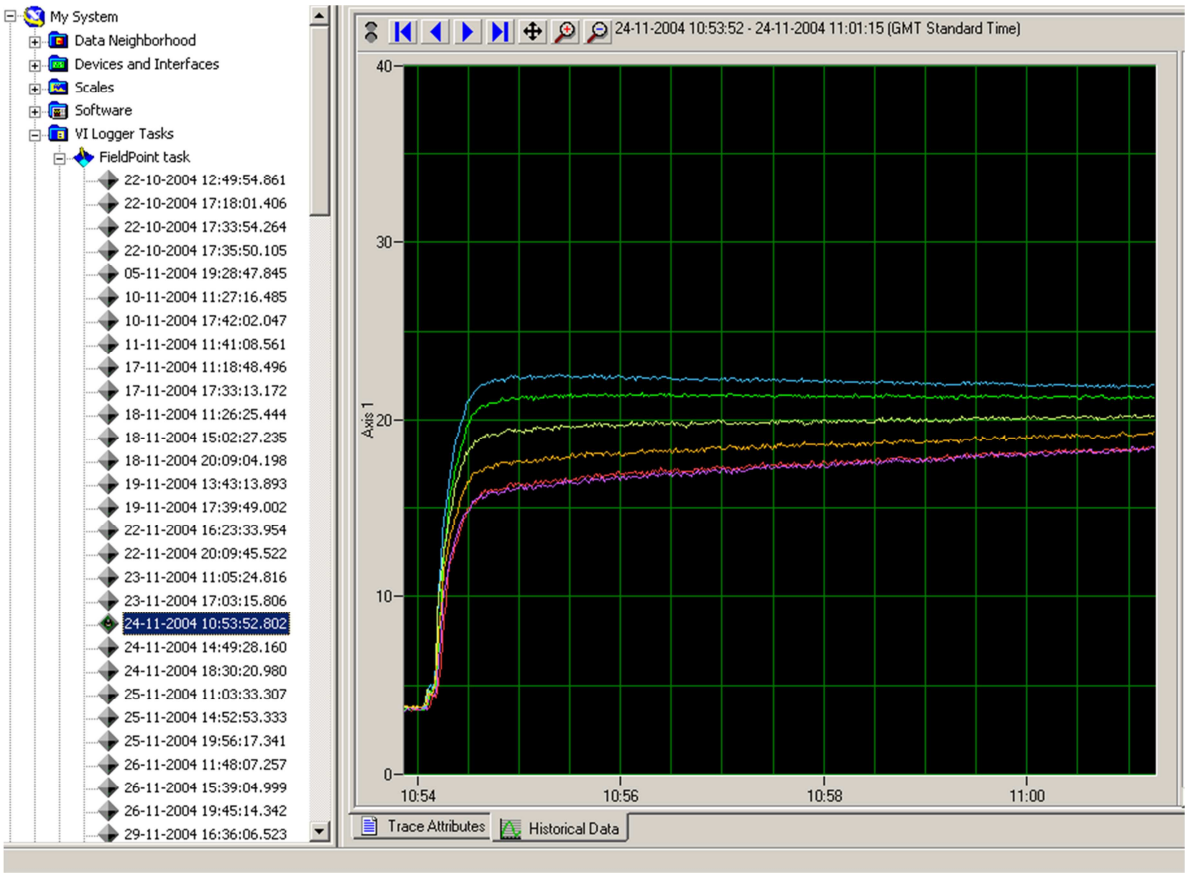


Figure A.1- Temperature profiles during a heat transfer experiment (in-line reading).

Table A.1- Average values of the mass flow rate, Reynolds (Re) and Prandtl (Pr) numbers of the cold and hot water and of the overall heat transfer coefficients (U), for each water/ water heat transfer experiment.

Experiment ID	Cold water			Hot water			U
	mass rate [kg s^{-1}]	Re [-]	Pr [-]	mass rate [kg s^{-1}]	Re [-]	Pr [-]	[W m^2K^{-1}]
1	0.187	977	6.63	0.189	1342	4.72	1105
2	0.085	393	7.63	0.102	613	5.69	601
3	0.085	414	7.21	0.089	568	5.29	582
4	0.113	524	7.63	0.108	623	5.98	705
5	0.228	1137	7.01	0.234	1591	4.93	1252
6	0.229	1168	6.82	0.217	1477	4.93	1245
7	0.057	291	6.82	0.055	389	4.72	413
8	0.057	289	6.82	0.055	367	5.05	418
9	0.226	1152	6.82	0.207	1408	4.93	1193
10	0.201	1151	5.98	0.213	1631	4.33	1207
11	0.202	1031	6.82	0.185	1157	5.42	1108
12	0.143	679	7.41	0.122	764	5.42	806
13	0.074	342	7.63	0.059	369	5.42	455
14	0.086	409	7.41	0.071	454	5.29	491
15	0.089	409	7.63	0.063	371	5.83	582
16	0.222	1078	7.21	0.211	1292	5.55	1178
17	0.225	1097	7.21	0.216	1415	5.17	1220
18	0.254	1296	6.82	0.258	1760	4.93	1364
19	0.144	666	7.63	0.129	757	5.83	881
20	0.113	536	7.41	0.103	620	5.70	742
21	0.202	959	7.41	0.176	1057	5.69	1138
22	0.097	582	5.69	0.087	582	5.05	694
23	0.100	574	5.98	0.087	583	5.05	738

Table A.2- Average values of the overall heat transfer coefficients (U), mean convective heat coefficients of cooling water (hcw) and mean convective heat coefficients of hot water (hhw) for each water/ water heat transfer experiment.

Experiment ID	**Reynolds number, Re [-]**	**h_{cw} [W m^2K^{-1}]**	**h_{hw} [W m^2K^{-1}]**
1	977	2329	2312
2	393	1251	1300
3	414	1278	1233
4	524	1541	1328
5	1137	2644	2597
6	1168	2675	2481
7	291	973	931
8	289	967	903
9	1152	2648	2395
10	1151	2547	2703
11	1031	2443	2114
12	679	1847	1526
13	342	1129	890
14	409	1276	1040
15	409	1288	906
16	1078	2565	2265
17	1097	2597	2386
18	1296	2887	2818
19	666	1837	1523
20	536	1554	1320
21	959	2375	1950
22	582	1528	1333
23	574	1534	1315

Table A.3- Average values of the local Nusselt number (Nu_L) of cooling water along the channel length (x_L) as a function of local Reynolds number, for section 1.

Local Reynolds number, Re [-]	**Channel length, x_L [m]**	**Local Nusselt number, Nu_L**
194	0.1395	43
	0.2595	42
	0.4295	28
	0.5745	24
311	0.1395	50
	0.2595	48
	0.4295	34
	0.5745	30
516	0.1395	60
	0.2595	57
	0.4295	43
	0.5745	38
734	0.1395	66
	0.2595	63
	0.4295	49
	0.5745	44
872	0.1395	71
	0.2595	67
	0.4295	54
	0.5745	49
999	0.1395	73
	0.2595	70
	0.4295	58
	0.5745	52

Table A.4- Average values of the local Nusselt number (Nu_L) of cooling water along the channel length (x_L) as a function of local Reynolds number, for section 2.

Local Reynolds number, Re [-]	**Channel length, x_L [m]**	**Local Nusselt number, Nu_L**
412	0,2425 0.3355 0.4835 0.6275	31 29 26 26
517	0.2425 0.3355 0.4835 0.6275	40 37 34 33
859	0.2425 0.3355 0.4835 0.6275	56 53 49 47
1271	0.2425 0.3355 0.4835 0.6275	69 65 61 58
1460	0.2425 0.3355 0.4835 0.6275	78 74 69 66
1625	0.2425 0.3355 0.4835 0.6275	84 79 74 71

Table A.5- Average values of the mass flow rate, Reynolds (*Re*) and Prandtl (*Pr)* numbers of the CMC solutions and cooling water and of the overall heat transfer coefficients (*U*), for each CMC/ water heat transfer experiment.

% CMC solution	**CMC**			**Cold water**			**U [W m^{2}K^{-1}]**
	mass rate [kg s^{-1}]	**Re [-]**	**Pr [-]**	**mass rate [kg s^{-1}]**	**Re [-]**	**Pr [-]**	
0.25	0.028	2.9	335	0.185	666	10.1	305
	0.040	4.3	326	0.187	776	8.6	431
	0.065	7.0	326	0.183	662	10.1	560
	0.066	6.8	341	0.222	752	10.8	604
	0.026	2.6	374	0.225	671	12.5	398
	0.095	10.2	326	0.224	882	9.2	715
	0.169	19.6	294	0.221	1021	7.6	933
	0.028	2.7	374	0.249	821	11.2	394
	0.061	6.2	351	0.253	941	9.8	535
	0.140	14.7	340	0.254	1115	8.1	843
1.0	0.051	4.7	378	0.250	955	9.4	453
	0.111	15.1	249	0.255	1238	7.2	590
	0.073	6.3	402	0.248	977	9.2	504
	0.122	12.4	342	0.249	1125	7.9	609
	0.175	20.4	295	0.226	1070	7.4	603
	0.180	23.5	261	0.249	1153	7.6	743
	0.217	26.4	281	0.263	1246	7.4	827
	0.265	37.3	241	0.261	1300	7.0	895
	0.229	35.3	219	0.260	1264	7.2	841
2.0	0.056	1.5	1268	0.271	1037	9.2	184
	0.080	2.5	1113	0.271	1254	7.6	214
	0.104	4.0	878	0.279	1321	7.4	281
	0.048	1.2	1423	0.278	1318	7.4	230
	0.071	1.9	1280	0.278	1285	7.6	254
	0.085	2.4	1223	0.278	1285	7.6	281
	0.101	3.1	1115	0.278	1285	7.6	291

Table A.6- Average values of the local Nusselt number (Nu_L) of 0.25% CMC solution along the channel length (x_L) as a function of local Reynolds number, for section 1.

Local Reynolds number, Re [-]	**Channel length, x_L [m]**	**Local Nusselt number, Nu_L**
3.5	0.1395	37.0
	0.2595	15.3
	0.4295	8.6
	0.5745	6.1
5.9	0.1395	22.5
	0.2595	16.2
	0.4295	11.8
	0.5745	9.4
8.9	0.1395	37.3
	0.2595	24.8
	0.4295	17.2
	0.5745	13.4
17.1	0.1395	35.7
	0.2595	30.7
	0.4295	22.8
	0.5745	19.0

Table A.7- Average values of the local Nusselt number (Nu_L) of 1.0% CMC solution along the channel length (xL) as a function of local Reynolds number, for section 1.

Local Reynolds number, Re [-]	**Channel length, x_L [m]**	**Local Nusselt number, Nu_L**
2.1	0.1395	60.5
	0.2595	21.2
	0.4295	11.9
	0.5745	8.4
6.2	0.1395	23.8
	0.2595	18.5
	0.4295	15.2
	0.5745	12.5
11.9	0.1395	20.4
	0.2595	19.4
	0.4295	17.8
	0.5745	16.0
18.5	0.1395	21.2
	0.2595	21.3
	0.4295	20.5
	0.5745	19.2

Table A.8- Average values of the local Nusselt number (Nu_L) of 2.0% CMC solution along the channel length (x_L) as a function of local Reynolds number, for section 1.

Local Reynolds number, Re [-]	**Channel length, x_L [m]**	**Local Nusselt number, Nu_L**
0.6	0.1395	12.8
	0.2595	9.6
	0.4295	6.9
	0.5745	5.9
1.2	0.1395	15.4
	0.2595	12.5
	0.4295	10.0
	0.5745	8.7
1.5	0.1395	16.7
	0.2595	12.4
	0.4295	9.2
	0.5745	7.8

Table A.9- Average values of the mass flow rate, Reynolds (*Re*) and Prandtl (*Pr*) numbers of the stirred yoghurt and cooling water and of the overall heat transfer coefficients (*U*), for each stirred yoghurt/ water heat transfer experiment.

Formulation ID	**Yoghurt**			**Cold water**			**U**
	mass rate [kg s^{-1}]	**Re [-]**	**Prg [-]**	**mass rate [kg s^{-1}]**	**Re [-]**	**Pr [-]**	**[W m^2K^{-1}]**
12% TS-YF	0.064	0.59	3303	0.260	995	9.4	616
	0.065	0.61	3244	0.271	1064	9.2	565
	0.017	0.06	9351	0.264	979	9.8	226
	0.083	0.92	2729	0.272	1162	8.3	613
	0.032	0.16	5865	0.272	1164	8.3	415
	0.056	0.45	3735	0.273	1168	8.3	514
	0.087	1.00	2640	0.270	1185	8.1	576
	0.073	0.72	3052	0.272	1289	7.4	554
	0.093	1.10	2522	0.270	1280	7.4	613
	0.119	1.72	2069	0.272	1325	7.2	783
	0.105	1.37	2302	0.275	1305	7.4	591
	0.157	2.75	1682	0.275	1473	6.5	697
	0.121	1.72	2065	0.275	1081	8.8	692
	0.087	0.96	2679	0.275	1404	6.8	636
12% TS-YC	0.021	0.07	9029	0.264	869	11.2	228
	0.059	0.45	3909	0.268	1055	9.2	382
	0.074	0.68	3284	0.265	1196	7.8	464
	0.035	0.18	5869	0.244	906	9.8	318
	0.057	0.44	4004	0.267	1078	8.9	407
	0.018	0.05	10379	0.265	1044	9.2	250
	0.073	0.66	3348	0.269	1246	7.6	434
	0.070	0.61	3461	0.273	1197	8.1	442
	0.047	0.30	4725	0.269	1148	8.3	324
	0.062	0.48	3835	0.271	1255	7.6	428
13% TS-YF	0.049	0.17	8574	0.273	1198	8.1	572
	0.106	0.69	4618	0.272	1225	7.9	724
	0.031	0.07	12574	0.274	1299	7.4	222
	0.121	0.84	4226	0.275	1337	7.2	542
	0.110	0.45	5672	0.110	1478	6.5	554
	0.120	0.72	4585	0.120	1478	6.5	695
13% TS-H50	0.052	0.34	4537	0.273	1263	7.6	292
	0.074	0.64	3408	0.273	1263	7.6	356
	0.089	0.90	2979	0.273	1293	7.4	413
	0.134	1.90	2099	0.273	1293	7.4	445
	0.111	1.34	2444	0.274	1301	7.4	494
	0.134	1.90	2125	0.274	1019	9.8	536
	0.142	2.10	2005	0.275	1338	7.2	565
13% TS-HMC	0.063	0.55	3465	0.274	1079	9.2	457
	0.062	0.32	5863	0.274	1269	7.6	466
	0.045	0.18	7670	0.273	1263	7.6	295
	0.072	0.42	5194	0.273	1263	7.6	356
	0.118	1.04	3411	0.277	1316	7.4	506
	0.063	0.55	3465	0.274	1079	9.2	457

Table A.10- Average values of the local Nusselt number (Nu_L) of 12%TS-YF stirred yoghurt along the channel length (x_L) as a function of local generalised Reynolds number, for section 2.

Local Reynolds number, Re [-]	**Channel length, x_L [m]**	**Local Nusselt number, Nu_L**
0.62	0.1020	4.5
	0.2460	4.2
	0.3940	3.8
	0.4870	3.7
1.72	0.1020	90.8
	0.2460	21.5
	0.3940	16.3
	0.4870	10.0
6.98	0.1020	62.3
	0.2460	22.9
	0.3940	20.3
	0.4870	15.6

Table A.11- Average values of the local Nusselt number (Nu_L) of 13%TS-YC stirred yoghurt along the channel length (x_L) as a function of local Reynolds number, for section 2.

Local Reynolds number, Re [-]	**Channel length, x_L [m]**	**Local Nusselt number, Nu_L**
0.07	0.1020	9.6
	0.2460	3.4
	0.3940	3.0
	0.4870	2.7
0.18	0.1020	17.5
	0.2460	12.3
	0.3940	6.3
	0.4870	5.0
0.66	0.1020	45.6
	0.2460	37.6
	0.3940	14.3
	0.4870	10.6

ANNEX A2 - SIMPLIFIED NUMERICAL SIMULATION TO OBTAIN HEAT TRANSFER CORRELATIONS FOR STIRRED YOGHURT IN A PLATE HEAT EXCHANGER

Isabel M. Afonso [1,2], Paulo Cruz [1], João M. Maia[3] and Luís F. Melo[1]

[1]Laboratório de Engenharia de Processos, Ambiente e Energia - LEPAE, Faculdade de Engenharia, Universidade do Porto, Rua Dr. Roberto Frias, s/n 4200-465 Porto, Portugal

[2]Escola Superior Agrária de Ponte de Lima, Instituto Politécnico de Viana do Castelo, Refóios, 4990-760 Ponte de Lima, Portugal

[3]IPC—Institute for Polymers and Composites, Departamento de Engenharia de Polímeros, Universidade do Minho, 4800-058 Guimarães, Portugal

ABSTRACT

In the present work a numerical investigation was conducted in order to obtain correlations for the determination of convective heat transfer coefficients of stirred yoghurt during the cooling stage in a plate heat exchanger, taking into account its rheological features. The main simplification in the simulation method was the assumption of bi-dimensional flow in a flat plate geometry. By combining the resulting theoretical equations for a flat geometry with the geometric parameters usually defined for corrugated parameters (aspect ratio, hydraulic diameter), correlations for the convective coefficients were obtained that compare well to the experimental ones. This simplified and much faster simulation methodology proved to be appropriate for highly viscous, low Reynolds number flow situations.

Keywords: plate heat exchanger, stirred yoghurt, parallel plates geometry, numerical simulation

CORRESPONDING AUTHOR´S ADDRESS

Correspondence concerning this paper should be addressed to Prof. Luis F. Melo, Laboratório de Engenharia de Processos, Ambiente e Energia - LEPAE, Faculdade de

Engenharia, Universidade do Porto, Rua Dr. Roberto Frias, s/n 4200-465 Porto, Portugal. Tel.: + 351 22-5081588; Fax: + 351-22-5081449. E-mail: lmelo@fe.up.pt

INTRODUCTION

Industrial processing of stirred yoghurt includes a cooling step which is usually carried out in plate heat exchangers built with special platage to ensure gentle mechanical treatment and a uniform product quality (Bylund, 1995). Yoghurt is a strongly non-Newtonian fluid and exhibits complex flow patterns that are dependent upon temperature, shear rate and elastic properties. Additionally, the rheological and thermal properties of yoghurt are affected by other factors as the total solid content and the type of starter culture. Such complexity may explain why the literature published on heat transfer in yoghurt is practically non-existent, although experimental data have been obtained on the rheology of the product, identifying its pseudoplastic flow behaviour and its partially thixotropic and viscoelastic characteristics (Benezech and Maingonnat, 1993; Benezech and Maingonnat, 1994; Afonso and Maia, 1999; Afonso et al., 2003).

The high apparent viscosity of yoghurt is the main factor limiting the cooling rates in heat exchangers due to flow distribution effects and low Reynolds numbers, resulting in low heat exchanger efficiency (Kakaç and Liu, 2002). In fact, the velocity of yoghurt in plate heat exchangers is quite low, often falling below 0.12 m s^{-1} (Tamine and Robinson, 1999). Moreover, the hydraulic diameter of the channels in these heat exchangers is typically very small and the length-to-diameter ratio (L / D_H) is relatively large. Due to these length scales and the viscous nature of the fluids being handled, the flow is usually laminar (Chaves et al., 2001). It should be stressed that in their study of the local heat transfer coefficients of Newtonian fluids in corrugated plate heat exchanger channels, Heggs et al. (1997) observed that pure laminar flow does not exist in the channels, showing how a core of fluid flows along the troughs of the plate corrugations. However, in the case of strongly viscous fluids such as stirred yoghurt, with very low Reynolds numbers (of the order of 0.1 to 10), it is conceivable that the flow might follow closely the irregularities of the surface and produce predominantly laminar boundary layers, without any significant generation of turbulent eddies. If so, laminar entry length effects may prevail and the local convective heat transfer coefficients will tend to decrease along the flow channel. This can be particularly

relevant in the optimisation of heat exchanger design for such processes as yoghurt cooling.

The industrial development of plate heat exchangers was considerable in recent decades. However, most of the industrial thermal performance data still remains confidential and only a limited number of studies were published focusing on plate exchangers experimental results (Bassiouny and Martin, 1984a; Bassiouny and Martin, 1984b; Rene et al., 1991; Heggs et al., 1997; Muley et al., 1999; Rao and Das, 2004; Carezzato et al., 2007) and modelling (Rene and Lalande, 1987; Kho and Müller-Steinhagen, 1999; Zettler and Müller-Steinhagen, 2001; Grijspeerdt et al., 2003; Gut and Pinto, 2003;). Apart from the experimental data recently published by the present authors (Afonso et al., 2003, see section below), only one study on heat transfer in stirred yoghurt processing in a plate heat exchanger has been reported, concerning either average or local convective heat transfer coefficients (Fernandes et al., 2006). Fernandes et al. (2006) compared the thermal correlations obtained numerically by using computational fluid dynamics (CFD) with the experimental ones obtained by the authors. Regarding stirred yoghurt flow behaviour, some studies have been published recently where both experimental and simulation results were reported (Fangary et al., 1999; Fernandes et al., 2005; Mullineux and Simmons, 2007).

Numerical simulation can be used to test hypotheses regarding the local heat transfer rates along the plates, particularly in the thermal entry zone. However, complex cases such as the present one, dealing with corrugated channels and a non-Newtonian fluid, require 3-D numerical analysis and are expensive in computing time. Avoiding this complexity would be quite useful for engineers trying to optimize plate heat exchanger design.

Therefore, the aim of present work was: a) to obtain a convective heat transfer correlation for stirred yoghurt cooling in a plate heat exchanger by using a simplified numerical approach, and compare it to the experimental correlation obtained in previous work by Afonso et al. (2003); b) to test whether the assumption of flat channel geometry with a developing laminar boundary layer simulates the more complex three-dimensional hydrodynamic pattern that actually exists in a plate heat exchanger, for the specific fluid under study.

PREVIOUS EXPERIMENTAL WORK ON THE RHEOLOGICAL AND THERMAL PROPERTIES OF STIRRED YOGHURT

An investigation was previously conducted in order to obtain an experimental correlation for convective heat transfer coefficients of stirred yoghurt in a small laboratory-scale plate heat exchanger (Afonso et al., 2003). A rheological study was also carried out to describe the stirred yoghurt flow behaviour, evaluating its dependency both on shear rate and temperature.

The effect of the temperature on the rheological behaviour of stirred yoghurt was assessed with the method reported by Afonso and Maia (1999). A shift in the temperature dependency was observed at approximately 25ºC. Thus, two distinct regions were observed, corresponding to different temperature dependencies with different activation energies (a measure of materials sensitivity to temperature changes).

The rheological model that better described the stirred yoghurt can be mathematically expressed as:

$$\tau = \tau_0 + K_1\dot{\gamma}, \text{ for } \tau < 6.7 \text{ Pa} \qquad (1)$$

$$\tau = K_2\dot{\gamma}^n, \text{ for } \tau > 6.7 \text{ Pa} \qquad (2)$$

where τ_0 is the yield stress, K_1 and K_2 consistency indexes and n is the flow behaviour index. At shear stresses lower than 6.7 Pa, the stirred yoghurt exhibited a Bingham viscoplastic features with a yield stress τ_0, of approximately 0.54 Pa and a consistency index K_1 of 1.45 Pa s. At shear stresses higher than 6.7 Pa, the stirred yoghurt exhibited a strong shear-thinning character described by a power-law model with a consistency index K_2 of 3.65 Pa s and a flow behaviour index n, of 0.42.

Temperature effects were included in the rheological model by means of an Arrhenius type term:

$$\mu_{app} = \left[\bar{\mu}_{app}(\dot{\gamma})\right] e^{(E/\Re T)} \qquad (3)$$

where μ_{app} is the apparent viscosity of stirred yoghurt, $\bar{\mu}_{app}(\dot{\gamma})$ is the term that takes in account the dependency of viscosity on shear rate, E is the activation energy, $\Re$ is the universal gas constant (8.314 J K^{-1} mol^{-1}) and T is the absolute temperature (K). For

temperatures below 25ºC, the activation energy is 3.39 kJ mol^{-1} and for temperatures above 25ºC is 94.8 kJ mol^{-1}.

Heat transfer experiments were carried out in the laboratory-scale plate heat exchanger with generalised Reynolds numbers (which take into account the rheological effects) of yoghurt varying from 0.51 to 14.47. The main geometrical characteristics of the heat exchanger plates used in the experimental work are given in Table 1.

The semi-empirical correlation obtained for the dimensionless average convective heat transfer coefficient of stirred yoghurt was:

$$Nu_m = 1.67 \cdot Re_g^{0.455} \cdot Pr_g^{0.3} \quad (4)$$

where Nu_m is the average Nusselt number. The generalised Reynolds (Re_g) and Prandtl (Pr_g) numbers were calculated considering that the apparent viscosity of stirred yoghurt assumed the power-law form presented in equations (2) and (3) because the stirred yoghurt under the operating conditions prevailing in the plate heat exchangers had a predominant pseudoplastic behaviour (shear stress > 6.7 Pa).

The generalised dimensionless numbers are mathematically expressed as:

$$Re_g = \frac{u \rho D_H}{\mu_{app}} \quad (5)$$

$$Pr_g = \frac{c_p \mu_{app}}{k} \quad (6)$$

The apparent viscosity μ_{app} was determined using a shear rate value calculated using the following expression:

$$\dot{\gamma} = \left(\frac{2n+1}{3n} \right) \cdot \frac{\dot{m}_v}{w \cdot b^2} \quad (7)$$

where $\dot{m}_v$ is the volumetric flow rate ($m^3\ s^{-1}$), w is the channel width (m) and b the mean channel spacing (m).

The study revealed significant thermal entrance effects associated to the high generalised Prandtl numbers (between 581 and 1867) and to the short length of the plates used in the experimental work.

The correlation obtained (Eq. (4)) includes a correction factor named as area enlargement factor (ϕ) of 1.105, related to the ratio of the developed length to the projected length (Hewitt et *al.*, 1994b; Kakaç and Liu, 2002).

The Reynolds number exponent in equation (4) was similar to those reported by Edwards (1988) in plate heat exchangers operating in the laminar regime with other non-Newtonian fluids, but higher than those obtained by Rene *et al.* (1991).

NUMERICAL APPROACH

Due to the very high Prandtl numbers (of the order of 1 000), the velocity entry length is much shorter than the thermal entry length. Therefore, in the numerical simulation the flow was considered to be fully developed from the momentum viewpoint but not from the thermal viewpoint. Also, in order to avoid time-consuming computer calculations, the flow channel was assumed to be flat. The idea was to verify whether the much simpler bi-dimensional approach is appropriate for particular cases of highly viscous fluids such as yoghurt.

The following analysis is thus subject to certain restrictions, namely: the heat exchanger is operated in steady state; the fluid thermal conductivity, k, heat capacity, c_p, and density, ρ, are independent of temperature and pressure; isothermal flow is fully developed hydrodynamically at the entrance to the heat transfer section in a duct; thermal energy generation in the fluid by viscous dissipation is negligible; the fluid is cooled either at constant wall temperature or at constant wall heat flux; the flow duct is modelled as parallel flat plates (lateral effects are discarded). Numerical tests were also run in the case of circular cross-section for comparison purposes.

The present analysis deals with the problem of determining the thermal development region of a non-Newtonian fluid whose rheological behaviour can be approximated by a temperature-dependent power law equation of the form:

$$\tau = K_2 \cdot (\dot{\gamma})^n e^{E/\Re T} \tag{8}$$

where τ is the shear stress and $\dot{\gamma}$ is the shear rate.

The dimensionless energy equation (for detailed derivation see Annex A) is given by:

$$\frac{\partial\theta}{\partial x^*} = 8(2-s)\frac{I_2}{I_1}\frac{1}{r^{*s}}\frac{\partial}{\partial r^*}\left(r^{*s}\frac{\partial\theta}{\partial r^*}\right) \tag{9}$$

where s is the heat transfer section geometric factor (0 – parallel flat plates, 1 - circular cross section), θ is the dimensionless temperature, $\theta = (T - T_{\text{in}})/(T_{\text{w}} - T_{\text{in}})$, x^* is the dimensionless axial coordinate, $x^* = (\text{Re}\,\text{Pr}\,D_H / x)^{-1}$, r^* is the dimensionless radial coordinate, $r^* = r/R$, T_{w} is the wall temperature ($x = 0$), T_{in} is the inlet temperature, Re is the Reynolds number, Pr is the Prandtl number, D_H is the hydraulic diameter and R is the tube radius or channel half-height. I_1 and I_2 are given by the following expressions:

$$I_1 = \int_{r^*}^{1} (r^*)^{1/n} \exp\left(E/n\Re T\right) \mathrm{d}r^* \tag{10}$$

$$I_2 = \int_{0}^{1} I_1\,(r^*)^s\ \mathrm{d}r^* \tag{11}$$

Equation (9) is a partial differential equation that can be solved by numerical techniques for various boundary conditions, limited in this study to two particular situations: constant wall temperature and constant wall heat flux

Boundary conditions:

$$x^* = 0;\quad \theta = \theta_{\text{in}};\quad \forall r^*$$

$$r^* = 0;\quad \frac{\partial\theta}{\partial r^*} = 0;\quad \forall x^*$$

Constant wall temperature: $r^* = 1;\quad \theta = 1$

Constant heat flux: $r^* = 1;\quad \dfrac{\partial\theta}{\partial r^*} = q_{\text{w}}^*$ (12)

where q_{w}^* is the dimensionless heat flux in the wall.

NUMERICAL SOLUTION

The discretisation of equation (9) is carried out in two stages. Firstly, the space derivatives appearing in the right hand side are computed with finite differences schemes. Then, the resulting initial value system of ordinary differential equations is integrated explicitly to obtain the grid point values. This integration is done with the package LSODA (Petzold, 1983). This package solves initial value problems for stiff or non-stiff systems of first-order ODE's. For non-stiff systems, it utilises the Adams method with variable order (up to $12^{\underline{\text{th}}}$ order) and step size, while for stiff systems it uses the Gear (or BDF) method with variable order (up to $5^{\underline{\text{th}}}$ order) and step size.

The average Nusselt number can be obtained by the following expression (for detail derivation see Annex B):

$$\mathrm{Nu_m} = \mathrm{Re}\,\mathrm{Pr}\frac{D_H}{L}\int_0^{(\mathrm{Re}\,\mathrm{Pr}\,D_H/L)^{-1}} \frac{2}{(\theta_\mathrm{w}-\theta_\mathrm{m})}\left(\frac{\partial\theta}{\partial r^*}\right)_{r^*=1} \mathrm{d}x^* \tag{13}$$

where θ_m is the average temperature, given by:

$$\theta_\mathrm{m} = \int_0^1 I_1 / I_2 \theta (r^*)^s \, dr^* \tag{14}$$

RESULTS AND DISCUSSION

The present study is a numerical approach of the plate heat exchanger corrugated channel flow to the laminar flow in a simple flat channel geometry. In order to test the consistency of the method, the numerical solutions obtained were compared to the ones obtained by several authors in their study of the heat transfer to Newtonian and non-Newtonian fluids in laminar flow in tubes of circular cross-section, with constant wall temperature and constant wall heat flux boundary conditions.

In both cases the temperature effects on the rheological properties were taken in account. Thus, in order to evaluate the temperature effects on the fluid viscosity (assessed by means of a Arrhenius type term), the numerical solutions obtained for constant wall temperature boundary condition were compared to the ones obtained by Christiansen and Craig (1962) in their study of the heat transfer to power-law fluids under laminar flow in a tube of circular cross-section, with constant wall temperature. The solutions obtained were in good agreement for $\mathrm{Re}\,\mathrm{Pr}\,D_H/L$ values higher than 20.

The difference observed may be due to the use of different methods in the calculation of the average Nusselt number values.

Figure 1 shows the heat transfer results obtained for a cylindrical tube, for constant wall temperature boundary condition. Several values of activation energy were computed in order to test its influence on the dimensionless heat transfer coefficient. Two limiting cases were considered: E=0 (temperature effects not included) and E=∞ (infinite activation energy). Figure 1 evidences the temperature effects for the whole range of $\mathrm{Re}\,\mathrm{Pr}\,D_H/L$ values, which are more pronounced for $\mathrm{Re}\,\mathrm{Pr}\,D_H/L$ values higher than 100.

From Figure 1, one can conclude that the asymptotic solution obtained for infinite activation energy can be satisfactorily correlated by the asymptotic solution obtained by Metzner *et al.* (1957), for plug flow given by:

$$\mathrm{Nu_m} = \frac{8}{\pi} + \frac{4}{\pi}\left(\mathrm{Re}\,\mathrm{Pr}\,D_H/L\right)^{1/2} \tag{15}$$

The asymptotic solution obtained without including the temperature effects on the apparent viscosity (E=0) is compared with the following correlation:

$$\mathrm{Nu_m} = 1.75\cdot\left(\frac{3n+1}{4n}\right)^{1/3}\left(\mathrm{Re}\,\mathrm{Pr}\,D_H/L\right)^{1/3} \tag{16}$$

Equation (16) is obtained for laminar heat transfer in the thermal entrance region assuming that a fully developed velocity profile exists, limited to $\mathrm{Re}\,\mathrm{Pr}\,D_H/L$ values higher than 33π (Metzner et al., 1957; Cho and Hartnett, 1985).

Numerical simulations were also carried for constant wall heat flux boundary condition, taking into account the temperature effects. In this case, the effect of the temperature dependent fluid consistency on heat transfer is not as marked as it was for the constant wall temperature situation, as one can observe in Figure 2. This is because, unlike the constant wall temperature case, the tube wall is not subjected to a sudden large increase of temperature at the entrance of the heated section but instead undergoes a gradual increase under the influence of a constant wall heat flux (Forrest and Wilkinson, 1973).

From Figure 2, one can conclude that the asymptotic solution obtained for zero activation energy can be satisfactorily correlated by Equation (17) given by (Kakaç and Yener, 1995; Hewitt *et al*., 1994a):

$$\mathrm{Nu}_{\mathrm{m}} = 1.953\left(\mathrm{Re}\,\mathrm{Pr}\,D_H/L\right)^{1/3}, \quad \left(\mathrm{Re}\,\mathrm{Pr}\,D_H/L\right) > 10^2 \tag{17}$$

Numerical solutions were also obtained for parallel flat plates, at the two limiting cases of constant wall temperature and constant wall heat flux boundary conditions. The energy equation was solved for fully developed flow with a flow behaviour index (n) of 0.42, considering that the apparent viscosity of stirred yoghurt assumed the power-law form presented in equation (2).

The temperature effects were assessed in two different situations, according to the two activation energies reported in section 2. Using the activation energy of 3.39 kJ mol^{-1}, the curve of the correspondent average Nusselt number was almost superimposed with the zero activation energy (E=0, no temperature correction); for an activation energy of 94.8 kJ mol^{-1}, the correspondent average Nusselt number curve was almost superimposed with an infinite activation energy (E=∞).

Figure 3 shows the heat transfer data obtained for parallel flat plates, for constant wall temperature. The numerical data plotted was obtained using the activation energy of 94.8 kJ mol^{-1}, as maximum value, and the zero activation energy (E=0) as a minimum.

Using the “channel aspect ratio” of the plate heat exchanger (defined as the mean channel gap divided by the corrugation pitch and the latter being the distance between two “peaks” of adjacent corrugations (Kakaç and Liu, 2002)) which is 0.52 in the present case, the values obtained from theoretical simulation fitted well the experimental data. It is possible to conclude from Figure 3 that the average Nusselt numbers obtained in the experimental work and the simulated ones are quite similar in this case, for constant wall temperature conditions.

Apparently, the results seem to indicate that the assumption of parallel flat plates is quite satisfactory to predict the convective heat transfer coefficients of stirred yoghurt flowing through plate heat exchanger channels, once the proper geometric parameters of the corrugated plates are introduced. In spite of the good agreement, one must have always in mind that this approach neglects the complex flow pattern of the fluid within

the plate heat exchanger channels and cannot be used for purposes different from the present ones.

Figure 4 compares the experimental correlation to the one obtained by numerical simulation. The correlation obtained from the numerical simulation for the dimensionless convective heat transfer coefficient of stirred yoghurt at constant wall temperature is:

$$\mathrm{Nu}_{\mathrm{m}} = 1.69 \cdot \mathrm{Re}_{g}^{0.362} \cdot \mathrm{Pr}_{g}^{0.3} \tag{18}$$

The correlations (Eqs. (4) and (18)) exhibit similar tendency, although the Reynolds number exponent is smaller in the simulation study (0.36 versus 0.46). Again, one must have in mind that the values of constants (1.69 versus 1.67) and Reynolds number exponent depend on flow characteristics and chevron plate angles (30º in the present plate heat exchanger).

For constant wall heat flux boundary condition, a similar analysis was carried out in order to compare the experimental correlation to the one obtained by numerical simulation, as it is shown in Figure 5.

The correlation obtained from numerical simulation for the dimensionless convective heat transfer coefficient of stirred yoghurt for constant wall heat flux is:

$$\mathrm{Nu}_{\mathrm{m}} = 1.94 \cdot \mathrm{Re}_{g}^{0.36} \cdot \mathrm{Pr}_{g}^{0.3} \tag{19}$$

Comparing the correlations (Eqs. (4) and (19)) one can observe their similarity, although the Reynolds number exponent is smaller in the simulation study (0.36 versus 0.46) and the constants are not equal (1.94 versus 1.67). The correlations obtained numerically for both boundary conditions (Eqs. (18) and (19)) exhibit the same Reynolds number exponent value. This could be expected since numerical simulations were run at the same operating conditions (similar to the experimental ones). The constants obtained in the numerical study have the same magnitude of the constants referred to in the literature (Cho and Hartnett, 1985; Kakaç and Yener, 1995; Hewitt *et al.*, 1994a; Fernandes *et al.*, 2006).

A statistical procedure by means of regression analysis of the experimental data was carried out in order to evaluate the confidence intervals of the constant and Reynolds number exponent in equation (4), with a confidence level of 95% (Kreyszig, 1999).

Figure 6 displays the slope of the confidence limits obtained by regression analysis. The confidence interval obtained for the constant in eq.(4) is 1.57 – 1.83 ($P<0.05$). For Reynolds number exponent, one obtained a lower and upper confidence limits ($P<0.05$) of 0.388 and 0.521, respectively. From the regression analysis performed, one can observe that the constant and Reynolds number exponent values were quite similar to the ones reported by Fernandes *et al*. (2006), 1.691-1.701 for the coefficient and 0.448-0.462 for the Reynolds number exponent.

Comparing the correlations obtained from numerical simulation (eqs.(18) and (19)) with the confidence limits from experimental data regression analysis one can observe that the constant in eq. (18) is within the confidence intervals and the constant in eq. (19) is slightly higher that the upper confidence limit. Concerning the values of the Reynolds number exponent, one can observe that both values are below the lower confidence limit. Thus, comparing both boundary conditions, one can say that the numerical approach carried out in this study may be considered appropriate for particular cases of highly viscous fluids such as yoghurt, mainly in the case of constant wall temperature.

CONCLUSIONS

Correlations for the convective heat transfer coefficients of stirred yoghurt during cooling in plate heat exchangers were obtained from experimental data and from a numerical simulation study. The simplifications introduced in the simulation method (namely, the assumption of bi-dimensional flow in a parallel flat plates geometry) were satisfactory for the prediction of the convective coefficients, once the geometric factors (channel aspect ratio, effective to projected area) are introduced in the simulation. One possible explanation for this agreement is that the effects of the high viscosity of stirred yoghurt prevail, in the sense that the corrugated surfaces do not seem to cause significant turbulent perturbations in the flow development in this particular case.

The temperature effect on the viscosity of the fluid was taken into account in the theoretical description and was shown to be of major importance.

NOMENCLATURE

b mean channel spacing (m)

c_p specific heat at constant pressure (J kg^{-1} K^{-1})

D_H hydraulic diameter (m)

E activation energy (J mol^{-1})

h_m average heat transfer coefficient (W $m^{-2}K^{-1}$)

k thermal conductivity (W $m^{-1}K^{-1}$)

K_1, K_2 consistency index (Pa s^n)

L length of heated channel (m)

$\dot{m}_v$ volumetric flow rate (m^3 s^{-1})

n flow behaviour index

Nu Nusselt number

Pr Prandtl number

p_T fluid pressure (Pa)

$\Re$ universal gas constant (J K^{-1} mol^{-1})

r local radius (m)

R tube radius or channel half-height (m)

r^* dimensionless radial coordinate

Re Reynolds number

s heat transfer section geometric factor

T absolute temperature (K)

u velocity (ms^{-1})

u^* dimensionless velocity

w channel width (m)

x axial coordinate (m)

x^* dimensionless axial coordinate

Greek symbols

ϕ area enlargement factor

$\dot{\gamma}$ shear rate (s^{-1})

μ_{app} apparent viscosity (Pa s)

θ dimensionless temperature

τ shear stress (Pa)

τ_0 yield stress (Pa)

Subscripts and superscripts

g generalised

in inlet

m average

w wall

ANNEX A. Derivation of non-dimensional energy equation (equation 9)

Based on the assumptions presented in section 3, the steady flow of an incompressible fluid with no external forces is described by the set of two basic equations: motion and energy.

Motion equation:

$$-\frac{\partial p_T}{\partial x} = \frac{1}{r^s}\frac{\partial\left(r^s \tau_{rx}\right)}{\partial r} \qquad \text{(A.1)}$$

Energy equation:

$$u(r)\cdot\rho\cdot cp\cdot\frac{\partial T}{\partial x} = k\frac{1}{r^s}\frac{\partial}{\partial r}\left(r^s\frac{\partial T}{\partial r}\right) \qquad \text{(A.2)}$$

where τ_{rx} is the shear stress in the x direction per unit area on an element of fluid surface of constant r, p_T is the fluid pressure, T is the fluid temperature and $u(r)$ is the velocity at radius r. The equation of motion, equation (A.1), can be integrated by taking $\partial p_T / \partial x$ independent of r to give:

$$\tau_{rx} = -\frac{r}{(s+1)} \frac{\mathrm{d}p_T}{\mathrm{d}x} \quad . \tag{A.3}$$

The shear stress at the wall, τ_{Rx} is given by:

$$\tau_{Rx} = -\frac{R}{(s+1)} \frac{\mathrm{d}p_T}{\mathrm{d}x} \tag{A.4}$$

And so the shear stress at radius r is given by:

$$\tau_{rx} = \frac{r}{R} \tau_{Rx} \tag{A.5}$$

The following dimensionless variables were introduced:

u^* = dimensionless velocity at radius r^*, $u^* = u / u_{\mathrm{m}}$

r^* = dimensionless radial coordinate, $r^* = r / R$

x^* =dimensionless axial coordinate, $x^* = (\mathrm{Re}\,\mathrm{Pr}\, D_H / x)^{-1}$

θ = dimensionless temperature, $\theta = \dfrac{T - T_{\mathrm{in}}}{T_{\mathrm{w}} - T_{\mathrm{in}}}$

where u_{m} is the average velocity, R is the tube radius or channel half-height, D_H is the hydraulic diameter, T_{w} is the wall temperature and T_{in} is the inlet temperature.

The energy equation, equation (A.2), can be written in the dimensionless form as follows:

$$u^*(r^*) \frac{\partial \theta}{\partial x^*} = 8 \frac{(2-s)}{(s+1)} \frac{1}{r^{*s}} \frac{\partial}{\partial r^*} \left(r^{*s} \frac{\partial \theta}{\partial r^*} \right) \tag{A.6}$$

and equation (A.1) as:

$$\tau_{rx} = r^* \tau_{Rx} \tag{A.7}$$

The velocity profile is obtained by the substitution of equation (7) into equation (A.1):

$$K_2 \cdot \left(-\frac{\mathrm{d}u}{\mathrm{d}r} \right)^n e^{E/\Re T} = \frac{r}{R} \tau_{Rx} \quad , \tag{A.8}$$

with integration between $u = 0$ to $u = u$ and $r = R$ to $r = r$ at a given x. The velocity profile is now given by:

$$u(r) = R \left(\frac{\tau_{Rx}}{m} \right)^{1/n} I_1 \tag{A.9}$$

where I_1 is defined as:

$$I_1 = \int_{r^*}^{1} (r^*)^{1/n} \exp\left(E / n\Re T \right) \mathrm{d}r^* \quad . \tag{A.10}$$

The average velocity u_{m} is given by:

$$u_{\mathrm{m}} = \frac{(s+1)}{R^{s+1}} \int_0^R u(r)\, r^s \, \mathrm{d}r \tag{A.11}$$

The substitution of equation (A.9) in equation (A.11) yields:

$$u_{\mathrm{m}} = (s+1) R \left(\frac{\tau_{Rx}}{m} \right)^{1/n} I_2 \tag{A.12}$$

where I_2 is defined as:

$$I_2 = \int_0^1 I_1 \, (r^*)^s \, \mathrm{d}r^* \tag{A.13}$$

And so the velocity profile is given by the following expression:

$$u^*(r^*) = u / u_{\mathrm{m}} = \frac{1}{(s+1)} \frac{I_1}{I_2} \tag{A.14}$$

ANNEX B Derivation of average Nusselt number (equation 13)

The heat transfer coefficient as a function of x coordinate, h_x, can be obtained by the two following relations:

$$q_x = h_x \cdot A \cdot (T_w - T_m) \tag{B.1}$$

$$q_x = k \cdot A \cdot \left(\frac{\partial T}{\partial r} \right)_{r=R} \tag{B.1}$$

where q_x is the heat flux as a function of x coordinate and the average heat transfer coefficient, $h_m = \int h_x dx / L$ can be obtained by the following expression:

$$h_m = \frac{1}{L} \int_0^L \frac{k}{(T_w - T_m)} \left(\frac{\partial T}{\partial r} \right)_{r=R} dx \tag{B.1}$$

And so, the average Nusselt number is given by the following expression:

$$Nu_m = Re\,Pr \frac{D_H}{L} \int_0^{(Re\,Pr\,D_H/L)^{-1}} \frac{2}{(\theta_w - \theta_m)} \left(\frac{\partial \theta}{\partial r^*} \right)_{r^*=1} dx^* \tag{B.1}$$

where θ_m is the average outlet temperature, given by:

$$\theta_m = \int_0^1 I_1 / I_2 \theta (r^*)^s dr^* \tag{B.6}$$

REFERENCES

Afonso, I. M. and Maia, J. M., 1999 Rheological monitoring of structure evolution and development of stirred yoghurt, Journal of Food Engineering 42: 183-190.

Afonso, I. M., Hes, L., Maia, J. M. and Melo, L.F.,2003, Heat transfer and rheology of stirred yoghurt during cooling in plate heat exchangers, Journal of Food Engineering 57: 179-187.

Bassiouny, M. K. and Martin, H., 1984a, Flow distribution and pressure drop in plate heat exchangers-I. U-type arrangement, Chemical Engineering Science 39 (4): 693-700.

Bassiouny, M. K. and Martin, H., 1984b, Flow distribution and pressure drop in plate heat exchangers-II. Z-type arrangement, Chemical Engineering Science 39 (4): 701-704.

Benezech, T. and Maingonnat, J. F., 1993, Flow properties of stirred yoghurt: structural parameter approach in describing time-dependency, Journal of Texture Studies 24: 455-473.

Benezech, T. and. Maingonnat J. F, 1994, Characterization of the rheological properties of yoghurt – a review, Journal of Food Engineering 21: 447-472.

Bylund, G., 1995, Culture milk products, in Dairy Processing Handbook, Tetra Pak Processing System AB, Lund, pp. 241-262.

Carezzato, A., Alcantara, M. R., Telis-Romero, J., Tadini, C. C. and Gut, J. A. W., 2007, Non-Newtonian Heat Transfer on a Plate Heat Exchanger with Generalized Configurations, Chem. Eng. Technol., 30, No. 1: 21-26

Chaves, C. L., Quaresma, J. N. N., Macêdo, E. N., Pereira, L. M. and Lima J. A., 2001, Hydrodynamically developed laminar flow of non-Newtonian fluids inside double-sine ducts, in: Proceedings of the 2nd International Conference on Computational Heat and Mass Transfer, COPPE/ UFRJ, Federal University of Rio de Janeiro, Brazil, (P91) pp.1-8.

Cho, Y. I. and Hartnett, J. P., 1985, Non-Newtonian fluids, in: W. M. Rohsenow, J. P. Hartnett, E. M. Ganic (Eds.), Handbook of Heat Transfer Applications, (McGraw-Hill).

Christiansen, E. B. and Craig, J. R., 1962 Heat transfer to pseudoplastic fluids in laminar flow, A.I.Ch.E. Journal 8 (2): 154-160.

Edwards, M. F., 1988, Heat transfer in plate heat exchangers at low Reynolds number, in S. Kakaç (Ed.), Low Reynolds number forced convection in channels and bundles applied to heat exchangers, NATO Advanced Study Institute, Ankara, Turkey, pp. 23-37.

Fangary, Y.S., Barigou, M. and Seville, J. P. K., 1999, Simulation of Yoghurt Flow and Prediction of Its End-of-Process Properties Using Rheological Measurements, Food and Bioproducts Processing 77 (C1): 33-39.

Fernandes, Carla S., Dias, R., Nóbrega, J. M., Afonso, I. M., Melo, L. F. and Maia, J. M., 2005, Simulation of stirred yoghurt processing in plate heat exchangers, Journal of Food Engineering, 69: 281-290.

Fernandes, Carla S., Dias, R. P., Nóbrega, J. M., Afonso, I. M., Melo, L. F. and Maia, J. M., 2006, Simulation of stirred yoghurt processing in plate heat exchangers, Journal of Food Engineering, 76: 433-439.

Forrest, G. and Wilkinson, W. L., 1973, Laminar heat transfer to temperature-dependent Bingham fluids in tubes, International Journal of Heat and Mass Transfer 16: 2377-2391.

Grijspeerdt, K., Hazarika, B. and Vucinic, D., 2003, Application of computational fluid dynamics to model the hydrodynamics of plate heat exchangers for milk processing, Journal of Food Engineering, 57: 237-242.

Gut, J. A. W. and Pinto, J. M., 2003, Modelling of plate heat exchangers with generalized configurations, International Journal of Heat and Mass Transfer 46: 2571-2585.

Heggs, P. J., Sandham, P.,. Hallam, R. A and Walton, C., 1997,Local heat transfer coefficients in corrugated plate heat exchanger channels, Transactions of the Institution of Chemical Engineers 75 (Part A): 641-645.

Hewitt, G. F., Shires, G. L. and Bott, T. R., 1994a, Process Heat Transfer (CRC Press LLC, Boca Raton), pp. 93-104.

Hewitt, G. F., Shires, G. L. and Bott, T. R., 1994b, Process Heat Transfer, (CRC Press LLC, Boca Raton), pp. 327-363.

Kakaç, S. and Y. Yener., Y., 1995, Convective Heat Transfer, (CRC Press, Boca Raton), pp. 279-309.

Kakaç, S. and Liu, H., 2002, The Gasketed-Plate Heat Exchangers, in Heat exchangers-selection, rating and thermal design, (CRC Press LLC, Boca Raton), pp. 373-396.

Kho, T. and Müller-Steinhagen, H., 1999, An experimental and numerical investigation of heat transfer fouling and fluid flow in flat plate heat exchangers, Transactions of the Institution of Chemical Engineers 77 (Part A): 124-130.

Kreyszig, E., 1999, Advanced Engineering Mathematics, (Wiley, Singapore) pp. 1145-1149.

Metzner, A. B., Vaughn, R. D. and Houghton, G. L, 1957, Heat transfer to non-Newtonian fluids, A.I.Ch.E. Journal 3 (1): 92-100.

Muley, A., Manglik, R. M. and Metwally, H. M., 1999, Enhanced heat transfer characteristics of viscous liquid flows in a chevron plate heat exchanger, Journal of Heat Transfer 121: 1011-1017.

Mullineux, G. and Simmons, M. J. H., 2007, Effects of processing on shear rate of yoghurt, Journal of Food Engineering 79: 850-857.

Petzold, L. R., 1983, Automatic selection of methods for solving stiff and nonstiff systems of ordinary differential equations, SIAM J. Sci. Stat. Comput. 4: 136-148.

Rao, B. P. and Das, S. K., 2004, An experimental study on the influence of flow maldistribution on the pressure drop across a plate heat exchanger, Transactions of the ASME 126:680-691.

René, F. and Lalande, M., 1987, Échangeur de chaleur à plaques et joints. Résolution numérique des équations d´échange thermique entre les différents canaux, Revue Générale Thermique Française 311: 577-583.

René, F., Leuliet, J.C. and Lalande, M., 1991, Heat transfer to Newtonian and non-Newtonian food fluids in plate heat exchangers: experimental and numerical approaches, Transactions of the Institution of Chemical Engineers 69 (Part C): 115-126.

Tamime, A. Y. and. Robinson, R. K., 1999, Yogurt- Science and Technology, second ed., (CRC Press LLC, Boca Raton).

Zettler, H.U. and Müller-Steinhagen, H., 2001, The use of CFD for the interpretation of fouling data in PHEs, in: Heat Exchangers Fouling- Fundamental Approaches & Technical Solutions (UEF- United Engineering Foundation, Inc., Davos, Switzerland).

ACKNOWLEDGMENTS

This research has been funded by the project POCTI/CTM/32970/99. The work of P. Cruz was supported by FCT (grant POSI - SFRH/BPD/13539/2003).

FIGURES

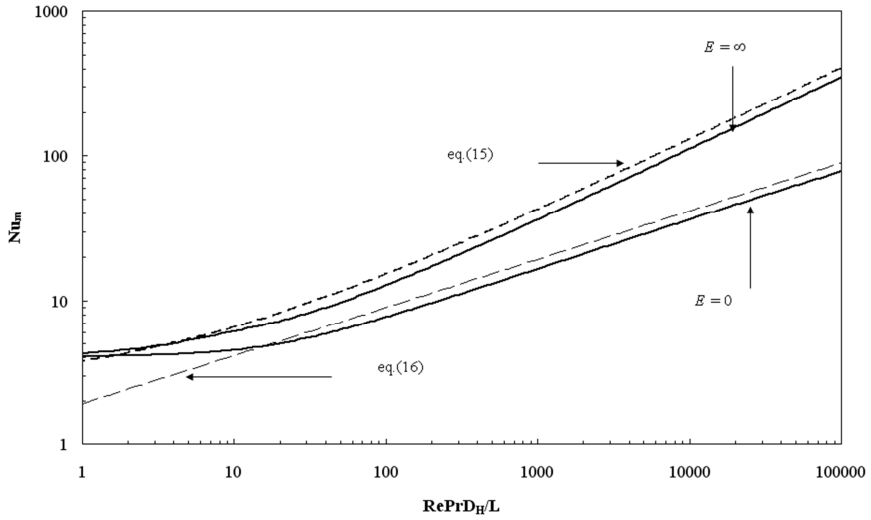


Figure1. Computed average Nusselt number as a function of ($RePrD_H/L$) and activation energy (*E*), for constant wall temperature boundary condition in a tube with circular cross-section. ═ simulation (with E= 0 and E= ∞ kJ mol^{-1}).

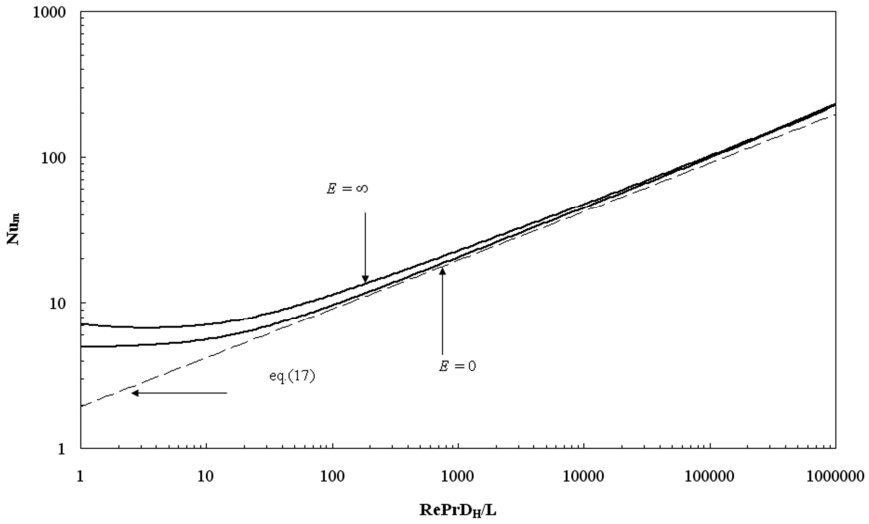


Figure2. Computed average Nusselt number as a function of ($RePrD_H/L$) and activation energy (*E*), for constant wall heat flux boundary condition in a tube with circular cross-section. ═ simulation (with E= 0 and E= ∞ kJ mol^{-1}).

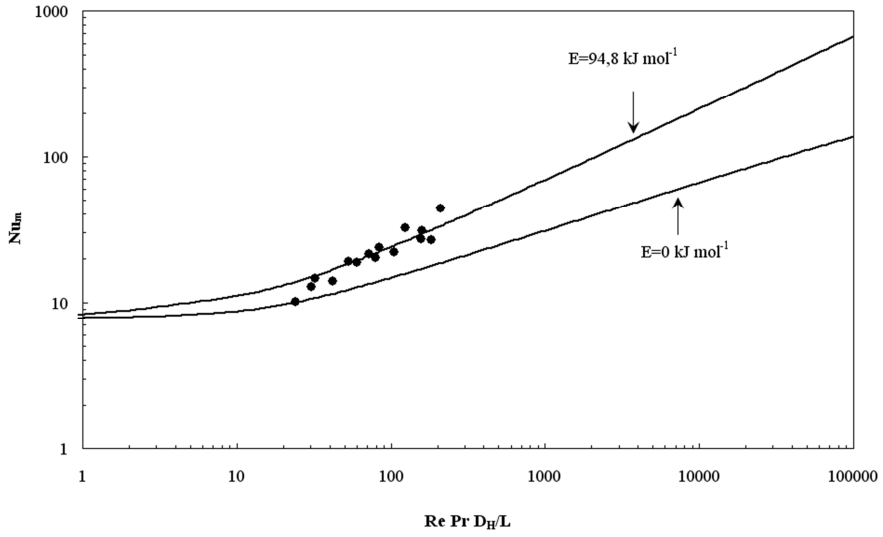


Figure 3. Computed average Nusselt number as a function of ($RePrD_H/L$) and activation energy (*E*), for constant wall temperature boundary condition. ● experimental and ── simulation (with E=0 kJ mol^{-1} and E=94.8 kJ mol^{-1})

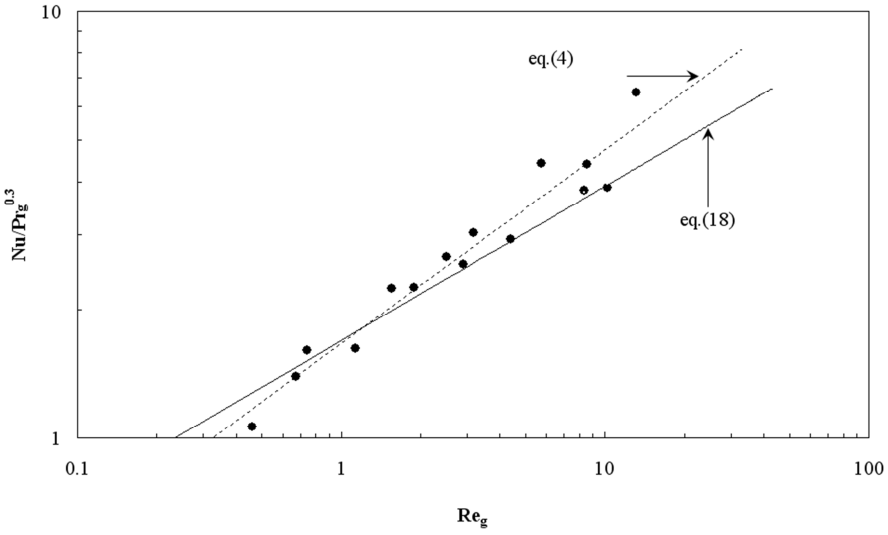


Figure 4. Experimental heat transfer correlation and numerical correlation computed for constant wall temperature boundary condition. ● experimental, ── simulation best fit and ···· experimental best fit.

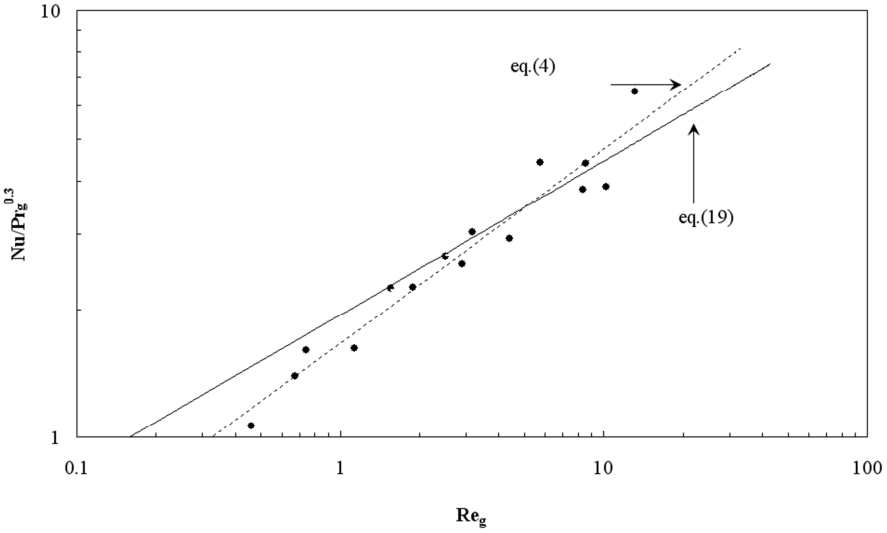


Figure 5. Experimental heat transfer correlation and numerical correlation computed for constant wall heat flux boundary condition. ● experimental, ── simulation best fit and ···· experimental best fit.

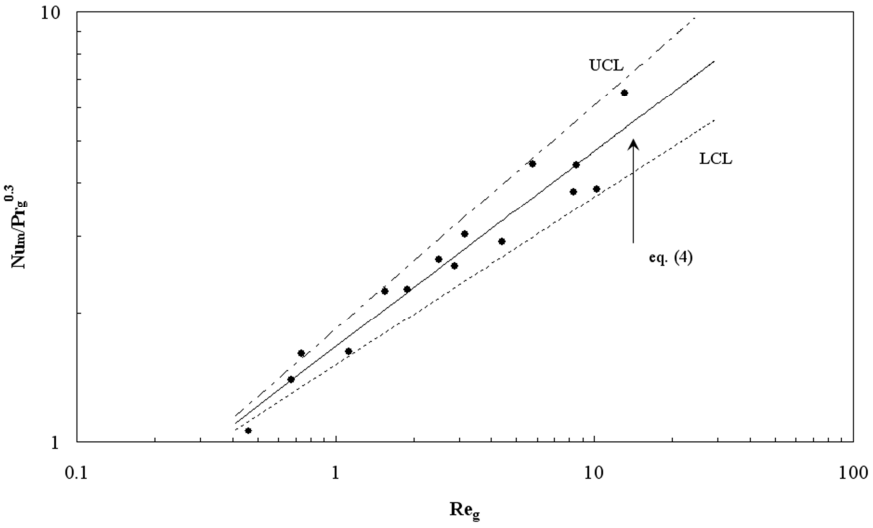


Figure 6. Experimental heat transfer correlation and lower and upper confidence limits. ● experimental, ── experimental best fit, - - - - lower confidence limit (LCL) fit and —·—·— upper confidence limit fit (UCL).

Table 1- Main geometrical characteristics of the herringbone plates

Material	Stainless steel AISI 316
Plate model	RS 22
Area, A (m^2)	0.015
Length, L (m)	0.265
Width, w (m)	0.102
Effective length, L_{eff} (m)	0.187
Effective width, w_{eff} (m)	0.0725
Area enlargement factor, ϕ (-)	1.105
Distance between plates, $b \times 10^{-3}$ (m)	2.6
Thickness, $x_p \times 10^{-3}$ (m)	0.5
Thermal conductivity, k_p (W $m^{-1}K^{-1}$)	16.3